Peedika Paramban, Rameees (2022)

Reductive Trapping of Novel Anionic Ligands using Divalent Organolanthanoid Complexes

A thesis submitted for the degree of

Doctor of Philosophy

by

Ramees Peedika Paramban

BS-MS (Chemistry)

College of Science and Engineering

James Cook University

October 2022

Declaration

I hereby declare that this thesis is my own work and contains no materials previously published or written by another person, or substantial proportions of material which have been accepted for the award of any other degree or diploma at any university or other institution, except where due reference is made in the text.

Ramees Peedika Paramban

College of Science and Engineering

James Cook University

October 2022

Acknowledgements

First of all, I would like to express my deepest gratitude to my supervisor Prof. Peter Junk. Being a part of your team and working with rare earths, which were completely new to me, was a tremendous honour. Without your unwavering support and guidance during my PhD journey, it would be hard for me. I really enjoyed our conversations, both about chemistry and cricket.

I am incredibly appreciative to Prof. Glen Deacon for his insightful counsel and assistance when my chemistry hits a roadblock. I appreciate his editorial help with my scientific writing as well. I would like to extend my thanks to Dr. Murray Davies, my secondary supervisor, for always being there whenever I needed him and leaving the chemical storage room open for us.

I am deeply indebted to Dr. Zhifang Guo for always being a big sister, friend, and mentor to me. It was always a pleasure to work with you and thanks for all that help with reactions and crystallography. Jun Wang deserves praise as well for introducing me to air-sensitive techniques and giving me my first laboratory training. Thanks should also go to the entire Junk gang, notably Angus, Vidushi, and Halim, as well as my office buddies Jayson, Alex, Kal and Mele for all the fun times, support and encouragement. Special thanks to Angus for your support, understanding and companionship throughout my PhD. I want to thank Owen Beaumont as well for his help with running crystals a few times.

Thank you to the entire chemistry team, especially Dr. Mark Robertson, for their support and assistance with the NMR spectroscopy and HPLC/MS, as well as Dr. Mark Barnes' aid with the lab demonstration. Special thanks to technical staff Dr. Winnie Lee, Shiyoh Nobile and Dr. Dana Roberts for their support during demonstration sessions.

Another person I'd like to recognise is Dr. Pradeep Kumar Mondal, who encouraged me to pursue a PhD despite my objections. If you were not there, this great journey would not have taken place, so thank you very much.

I'd want to thank all of my close friends, with special thanks to Naisham, Vivian, Kevin, Teddy, Saul, Tejas, Emenike, Neha, Adeel and Juan for all the laughs and wonderful times we shared. These experiences helped me get through all the frustrations and hard times I've faced over the past three and a half years.

My amazing landlords, Jack and Marian Worsfold, who have been likened to my foreign grandparents and have given me all the love and support throughout the years, deserve a special thanks as well.

Finally, a big thanks to my family (Dady, Umma, Rashamol and Anu), for their endless support and affection. And for encouraging me wholeheartedly in whatever decision I make.

And to my soulmate, Jumana. I wish you were here with me. It was always a pleasure to have someone in the family to talk research, especially when things are not going smoothly. Thanks a lot.

To all my well-wishers, thank you!

Statement of the contribution of others

Outside of personal contributions outlined in the acknowledgements, there have been several key bodies who have provided contributions in direct support of this thesis:

Nature of Assistance	Contribution	Names, Titles and Affliations of Co-Contributors
Intellectual Support	Proposal writing, data analysis and editorial assistance	Prof. Peter Junk Prof. Glen Deacon Dr. Murray Davies
Financial Support	Fee offset/waiver and stipend (through JCUPRS fellowship)	James Cook University
	Research costs (through ARC Discovery Project grants)	Australian Research Council
	Travel grants for attending conference (through CRT Project Grant)	College of Science and Engineering
Data Collection	X-ray diffraction data from crystals, solving and refining of crystal structures	Dr. Zhifang Guo Dr. Jun Wang Owen Beaumont

Abstract

Divalent organolanthanoid complexes have been used as single electron transfer reagents in several chemical transformations owing to their strong reduction potential and continue to offer fascinating results. Their application in trapping novel and unusual anionic ligands has been attracting chemists recently. Starting from dinitrogen to the recently reported ditungsten decacarbonyl ligand, complexes of classical divalent lanthanoids samarium and ytterbium with cyclopentadienyl and its N- and O-donor alternative ligand sets have eased the trapping of a vast array of notable ligands. However, this fascinating area is open to further exploration. This thesis extends the studies towards developing new reaction chemistry using recently synthesized organolanthanoid complexes, especially utilizing the ligand trapping capabilities of [$Sm(DippForm)_2(THF)_2$] (and its Yb analogue).

Beginning with the fundamentals, Chapter 1 presents an overview of rare earth chemistry and covers the characteristics, occurrence, abundance, and applications of rare earth elements. A discussion of the evolution of organolanthanoid chemistry, the use of Ln (II) complexes as SET reagents and their application in the reductive trapping of unique ligand fragments is provided. Additionally, information regarding the syntheses of divalent organolanthanoid starting materials is also given at the end of the chapter.

Chapter 2 mainly focuses on the interaction of divalent [$Sm(DippForm)_2(THF)_2$] with unsaturated alkyl and aromatic hydrocarbons. 1,3,5,7-Cyclooctatetraene has been utilized in this particular application and succeeded in the solvent-dependent synthesis of three different trivalent samarium complexes [$Sm^{III}(DippForm)(COT)(THF)_2$], [$Sm(DippForm)_2(O\text{-}C_4H_8\text{-}DippForm)(THF)$] and [$Sm_2(DippForm)_4(COT)$], in which the COT^{2-} dianion is trapped in two of them. It also demonstrated the remarkably similar reactivity between well-known divalent complex [$SmCp^*_2$] and its N- donor alternative [$Sm(DippForm)_2(THF)_2$], which yielded the syntheses of similar reaction products upon reaction with COT in THF. Interestingly, a change of solvent for the same reaction

resulted in the encapsulation of a planar COT^{2-} ligand flanked by two η^8-bound trivalent samarium moieties forming a rare dinuclear inverse sandwich complex.

Chapter 3 explores the interaction of divalent $[Ln(DippForm)_2(THF)_2]$ (Ln = Sm, Yb) with substrates containing dipnictide linkages. Treatment of $[Sm(DippForm)_2(THF)_2]$ with *trans*-azobenzene demonstrates similar reactivity to that of $[SmCp^*_2(THF)_2]$ and resulted in interesting mono- and dinuclear complexes $[(DippForm)_2Sm^{III}(Ph_2N_2)(THF)]$ and $[(DippForm)Sm^{III}(Ph_2N_2)(THF)]_2$ respectively, where azobenzene has undergone both one and two electron reduction. Even the less powerful reducing agent ytterbium analogue $[Yb(DippForm)_2(THF)_2]$ also reacts with *trans*-azobenzene to form $[(DippForm)Yb^{III}(Ph_2N_2)(THF)]_2(OH)_2$ where an influence of partial hydrolysis can be seen. The reaction with 1*H*-1,2,3-benzotriazole also yielded a trivalent samarium complex containing benzotriazolate, $[Sm^{III}(DippForm)_2(Btz)(THF)]$, suggesting more utilization of 1*H*-1,2,3-benzotriazole in divalent lanthanoid reduction chemistry. Synthesis of $[(Sm^{III}(DippForm)_2(\mu\text{-}DippForm)(PPh_2)O]$ by the reaction of $[Sm(DippForm)_2(THF)_2]$ with P_2Ph_4 provides a perfect start for substrates containing dipnictogen bonds other than azo linkages in reductive trapping using non-cyclopentadienyl derivatives.

Chapter 4 expands the discussion of reductive trapping using Ln(II) complexes towards other unsaturated small organic molecules. An unusual samarium amidinate ketyl complex $[(DippForm)_2Sm^{III}(bnzl^{\cdot}\text{-}O)(THF)]$, which exhibits extraordinary stability in the non-coordinating solvents benzene-d_6 and toluene, was produced through the reaction of $[Sm(DippForm)_2(THF)_2]$ with benzil. Interaction of $[Sm(DippForm)_2(THF)_2]$ with naphthyl isothiocyanate resulted in the formation of a highly remarkable samarium complex $[Sm^{III}(DippForm)_2(Nap\text{-}NCHS)(THF)]$, in which both nitrogen and sulfur coordinate to the samarium centre. The formation of $[Sm(DippForm)_3]$ and a few related organic substrates can be observed upon treatment of phenyl isocyanate, phenyl isothiocyanate, benzonitrile and *o*-tolunitrile with $[Sm(DippForm)_2(THF)_2]$, suggesting the possibility of an unknown samarium complex in the reaction mixture.

A brief chapter of supporting research, Chapter 5, describes the treatment of [Yb(DippForm)$_2$(THF)$_2$] with $Co_2(CO)_8$ and the formation of [Co(DippFormCO)(CO)$_3$]. This work formed part of a research paper published in *Dalton Transactions*.

Overall, these observations demonstrate that DippForm$^-$ is a very suitable substitute for the Cp*$^-$ ligand and points towards the possibility of the N-donor alternative [Sm(DippForm)$_2$(THF)$_2$] acting as a successor for the most successful complex in organolanthanoid chemistry, [SmCp*$_2$], with much more versatile reaction chemistry and promises to have an exciting future in reduction chemistry. Moreover, the reactivity of less powerful [Yb(DippForm)$_2$(THF)$_2$] was also examined and highlights its highly reactive nature towards different substrates.

Abbreviations

Å	Ångström unit, 10^{-10}m
Bnzl	Benzil
BtzH	1*H*-1,2,3-benzotriazole
Cen	Centroid
Cp	Cyclopentadienyl ($C_5H_5^-$)
Cp*	Pentamethylcyclopentadienyl ($C_5Me_5^-$)
COT	1,3,5,7-cyclooctatetraene
DippForm	N,N′-Bis(2,6-diisopropylphenyl)formamidinate
DME	1,2-Dimethoxyethane
DMF	Dimethylformamide
h	Hour
HMDS	trimethylsilyl)amide
^{i}Pr	Isopropyl
IR	Infrared
Ln	Lanthanoid
Me	Methyl
^{n}Bu	*n*-Butyl
NHE	Normal Hydrogen Electrode
NMR	Nuclear magnetic resonance
ODS	Oxide Dispersion Strengthened
ORTEP	Oak Ridge Thermal Ellipsoid Plot
OTf	Triflate ($CF_3SO_3^-$)
Ph	Phenyl
PhMe	Toluene

pm	picometre
ppm	Parts per million
ppb	Parts per billion
Pz	Pyrazole
RT	Room temperature
REE	Rare earth element
RTP	Redox transmetallation/protolysis
SCE	Saturated Calomel Electrode
SET	Single Electron Transfer
$t_{1/2}$	Half-life
^{t}Bu	*tert*-Butyl
TM	Transition Metal
THF	Tetrahydrofuran
XylForm	N,N'-bis(2,6-dimethylphenyl)formamidinate
YAG	Yttrium-aluminum-garnet

Table of Contents

Chapter 1

Introduction to Rare Earths and their application in reductive trapping

1.1 Rare Earth Elements

Rare Earth Elements (REEs) are a series of 17 soft heavy metals which includes 14 f-block elements (ranging from cerium to lutetium) along with group 3 metals yttrium, scandium and lanthanum.[1] The group of elements with atomic numbers 57 to 71, lanthanum to lutetium, are referred to as lanthanoid elements. These elements are generally denoted by the symbol 'Ln'. Scandium and yttrium are often grouped with lanthanoids as their chemistry is similar to these metals due to their physical and chemical properties.[2] The history of rare earths started in 1794 when Finnish chemist Johan Gadolin succeeded in obtaining yttria (an impure yttrium oxide) from a black mineral, which was later known as 'gadolinite'. In 1804, M.H. Klaproth, W. Hisinger and J.J. Berzelius isolated the first cerium compound ceria from another oxide cerite. However, the separation of these compounds into their component oxides was only achieved 3 decades later, during 1839 – 1843, when C.G. Mosander first separated cerium and lanthanum from ceria along with mixed oxide 'didymia' (a mixture of the oxides of the metals from praseodymium through gadolinium). Similarly, erbium, terbium and yttrium were separated from the original oxide yttria. Subsequent research continued for several decades and the identification of all the naturally occurring rare earth elements was completed in 1907 with the discovery of lutetium by Carl Auer von Welsbach and Georges Urban.[3, 4] Without realizing this fact, the quest for new elements continued until the development of atomic theory and the concept of atomic number by Henry Moseley's work on X-ray spectra of elements in 1913. The radioactive element promethium was isolated by Marinsky, Glendlin and Goryell in 1948, using ion-exchange chromatography. They obtained the element from the fission products of uranium and of bombardment of neodymium.[3-5]

1.1.1 Occurrence and Isolation

Except for radioactive promethium (Pm), all the rare earth elements occur naturally. Rare earths are not 'rare' as the name suggests, it is indeed a misnomer. **Table 1.1** shows the continental crustal abundance data of elements and it is evident from the table that rare earths are fairly abundant elements in the earth's crust.[6] Cerium is positioned higher in the table among lanthanoids and their abundance is higher than the common elements cobalt and copper. Even the rarest lanthanoids lutetium and thulium are more abundant than silver, gold or platinum metals. A higher abundance of lighter lanthanoids compared to heavier ones and that of elements with even atomic numbers than the elements with odd atomic numbers is also evident from **Table 1.1**. The radioactive promethium, ^{147}Pm (most stable isotope; β-emitter, $t_{1/2}$ = 2.6 yr) can be synthetically produced by the spontaneous fission of ^{238}U.[1, 2]

Table 1.1: Elemental concentrations in the Continental Crust (the rare earth metals are shaded grey) [5]

O	47.2 %	La	30 ppm	Pr	6.7 ppm	Br	1.0 ppm
Si	28.8 %	Nd	27 ppm	Sm	5.3 ppm	Ho	800 ppb
Al	7.96 %	Cu	25 ppm	Gd	4.0 ppm	Tb	650 ppb
Fe	4.32 %	Co	24 ppm	Dy	3.8 ppm	Lu	350 ppb
P	757 ppm	Y	24 ppm	Cs	3.4 ppm	Tm	300 ppb
Cl	472 ppm	Li	18 ppm	Er	2.1 ppm	Ag	70 ppb
Zn	65 ppm	Sc	16 ppm	Yb	2.0 ppm	Au	2.5 ppb
Ce	60 ppm	B	11 ppm	Eu	1.3 ppm	Pt	0.4 ppb

Rare earth elements cannot be found in elemental states in nature, which could be one reason they were considered ‘rare’. Rare earths mostly occur as oxidic compounds owing to their strong affinity toward oxygen.[3] They also can be found in other forms such as phosphates, carbonates and silicides in minerals. Over hundreds of such mineral deposits are located in different parts of the world but only a few of them are of commercial importance. Monazite [$(Ln,Th)PO_4$] and bastnasite ($LnFCO_3$) are two principal sources of lanthanoids in which monazite is rare-earth phosphate while bastnasite is a fluorocarbonate of rare earths.[2, 7] All metals (excluding Pm) can be obtained from the mineral monazite while bastnasite is richer in lighter lanthanoids. Xenotime [$(Y,Ln)PO_4$] containing heavier lanthanoids and euxenite $(Y, Ce, Ca, U, Th)(Ti, Nb,Ta)_2O_6$ having fairly even distribution of metals are examples of other rare earth sources.[3, 8] Major rare earth deposits can be found in China, Australia, USA, India and Brazil.

The extraction and separation of lanthanoids from individual mineral deposits are very hard because of the similarity in the size of ions and properties. That is why it took over 150 years to finish the story of rare earth discovery. The processing of these ores includes multi-stage tedious jobs starting with conventional mineral dressing, which yields mineral concentrates of high purity (over 90%).[7] This is followed by a series of acid or alkaline digestions, which ultimately results in the formation of a solution of trivalent rare earth metal compounds (chlorides, sulphates, oxalates etc.) to complete the extraction procedure.[3] Further separation of individual elements from these RE compounds is the hardest part. In earlier days, continuous fractional crystallization was the only possible way of obtaining pure RE elements. Things got better and simpler with the introduction of modern techniques such as ion-exchange and solvent extraction methods, which replaced the classical methods and made the separation of these elements easily achievable. The ion exchange method will be the most powerful by which high-purity and smaller-scale separation are feasible. For commercial purposes, solvent extraction using tri-*n*-butylphosphate [$(^nBuO)_3PO$] is used as it is ideal for large-scale production.[8] There is still a lots of scope for improving the separation techniques because the extraction process utilises significant quantities of acid and hydrocarbons, which have negative environmental effects.

1.1.2 Properties

Several intrinsic and exceptional properties of lanthanoids impart unparalleled electronic and steric features to rare earth compounds. Rare earth elements are soft with a silvery shining appearance and very reactive, tarnishing readily in the air due to the formation of corresponding oxides. They react slowly with cold water liberating hydrogen but show rapid reactivity with dilute acids. Except for cerium, gadolinium (half-filled) and lutetium (full-filled), the general electronic configuration for lanthanoids is $[Xe]4f^n5d^06s^2$. **Table 1.2** shows the electronic configuration and ionic radius of the lanthanoids. For scandium and yttrium, electronic configuration is $[Ar]3d^14s^2$ and $[Ke]4d^15s^2$ respectively. Unlike transition metals, 4f electrons are accountable for the properties of lanthanide ions and the 4f orbitals are deeply buried inside the xenon core which is effectively capped from the impact of the external forces by the overlying 5s and 5p orbitals. This is the reason for the remarkable similarity in the chemical properties among the lanthanoids as the addition of each f-electron provides only slight differences in their chemistry. Compared to the d-block elements in each row, lanthanoids show a much more close resemblance to each other.[2] In addition, they show fundamentally different magnetic and spectral behaviour from that of d-transition metals. The reason for their metallic behaviour is the high contribution and overlap of 5d and 6s atomic orbitals compared to the 4f orbitals.[9]

The sum of the first three ionization potentials of rare earth elements is relatively low and these metals are highly electropositive (1.1 on Pauling scale).[10] So their most easily accessible oxidation state is +3, especially in aqueous solutions. However, a few exceptions are also found such as a divalent state for samarium, europium and ytterbium as well as an oxidized tetravalent state for cerium. The existence of these oxidation states is due to the special stability associated with empty, half- and full-filled 4f shells (except for Sm^{2+} which has a $4f^6$ configuration). Another phenomenal feature of these elements is the lanthanide contraction, which is the steady decrease of Ln^{3+} ionic radii (for an 8-coordinate ion) as we proceed from La (116pm) to Lu (98pm), as shown in **Table 1.2**. This is caused by the imperfect shielding effect of 4f electrons within the subshell. Due to the shapes of the orbitals, the shielding of one 4f electron by the other is very poor (compared to d electrons) along with the series of elements

La-Lu. This cannot neutralize the effect of nuclear charge after the addition of each 4f electron. As a result, a gradual reduction in the size of the $4f^n$ subshell is observed.[1, 2] As a consequence of this contraction, lanthanoids tend to have similar (not identical) properties and it makes the chemical separation of these elements possible.[11]

Table 1.2: Electronic configuration, atomic and ionic radii (for an 8-coordinate ion) of lanthanoids.[2]

Rare Earth Element & Symbol	Electronic Configuration		Radius/pm	
	Ln	Ln^{3+}	Ln	Ln^{3+}
Lanthanum (La)	$[Xe]5d^16s^2$	$[Xe]4f^0$	188	116
Cerium (Ce)	$[Xe]4f^15d^16s^2$	$[Xe]4f^1$	183	114
Praseodymium (Pr)	$[Xe]4f^36s^2$	$[Xe]4f^2$	182	113
Neodymium (Nd)	$[Xe]4f^46s^2$	$[Xe]4f^3$	181	111
Promethium (Pm)	$[Xe]4f^56s^2$	$[Xe]4f^4$	181	109
Samarium (Sm)	$[Xe]4f^66s^2$	$[Xe]4f^5$	180	108
Europium (Eu)	$[Xe]4f^76s^2$	$[Xe]4f^6$	199	107
Gadolinium (Gd)	$[Xe]4f^76s^25d^1$	$[Xe]4f^7$	180	105
Terbium (Tb)	$[Xe]4f^96s^2$	$[Xe]4f^8$	178	104
Dysprosium (Dy)	$[Xe]4f^{10}6s^2$	$[Xe]4f^9$	177	103
Holmium (Ho)	$[Xe]4f^{11}6s^2$	$[Xe]4f^{10}$	176	102
Erbium (Er)	$[Xe]4f^{12}6s^2$	$[Xe]4f^{11}$	175	100
Thulium (Tm)	$[Xe]4f^{13}6s^2$	$[Xe]4f^{12}$	174	99
Ytterbium (Yb)	$[Xe]4f^{14}6s^2$	$[Xe]4f^{13}$	194	99
Lutetium (Lu)	$[Xe]4f^{14}6s^25d^1$	$[Xe]4f^{14}$	173	98

In the stable oxidation state of REs, the 4f-orbitals containing valence electrons are deeply buried inside the xenon core, which makes them unavailable for covalent bonding, as they were not able to interact with ligands. So, in rare earth complexes, metal-to-ligand bonding is considered to be mostly ionic, where they are held together by electrostatic interactions. Consequently, lanthanoid chemistry is far different from that of transition metals and most of the well-established principles such as "18-electron rule", σ-π bonding, metal-metal multiple bonds etc. in d-metal chemistry are not observed for f-metals.[11] The steric effects tend to exclusively control their formal electron count, coordination numbers and geometries.[12, 13] Lanthanoids generally prefer higher coordination numbers ranging from 6-12 in both ionic crystals and complexes, especially due to large ionic radii and high charge, in which 8 and 9 are the most common. Low coordination numbers in the range of 2-5 are also possible, but the use of bulky ligands is mandatory as it requires substantial steric protection.[1, 11]

1.1.3 Applications

The enormous commercial value and increased demand for the rare earth metal over the last few decades are attributed to their widely divergent availabilities and applications, which made them critical to numerous key technologies in the field of medicine, transportation, communication, energy generation, surveillance and in the military. The beginning of the rare earth industry was in 1891 when Carl Auer came up with Auer light, a gas mantle constituting 99% thoria and 1% ceria. It was followed by the introduction of a pyrophoric alloy called flintstone (70% mischmetal and 30% iron) and the addition of rare earth fluoride as a wick in arc light carbons.[3] Mischmetal is the oldest rare earth alloy consisting mainly lighter lanthanides, cerium in particular (~55% Ce).[8] For various metallurgical applications, rare earths were introduced in the form of mischmetal (as constituents) to numerous other alloys including ductile iron (for graphite nodularization in cast iron), steels (caused improved mechanical properties), superalloys (high-temperature corrosion resistance), magnesium alloys (Mg-Al-Zn-Nd alloy shows high corrosion resistance in aqueous saline solution), aluminium alloys (Y-Mg-Al alloy for transmission cabling), titanium alloys, copper alloys, zinc alloys (used in galvanizing baths), ODS (oxide dispersion strengthened) alloys and long-range ordered alloys.[3] Apart from metallurgy, rare earths have been used extensively in the area of magnets and magnetic properties, as chemical and petroleum refining catalysts, glass polishing and ceramics, semiconducting and other electric properties, catalytic converters in automobiles, in opticals, as rare earth phosphors, nuclear applications and in hydrogen storage.

Some applications are: Nickel-metal hydride (NiMH) batteries containing $LaNi_5$ widely used for hydrogen storage, with application in fuel cells and catalytic hydrogenation.[8] YAG-Nd lasers containing a low concentration of Nd^{3+} are very efficient for etching, cutting and welding metals. Europium(III) complex (with commercial name Resolve-Al™) and $[Ln(DPA)_3]^{3-}$ (H_3DPA is pyridine-2,6-dicarboxylic acid) are very useful shift reagents in NMR spectroscopy.[2] Erbium, which changes to pink when oxidized, has been used in glass colouring, as an amplifier in fibre optic cables and lasers for surgical applications. Nd-Fe-B and its Dy additive are strong permanent magnets that are used in hybrid and electric vehicles, hard drives and wind turbines.[14] The unique luminescent behaviour of europium (due to the sharp 4f-4f transition of Eu^{3+}) has been utilized in red-emitting phosphors in TV-computer screens and fluorescent lamps.[15] Cerium, lanthanum (green), gadolinium, terbium and yttrium are the other rare earth elements having several applications in phosphors. Thulium has been used in the production of portable x-ray sources which has important applications in the area of medicine. Holmium lasers also have a variety of uses in medical and dental applications. Praseodymium is another metal widely used in the medical field, which has application in the scintillator for CAT scans. Samarium-cobalt (Sm_2Co_{17}) permanent magnets have been used extensively in aerospace equipment, electric watches and servomotors. In ceramics, cerium has a lot of applications which include acting as phase stabilizer in zirconia-based products.[3]

1.2 Organometallic chemistry of Rare Earth Elements

The chemistry of rare-earth elements is currently one of the most rapidly developing fields in the area of organometallics and coordination compounds.[16-18] It is a great achievement indeed as it has overthrown several false assumptions and misinterpretations related to the chemistry of lanthanoids, especially the possibility of organolanthanoids and unfolded astonishing research avenues.[6] The synthesis of the first trivalent tris(cyclopentadienyl)lanthanoid complexes, Cp_3Ln, by Birmingham and Wilkinson in 1954 marked the commencement of organolanthanoid chemistry.[19] Although few organic derivatives of rare earth metals were reported previously, the kinetic instability of complexes and lack of adequate synthetic and characterization techniques prevented the field from advancing further. Credit should be given to the arrival of dry-box and single-crystal x-ray diffraction technology, which made it feasible to deal with these air and moisture-sensitive compounds and determine the structural characteristics of these interesting compounds. Since then, the field has changed drastically and organolanthanoid chemistry flourished from being a mere laboratory curiosity. As a result, we have witnessed numerous unprecedented reaction pathways and novel organolanthanoid compounds in recent years.[20]

Rare earth organometallics are rewarded by several elemental features of lanthanoid ions which provide unique steric and electronic properties to these versatile complexes.[21, 22] These features allow organolanthanoids to deviate from certain rules created by d-transition metals in organometallics and follow their own path. As a result, many universally established principles of d-organometallics are not applied for the compounds of organolanthanoids including the popular “18-electron rule”.[11, 23] Moreover, lanthanoid ions are considered to be hard acids according to HSAB (= hard and soft acids and bases) concept, which is mainly because of the presence of vacant d, s and p orbitals.[24] The strong oxophilicity of lanthanoids can be explained based on this hard acidic character along with predominantly ionic bonding.[22, 25] The reactivity of organolanthanoid compounds is strongly influenced by the oxophilic nature of the metal centre. As a consequence, these compounds have a strong preference for hard nitrogen or oxygen-based ligands (including bases having light halide donor atoms) compared with soft phosphorus or sulfur-containing ligands.

Although organic chemistry has benefited from lanthanoids for the first time as their use as NMR shift reagents, their major applications are in two fields. One includes organometallic compounds as catalysts for organic transformations and reactions. For example, lanthanoid metallocenes (containing (η^5-C_5R_5)Ln or (η^5-C_5R_5)$_2$Ln units where R = Me, H) have turned out to be remarkably useful catalysts for a range of olefin transformations involving hydroamination, hydroboration, hydrogenation, hydrosilylation, hydrophosphination and polymerization.[2] Rare earth triflates ($Ln(OTf)_3$) have proven to be very active catalysts for Michael, aldol, glycosylation, allylation, and Diels-Alder reactions as well as for Friedel-Crafts acylations, while rare earth alkoxides ($Ln(OR)_3$) have appeared to be efficient catalysts for the hydrocyanation and the Meerwein-Ponndorf-Verley reduction.[12, 26-31] The other major application is reduction chemistry, where the lanthanides of divalent oxidation states act as strong reductants in synthetic chemistry. This thesis focuses on these latter directions.

1.2.1 Lanthanoids as single electron transfer (SET) reagents

Electron transfer has facilitated many important reduction reactions in organic chemistry.[32] Recently lanthanoids have inevitably played a role in this area. The oldest use of lanthanoids can be attributed to the use of Eu(II) for many years as a simple one-electron reductant in aqueous redox chemistry.[33, 34] Studies show that lanthanoids are highly electropositive and +3 is the most stable oxidation state for lanthanoids, particularly in aqueous solutions.[16, 17] This describes the potential of divalent lanthanoid salts acting as strong reducing agents. In earlier times, the divalent state was only accessible to europium (f^7 configuration; half-filled shell), ytterbium (f^{14}; completely filled shell) and samarium (f^6; approaches a half-filled shell), which are termed as ‘classical’ divalent metal ions.

The reduction of pyridine carboxylic acids using Eu(II) by Vrachnou and Katakis in 1975 can be considered as one of the earlier attempts in this field.[35] The preparation of divalent europium salts is easy compared with other divalent lanthanoids, for which severe conditions or unconventional techniques are required. However, the compounds of these europium salts are less reactive toward various organic reagents.[36] In addition, among our 'classical' ions, ytterbium (II) and samarium (II) have comparatively higher reducing properties than europium (II). This is evident from their standard reduction potentials; Eu^{2+}/Eu^{3+} = -0.43, Yb^{2+}/Yb^{3+} = -1.15, and Sm^{2+}/Sm^{3+} = -1.55 V.[33, 34] This thought guided organometallic chemists towards synthesizing samarium and ytterbium compounds and analyzing their performance as potentially powerful reducing agents. In 1979, P. Girard *et al* succeeded in preparing YbI_2 and SmI_2 from the corresponding metals and 1,2-diiodoethane in THF and tested their reactivity as a reductant toward a variety of functional groups.[36] Positive results from those experiments allowed YbI_2 and SmI_2 to be placed amongst the most powerful reducing agents (which are soluble in organic media) at that time. These findings marked the beginning of an era of reduction chemistry controlled by divalent lanthanide derivatives.[20, 37] Furthermore, SmI_2 is now commercially available as a THF solvate.

Sm^{2+}, being the most reactive of the three, promoted a number of organic reactions, which brought a proper entry point for the synthesis of organic derivatives.[38-40] Some additives and co-solvents of SmI_2, having the ability to tune the properties of the reagent, also contributed to its wide popularity. The complexation of water and amine to SmI_2 is an example.[41-45] A lot of sensational advancements in the reductive chemistry of divalent lanthanoids in recent years have exploited the high reductive power of samarium (II). These include new Sm (II) reagents other than SmI_2 such as samarium(II) bromide, samarium(II) chloride and their complexation with some additives, which possess higher reduction potentials than samarium diiodide. Moreover, these single-electron reductants impart a remarkable level of chemo-, region-, and diastereoselectivity, and are readily available under standard laboratory conditions.[46] Samarium(II) amides and samarium(II) alkoxides can also be added to this list. Among samarium amides, it was found that bis(trimethylsilyl)amide (HMDS) can be a ligand of choice for the samarium(II) complex.[47, 48] In alkoxides, samarium(II) triflate [$Sm(OTf)_2$]

is a worthwhile reductant in a divalent samarium system that provides greater yields and better diastereoselectivities for reductive processes.[49-51]

1.2.2 Divalent lanthanoid complexes in organometallic chemistry

In the organometallic area, Yb and Eu made an early entry to divalent chemistry in 1964 before samarium as both metals can be dissolved in liquid ammonia, thus facilitating suitable access to the lower oxidation state.[52, 53] Being larger and a stronger reductant, it would be quite difficult to handle samarium experimentally. Also, smaller metals were a more popular choice in early organometallic lanthanide chemistry due to the stability provided for the complex as the steric saturation of the coordination sphere could be attained more easily. Moreover, the lack of a suitable starting material and being insoluble in liquid ammonia also retarded the growth of divalent samarium chemistry in the organometallic field.[54]

The first crystallographically characterized divalent samarium organometallic compound, $[Cp^*_2Sm(THF)_2]$ (where Cp = C_5Me_5) was synthesized in 1981 using metal vapour methods.[55] Introduction of THF-soluble $[SmI_2(THF)_2]$ by Kagan *et al*.[36] acted as an efficient starting material for divalent samarium complexes. Furthermore, the incorporation of a bulky ligand than a simple cyclopentadienide provided stability to the complex and helped to solubilize this large metal.[54] Thus the $(C_5Me_5)^-$ ligand emerged as a turning point in the development of divalent chemistry of samarium complexes. Without a doubt, the synthesis of $[Cp^*_2Sm(THF)_2]$ and its unsolvated analogue, the strangely bent $[Cp^*_2Sm]$,[56, 57] was one of the crucial discoveries at the end of the 20th century that expanded the solution chemistry of divalent lanthanoids.

$[Cp^*_2Sm]$ turned out to be a very powerful samarium(II) reductant with a higher estimated reduction potential ($[Cp^*_2Sm]$: -2.44 V vs SCE in DMF).[58] The activation of dinitrogen can be considered as one of the most important achievements of this highly reactive samarium(II) complex.[59] The unusual reactivity of this samarium(II) complex is exemplified in the synthesis of the dihydroxyindenoindene unit via a samarium-mediated CO and CH activation.[60] Because of the limited radial expansion of the 4f orbitals, it was assumed that effective back-bonding would not be possible between alkyne or CO substrates with lanthanides like those in transition metals. As a result, little reactivity was expected with these compounds. Surprisingly, the reaction proceeded in a unique way to generate a tetracyclic hydrocarbon from simple reagents. Different types of reactivity modes have been noticed for these complexes which include unique small molecule transformations,[58, 61-66] olefin[67] and polar monomer polymerizations.[68-71]

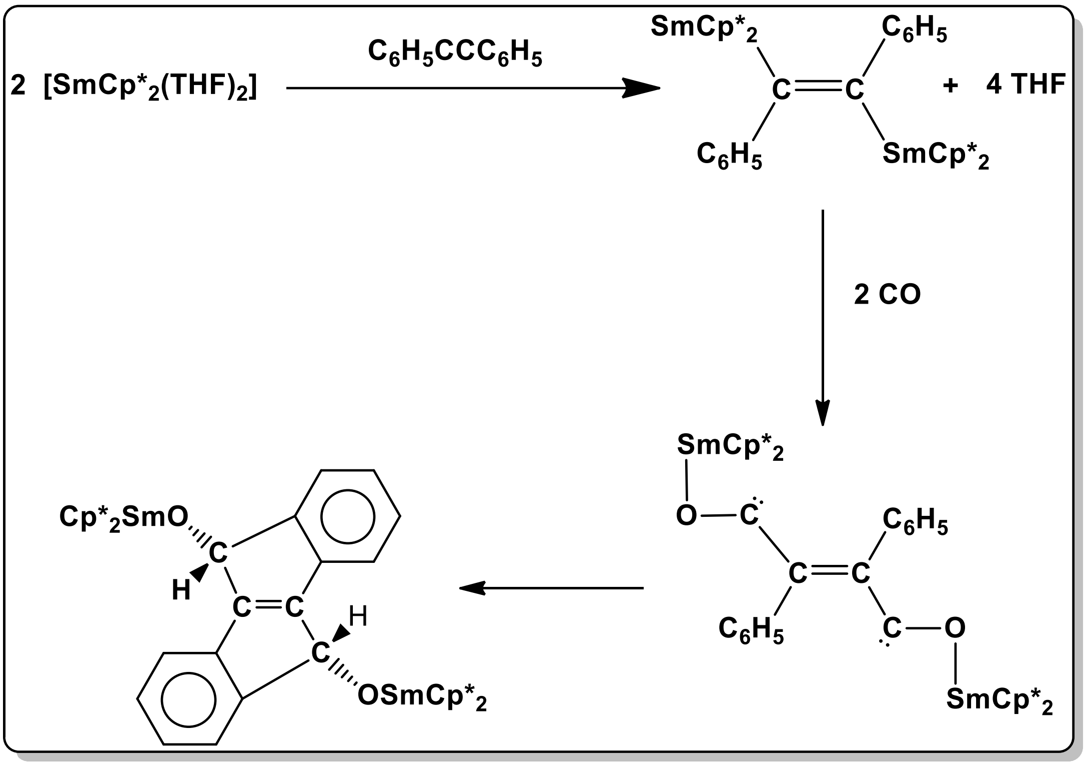

Scheme 1.1 Synthesis of the dihydroxyindenoindene unit via a samarium-mediated CO and CH activation.[60]

A diversion from cyclopentadienyl chemistry and the quest for other ligand sets with the same useful effects can be seen in recent organolanthanoid research. The guiding idea in this chemistry was the electronic and steric saturation of the coordination sphere in the vicinity of sizable and electropositive f-ions, which can be accomplished by the use of ligand architectures. The use of anionic heteroallylic ligands was one of the most rewarding advancements in this angle providing much more diverse derivative chemistry. Among various heteroallylic ligands **(Figure 1.1)**, guanidinates and amidinates stand out as they show superior performance and versatility by forming rare earth metal complexes containing *N*-chelating ligands. In addition, they are a readily approachable ligand system in the series compared with other heteroallylic ligands used in rare-earth metal chemistry such as phosphaguanidinates, trizaenides, diiminosulfinates, boraamidinates and silaaminidinates.[11, 23] The synthesis of N-silylated benzamidinate ligands such as [$PhC(NSiMe_3)_2$] in 1987 was the beginning of this interesting chemistry.[72] The non-cyclopentadienyl chemistry of lanthanoids flourished rapidly and was soon utilized in divalent reduction chemistry. The samarium(II) bis(trimethylsilyl)amido species, [$Sm(N(SiMe_3)_2)_2(THF)_2$], introduced by Evans,[73] is one of the major reducing agents that mirrored [$Cp^*{}_2Sm(THF)_2$] in the reduction of O- and N- containing substrates.[74]

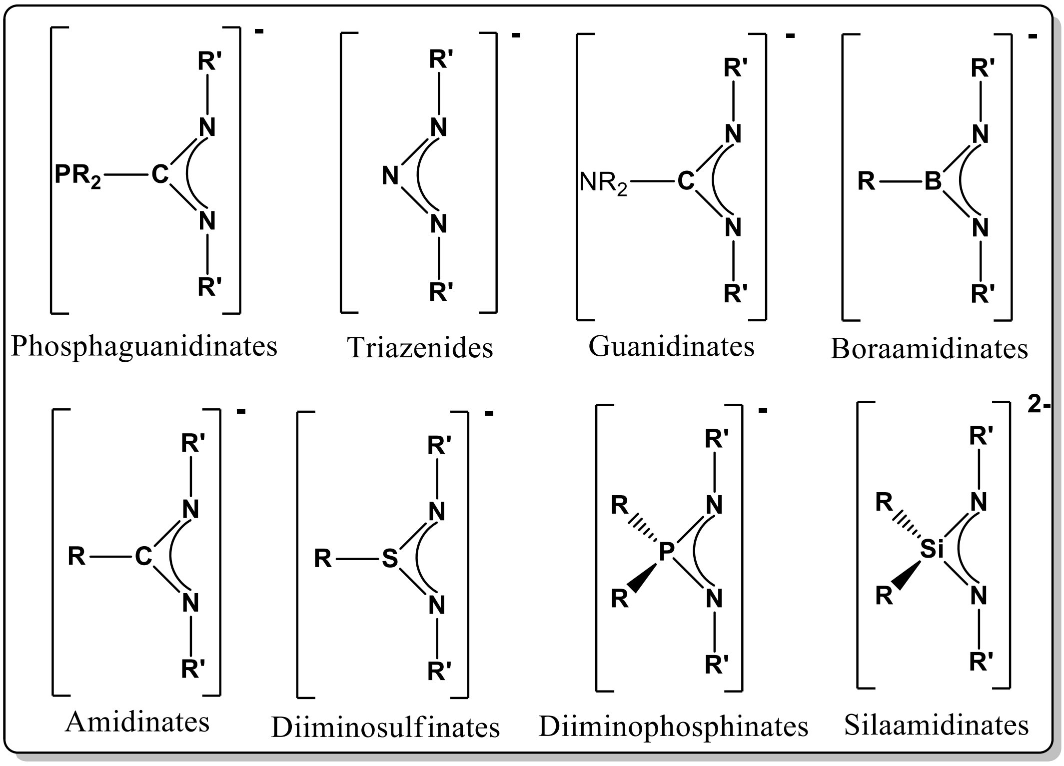

Fig 1.1 Anionic heteroallylic ligands.

1.2.3 New molecular divalent oxidation states

The development of organolanthanoid chemistry intensified by the entry of new molecular divalent oxidation states of thulium, dysprosium and neodymium. The first molecular complex of divalent thulium, [$TmI_2(DME)_3$], was identified by X-ray crystallography in 1997 as a result of a combined effort by the Evans and Bochkarev groups.[75] The high reduction potential of this complex even facilitated instantaneous dinitrogen reduction (which was supposed to provide the inert atmosphere) during another synthetic attempt.[76, 77] The first metallocene of Tm^{2+}, [$C_5H_3(SiMe_3)_2]_2Tm(THF)$, was isolated and structurally characterized by using a carefully chosen combination of ligands, solvent and reaction conditions.[78] The first structurally validated complex of dysprosium(II), [$DyI_2(DME)_3$], was introduced by Evans et al. in 2000.[79] In 2001, Bocharkev and Schumann reported the completely characterized divalent complex of neodymium for the first time, [$NdI_2(thf)_2$], which is isotypic to the samarium diiodide complex.[80] Among SmI_2 analogues, neodymium(II) iodide is the strongest lanthanoid reductant ($Nd^{3+}I/Nd^{2+}$ redox potential of -2.6 V vs NHE). The entry of Tm^{2+}, Dy^{2+} and Nd^{2+} doubled the number of isolable Ln^{2+} complexes. Further research led to the discovery that the +2 oxidation state is attainable to all of the lanthanoid elements in soluble crystalline molecular species except radioactive promethium.[81-83] This established the fact that there will always be room for expansion in the case of lanthanoids, especially for the development of divalent lanthanoid reduction chemistry.

1.2.4 Application in trapping anionic ligands

The high reduction potential of divalent organolanthanoids promotes electron transfer reactions in various organic and organometallic transformations. By using them as single electron transfer (SET) agents, they have been utilized in different applications recently, among them trapping novel anionic ligands.

Reductive trapping of dinitrogen in 1988 using the bent metallocene [$Cp^*{}_2Sm$][59] was a major discovery that played a great role in the development of solution chemistry of divalent lanthanoids **(Scheme 1.2a)**. The structural characterization of [$Cp^*{}_2Sm]_2$(μ-

η^2:η^2-N_2) was the first X-ray crystal structure of an f-element dinitrogen complex. Another peculiarity of this complex was the coplanar arrangement between N_2 and the samarium metal in the structure, which had not been observed before in a dinitrogen complex of any metal.[84] Divalent thulium also contributed to dinitrogen trapping[76] and showed that it is not limited to the $(C_5Me_5)^-$ ligand. Complexes of thulium with the $[C_5H_3(SiMe_3)_2]^-$ ligand **(Scheme 1.2b)** and even with the mono-substituted $[C_5H_4(SiMe_3)]^-$ ligand have been employed in trapping dinitrogen. The dysprosium complex $[(C_5H_3(SiMe_3)_2)_2Dy]_2(\mu$-$\eta^2$:$\eta^2$-$N_2)$ also can be added to the list.[78]

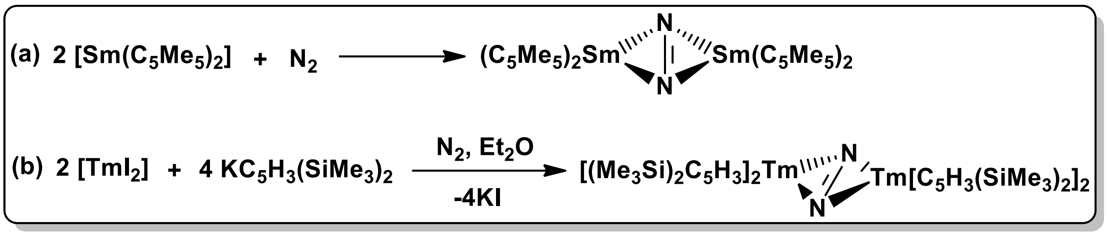

Scheme 1.2 Dinitrogen trapping using divalent samarium and thulium.[59,76]

Electron transfer from bis(pentamethyl-cyclopentadienyl) samarium $[Cp^*_2Sm]$ has led to a range of remarkable ligands. It has been used to make crystallographically characterizable complexes of other polyanions, other than dinitrogen. $[Cp^*_2Sm]$ has been utilized in trapping Bi_2^{2-} by reaction with $BiPh_3$[64] **(Scheme 1.3a)** and Sb_3^{3-} from reaction with $Sb(Bu^n)_3$ in toluene.[85] The reductive homologation of CO with $[Cp^*_2Sm]$ resulted in trapping the $O_2C_2O_3^{2-}$ anion.[86] The one-electron redox reaction of divalent samarocene also gave rise to polyphosphide (P_8^{4-}) **(Scheme 1.3b)**[87], carbonyl sulfide iron clusters[88], and arsenic sulfide species.[89] The ytterbium analogue of $[Cp^*_2Sm]$ was also found to be useful in this case, trapping the iron and cobalt carbonyl anions **(Scheme 1.3c)**, $Fe_3(CO)_{11}^{2-}$ and a tetracarbonylcobaltate anion respectively.[90, 91] Furthermore, the reaction of $[Yb(C_5Me_5)_2(OEt_2)]$ with $[Co(C_5H_4R)(CO)_2]$ yielded an odd-electron-numbered complex, $[\{Yb(C_5Me_5)_2\}_2\{Co_3(C_5H_4R)_2(\mu_3$-$C0)_4\}]$, where R = H, Me, $SiMe_3$.[92]

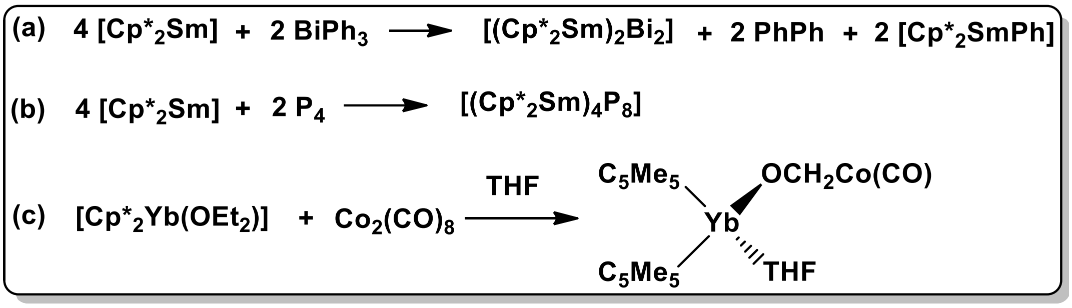

Scheme 1.3 Anionic ligands trapping using bis-pentamethyl complexes of samarium and ytterbium.[64,87,90]

Among various N-donor alternatives to LnCp*$_2$ reagents, [Sm(DippForm)$_2$(THF)$_2$] (DippForm = N,N' – bis(2,6-di-isopropyl phenyl)formamidinate), firstly synthesized in 2005,[93] has contributed enormously to anionic ligand trapping. It's reductive trapping of the bridging ligand $[OC(Ph)=(C_6H_5)\text{-}C\text{-}(Ph)_2O]^{2-}$ upon reaction with benzophenone demonstrated the unexpected, rare head-to-tail C-C coupling while its reaction with CS_2 shows the formation of unusual C-S bond instead of C-C coupling which leads to the trapping of $[SCSCS_2]^{2-}$ ligand (**Scheme 1.4**).[94] Its treatment with metal carbonyls[95] and reduction of polypnictogenides[96] are also followed by the synthesis of impressive polynucleated complexes with unusual trapping fragments such as [(DippForm)$_2$Sm(thf)]$_2$[(μ-CO)$_2$Co(CO)$_2$]$_2$, [(DippForm)$_2$Sm]$_2$](μ$_3$-CO)$_2$Fe$_3$(CO)$_9$] and [(DippForm)$_2$Sm(Cp*Fe)E$_5$[(CH$_2$)$_4$O][(DippForm)$_2$Sm(thf)] (E = P, As) **(Figure 1.2)**.

Its ytterbium analogue, [Yb(DippForm)$_2$(THF)$_2$], has accomplished the trapping of a range of ketyl ligands when treated with 9-fluorenone and 2,3,4,5-tetraphenylcyclopentadienone.[97] Besides, it has also been used in the formation of the trinuclear polysulfide coordination clusters[98] and iron polypnictide trapping.[96]

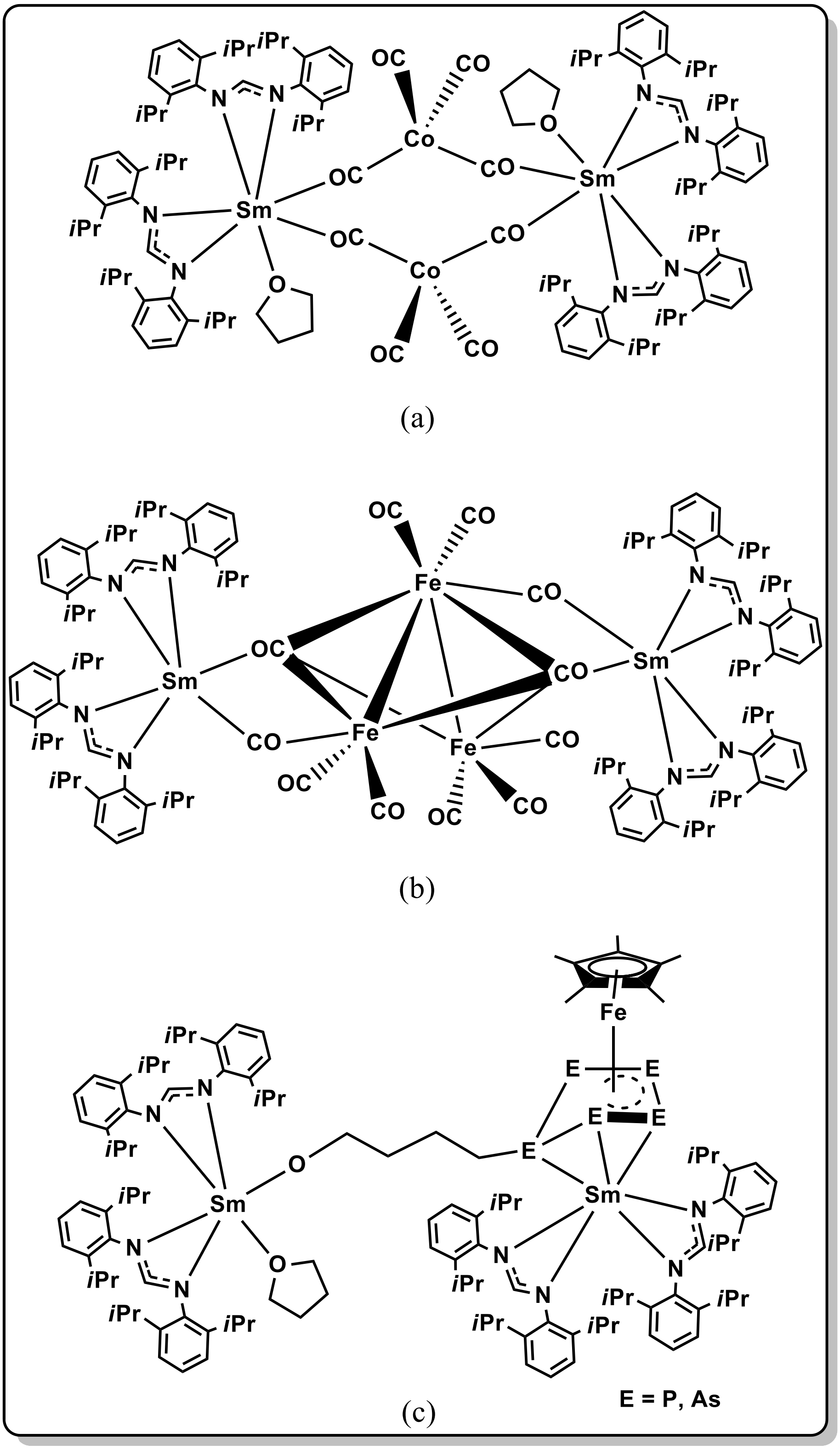

Fig 1.2 Polynucleated complexes with unusual trapping fragments (a) $[(\mathrm{DippForm})_2\mathrm{Sm(thf)}]_2[(\mu\text{-CO})_2\mathrm{Co(CO)}_2]_2$, (b) $[(\mathrm{DippForm})_2\mathrm{Sm}]_2](\mu_3\text{-CO})_2\mathrm{Fe}_3(\mathrm{CO})_9]$ and (c) $[(\mathrm{DippForm})_2\mathrm{Sm(Cp^*Fe)E_5}[(\mathrm{CH_2})_4\mathrm{O}][(\mathrm{DippForm})_2\mathrm{Sm(thf)}]$ (E = P, As) .

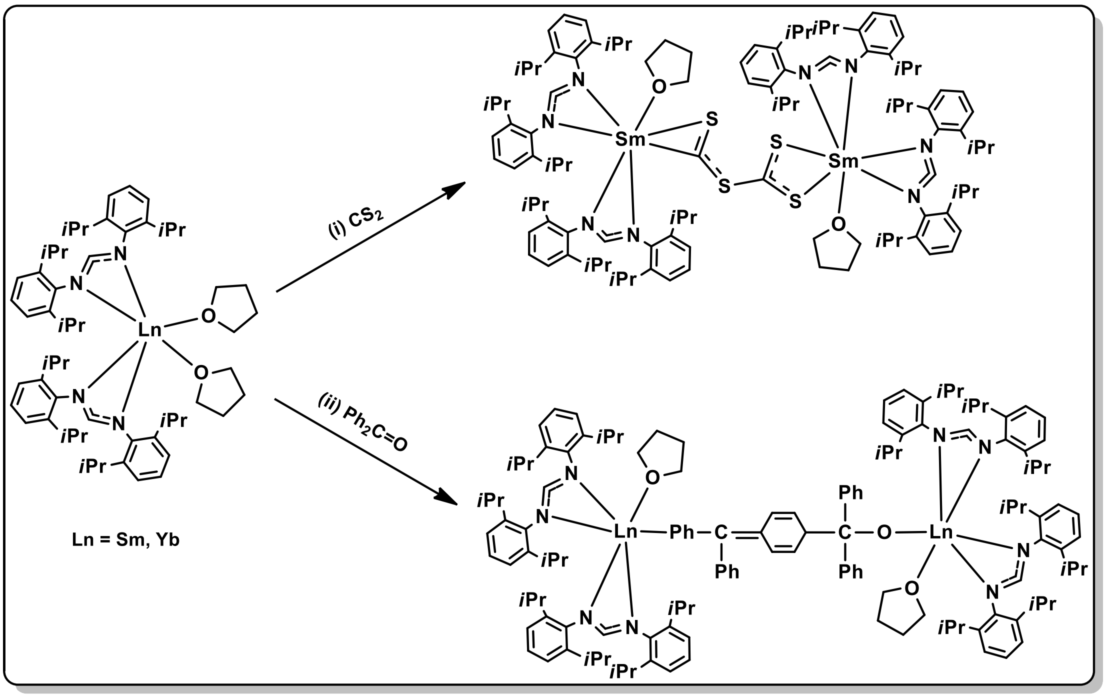

Scheme 1.4 [Ln(DippForm)$_2$(thf)$_2$] entrapping bulky anions (i) [SCSCS$_2$]$^{2-}$ and (ii) [OC(Ph)=(C$_6$H$_5$)CPh$_2$O]$^{2-}$.[94]

Another lanthanoid N-donor reductive trapping agent, the divalent samarium *meso*-octaethylcalyx[4]pyrrolide complex [Sm$_2$(N$_4$Et$_8$)(THF)$_4$] treated with tungsten hexacarbonyl resulted in the entrapment of very rare anionic ditungsten decacarbonyl [W$_2$(CO)$_{10}$$^{2-}$], in a sandwich complex [(THF)$_2$Sm^{II}(N$_4$Et$_8$)Sm^{III}(THF)]$_2$[(μ-OC)$_2$W$_2$(CO)$_8$] having mixed oxidation state samarium ions.[99] This is also the first reductive entrapping reported of any fragment containing metal, which is in a mixed-valent rare-earth metal complex. Within this productive area, further research is underway using various divalent organolanthanoids aimed at trapping novel anionic ligands.

1.3 Synthetic pathways to divalent lanthanoid formamidinate complexes

The common synthetic approaches for organolanthanoid starting materials are salt elimination/metathesis, insertion/oxidation (direct metalation), protolysis, and redox transmetalation/protolysis (RTP)[100-102]. Since this thesis employed only metathesis (for the divalent samarium reagent) and RTP (for divalent ytterbium reagent), they are briefly discussed below.

1.3.1 Metathesis

Metathesis is a useful synthetic method, especially for the preparation of homoleptic complexes that involve the treatment of a lanthanoid salt precursor (usually a halide) and a ligand transfer reagent (alkali metal substituted ligands) as shown in **Equation 1.1**.[100, 103]

$$LnX_n + nML \rightarrow [LnL_n] + n\ MX \qquad \textbf{(1.1)}$$

where L= anionic ligand, M=alkali metal, n = 2,3 and X = halide

The choice of reagents is very critical here as they occasionally result in low yields or the formation of undesirable side products, such as halide or alkali metal retention, which may prevent the isolation of the desired products.[104]

1.3.2 Redox transmetalation/protolysis (RTP)

Redox transmetalation protonolysis or protolysis (RTP) provides a simple route to divalent organolanthanoid complexes which involves the treatment of rare earth metals with organomercurial oxidants such as $Hg(C_6F_5)_2$/$Hg(CCPh)_2$ or $HgPh_2$ and a protic ligand LH **(Eqn. 1.2)**.

$$Ln + (n/2)\ HgAr_2 + n\ LH \rightarrow Ln(L)_n + (n/2)\ Hg + n\ ArH \qquad \textbf{(1.2)}$$

where Ar = C_6F_5, CCPh or Ph; LH = formamidine, phenol, triazene, cyclopentadiene, pyrazole, or amine; n =2, 3

This method is very useful for synthesizing divalent homoleptic complexes, generally in good yields. This is a more straightforward synthetic route compared to metathesis or protolysis as it is a one-pot procedure with a single air-sensitive material (Ln metal) and products can be easily isolated via crystallization (after filtering to remove excess Ln metal and Hg formed during the reaction). The reaction often required coordinating solvents such as 1,2-dimethoxyethane (DME) or tetrahydrofuran (THF) which results in the formation of solvated derivatives and also needed activation of metals in some cases which can be obtained by a few methods (e.g., adding few amounts of Hg and I_2).[100] More forcing conditions (e.g. heating) might be essential for the reaction if using diphenylmercury or using a non-donor solvent (such as toluene).[105, 106] These types of reactions required careful handling as they contain mercury reagents which raises environmental concerns.[107]

1.4 The current study

The complexes of divalent lanthanoids have been utilized as single electron transfer reagents in various chemical transformations and continue to produce exciting results. Recently, their application in trapping novel anionic ligands has been attracting chemists. Within a short span of time, they have been used to trap a variety of anionic ligands, starting from dinitrogen to the recently reported ditungsten decacarbonyl ligand. However, this fascinating area is open to further exploration. This thesis extends the studies towards developing new reaction chemistry using recently synthesized organolanthanoid complexes, especially utilizing the capacity of [Sm(DippForm)$_2$(THF)$_2$] (and its Yb analogue) in ligand trapping.

Chapter 2 mainly focuses on the interaction of divalent [Sm(DippForm)$_2$(THF)$_2$] with unsaturated alkyl and aromatic hydrocarbons. 1,3,5,7-cyclooctatetraene ligand has been utilized in this particular application and succeeded in the solvent-dependent synthesis of three different trivalent samarium complexes in which the COT^{2-} dianion is trapped in two of them. Their crystal structures where obtained and structural features were extensively studied. In addition, the similarity and differences in the reactivity of [Sm(DippForm)$_2$(THF)$_2$] and [SmCp*$_2$] towards COT were investigated.

Chapter 3 describes the interaction of [Ln(DippForm)$_2$(THF)$_2$] (Ln = Sm, Yb) with substrates containing dipnictide linkages. The highly reactive substrate *trans*-azobenzene is the one targeted reagent, along with 1*H*-1,2,3-benzotriazole which has not been utilized extensively in rare earth chemistry. Treatment of divalent [Sm(DippForm)$_2$(THF)$_2$] with *trans*-azobenzene demonstrates similar reactivity to that of [SmCp*$_2$(THF)$_2$] and resulted in interesting mono- and dinuclear complexes. Reaction with 1*H*-1,2,3-benzotriazole also yielded a trivalent samarium complex containing benzotriazolates. Among ligands containing dipnictide linkages other than N=N double bond, tetraphenyl diphosphide has been employed and its reaction with [Sm(DippForm)$_2$(THF)$_2$] produced an exciting dinuclear samarium complex, which might lead to a wide range of new synthesis and reactivity in future work.

Chapter 4 reports the reaction of [Ln(DippForm)$_2$(THF)$_2$] (Ln = Sm, Yb) towards unsaturated small organic molecules. Important substrates used for the study are benzil, naphthyl isothiocyanate, phenyl isocyanate, phenyl isothiocyanate, methyl benzoate, benzonitrile and *o*-tolunitrile. The [Ln(DippForm)$_2$(THF)$_2$] (Ln = Sm, Yb) reacted with each substrate in unique ways which resulted in the formation of various interesting organic and organometallic complexes.

Chapter 5 is a small chapter of supporting research where [Yb(DippForm)$_2$(THF)$_2$] was treated with $Co_2(CO)_8$ and resulted in [Co(DippFormCO)(CO)$_3$]·THF. This work formed part of a research paper published in *Dalton Transactions*.

1.5 References

1. F. A. Cotton and G. Wilkinson, *Advanced inorganic chemistry; a comprehensive text*, Interscience Publishers, New York,, 3d edn., 1972.
2. C. E. Housecroft and A. G. Sharpe, *Inorganic chemistry*, Pearson, Harlow, England ; New York, 4th edn., 2012.
3. C. K. Gupta and N. Krishnamurthy, *Extractive metallurgy of rare earths*, CRC Press, Boca Raton, Fla., 2005.
4. T. Moeller, *The chemistry of the lanthanides*, Reinhold Pub. Corp., New York,, 1963.
5. B. T. Kilbourn, *A lanthanide lanthology : a collection of notes concerning the lanthanides and related elements*, Molycorp, White Plains, NY, U.S.A., 1993.
6. W. J. Evans, *Inorg. Chem.*, 2007, **46**, 3435-3449.
7. N. N. Greenwood and A. Earnshaw, *Chemistry of the elements*, Butterworth-Heinemann, Oxford ; Boston, 2nd edn., 1997.
8. S. A. Cotton, *Lanthanide and actinide chemistry*, Wiley, Chichester, England ; Hoboken, NJ, 2006.
9. N. Kaltsoyannis and P. Scott, *The f elements*, Oxford University Press, Oxford ; New York, 1999.
10. M. Husain, A. Batra and K. S. Srivastava, *Polyhedron*, 1989, **8**, 1233-1237.
11. F. T. Edelmann, *Chem. Soc. Rev.*, 2012, **41**, 7657-7672.
12. P. W. Roesky, *Z. Anorg. Allg. Chem.*, 2003, **629**, 1881-1894.
13. K. Dehnicke and A. Greiner, *Angew Chem. Int. Ed. Engl.*, 2003, **42**, 1340-1354.
14. J. M. Klinger, *Extr. Ind. Soc.*, 2015, **2**, 572-580.
15. C. R. Ronda, *Luminescence : from theory to applications*, Wiley-VCH, Weinheim, 2008.
16. N. E. Topp, *The Chemistry of the Rare-earth Elements*, Elsevier Publishing Company, Amsterdam, 1965.
17. S. Cotton, *Lanthanides and actinides*, Macmillan Education Ltd, London, First edn., 1991.
18. T. J. Marks, *Organometallics*, 2013, **32**, 1133-1136.
19. G. Wilkinson and J. M. Birmingham, *J. Am. Chem. Soc.*, 1954, **76**, 6210-6210.

20. G. A. Molander, *Chem. Rev.*, 1992, **92**, 29-68.
21. A. J. Freeman and R. E. Watson, *Phys. Rev.*, 1962, **127**, 2058-2075.
22. L. R. Morss, *Chem. Rev.*, 1976, **76**, 827-841.
23. F. T. Edelmann, *Chem. Soc. Rev.*, 2009, **38**, 2253-2268.
24. R. G. Pearson, *J. Am. Chem. Soc.*, 1963, **85**, 3533-3539.
25. H. Tsuruta, K. Yamaguchi and T. Imamoto, *Chem. Commun.*, 1999, 1703–1704.
26. P. L. Watson, *J. Am. Chem. Soc.*, 1982, **104**, 337-339.
27. S. Kobayashi and H. Ishitani, *J. Am. Chem. Soc.*, 1994, **116**, 4083-4084.
28. S. Kobayashi and I. Hachiya, *J. Org. Chem.*, 1994, **59**, 3590—3596.
29. A. Kawada, S. Mitamuraa and S. Kobayashi, *J. Chem. Soc., Chem. Commun.*, 1993, 1157-1158.
30. G. Jeske, H. Lauke, H. Mauermann, H. Schumann and T. J. Marks, *J. Am. Chem. Soc.*, 1985, **107**, 8111-8118.
31. M. R. Douglass and T. J. Marks, *J. Am. Chem. Soc.*, 2000, **122**, 1824-1825.
32. H. Taube and E. S. Gould, *Acc. Chem. Res.*, 1969, **2**, 321-329.
33. J. Doyle and A. G. Sykes, *J. Chem. Soc. A.*, 1968, 2836-2839.
34. P. K. Thamburaj and E. S. Gould, *Inorg. Chem.*, 1975, **14**, 15-17.
35. E. Vrachnou-Astra and D. Katakis, *J. Am. Chem. Soc.*, 1975, **97**, 5357-5363.
36. P. Girard, J. L. Namy and H. B. Kagan, *J. Am. Chem. Soc.*, 1980, **102**, 2693-2698.
37. H. B. Kagan and J. L. Namy, *Tetrahedron*, 1986, **42**, 6573-6614.
38. T. P. Ananthanarayan, T. Gallagher and P. Magnus, *J. Chem. Soc., Chem. Commun.*, 1982, 709-710.
39. J. L. Namy, J. Souppe and H. B. Kagan, *Tetrahedron Lett.*, 1983, **24**, 765-766.
40. J. Souppe, L. Danon, J. L. Namy and H. B. Kagan, *J. Organomet. Chem.*, 1983, **250**, 227-236.
41. J. Wettergren, T. Ankner and G. Hilmersson, *Chem. Commun.*, 2010, **46**, 7596-7597.
42. D. Parmar, K. Price, M. Spain, H. Matsubara, P. A. Bradley and D. J. Procter, *J. Am. Chem. Soc.*, 2011, **133**, 2418-2420.
43. D. Parmar, L. A. Duffy, D. V. Sadasivam, H. Matsubara, P. A. Bradley, R. A. Flowers and D. J. Procter, *J. Am. Chem. Soc.*, 2009, **131**, 15467–15473.

44. L. A. Duffy, H. Matsubara and D. J. Procter, *J. Am. Chem. Soc.*, 2008, **130**, 1136-1137.
45. A. Dahlén, A. Nilsson and G. Hilmersson, *J. Org. Chem.*, 2006, **71**, 1576-1580.
46. M. Szostak and D. J. Procter, *Angew. Chem. Int. Ed. Engl.*, 2012, **51**, 9238-9256.
47. E. Prasad, B. W. Knettle and R. A. Flowers, *J. Am. Chem. Soc.*, 2002, **124**, 14663-14667.
48. T. Ankner, M. Fridén-Saxin, N. Pemberton, T. Seifert, M. Grøtli, K. Luthman and G. r. Hilmersson, *Org. Lett.*, 2010, **12**, 2210-2213.
49. K. Mashima, T. Oshiki and K. Tani, *J. Org. Chem.*, 1998, **63**, 7114-7116.
50. S.-i. Fukuzawa, Y. Yahara, A. Kamiyama, M. Hara and S. Kikuchi, *Org. Lett.*, 2005, **7**, 5809-5812.
51. S.-i. Fukuzawa, K. Mutoh, T. Tsuchimoto and T. Hiyama, *J. Org. Chem.*, 1996, 5400-5405.
52. S. Salot and J. C. Warf *J. Am. Chem. Soc.*, 1968, **90**, 1932-1933.
53. R. Navaneethakrishnan and J. C. Ware, *Inorg. Chem.*, 1976, **15**, 2849-2852.
54. W. J. Evans, *Coord. Chem. Rev.*, 2000, **206–207**, 263–283.
55. W. J. Evans, I. Bloom, W. E. Hunter and J. L. Atwood, *J. Am. Chem. Soc.*, 1981, **103**, 6508-6510.
56. W. J. Evans, L. A. Hughes and T. P. Hanusa, *J. Am. Chem. Soc.*, 1984, **106**, 4270-4272.
57. W. J. Evans, L. A. Hughes and T. P. Hanusa, *Organometallics*, 1986, **5**, 1285-1291.
58. W. J. Evans, S. L. Gonzales and J. W. Ziller, *J. Am. Chem. Soc.*, 1994, **116**, 2600-2608.
59. W. J. Evans, T. A. Ulibarri and J. W. Ziller, *J. Am. Chem. Soc.*, 1988, **110**, 6877-6879.
60. W. J. Evans, L. A. Hughes, D. K. Drummond, H. Zhang and J. L. Atwood, *J. Am. Chem. Soc.*, 1986, **108**, 1722-1723.
61. W. J. Evans, T. A. Ulibarri and J. W. Ziller, *J. Am. Chem. Soc.*, 1990, **110**, 219-223.
62. W. J. Evans, T. A. Ulibarri and J. W. Ziller, *J. Am. Chem. Soc.*, 1990, **112**, 2314-2324.

63. W. J. Evans, R. A. Keyer, H. Zhang and J. L. Atwood, *J. Chem. Soc., Chem. Commun.*, 1987, 837-838.

64. W. J. Evans, S. L. Gonzales and J. W. Ziller, *J. Am. Chem. Soc.*, 1991, **113**, 9880-9882.

65. W. J. Evans and D. K. Drummond, *J. Am. Chem. Soc.*, 1989, **111**, 3329-3335.

66. W. J. Evans and D. K. Drummond, *J. Am. Chem. Soc.*, 1988, **110**, 2772-2774.

67. W. J. Evans, L. R. Chamberlain, T. A. Ulibarri and J. W. Ziller, *J. Am. Chem. Soc.*, 1988, **110**, 6423-6432.

68. H. Yasuda, H. Yamamoto, K. Yokota, S. Miyake and A. Nakamura, *J. Am. Chem. Soc.*, 1992, **114**, 4908-4910.

69. H. Yasuda, M. Furo and H. Yamamoto, *Macromolecules*, 1992, **25**, 5115-5116.

70. M. Yamashita, Y. Takemoto, E. Ihara and H. Yasuda, *Macromolecules*, 1996, **29**, 1798-1806.

71. W. J. Evans and H. Katsumata, *Macromolecules*, 1994, **27**, 4011-4013.

72. F. T. Edelmann, *Coord. Chem. Rev.*, 1994, **137**, 403-481.

73. W. J. Evans, D. K. Drummond, H. Zhang and J. L. Atwood, *Inorg. Chem.*, 1988, **27**, 575-579.

74. G. B. Deacon, C. M. Forsyth, P. C. Junk and J. Wang, *Inorg. Chem.*, 2007, **46**, 10022–10030.

75. M. N. Bochkarev, I. L. Fedushkin, A. A. Fagin, T. V. Petrovskaya, J. W. Ziller, R. N. R. Broomhall-Dillard and W. J. Evans, *Angew Chem. Int. Ed. Engl.*, 1997, **36**, 133-135.

76. W. J. Evans, N. T. Allen and J. W. Ziller, *J. Am. Chem. Soc.*, 2001, **123**, 7927-7928.

77. W. J. Evans, *J. Alloys Compd.*, 2009, **488**, 493-510.

78. W. J. Evans, N. T. Allen and J. W. Ziller, *Angew. Chem. Int. Ed. Engl.*, 2002, **41**, 359-361.

79. W. J. Evans, N. T. Allen and J. W. Ziller, *J. Am. Chem. Soc.*, 2000, **122**, 11749-11750.

80. M. N. Bochkarev, I. L. Fedushkin, S. Dechert, A. A. Fagin and H. Schumann, *Angew. Chem. Int. Ed. Engl.*, 2001, **40**, 3176-3178.

81. M. R. MacDonald, J. W. Ziller and W. J. Evans, *J. Am. Chem. Soc.*, 2011, **133**, 15914-15917.

82. M. R. MacDonald, J. E. Bates, M. E. Fieser, J. W. Ziller, F. Furche and W. J. Evans, *J. Am. Chem. Soc.*, 2012, **134**, 8420-8423.
83. M. R. MacDonald, J. E. Bates, J. W. Ziller, F. Furche and W. J. Evans, *J. Am. Chem. Soc.*, 2013, **135**, 9857-9868.
84. W. J. Evans and D. S. Lee, *Can. J. Chem.*, 2005, **83**, 375-384.
85. W. J. Evans, S. L. Gonzales and J. W. Ziller, *J. Chem. Soc., Chem. Commun.*, 1992, 1138-1139.
86. W. J. Evans, J. W. Grate, L. A. Hughes, H. Zhang and J. L. Atwood, *J. Am. Chem. Soc.*, 1985, **107**, 3728-3730.
87. S. N. Konchenko, N. A. Pushkarevsky, M. T. Gamer, R. Koppe, H. Schnöckel and P. W. Roesky, *J. Am. Chem. Soc.*, 2009, **131**, 5740–5741.
88. S. N. Konchenko, T. Sanden, N. A. Pushkarevsky, R. Koppe and P. W. Roesky, *Chem. Eur. J.*, 2010, **16**, 14278-14280.
89. N. Arleth, S. Bestgen, M. T. Gamer and P. W. Roesky, *J. Am. Chem. Soc.*, 2014, **136**, 14023-14026.
90. T. D. Tilley and R. A. Anderse, *J. Chem. Soc., Chem. Commun.*, 1981, 985-986.
91. T. D. Tilley and R. A. Andersen, *J. Am. Chem. Soc.*, 1982, **104**, 1772-1774.
92. J. M. Boncella and R. A. Andersen, *J. Chem. Soc., Chem. Commun.*, 1984, 809-810.
93. M. L. Cole and P. C. Junk, *Chem. Commun.*, 2005, 2695-2697.
94. G. B. Deacon, P. C. Junk, J. Wang and D. Werner, *Inorg. Chem.*, 2014, **53**, 12553-12563.
95. R. Yadav, M. E. Hossain, R. Peedika Paramban, T. Simler, C. Schoo, J. Wang, G. B. Deacon, P. C. Junk and P. W. Roesky, *Dalton. Trans.*, 2020, **49**, 7701-7707.
96. C. Schoo, S. Bestgen, M. Schmidt, S. N. Konchenko, M. Scheer and P. W. Roesky, *Chem. Commun.*, 2016, **52**, 13217-13220.
97. D. Werner, X. Zhao, S. P. Best, L. Maron, P. C. Junk and G. B. Deacon, *Chem. Eur. J.*, 2017, **23**, 2084-2102.
98. Y. Z. Ma, S. Bestgen, M. T. Gamer, S. N. Konchenko and P. W. Roesky, *Angew. Chem. Int. Ed. Engl.*, 2017, **56**, 13249-13252.
99. G. B. Deacon, Z. Guo, P. C. Junk and J. Wang, *Angew. Chem. Int. Ed. Engl.*, 2017, **56**, 8486-8489.

100. F. Ortu, *Chem. Rev.*, 2022, **122**, 6040-6116.
101. W. A. Herrmann, *Synthetic methods of organometallic and inorganic chemistry: (Herrmann/Brauer)*, Georg Thieme Verlag; Thieme Medical Publishers, Stuttgart; New York, 1996.
102. Z. Guo, V. L. Blair, G. B. Deacon and P. C. Junk, *Dalton Trans.*, 2020, **49**, 13588-13600.
103. J. A. McCleverty and T. J. Meyer, *Comprehensive coordination chemistry II : from biology to nanotechnology*, Elsevier Pergamon, Amsterdam; Boston, 1st edn., 2004.
104. K. Izod, S. T. Liddle and W. Clegg, *Inorg. Chem.*, 2004, **43**, 214-218.
105. G. B. Deacon, C. M. Forsyth and S. Nickel, *J. Organomet. Chem.*, 2002, **647**, 50-60.
106. G. B. Deacon, T. C. Feng, C. M. Forsyth, A. Gitlits, D. C. R. Hockless, S. Qi, B. W. Skelton and A. H. White, *J. Chem. Soc., Dalton Trans.*, 2000, 961-966.
107. W. F. Fitzgerald and R. P. Mason, *Met. Ions Biol. Syst.*, 1997, **34**, 53-111.

Chapter 2

Reductive trapping of large planar COT^{2-} by divalent samarium complex

2.1 Introduction

The field of organolanthanoid chemistry has a lot of misleading assumptions and inaccurate assessments at the beginning.[1] The cations being oxophilic hard acids and their fondness towards electrostatic interactions to form ionic bonds made them the least expected candidates to have an affinity with neutral hydrocarbons and other nonpolar substrates.[2-4] Investigation into zero valent lanthanide chemistry and the metal vapour technique synthetic approach later resulted in the formation of a variety of new classes of organolanthanoids in which lanthanoid metals interacted with neutral unsaturated hydrocarbons.[5-9] Subsequently, divalent lanthanoid complexes were used to trap some unusual anionic species via single electron transfer from these highly reducing compounds. In this chemistry lanthanoid complexes of the cyclopentadienide ion (and its derivatives) were able to satisfy both the ionic and steric requirements in these complexes.[4]

2.1.1 Interaction of divalent organolanthanoid complexes with unsaturated hydrocarbons

The reaction of unsaturated alkyl hydrocarbons towards divalent organolanthanoid complexes (divalent lanthanoid centre) was first reported by Bill Evans using very reactive $[SmCp^*_2(THF)_2]$ (where $Cp^* = C_5Me_5$) in a reaction with diphenylacetylene, which resulted in the formation a new type of organolanthanoid complex, an enediyl complex $[(Cp^*_2Sm)(C_6H_5)C{=}C(C_6H_5)(Cp_2Sm)]$ **(Scheme 2.1a)**.[4, 10, 11] This reaction construes a new reductive type of interaction between lanthanoid and unsaturated hydrocarbons, where the product can be converted into the first organosamarium hydride complex (a reaction with interesting implications). Later in 1987, it was reported the first structure had η^2-coordination of carbon-carbon multiple bonds to samarium, which wasn't expected because of its ionic nature and limited radial extension of their 4f valence orbitals.[12] Later $[SmCp^*_2(THF)_2]$ was treated with the diyne $PhC{\equiv}CC{\equiv}CPh$ in THF to form highly soluble $[(Cp^*_2Sm)_2C_4Ph_2]$ **(Scheme 2.1b)**. Even though these results suggest a resemblance with alkali-metal chemistry, the high solubility of $[SmCp^*_2(THF)_2]$ made their chemistry different and novel. This is evident from the reaction of $[SmCp^*_2(THF)_2]$ and the more reactive unsolvated species

[SmCp*$_2$] with alkenes and dienes which resulted in the formation of trivalent and mixed valent products **(Scheme 2.1c-e)**.[13] Reactions of [SmCp*$_2$] with stilbene[2], styrene[2], isoprene[14] and myrcene[14] also exhibit similar reactivity which resulted in reductive trapping of hydrocarbon fragments. Examples of successful alternatives to [SmCp*$_2$]/[SmCp*$_2$(THF)$_2$] in these applications are [YbCp*$_2$(OEt$_2$)][15], [Sm(C$_5$H$_4$^{t}Bu)$_2$][16] and [YbL(THF)$_2$]·0.5C$_7$H$_8$ (where L = [Me$_2$NCH$_2$CH$_2$N(CH$_2$-2-OC$_6$H$_2$-3,5-Bu^t$_2$)$_2$][17] and their reactions with phenylacetylene are illustrated in the scheme below **(Scheme 2.1f)**.

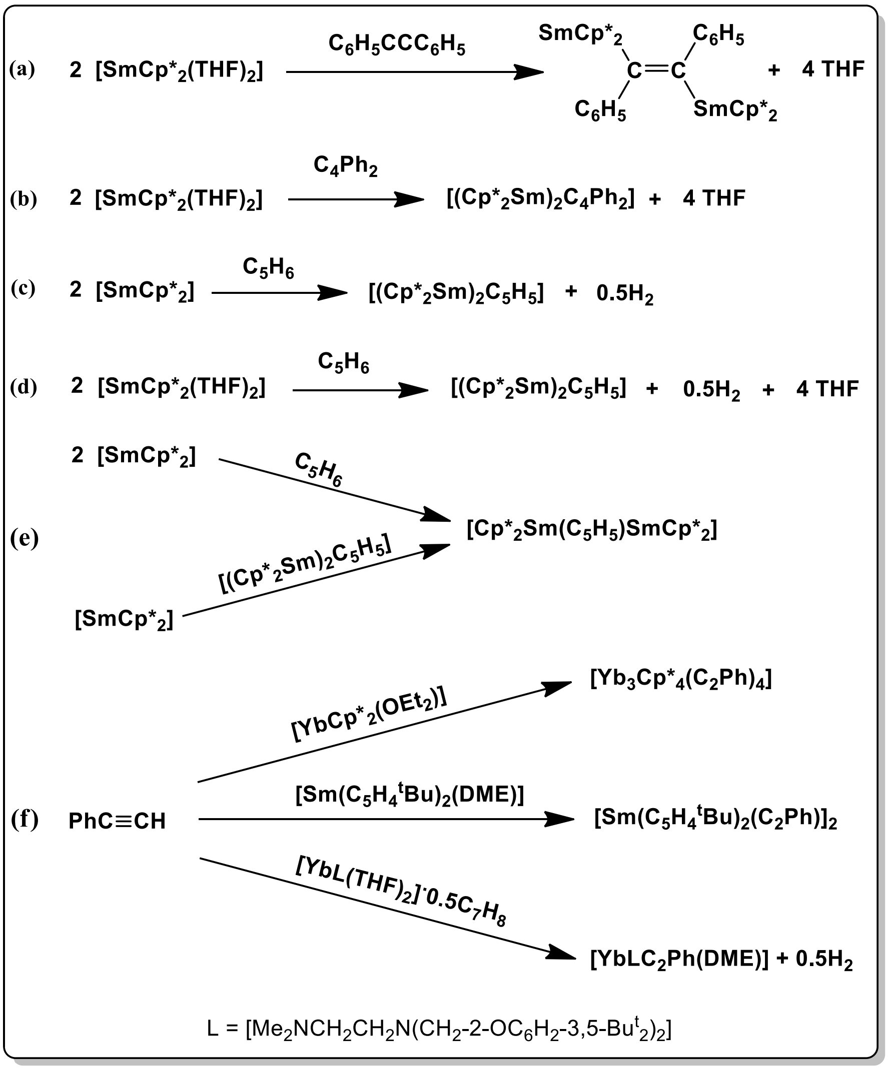

Scheme 2.1 Trapping of various unsaturated hydrocarbons using divalent organolanthanoid complexes.[2,4,10-17] Byproducts for some reactions are not identified by the authors.

Divalent samarium metallocenes [$SmCp^*_2(THF)_2$] and [$SmCp^*_2$] also proved to be successful in reactions with bulkier polycyclic aromatic hydrocarbons. Their reaction with COT (cyclooctatetraene) resulted in unusual and interesting products which will be discussed in detail in the coming paragraphs. Unsolvated decamethylsamarocene, [$SmCp^*_2$], was more reactive than its solvated counterpart due to its high reduction potential, sterically unsaturated and unusually bent metallocene geometry, which provide sufficient solubility and crystallinity to reaction products.[18] They were treated with anthracene ($C_{14}H_{10}$), pyrene ($C_{16}H_{10}$), 2,3-benzanthracene ($C_{18}H_{12}$), 9-methylanthracene ($C_{15}H_{12}$) and acenaphthylene ($C_{12}H_8$), which yielded the formation of dinucleated organolanthanoid complexes with general formula $(SmCp^*_2)_2$(substrate dianion) as shown in **Scheme 2.2**, where planar dianions are having an allylic interaction with $SmCp^*_2$ unit.[19] One recent example of a similar application is the reduction of naphthalene and biphenyl using divalent complexes [K(2.2.2-cryptand)][$(C_5H_4SiMe_3)_3Ln$], where Ln = Y, La, Ce and Dy).[20]

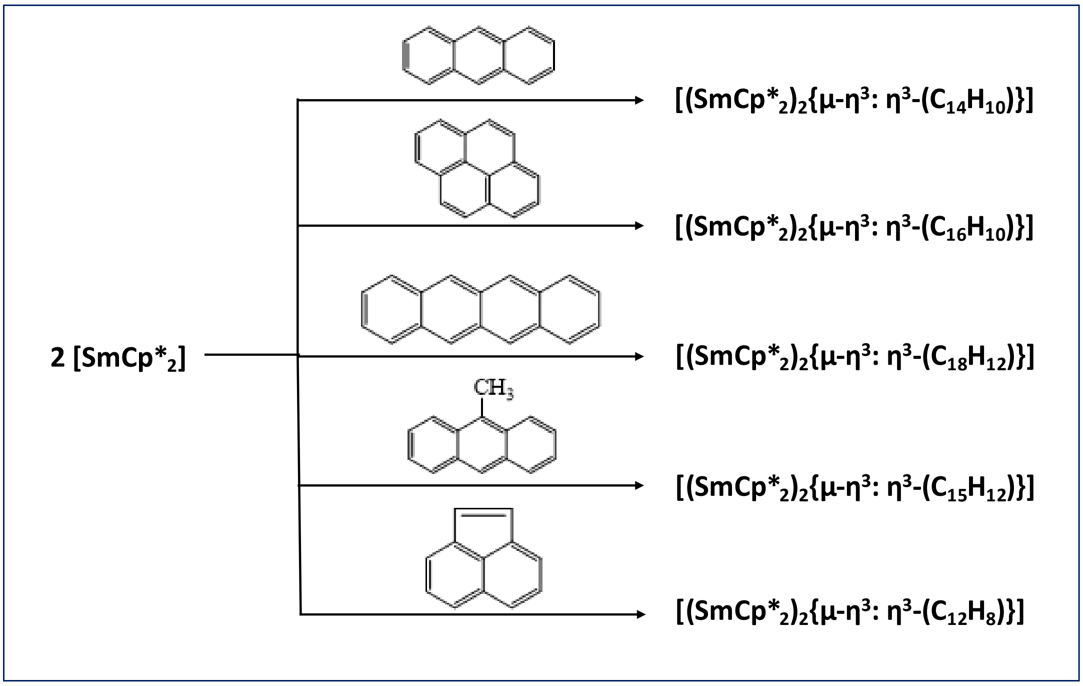

Scheme 2.2 Trapping of various polycyclic aromatic hydrocarbons by [$SmCp^*_2$].[19]

2.1.2 COT in organolanthanoid chemistry

While cyclopentadiene (Cp) and its derivatives (eg. Cp*) have been extensively used in organolanthanoid chemistry, cyclooctatetraene (generally abbreviated as COT) has also provided some very exciting results. Even the first divalent organolanthanoid complexes were synthesized using cyclooctatetraene which they prepared by taking advantage of the solubility of Eu and Yb in liquid ammonia.[21] The flat 1,3,5,7-$C_8H_8^{2-}$ ring with a redox potential of -1.86V (vs SCE)[22] usually binds in a η^8-coordination fashion, even if binding modes other than 8 are also reported in some cases.[23] The metal atom can bind to one or both faces of cyclooctatetraene dianion ($C_8H_8^{2-}$) which has a 10 π-electron system. COT^{2-} is an exciting ligand in f-element chemistry which gives rise to numerous complexes such as conventional, half-, and inverse sandwiches, as well as multi-decker compounds **(Fig 2.1)**. Initial organolanthanoid complexes containing COT^{2-} such as [Eu(COT)] and [Yb(COT)] were 'half-sandwich' type structures **(Fig. 2.1a)** with COT^{2-} bound to a single metal in an η^8-coordination fashion.[21] Conventional 'sandwich' type structures are those having a single metal centre, featuring two COT^{2-} ligands placed symmetrically on either side **(Fig. 2.1b)**. Cerocene, $[Ce(COT)_2]$ is an example of this type of COT^{2-} complex.[24] Inverse sandwich complexes feature two metal centres with a single COT^{2-} ligand in between as shown in **Fig. 2.1c**.[25] COT^{2-} compounds with much higher structural complexity are also reported including linear tetranuclear structures[26, 27] and nanowires[28] (**Fig. 2.1c, d)**.

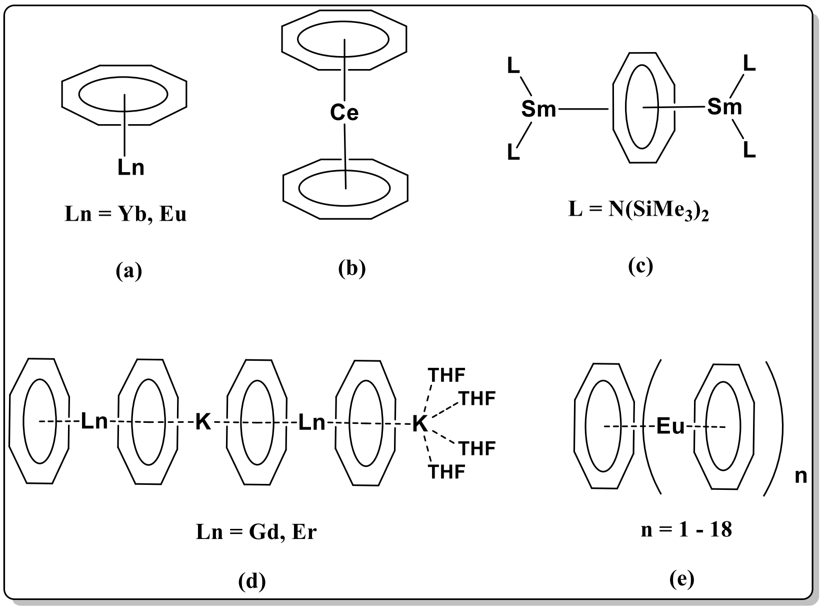

Figure 2.1 Different types of organolanthanoid complexes containing COT^{2-} ligand.

Encapsulation of an anionic COT^{2-} ring using divalent $[SmCp^*_2(THF)_2]$ and its unsolvated analogue give rise to a common product $[Cp^*Sm(C_8H_8)]$ and two different additional products as shown in **Scheme 2.3**.[29, 30] The reaction with bent $[SmCp^*_2]$ leads to the synthesis of the first $(\eta^5\text{-}C_5Me_5)_3Ln$ type complex, which wasn't an expected structure because of its steric bulkiness and that leads to a lot of interesting reaction chemistry.[31] This was entirely different from reaction products observed for other similar polycyclic aromatic hydrocarbons **(Scheme 2.2)**.[19] Later similar sandwich compounds incorporating the COT^{2-} ligand were synthesized through alternative routes.[32-34]

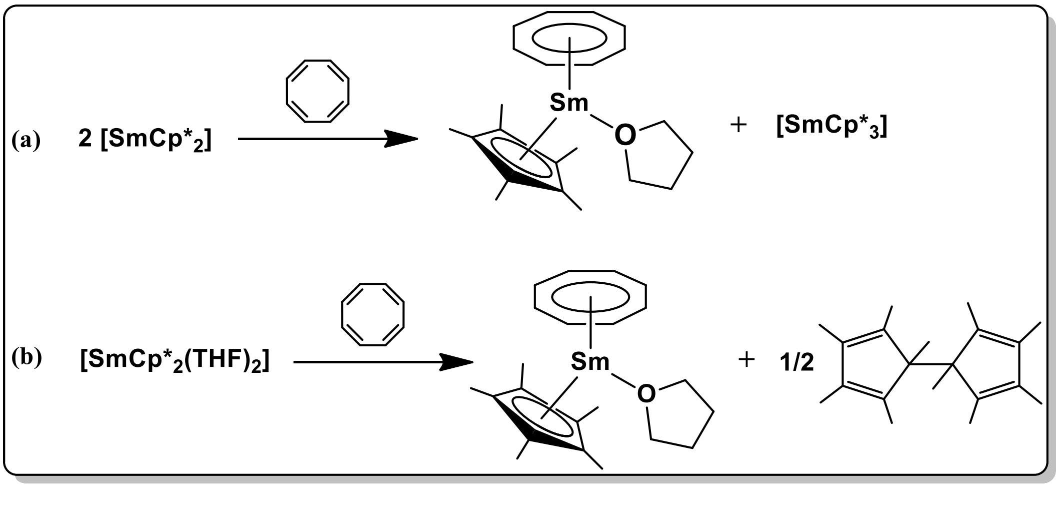

Scheme 2.3 Reaction of $[SmCp^*_2]$ (a) and $[SmCp^*_2(THF)_2]$ (b) with COT.[29, 30]

2.1.3 Solvent dependency and ring-opening of THF

Two major solvents that are widely used to carry out chemical reactions involving organolanthanoid complexes are toluene and tetrahydrofuran (THF) owing to the reagents having good solubility. The major difference between them arises when it comes to their coordinating ability, where THF typically solvates the metal centre while in toluene, these coordination positions become free due to the dissociation of some THF.[3] These contrasting characteristics will sometimes make certain reactions proceed differently in each solvent, resulting in the formation of different reaction products. Besides, THF is capable of being activated, by Lewis acids, to nucleophilic ring opening.[35-37] Reactions involving ring-opening of the cyclic ether THF has been reported many times in the past, a handful of them being in organolanthanoid chemistry.[31, 38-41] Nucleophilic ring-opening is illustrated in **Scheme 2.4** where a Lewis acid initiates the nucleophilic ring-opening of THF through the formation of a tetrahydrofuran oxonium ion and that is opened by the nucleophilic addition of another THF. Ring-opening of THF is dependent on various factors that affect the nucleophilicity, which includes size, counter ion and pK_a of the conjugate acid.[42]

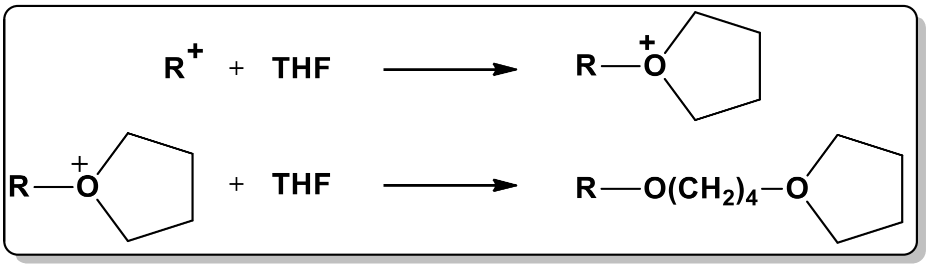

Scheme 2.4 Nucleophilic ring-opening of tetrahydrofuran.

2.2 Research Plan

The potential of divalent [Sm(DippForm)$_2$(THF)$_2$] in reductive trapping of novel anionic ligands has been discussed in the previous chapter. The interaction of [Sm(DippForm)$_2$(THF)$_2$] with unsaturated alkyl and aromatic hydrocarbons is yet to be explored. Cyclooctatetraene could be a good starting point in this regard as it is a two electron acceptor generating the COT^{2-} dianion and is typically η^8-coordinated to the metal centre. It was expected that [Sm(DippForm)$_2$(THF)$_2$] with its strongly reducing power coupled with the tendency of COT^{2-} to form polyhapto complexes, some exciting chemistry similar to that of [SmCp$^*_2$] could be expected.

2.3 Results and Discussion

2.3.1 *Synthesis and characterisation*

2.3.1.1 The reaction of [Sm(DippForm)$_2$(THF)$_2$] with COT in THF

The primary target compound of the reaction was a dinuclear inverse sandwich-type complex where the COT^{2-} ligand is flanked by two [Sm^{III}(Dippform)$_2$]$^-$ fragments on opposing sides. So the reaction was carried out in a 2:1 stoichiometric ratio of [Sm(DippForm)$_2$(THF)$_2$] to COT. The high solubility of reagents made THF the first-choice solvent to facilitate the reaction. The COT reagent was added slowly to a solution of [Sm(DippForm)$_2$(THF)$_2$] in THF, which caused a rapid colour change from dark green to red without stirring or heating. Crystallization after layering hexane onto the reaction mixture resulted in the formation of purple crystals of **[Sm^{III}(DippForm)(COT)(THF)$_2$] (1)**. The other product, **[Sm(DippForm)$_2$(O-C$_4$H$_8$-DippForm)(THF)]·THF (2)**, which has the ring-opened THF component, was obtained by fractional crystallization of the remaining solution. The reaction scheme and structures of products are given below **(Scheme 2.5)**.

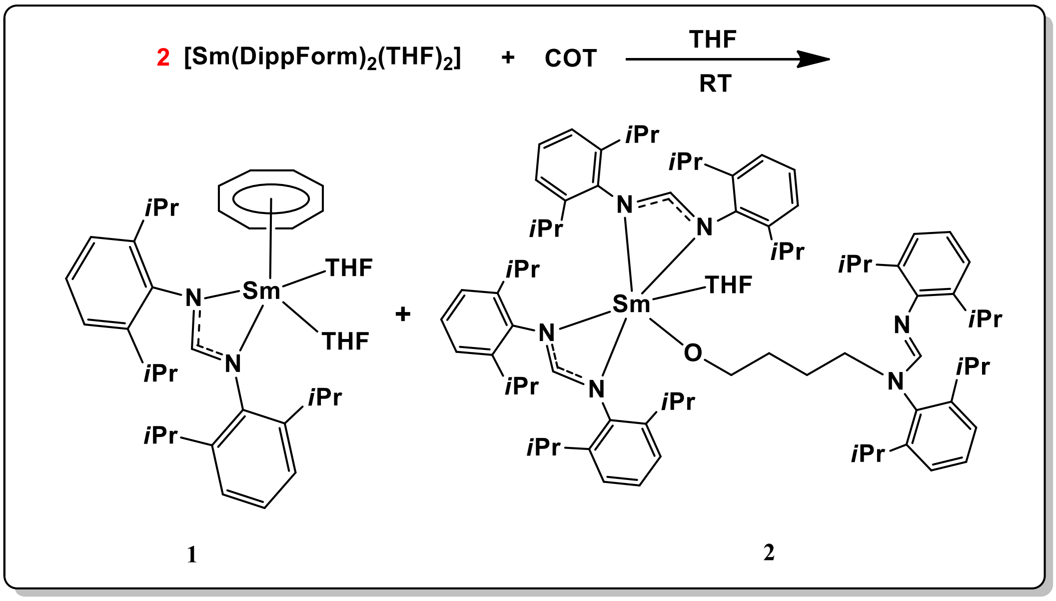

Scheme 2.5 Reaction of [Sm(DippForm)$_2$(THF)$_2$] with COT in THF.

Satisfactory ^{1}H NMR and ^{13}C NMR spectra were obtained for compound **1** (figure 2.2 & 2.3). The η^8-C_8H_8 ligand protons appear as a singlet at δ = 10.93 ppm while NC*H*N (DippForm) signal is at δ = 8.31 ppm, and their integration is in 8:1 ratio as expected. For Evan's product [SmCp*COT(THF)][30], the coordinated COT^{2-} resonances were at δ = 8.88 ppm. The C*H*$_2$ signals of coordinated THF can be observed at δ = 3.79 and 1.56 ppm, while the proton signals for the isopropyl group of DippForm appear at δ = 2.55 ppm (Dipp-C*H*) and in the range of δ = 1.16 – 1.18 ppm (Dipp-C*H*$_3$). For ^{13}C NMR, the η^8-C_8H_8 signals are visible at δ = 82.58 ppm, which is comparable to the reported value of δ = 85.15 ppm for [SmCp*COT(THF)]. ^{13}C NMR signals for coordinated THF are at δ = 71.82 and 25.95 ppm, while those of the isopropyl group are at δ = 24.63 (Dipp-*C*H$_3$) and 25.95 ppm (Dipp-*C*H). In addition, the product is also confirmed by IR spectroscopy and elemental analysis.

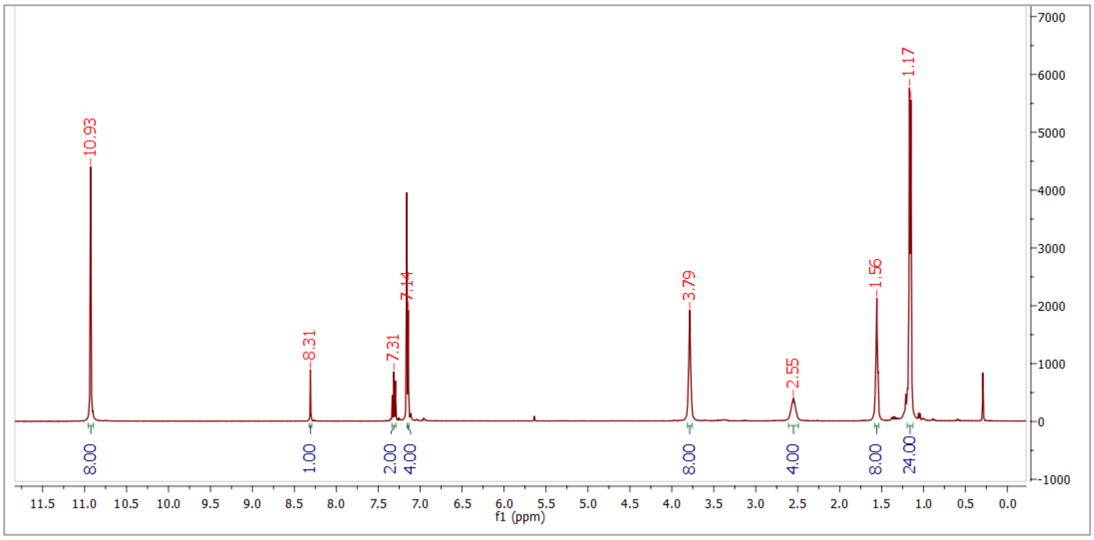

Fig. 2.2 ^{1}H NMR spectrum of [Sm(DippForm)(COT)(THF)$_2$] (**1**)

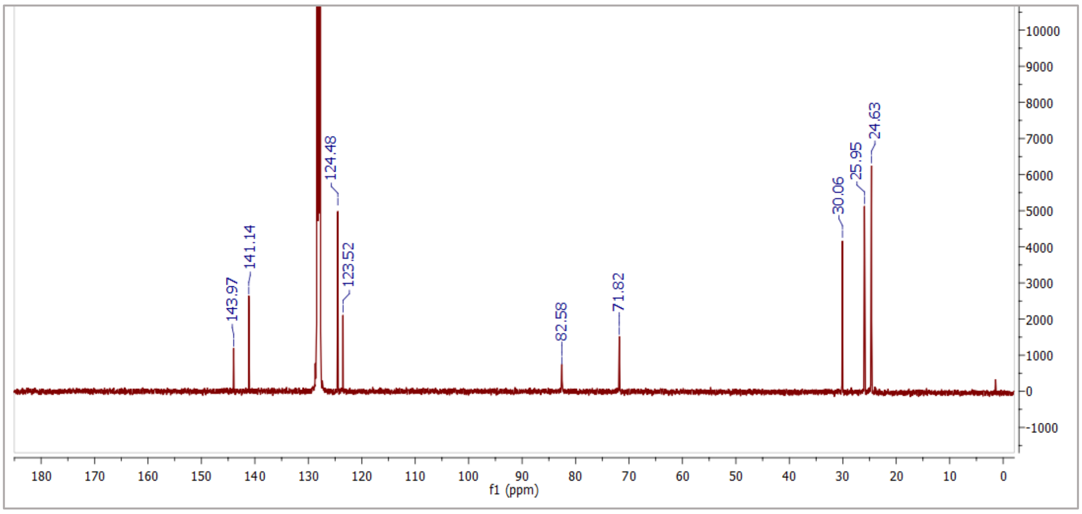

Fig. 2.3 ^{13}C NMR spectrum of [Sm(DippForm)(COT)(THF)$_2$] (**1**)

Ring-opened THF complex **2** was also characterized by ^{1}H NMR, ^{13}C NMR, IR and elemental analysis. Even though the broadening of signals due to paramagnetic effects of trivalent samarium makes it difficult to integrate certain regions of ^{1}H NMR spectra, the data is interpretable to an extent and is consistent with the obtained X-ray crystal structure (**Fig. 2.4**). The existence of two separate THF and DippForm moieties is evident from the ^{1}H NMR spectra. The NC*H*N proton of the typical DippForm ligand shows signals at δ = 9.67 ppm with an integration of 2 while that of DippForm in the ring-opened component is at δ = 7.36 ppm with an integration value of one. The four CH$_2$ signals of ring-opened THF are at δ = 7.25 (N-CH$_2$), 5.36, 4.42 and 2.73 ppm (O-CH$_2$), all with integration of ca. 2. One of the CH$_2$ signals of coordinated THF can be observed at δ = 2.89 ppm, but the other signal and the remaining Dipp-CH_3 proton signals are expected to be at the broad upfield region of the spectrum where they are indistinguishable. The singlet at δ = 5.6 ppm is attributed to proton signals of unreacted COT. The ^{13}C NMR spectrum is shown in **Fig. 2.5** indicating two ^{13}C signals at δ = 68.31 and 25.36 ppm for coordinated solvent THF. The signals for ring-opened-THF (CH$_2$) components can be seen at δ = 72.59, 51.58, 34.78 and 24.51 ppm. IR spectroscopy confirmed the same structure and elemental analysis confirmed purity of the sample.

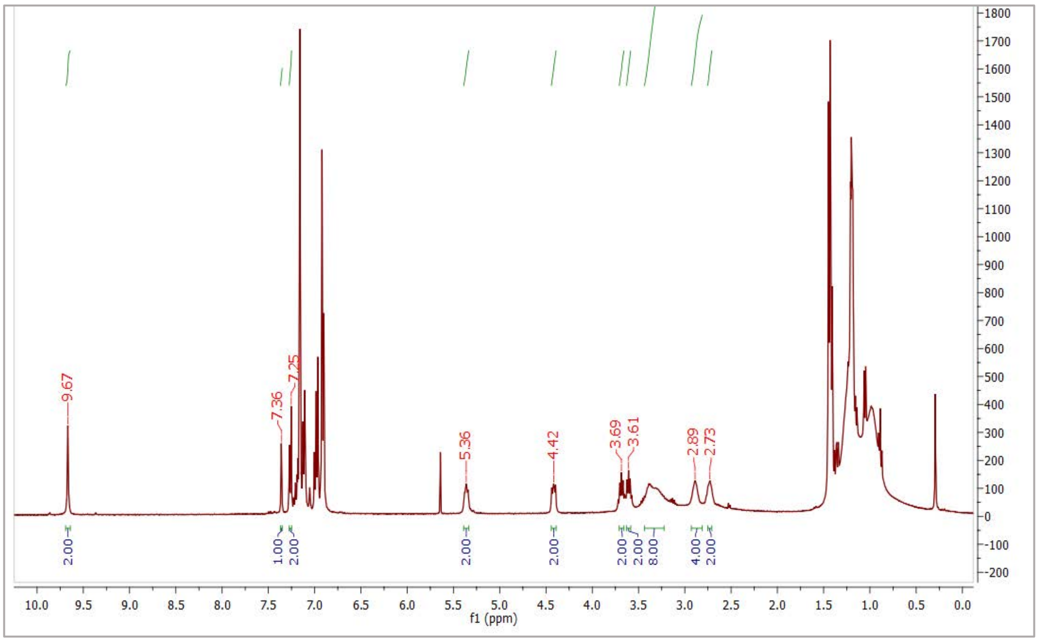

Fig. 2.4 ^{1}H NMR spectrum of $[Sm(DippForm)_2(O\text{-}C_4H_8\text{-}DippForm)(THF)]\cdot THF$ (**2**)

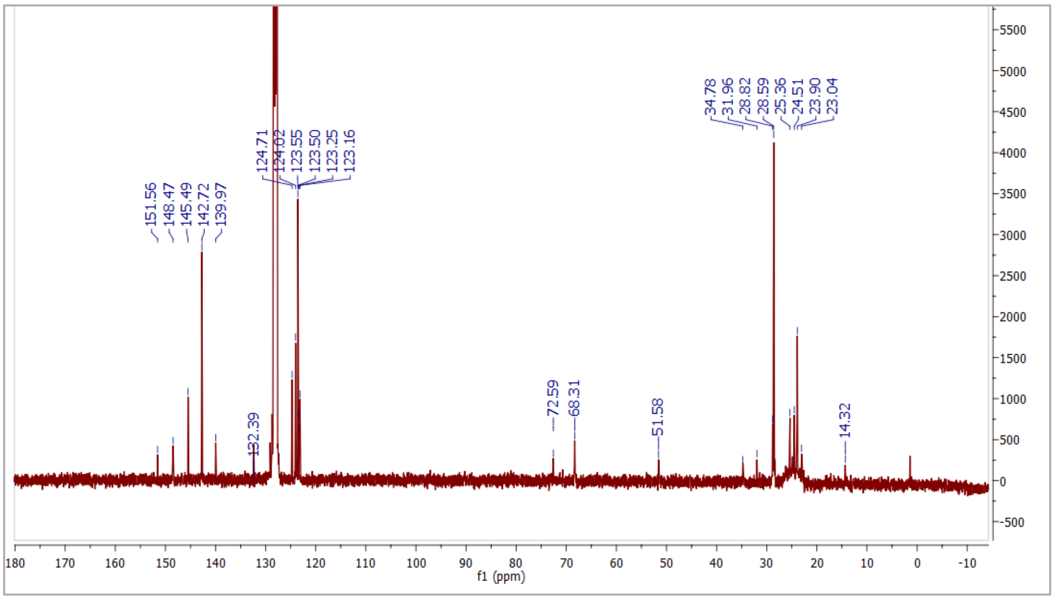

Fig 2.5 ^{13}C NMR spectrum of $[Sm(DippForm)_2(O\text{-}C_4H_8\text{-}DippForm)(THF)]\cdot THF$ (**2**)

2.3.1.2 The reaction of [Sm(DippForm)$_2$(THF)$_2$] with COT in toluene

The reaction of [Sm(DippForm)$_2$(THF)$_2$] and COT in the non-coordinating solvent toluene was carried out in similar conditions to that of THF (above). The result was also an instant colour change from dark green to red. Here, no further colour changes occurred, unlike the reaction in THF above, and red crystals of an inverse dinuclear cyclooctatetraenyl sandwich samarium(III) complex **[Sm$_2$(DippForm)$_4$(COT)]·4C$_6$D$_6$ (3)** deposited in good yield in toluene/C$_6$D$_6$ after several hours. The complete reaction scheme is provided below along with the product structure **(Scheme 2.6)**.

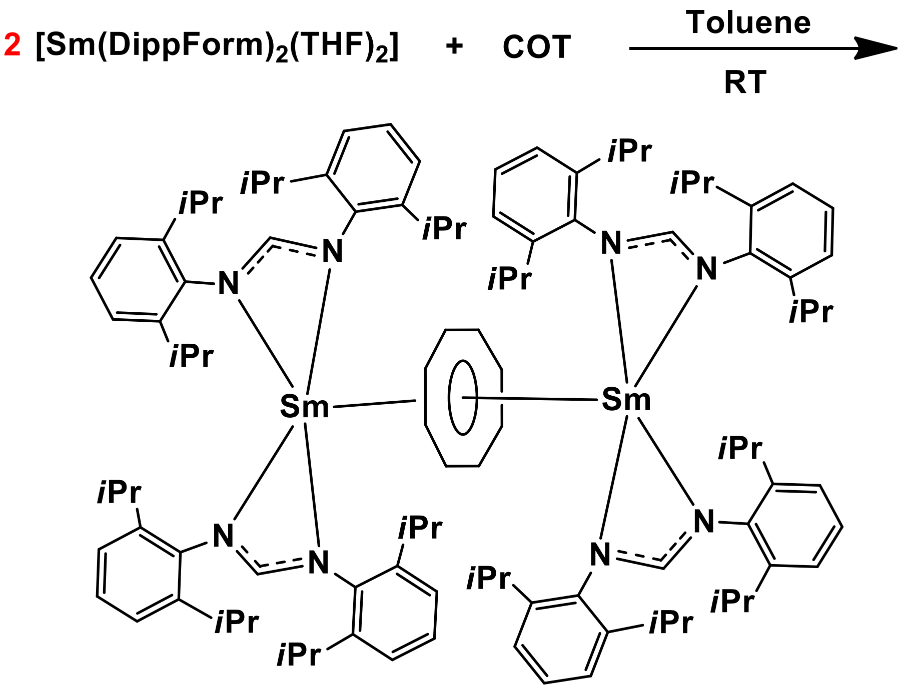

3

Scheme 2.6 Reaction of [Sm(DippForm)$_2$(THF)$_2$] with COT in toluene.

Here again, the paramagnetic nature of Sm^{3+} acted as a barrier to obtaining interpretable ^{1}H NMR spectra. There is a significant broadening of the proton signals in the upfield region while the sharp resonances in the downfield area can be more easily analysed and agree with the composition of the obtained Xray crystal structure **(Fig 2.6)**. The proton signals of the COT^{2-} ring and NC*H*N (DippForm) are at δ = 10.71 and 8.34 ppm respectively with an integration ratio of 1:2, showing they interchanged their position compared to complex **1**. Here the signals of entrapped COT^{2-} protons are well inside the expected range (8-11ppm) based on previously reported trivalent samarium cyclooctatetraenides.[34] In addition, ^{13}C signals for the COT^{2-} ligand **(Fig 2.7)** are at δ = 67.90 ppm, which is shifted a little to high field compared to δ = 82.58 ppm of complex **1**. Moreover, suitable IR spectra and a satisfactory microanalysis were obtained.

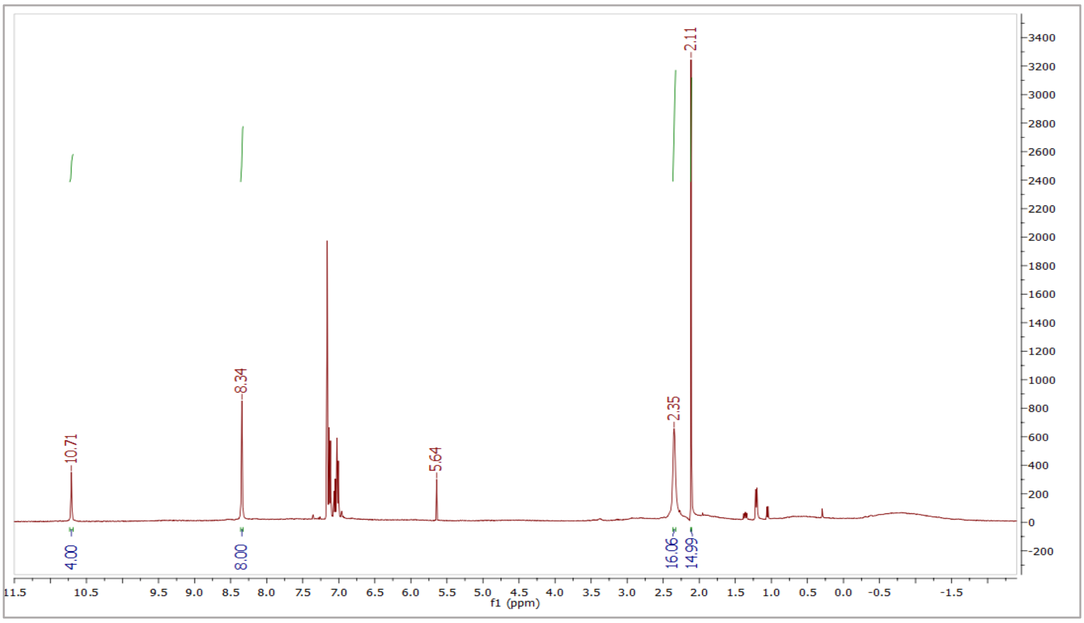

Fig. 2.6 ^{1}H NMR spectrum of $[Sm_2(DippForm)_4(COT)]\cdot 4C_6D_6$ (**3**)

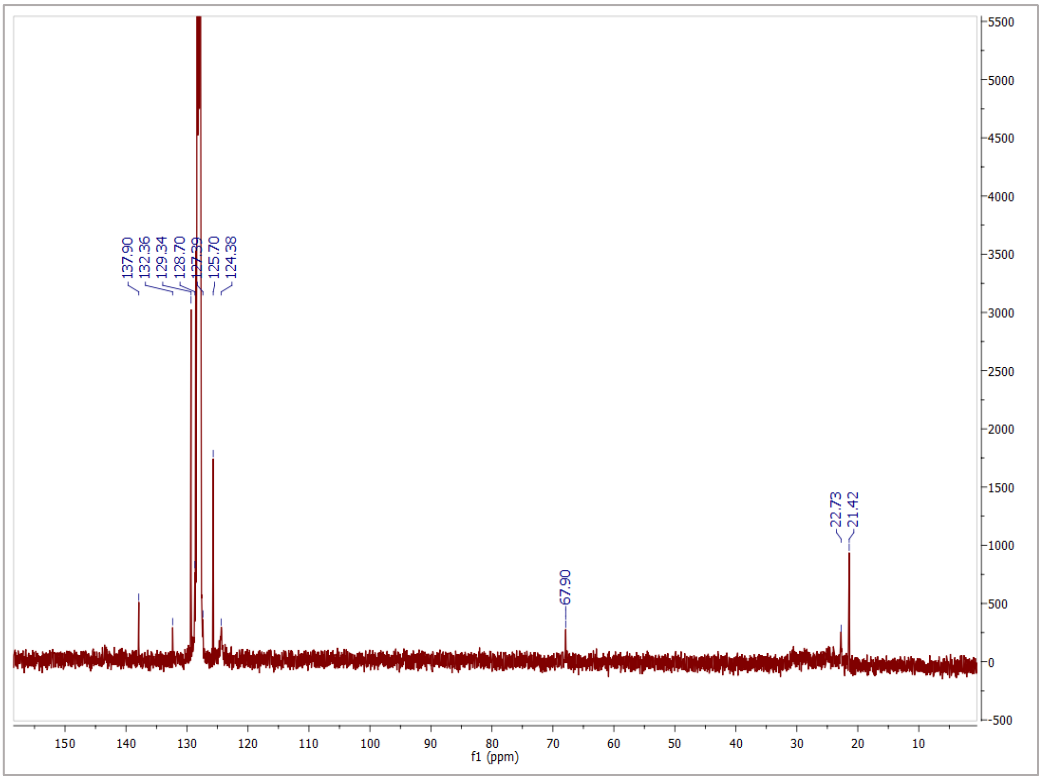

Fig. 2.7 ^{13}C NMR spectrum of [Sm_2(DippForm)$_4$(COT)]·4C_6D_6 (**3**)

2.3.2 X-ray Crystal Structures

2.3.2.1 [Sm(DippForm)(COT)(THF)$_2$] ***1***

Complex **1** crystallizes in orthorhombic space group *P*$2_12_12_1$. The planar COT^{2-} ligand binds in an η^8-coordination fashion while one DippForm ligand binds in κ^1: κ^1 fashion to the samarium atom, along with two coordinating THF molecules. The samarium atom to COT^{2-} ring centroid distance is 1.957 Å while the angle between the samarium atom and COT^{2-} plane is 88.83°. The Sm-COT^{2-} (centroid) distance is slightly longer compared to that of a similar complex [Sm(COT)Cp*$_2$], which is 1.838 Å.[43] The same trend can be seen in the case of average Sm-C(COT) distance, which is 2.663 Å for complex **1** and 2.558 Å for [Sm(COT)Cp*$_2$]. Moreover, the Sm-N bond lengths are marginally shorter [between 2.542(4) Å & 2.545(4) Å] compared with the divalent starting material [Sm(DippForm)$_2$(THF)$_2$] [2.529(4) Å & 2.617(4) Å], suggesting the trivalent oxidation state for all the samarium atoms. This is attributed to the high Lewis acidity of the Sm^{3+} and smaller ionic radius compared with Sm^{2+}.[44]

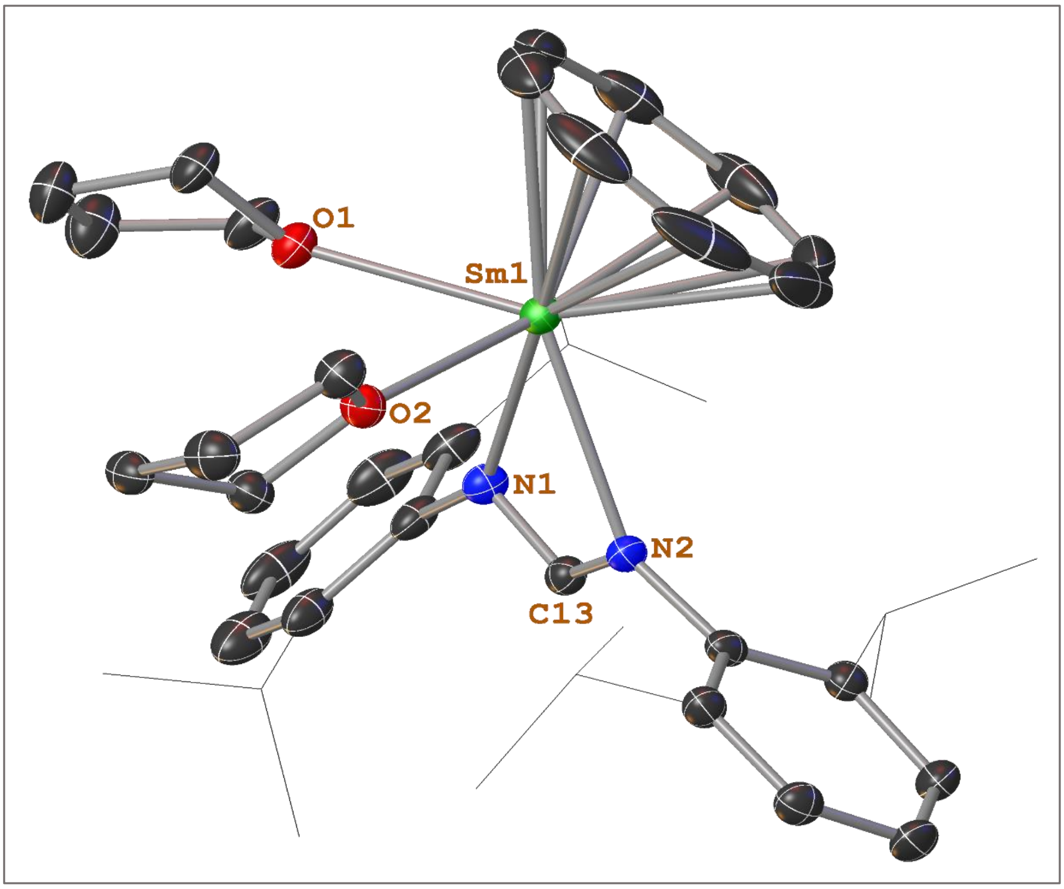

Fig. 2.6 ORTEP diagram of complex **1** in which relevant atoms are labelled. Thermal ellipsoids are drawn at a 50% probability level. Isopropyl groups of DippForm are shown as lines and hydrogen atoms are omitted for clarity. Selected bond angles (°) and lengths (Å): Sm1-COT(cen) 1.957, Sm-O1 2.553(4), Sm-O2 2.495(3), Sm-N1 2.542(4), Sm-N2 2.545(4), N1-C13 1.322(6), N2-C13 1.310(6), C13-N2-Sm 93.0(3), N2-C13-N1 120.6(4), N1-C13-Sm 60.3(2).

2.3.2.2 [Sm(DippForm)$_2$(O-C$_4$H$_8$-DippForm)(THF)]·THF (**2**)

The X-ray crystal structure of complex **2** was solved and refined in the triclinic space group *P*-1 with two lattice THF molecules in the asymmetric unit. Two DippForm ligands are $\kappa^1 : \kappa^1$ coordinated to the samarium atom whereas the third DippForm creates a new N-C bond with a butoxide component, which was a result of the ring-opening of one of the two coordinating THF molecules. There is a significant difference in the Sm-O bond lengths between coordinating THF [2.481(4) Å] and ring-opened THF unit [2.064 (4) Å], in which the latter is comparable to the usual Sm-O bond distance for samarium-amidinate alkoxides. This indicates the anionic character of the ring-opened THF component. These bond lengths are very similar to [Cp*Sm(O-$C_4H_8C_5Me_5$)THF],[40] in which Sm-O bond lengths or coordinating THF and ring-opened THF are 2.49 (1) Å and 2.08 (2) Å respectively. Here again, the Sm-N bond lengths are slightly shorter [2.436(4) Å & 2.531(4) Å] compared with the divalent starting material [Sm(DippForm)$_2$(THF)$_2$] [2.529(4) Å & 2.617(4) Å] reflecting the smaller Sm^{3+} compared with Sm^{2+}.[44]

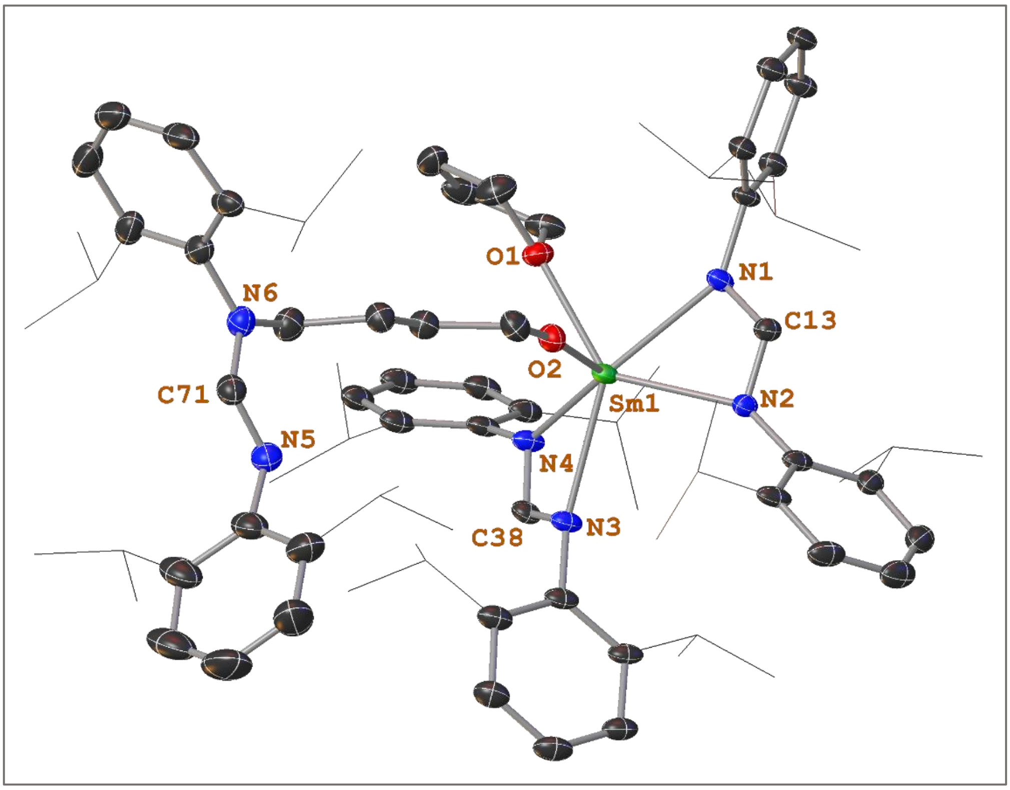

Fig. 2.7 ORTEP diagram of complex **2** in which relevant atoms are labelled. Thermal ellipsoids are drawn at a 50% probability level. Isopropyl groups of DippForm are shown as lines and hydrogen atoms along with two lattice THF are omitted for clarity.[45] Selected bond angles (°) and lengths (Å): Sm1-O2 2.064(4), Sm1-N2 2.453(5), Sm1-O1 2.481(4), Sm1-N1 2.470(4), Sm1-N4 2.436(5), Sm1-N3 2.531(4), N2-C13 1.321(7), N1-C13 1.334(7), N6-C58 1.448(9), N4-C38 1.328(7), N3-C38 1.317(8), N6-C71 1.360(9),

N5-C71 1.281(9), O2-Sm1-O1 85.73(16), N2-Sm1-N1 55.26(15), N4-Sm1-N3 54.52(15), C55-O2-Sm1 171.7(4), C13-N2-Sm1 92.0(3), C71-N6-C58 119.5(6), C71-N6-C67 119.8(5), C67-N6-C58 120.5(6), C38-N4-Sm1 95.2(3), C38-N3-Sm1 91.2(3), N2-C13-N1 118.6(5), N3-C38-N4 118.8(5), N5-C71-N6 123.9(6).

*2.3.2.3 [Sm_2(DippForm)$_4$(COT)]·4C_6D_6 (**3**)*

Complex **3** crystallizes in triclinic space group *P*-1 with four lattice deuterated benzene molecules in the asymmetric unit, and there is a disorder in one of the isopropyl groups of a DippForm ligand. This bimetallic inverse sandwich complex contains a COT^{2-} ligand at the centre which is η^8-coordinated to two samarium atoms on either side. In addition, each samarium atom is ligated by two DippForm moieties. The distance between Sm and COT^{2-} ring centroid is 2.217 Å and 2.219 Å, which is longer compared to their non-bridging counterparts in complex **1** (1.957 Å). This difference is expected between the terminal and bridging COT^{2-} ligands. Like the previous two structures, Sm^{III}-N bond lengths are slightly shorter [2.437(4) Å & 2.541(4) Å] compared to [Sm^{II}(DippForm)$_2$(THF)$_2$].

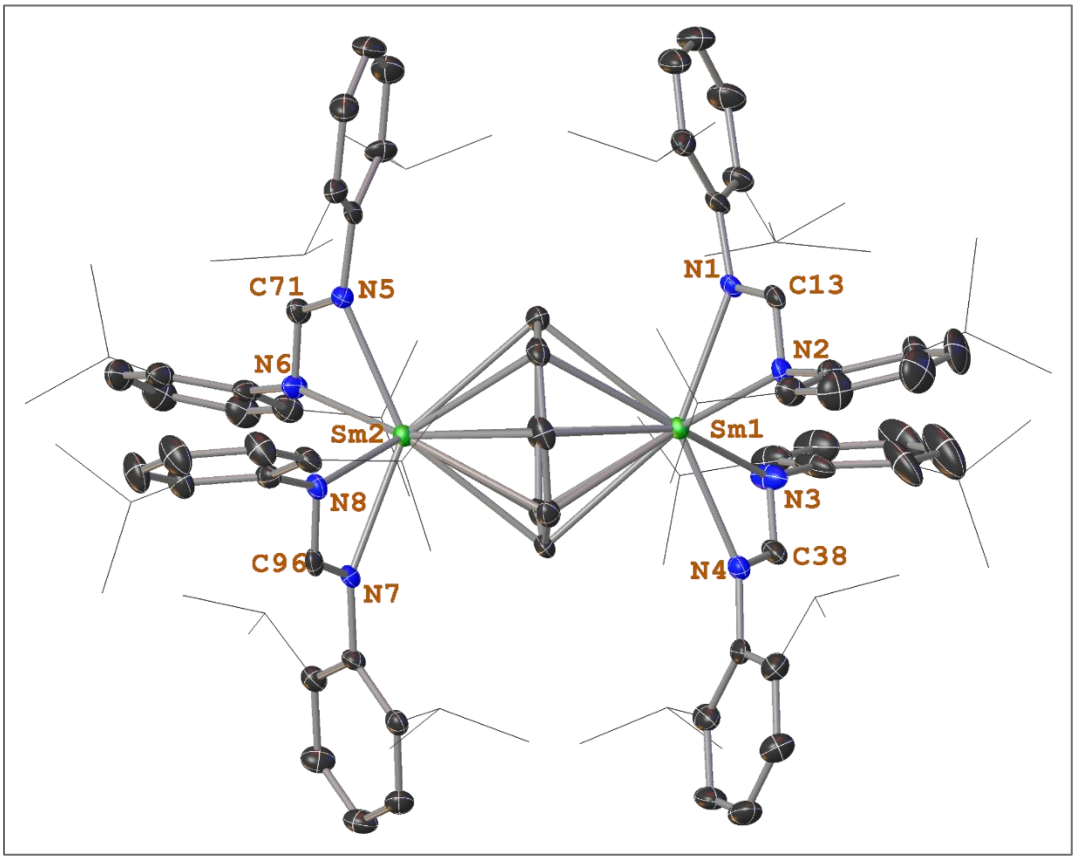

Fig. 2.8 ORTEP diagram of complex **3** in which relevant atoms are labelled. Thermal ellipsoids are drawn at a 50% probability level. Isopropyl groups of DippForm are shown as lines and hydrogen atoms along with four lattice benzene molecules are omitted for clarity. Selected bond angles (°) and lengths (Å): Sm1-COT(cen) 2.218, Sm2-COT(cen) 2.221, Sm1-N1 2.447(4), Sm1-N2 2.534(4), Sm1-N3 2.511(4), Sm1-N4 2.458(4), Sm2-N5 2.440(4), Sm2-N6 2.541(4), Sm2-N7 2.437(4), Sm2-N8 2.525(4), N1-Sm1-N2 54.98(12), N4-Sm1-N3 55.03(13), N7-Sm2-N8 55.25(12), N5-Sm2-N6 55.06(12).

2.3.3 Discussion

The high reactivity of COT towards acceptance of two electrons was easily visible from the instant colour change of the reaction mixture to red. The products resulting from the reaction in THF were similar to those obtained in previous work with [SmCp*$_2$] carried out by Evans *et al* (**Scheme 2.7b**)[30], where they obtained [SmCp*COT] and sterically bulkier [SmCp*$_3$]. In a later publication by Evans *et al* [SmCp*$_3$] was shown to ring-open THF due to the steric bulk and form product **C** (in **Scheme 2.7b**), which is analogous to our ring-opened THF complex **3**.[31] This shifted our focus to the missing piece of the puzzle, namely detection of [Sm(DippForm)$_3$]. To avoid the ring-opening of THF, the reaction was attempted in the typically non-coordinating solvent, toluene, hoping to see the formation of this desired *tris*-homoleptic samarium complex. A previous synthesis of this tris(formamidinato)samarium(III) complex was also reported in toluene supporting this decision.[46] Surprisingly, the result was the formation of complex **3**, which is quite interesting as that was the primary target. Another approach was treating [Sm(DippForm)$_3$] in THF, expecting a reaction similar to the one illustrated in scheme **2.7a** (**B** → **C**). However, no reaction was observed even after heating the reaction mixture for a few days. These outcomes forced us to disregard the theory of the formation of [Sm(DippForm)$_3$] as an intermediate in this reaction pathway.

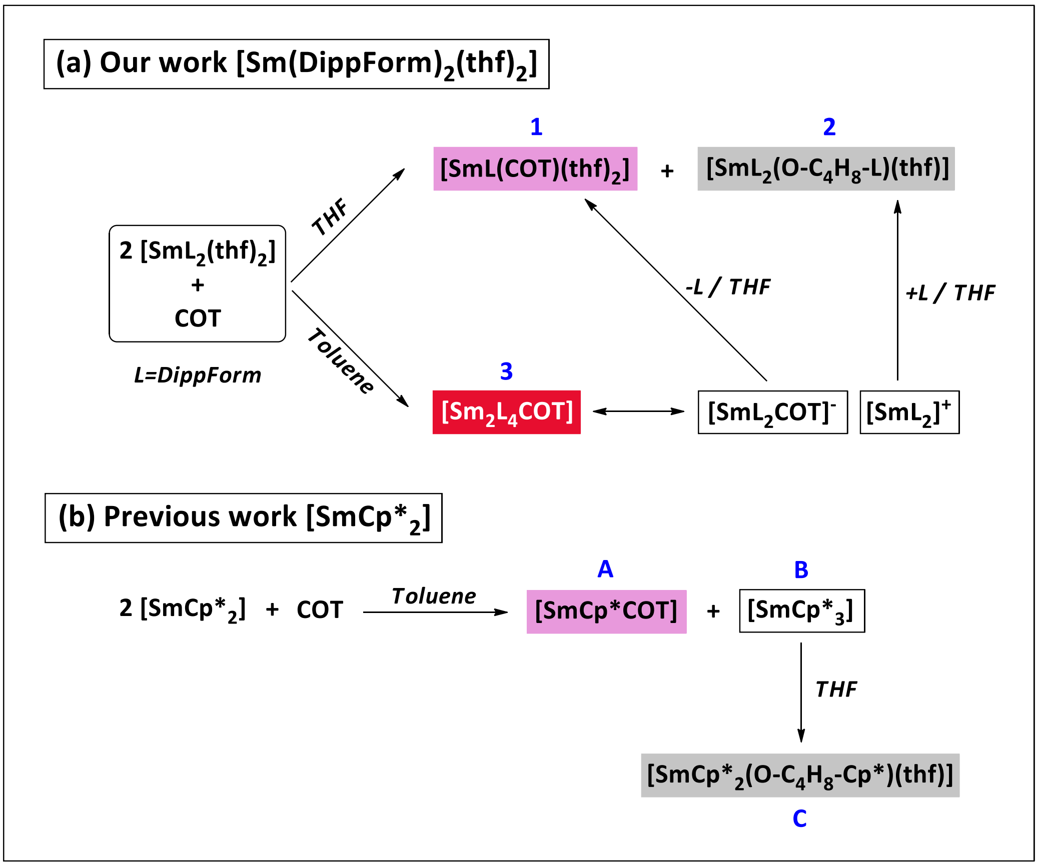

Scheme 2.7 (a) Reaction of COT with [Sm(DippForm)$_2$(THF)$_2$] (*Our work*). (b) Reaction of COT with [SmCp*$_2$] *(Previous work)*.

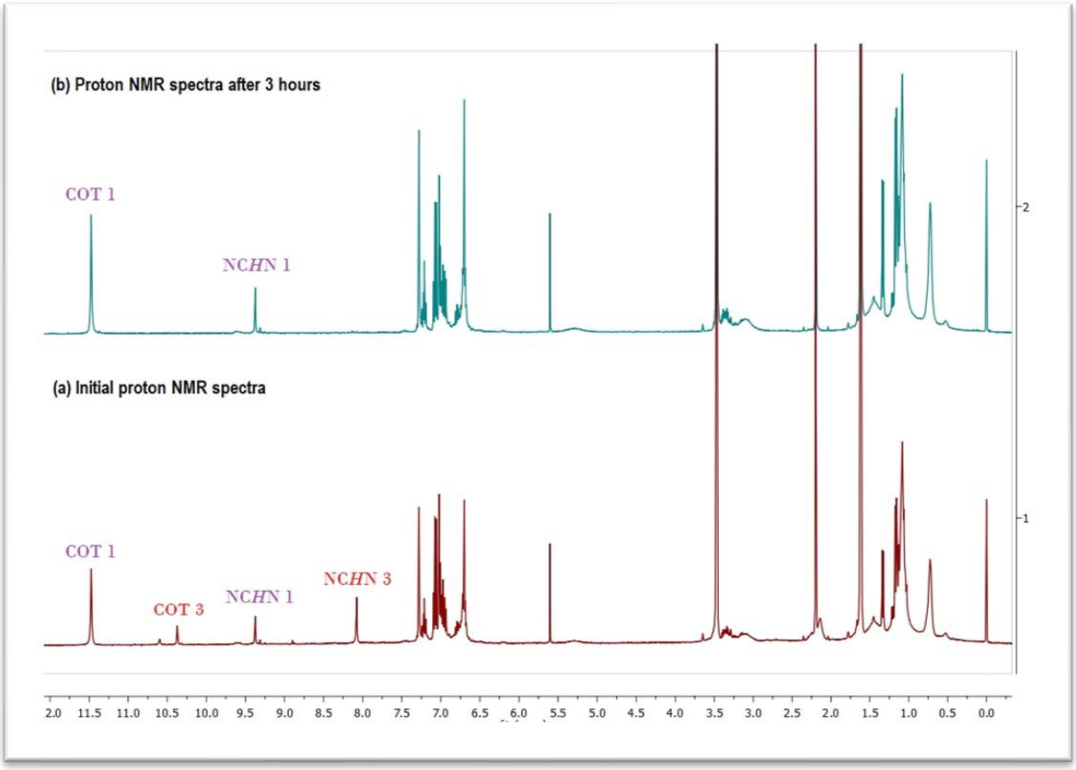

Fig. 2.9 ^{1}H NMR of complex **3** in d$_8$-THF (a) initially and (b) after 3 hours.

Having these results in hand, unravelling the chemistry occurring in the reactions performed herein was reasonably straightforward. The immediate, red-coloured solution obtained before turning purple during the synthesis of complex **1** signalled the possibility of the initial formation of red complex **3**. To confirm this, d$_8$-THF was added to crystals of complex **3** in an NMR tube and the reaction was monitored by ^{1}H NMR spectroscopy. **Figure 2.9** depict the stacked ^{1}H NMR spectra where the lower portion (a) shows initial reaction spectra, and the upper part (b) is the spectrum taken after three hours. Since the reaction is fast, **Figure 2.9a** shows the presence of both complex **1** and **3** as the signals of trapped COT^{2-} ring and DippForm backbone (NC*H*N) are evident from the spectrum. The disappearance of signals of **3** and increased intensity of complex **1** signals after three hours **(Fig 2.9b)** indicates the formation of **1** from **3**. In addition, we also witnessed a colour change in the solution from red to purple. The presence of complex **2** was also detected using ^{1}H NMR spectroscopy after repeating the reaction in bulk scale. We do however consider the reaction irreversible because the formation of ring-opened THF would hinder the reverse reaction. These observations point toward chemistry in which the reductive trapping triggers the formation of two products in equilibrium as shown in **Scheme 2.7b**. So, complex **3** can be a precursor of a charge-separated species and it probably exists as $[Sm(DippForm)_2]^+[Sm(DippForm)_2COT]^-$ in THF, where the anion loses one DippForm to form complex **1.** On the other hand, the cation acts as Lewis acid which activates THF to nucleophilic ring-opening and results in the formation of an oxonium ion component, which later binds with the remaining DippForm to give complex **2**. The chemistry of nucleophilic ring-opening of THF is explained in the introduction part of this chapter.

2.4 Conclusions & Future Outlook

The results obtained in this chapter underline the fact that [Sm(DippForm)$_2$(THF)$_2$] is a potential divalent reagent in the reductive trapping of aromatic hydrocarbons. It also demonstrated the remarkably similar reactivity between well-known divalent complex [SmCp*$_2$] and its N- donor alternative [Sm(DippForm)$_2$(THF)$_2$], which yielded the syntheses of similar reaction products upon treatment with COT in THF. These observations demonstrate that DippForm$^-$ is a very suitable substitute for the Cp*$^-$ ligand. Interestingly, the change of solvent for the same reaction resulted in the encapsulation of a planar COT^{2-} ligand flanked by two η^8-bound trivalent samarium moieties forming a bimetallic inverse sandwich complex. These findings point to the possibility of [Sm(DippForm)$_2$(THF)$_2$] acting as a successor for [SmCp*$_2$] with much more versatile reaction chemistry and the promise to have an exciting future in reduction chemistry along the lines of the cyclopentadienyl chemistry of [SmCp*$_2$].

These studies can be expanded to other unsaturated hydrocarbons and two promising ligands among them are phenyl acetylene and 2,3,4,5-tetraphenyl fulvene. The reaction of [Sm(DippForm)$_2$(THF)$_2$] with phenylacetylene resulted in a colour change to brown and two types of crystals were obtained from the solution. Unfortunately, both were poorly diffracting and no interpretable data was able to be obtained. The reaction with 2,3,4,5-tetraphenyl fulvene also resulted in a colour change to brown but attempts to obtain crystals were futile. Treatment of [Sm(DippForm)$_2$(THF)$_2$] with related nitrogen heterocycles phenazine and acridine also resulted in a change in the solution colour to yellowish green and reddish brown respectively. Here again, failure to obtain characterizable crystals restricted further advancement. These promising results suggest the necessity of further investigations in this area, which will lead to interesting outcomes in future.

2.5 Experimental

2.5.1 General Considerations

The lanthanoid compounds described here are highly air and moisture sensitive and were prepared and handled with vacuum-nitrogen line techniques and in a dry box in an atmosphere of purified nitrogen. [Sm(DippForm)$_2$(THF)$_2$] was prepared by the literature method.[45] Lanthanoid metals were from Santoku/Molycorp/Eutectix. Large chunks were filed in the drybox before use. Solvents (THF, C_6D_6, toluene, hexane) were pre-dried by distillation over sodium or sodium benzophenone ketyl before being stored under an atmosphere of nitrogen. Cyclooctatetraene (COT) was purchased from Sigma Aldrich, degassed and stored over dried 4Å molecular sieves. IR spectra were recorded as Nujol mulls between NaCl plates using an Agilent Technologies Cary 630 FTIR instrument within the range 4000–700 cm^{-1}. ^{1}H NMR and ^{13}C NMR spectra were recorded with a Bruker 400MHz instrument. Chemical shifts were referenced to the residual ^{1}H resonances of the deuterated solvents (^{1}H). Microanalyses were determined by the Chemical Analysis Facility, Macquarie University, and all the samples were sealed in tubes under nitrogen. Melting points were determined in sealed glass capillaries under nitrogen and are uncalibrated. Crystals were immersed in viscous hydrocarbon oil and were measured on a Rigaku SynergyS diffractometer or the MX1 beamline at the Australian Synchrotron.

2.5.2 General Procedure

COT (0.09mmol) was added dropwise to a Schlenk charged with [Sm(DippForm)$_2$(THF)$_2$] (0.18mmol) in 5mL of THF (for **1** and **2**) / Toluene (for **3**) at room temperature under nitrogen atmosphere, and left undisturbed for one day.

2.5.3 [Sm(DippForm)(COT)(THF)$_2$] 1

Purple crystals were obtained after layering the reaction mixture with hexane followed by concentrating the solution in vacuo. (0.0196 g, 28.56%), (Found: C, 64.57; H, 8.69; N, 5.60; $C_{41}H_{59}N_2O_2Sm$ (762.25) requires C, 64.60; H, 7.80; N, 3.67 %). IR (Nujol): 2722m, 1667w, 1526s, 1324m, 1312m, 1285s, 1251m, 1188m, 1099w, 1054m, 1030m, 1008m, 927w, 889m, 873m, 770m, 758m, 722m, 705s cm $^{-1}$. ^{1}H NMR (C_6D_6, 300 MHz): 10.93 (s, 8H, $C_8\boldsymbol{H}_8$), 8.31 (s, 1H, NC***H***N), 7.4 - 7.0 (m, 6H, aromatic Hs), 3.79 (8H, THF: 2,5-C$\boldsymbol{H}_2$), 2.55 (m,4H, Dipp-C***H***), 1.56 (8H, THF: 3,4-C$\boldsymbol{H}_2$), 1.16 – 1.18 (m, 24H, Dipp-C$\boldsymbol{H}_3$). ^{13}C NMR (75.5 MHz, C_6D_6, 296K): 24.63 (Dipp-***C***H$_3$), 25.95 (THF: 3,4-***C***H$_2$), 30.06 (Dipp-***C***H), 71.82 (THF: 2,5-***C***H$_2$), 82.58 ($\boldsymbol{C}_8H_8$), 123.52, 124.48, 141.14, 143.97 (aromatic C resonances – not assigned)

2.5.4 [Sm(DippForm)$_2$(O-C_4H_8-DippForm)(THF)]·THF (2)

Colourless crystals were obtained after concentrating the supernatant solution separated from the product **1** crystals and keeping in refrigerator overnight. (0.0254 g, 20.3%), M.p. 210°C, (Found: C, 71.91; H, 9.46; N, 5.83; $C_{83}H_{121}N_6O_2Sm$ (1385.25) requires C, 72.60; H, 9.31; N, 5.71 %). IR (Nujol): 2723w, 1666m, 1637s, 1587m, 1525s, 1361m, 1319s, 1279s, 1235m, 1190m, 1112s, 1072m, 1056m, 1044m, 1030m, 933m, 873w, 800m, 767w, 755s cm $^{-1}$. ^{1}H NMR (C_6D_6, 300 MHz): 9.67 (s, 2H, Dipp-NC***H***N), 7.36 (s, 1H, Dipp-NC***H***N: RO-THF), 7.25 (m, 2H, N-C$\boldsymbol{H}_2$: RO-THF), 7.24 - 6.8 (m, 18H, aromatic Hs), 5.36 (m, 2H, C$\boldsymbol{H}_2$: RO-THF), 4.42 (m, 2H, C$\boldsymbol{H}_2$: RO-THF), 3.69 & 3.61 (2H+2H, Dipp-C***H***: RO-THF), 3.5 - 3.1 (8H, Dipp-C***H***), 2.89 (4H, THF-C$\boldsymbol{H}_2$), 2.73 (2H, C$\boldsymbol{H}_2$: RO-THF), 1.5 – 0.8 (24H, Dipp-C$\boldsymbol{H}_3$:RO-THF; 48H, Dipp-C$\boldsymbol{H}_3$; 4H, THF-C$\boldsymbol{H}_2$). ^{13}C NMR (75.5 MHz, C_6D_6, 296K): 14.32, 23.04, 23.90, 24.51, 25.36, 28.59, 28.82, 31.96, 34.78, 51.58, 68.31, 72.59, 123.16, 123.25, 123.50, 123.55, 124.02, 124.71, 132.39, 139.97, 142.72, 145.49, 148.47, 151.56.

2.5.5 [Sm$_2$(DippForm)$_4$(COT)]·4C_6D_6 (3)

Red crystals were obtained in toluene/C_6D_6 after concentrating the solution and leaving it overnight at room temperature. (0.102g, 71.2%), (Found: C, 69.87; H, 8.61; N, 6.01; $C_{108}H_{148}N_8Sm_2$ (1859.1) requires C, 69.77; H, 8.02; N, 6.03%). IR (Nujol): 3060m, 2728w, 1665m, 1594m, 1517s, 1363m, 1337m, 1289s, 1255m, 1235m, 1190s, 1116m, 1081w, 1056m, 1030m, 1018m, 932m, 907w, 798m, 764m, 764s, 754s, 741s, 728s, 694m cm $^{-1}$. ^{1}H NMR (C_6D_6, 300 MHz): 10.71 (s, 4H, NC***H***N), 8.34 (s, 8H, $C_8\boldsymbol{H}_8$), 7.2 - 6.9 (m, 24H, aromatic Hs), 2.35 (m,16H, Dipp-C***H***), 2.11 (Toluene-C$\boldsymbol{H}_3$), 1.5 - -2.0 (Dipp-C$\boldsymbol{H}_3$). ^{13}C NMR (75.5 MHz, C_6D_6, 296K): 21.42 (Toluene: ***C***H$_3$), 22.73 (Dipp- ***C***H$_3$), 67.90 ($\boldsymbol{C}_8H_8$), 125.70 (Toluene: ***C***H(4)), 128.70 (Toluene: ***C***H(3,5)), 129.34 (Toluene: ***C***H(2,6)), 137.90 (Toluene: ***C***H(1)), 124.38, 127.39, 132.90 (aromatic C resonances – not assigned).

2.6 X-ray crystal data

Single crystals coated with viscous hydrocarbon oil were mounted on glass fibres or loops. Complex **1** was measured at the Australian Synchrotron on the MX1 macromolecular beamlines, data integration was completed using Blue-ice[47] and XDS[48] software programs. Complexes **2** and **3** were measured on a Rigaku SynergyS diffractometer. The SynergyS operated using microsource Cu-Kα radiation (λ = 1.54184 Å) for **2** and Mo-Kα radiation (λ = 0.71073 Å) for **3** at 123 K. Data processing was conducted using CrysAlisPro.55 software suite.[49] Structural solutions were obtained by either direct methods[50] or charge flipping[49] methods and refined using full-matrix least-squares methods against F^2using SHELX2015,[51] in conjunction with Olex2[49] graphical user interface. All hydrogen atoms were placed in calculated positions using the riding model. Crystal data and refinement details are given in **Table 2.1**. X-ray crystal data were collected by my colleagues Owen Beaumont (for **1** and **2**) and Dr. Zhifang Guo (for **3**). Dr. Zhifang Guo solved and refined the X-ray structures of all three complexes.

Table 2.1 Crystal data and structural refinement for lanthanoid complexes **1-3**

	1	2	3
Formula	$C_{41}H_{59}N_2O_2Sm$	$C_{87}H_{129}N_6O_3Sm$	$C_{132}H_{172}N_8Sm_2$
M_r	762.25	1457.30	2171.47
Crystal System	Orthorhombic	Triclinic	Triclinic
Space group	$P2_12_12_1$	P-1	P-1
a (Å)	10.842(2)	12.6902(4)	15.9605(2)
b (Å)	18.607(4)	17.9896(7)	17.7059(2)
c (Å)	18.765(4)	20.6655(4)	21.0634(3)
α (°)	90	97.357(2)	95.1820(10)
β (°)	90	103.624(2)	96.0570(10)
γ (°)	90	108.342(3)	98.3200(10)
V (Å^3)	3785.6(13)	4246.3(2)	5823.06(13)
Z	4	2	2
ρ_{calc}, g cm^{-3}	1.337	1.141	1.238
μ, mm^{-1}	1.586	5.551	1.050
N_τ	47416	76924	20432
N (R_{int})	7196 (0.0654)	16575(0.1189)	20432 (-)
R_1($I > 2\sigma(I)$)	0.0292	0.0763	0.0448
wR_2 (all data)	0.0767	0.1908	0.1069
GOF	1.040	1.072	1.140

2.7 References

1. W. J. Evans, *Inorg. Chem.*, 2007, **46**, 3435-3449.
2. W. J. Evans, T. A. Ulibarri and J. W. Ziller, *J. Am. Chem. Soc.*, 1990, **112**, 219-223.
3. W. J. Evans, *Polyhedron*, 1987, **6**, 803-835.
4. W. J. Evans, *J.Organomet. Chem.*, 1983, **250**, 217-226.
5. P. S. Skell and M. J. Mcglinchey, *Angew. Chem. Int. Edit.*, 1975, **14**, 195-199.
6. W. J. Evans, S. C. Engerer and A. C. Neville, *J. Am. Chem. Soc.*, 1978, **100**, 331-333.
7. W. J. Evans, S. C. Engerer and K. M. Coleson, *J. Am. Chem. Soc.*, 1981, **103**, 6672-6677.
8. W. J. Evans, K. M. Coleson and S. C. Engerer, *Inorg. Chem.*, 1981, **20**, 4320-4325.
9. J. R. Blackborow and D. Young, *Metal vapour synthesis in organometallic chemistry*, Springer-Verlag, Berlin ; New York, 1979.
10. W. J. Evans, L. A. Hughes, D. K. Drummond, H. M. Zhang and J. L. Atwood, *J. Am. Chem. Soc.*, 1986, **108**, 1722-1723.
11. W. J. Evans, I. Bloom, W. E. Hunter and J. L. Atwood, *J. Am. Chem. Soc.*, 1983, **105**, 1401-1403.
12. W. J. Evans, R. A. Keyer, H. Zhang and J. L. Atwood, *J. Chem. Soc., Chem. Commun.*, 1987, 837-838.
13. W. J. Evans and T. A. Ulibarri, *J. Am. Chem. Soc.*, 1987, **109**, 4292-4297.
14. W. J. Evans, D. G. Giarikos, C. B. Robledo, V. S. Leong and J. W. Ziller, *Organometallics*, 2001, **20**, 5648-5652.
15. J. M. Boncella, T. D. Tilley and R. A. Andersen, *J. Chem. Soc., Chem. Commun.*, 1984, 710-712.
16. Q. Shen, D. S. Zheng, L. Lin and Y. H. Lin, *J.Organomet. Chem.*, 1990, **391**, 307-312.
17. H. Zhou, H. D. Guo, Y. M. Yao, L. Y. Zhou, H. M. Sun, H. T. Sheng, Y. Zhang and Q. Shen, *Inorg. Chem.*, 2007, **46**, 958-964.
18. W. J. Evans, L. A. Hughes and T. P. Hanusa, *J. Am. Chem. Soc.*, 1984, **106**, 4270-4272.

19. W. J. Evans, S. L. Gonzales and J. W. Ziller, *J. Am. Chem. Soc.*, 1994, **116**, 2600-2608.

20. C. M. Kotyk, M. R. MacDonald, J. W. Ziller and W. J. Evans, *Organometallics*, 2015, **34**, 2287-2295.

21. M. Tsutsui, *Fundamental research in homogeneous catalysis, volume 3 : [proceedings of the First International Conference on Homogeneous Catalysis, held in Corpus Christi, Texas, November 1978]*, Plenum Press, New York, 1979.

22. C. K. Mann and K. K. Barnes, *Electrochemical reactions in nonaqueous systems*, M. Dekker, New York,, 1970.

23. A. S. P. Frey, M. G. Gardiner, D. N. Stringer and B. F. Yates, *Organometallics*, 2007, **26**, 1299-1302.

24. K. O. Hodgson and K. N. Raymond, *Inorg. Chem.*, 1972, **11**, 3030-3035.

25. H. Schumann, J. Winterfeld, L. Esser and G. Kociokkohn, *Angew. Chem. Int. Ed.*, 1993, **32**, 1208-1210.

26. J. S. Xia, Z. S. Jin and W. Q. Chen, *J. Chem. Soc., Chem. Commun.*, 1991, 1214-1215.

27. J. J. Le Roy, L. Ungur, I. Korobkov, L. F. Chibotaru and M. Murugesu, *J. Am. Chem. Soc.*, 2014, **136**, 8003-8010.

28. T. Tsuji, N. Hosoya, S. Fukazawa, R. Sugiyama, T. Iwasa, H. Tsunoyama, H. Hamaki, N. Tokitoh and A. Nakajima, *J. Phys. Chem. C.*, 2014, **118**, 5896-5907.

29. A. Recknagel, M. Noltemeyer and F. T. Edelmann, *J.Organomet. Chem.*, 1991, **410**, 53-61.

30. W. J. Evans, S. L. Gonzales and J. W. Ziller, *J. Am. Chem. Soc.*, 1991, **113**, 7423-7424.

31. W. J. Evans, K. J. Forrestal and J. W. Ziller, *J. Am. Chem. Soc.*, 1998, **120**, 9273-9282.

32. W. J. Evans, M. A. Johnston, M. A. Greci and J. W. Ziller, *Organometallics*, 1999, **18**, 1460-1464.

33. W. J. Evans, M. A. Johnston, R. D. Clark, R. Anwander and J. W. Ziller, *Polyhedron*, 2001, **20**, 2483-2490.

34. W. J. Evans, R. D. Clark, M. A. Ansari and J. W. Ziller, *J. Am. Chem. Soc.*, 1998, **120**, 9555-9563.

35. M. E. Woodhouse, F. D. Lewis and T. J. Marks, *J. Am. Chem. Soc.*, 1982, **104**, 5586-5594.
36. S. Penczek, P. Kubisa and K. Matyjaszewski, *Adv. Polym. Sci.*, 1980, **37**, 1-144.
37. P. Dreyfuss and M. P. Dreyfuss, *Adv. Chem. Ser.*, 1969, 335-349.
38. C. Schoo, S. Bestgen, M. Schmidt, S. N. Konchenko, M. Scheer and P. W. Roesky, *Chem. Commun.*, 2016, **52**, 13217-13220.
39. Z. Guo, V. L. Blair, G. B. Deacon and P. C. Junk, *Dalton Trans.*, 2020, **49**, 13588-13600.
40. W. J. Evans, T. A. Ulibarri, L. R. Chamberlain, J. W. Ziller and D. Alvarez, *Organometallics*, 1990, **9**, 2124-2130.
41. M. L. Cole, G. B. Deacon, C. M. Forsyth, P. C. Junk, K. Konstas and J. Wang, *Chem. Eur. J.*, 2007, **13**, 8092-8110.
42. A. Solovyev, S. J. Geib, E. Lacote and D. P. Curran, *Organometallics*, 2012, **31**, 54-56.
43. W. J. Evans, M. A. Johnston, R. D. Clark and J. W. Ziller, *J. Chem. Soc., Dalton Trans.*, 2000, 1609-1612.
44. R. D. Shannon, *Acta Crystallogr. Sect. A.*, 1976, **32**, 751-767.
45. M. L. Cole and P. C. Junk, *Chem. Commun.*, 2005, 2695-2697.
46. M. L. Cole, G. B. Deacon, C. M. Forsyth, P. C. Junk, D. P. Ceron and J. Wang, *Dalton Trans.*, 2010, **39**, 6732-6738.
47. T. M. McPhillips, S. E. McPhillips, H. J. Chiu, A. E. Cohen, A. M. Deacon, P. J. Ellis, E. Garman, A. Gonzalez, N. K. Sauter, R. P. Phizackerley, S. M. Soltis and P. Kuhn, *J. Synchrotron Radiat.*, 2002, **9**, 401-406.
48. W. Kabsch, *J. Appl. Crystallogr.*, 1993, **26**, 795-800.
49. O. V. Dolomanov, L. J. Bourhis, R. J. Gildea, J. A. K. Howard and H. Puschmann, *J. Appl. Crystallogr.*, 2009, **42**, 339-341.
50. G. M. Sheldrick, *Acta Crystallogr. A.*, 2008, **64**, 112-122.
51. G. M. Sheldrick, *Acta Crystallogr. C.*, 2015, **71**, 3-8

Chapter 3

Reactivity of [Ln(DippForm)$_2$(THF)$_2$] (Ln = Sm, Yb) towards substrates containing dipnictide linkages

3.1 Introduction

Reactions of unsaturated substrates with highly reactive divalent lanthanoid complexes are always impressive and the previous chapter unveiled that divalent samarium complexes can enforce several exceptional, unanticipated, and potentially effective transformations with unsaturated hydrocarbons. Substrates containing dipnictide linkages will be a topic of great interest in this area as it is expected that Ln(II) complexes can manipulate and derivatize those ligands. Among dipnictogens, the reactivity of organolanthanoid complexes towards hard N-donor ligands is a well-investigated area since they have a strong preference for them (along with O-donor ligands) due to the corresponding hard Lewis acid nature of the metal centre.[1, 2] Recently, a few studies based on soft heavier group 15 ligands also resulted in the formation of novel structures with interesting properties illustrating that such soft ligands are also useful to this fascinating chemistry.[3, 4]

Azo compounds (containing NN linkages) are often termed as highly reactive substrates and the behaviour of the N=N double bond in the vicinity of divalent lanthanoid complexes always leads to interesting outcomes. This is crystal clear from the discovery of dinitrogen trapping by [SmCp*$_2$], which is mentioned briefly in chapter 1 (**Scheme 1.2a**).[5] Previously reported examples of azo ligands for their interaction with divalent lanthanoid complexes (especially samarium(II) and ytterbium(II) complexes) are azobenzene, hydrazine, diphenylhydrazine, pyridazine and benzaldehyde azine, where these all resulted in either N-N cleavage or their retention. Among these azo compounds, interaction with azobenzene is discussed in detail in the next paragraph since it delivers much more structural and reaction factors to their reduction chemistry. The reaction of diphenylhydrazine with solvated samarocene [SmCp*$_2$(THF)$_2$] resulted in a trivalent product with NN cleavage (**Scheme 3.1a**) while retention of the azo linkage is observed during the interaction with unsolvated analogue [SmCp*$_2$] (**Scheme 3.1b**).[6] Reaction of [SmCp*$_2$] with hydrazine is also accompanied by retaining NN bonds where it forms a trivalent product [(SmCp*$_2$)$_2$(HNNH)] along with dihydrogen as a by-product (**Scheme 3.1c**).[6] Unlike dinitrogen reduction, no reductive trapping products were obtained in all these three reactions and deprotonation can be observed in the latter two reactions. Studies on the reaction of pyridazine and benzaldehyde azine with [SmCp*$_2$] resulted in reductive coupling products with C-C bond formation as shown in **Scheme 3.2.**[7] Both pyridazine and benzaldehyde azine undergo one-electron transfer to give intermediate radicals which dimerize without going through further reduction to form trivalent samarium complexes. This is different from the reduction of other multiple bonded complexes by divalent samarocene [SmCp*$_2$(THF)$_2$], where usually two-electron reduction is observed. [8-11]

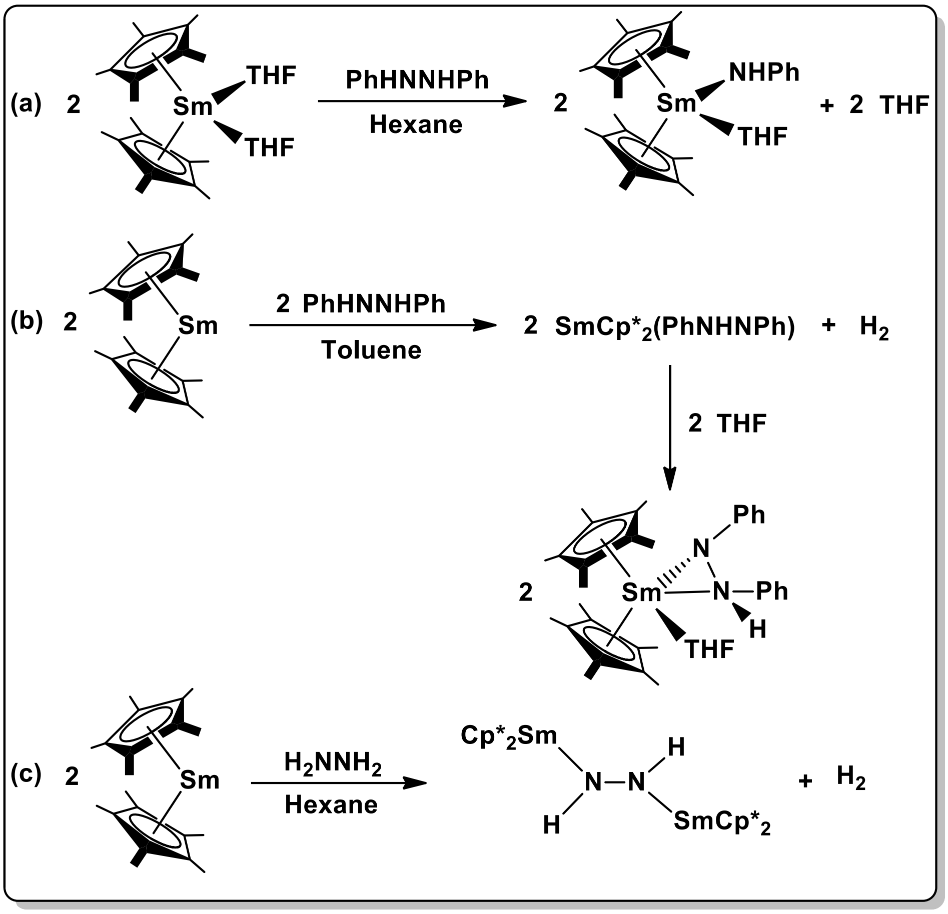

Scheme 3.1. The reaction of hydrazine and diphenylhydrazine with solvated samarocene [SmCp*$_2$(THF)$_2$].[6]

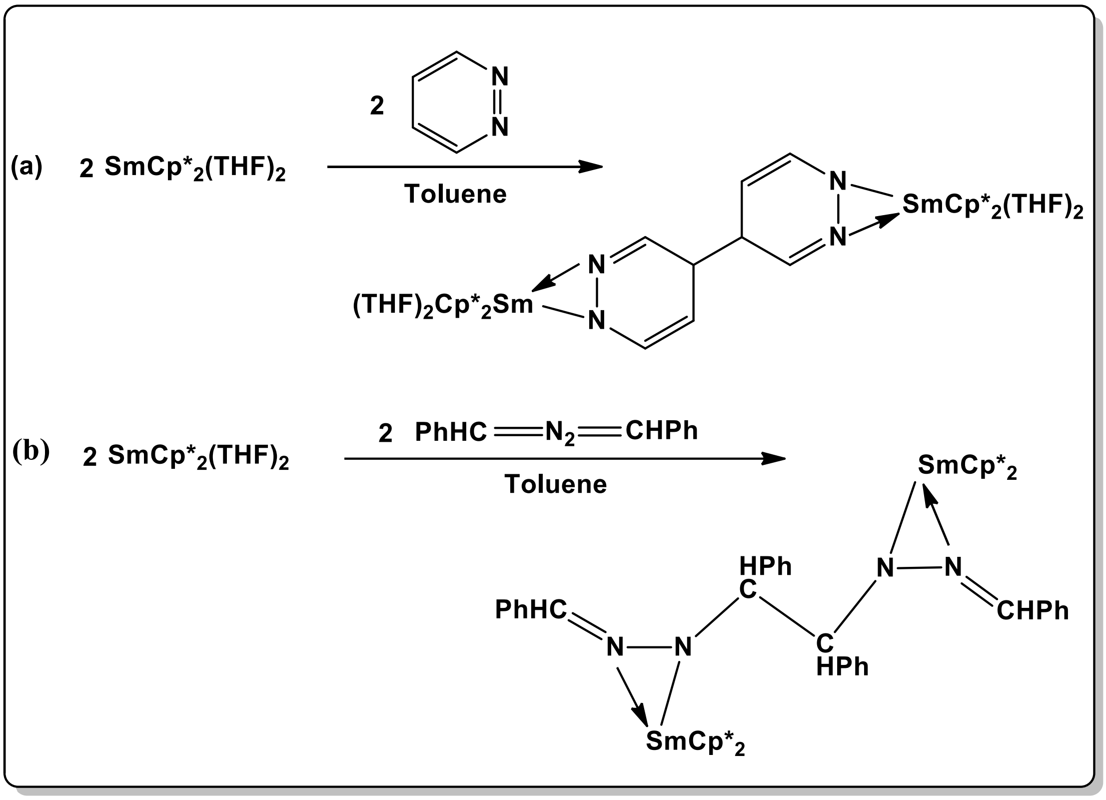

Scheme 3.2. The reaction of pyridazine and benzaldehyde azine with [SmCp*$_2$].[7]

The reaction of divalent lanthanoid complexes with soft ligands containing pnictogens also gives rise to a lot of fascinating trivalent organolanthanoid compounds. Tetraphenyl diphosphine and its other pnictogen analogues (Ph_2EEPh_2, where E = P, As, Sb & Bi) are one of the intriguing series of ligands where the versatility of the dipnictogen bond in reacting with low valent lanthanoids is quite impressive. Their reactivity toward different types of divalent organosamarium complexes is discussed in detail in the coming paragraphs. Other ligands involved in these types of reactions are polypnictides and polypnictide-containing metal/sulfur clusters. The reaction of divalent samarium and ytterbium metallocenes with cage compounds As_4S_3 and As_4S_4 resulted in the formation of closed and open core lanthanoid As/S clusters.[12] Reactivity of Ln(II) amidinates [Ln(DippForm)$_2$(THF)$_2$] (Ln = Sm, Yb) towards As_4S_4 also produces interesting trivalent organolanthanoid species.[13] Treatment of divalent lanthanocenes [Cp*$_2$Sm(THF)$_2$ and its Yb analogue] with molybdenum polyphosphides give rise to synthesis of the first 4d/4f polyphosphides.[14] Reduction of polyphosphides and polyarsenides using [Cp*$_2$Sm(THF)$_2$] also resulted in the synthesis of respective polypnictide lanthanoid complexes.[15, 16] Other interesting trivalent organosamarium complexes were obtained by treating them with [$Cp^*Fe(\eta^5\text{-}E_5)$] (E = P, As)[17] and [$(Cp'''Co)_2(\mu,\eta^{2:2}\text{-}P_2)_2$] (Cp''' = 1,2,4-$tBu_3C_5H_2$)[18] where we can see a formation of intramolecular P-P bond within a Co_2P_4 core in the latter case.

3.1.1 *Role of trans-azobenzene and 1H-1,2,3-benzotriazole in reductive ligand trapping*

Azobenzene is a very reactive substrate which is capable of undergoing two one-electron reductions, with a first reduction potential in the range of -1.35 to -1.41 V and the second is around -1.75 to -2.03 V (versus SCE)[19] depending on the solvent. This reagent gathered a lot of attention in the research field not only because of its high reactivity but also due to some peculiar structural features demonstrated by them. The coordination pattern of reduced azobenzene ligand (anionic $Ph_2N_2^{-}$ or a dianionic $Ph_2N_2^{2-}$ species) resulting from reduction by organolanthanoid complexes differs in many ways as it can bind through various structural motifs. **Figure 3.1** illustrates various binding modes of azobenzene moieties in Ln complexes, where each binding motif is assigned either based on the steric crowding of starting divalent lanthanoid complex or the reaction stoichiometry in other few cases.[20-29] Azobenzene has undergone two-electron reduction with organolanthanoid complexes of divalent lanthanum, samarium, ytterbium, and thulium previously, those having sterically supporting ligand systems containing cyclopentadienyl derivatives, amides and naphthalenides.[20, 22-24, 26, 28, 30] Reductive trapping of azobenzene in rare-earth chemistry is first reported by using [$Cp^*_2Sm(THF)_2$] [26], where it displayed three different binding modes out of four (**A**, **C** and **D** in **Fig. 3.1**). Analogous trapping reactions also reported by other divalent samarium complexes such as [$\{(Me_3Si)_2N\}_2Sm(THF)_2$] [28], [$Sm\{HB(3,5\text{-}Me_2Pz)_3\}_2$] (Pz = pyrazole)[31], [$(C_5Me_5)Sm_2\{OSi(O^tBu)_3\}_3$] [32], and [$Sm\{(^iPr_3Si)_2N\}_2$] [33], in which some of them are illustrated in **Fig 3.2** (a, b and e). Azobenzene is also capable of oxidising even less powerful reductant ytterbium(II), which is evident from its reaction with [$(C_5H_5)_2Yb(THF)$] [26] and [$Yb(Me_2Si)(C_5Me_4)(NPh)(THF)_3$] [23] (**Fig 3.2c**). Another example is use of huge sterically encumbered metallasilsesquioxane of divalent ytterbium which afforded formation of bulky azobenzene trapped Yb(III) complex $[Yb(Cy_7Si_7O_{11}(OSiMe_3))(THF)_2]_2(PhNNPh)$ **(Fig 3.2d)**.[34]

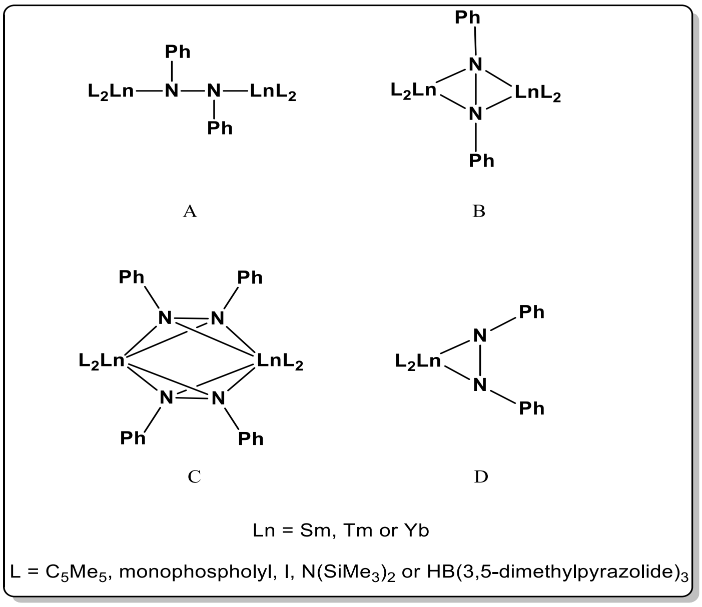

Ln = Sm, Tm or Yb

L = C_5Me_5, monophospholyl, I, $N(SiMe_3)_2$ or HB(3,5-dimethylpyrazolide)$_3$

Fig 3.1. Various coordinating patterns of azobenzene moieties.[20-29]

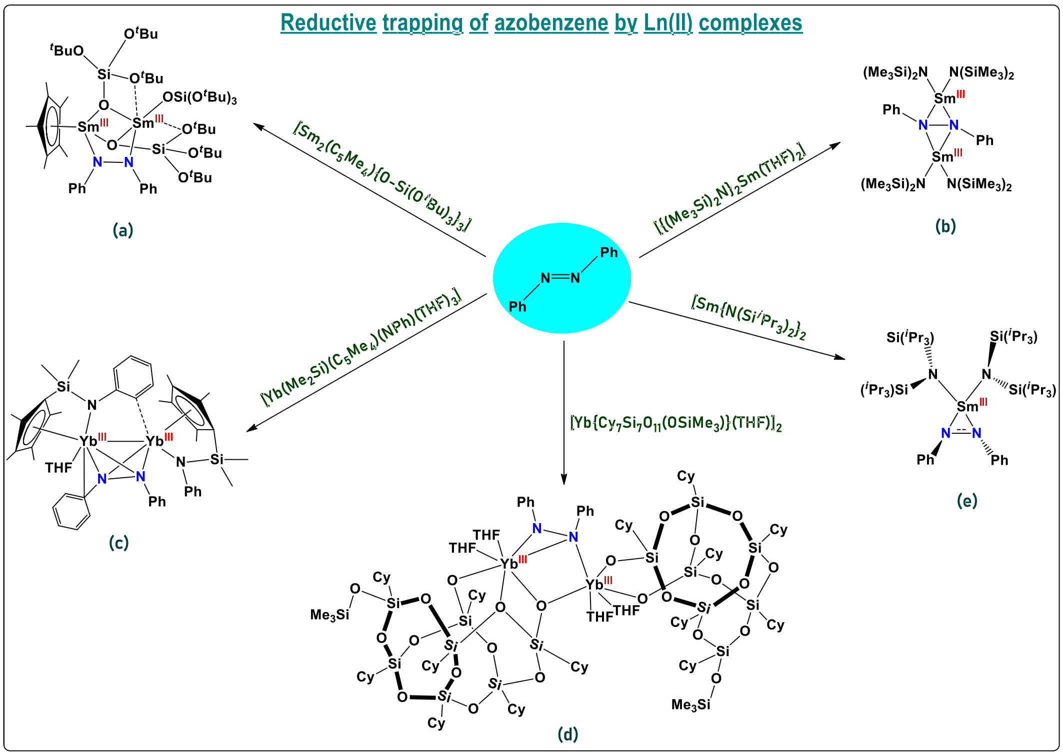

Fig 3.2. Examples of a few azobenzene trapping reactions exhibited by divalent organolanthanoid complexes.[23,31-34]

A detailed discussion regarding the reaction of azobenzene with bis(pentamethylcyclopentadienyl)samarium(II) is very important as our reagent [Sm(DippForm)$_2$(THF)$_2$] has demonstrated a parallel reaction pathway on previous occasions. Since Sm(II) has a very high reduction potential, reduction of azobenzene to both monoanionic ($Ph_2N_2^{-}$) and dianionic ($Ph_2N_2^{2-}$) forms by [Cp*$_2$Sm(THF)$_2$] will be expected. Evans *et al* performed this reaction and obtained fascinating results and remarkable crystal structures.[26] Initially, they treated azobenzene with [Cp*$_2$Sm(THF)$_2$] in a 1:1 stoichiometric ratio in toluene, which resulted in a green solution with the formation of trivalent samarium complex containing $Ph_2N_2^{-}$ anion (complex **A** in **Fig 3.3**). Here azobenzene is subjected to the one-electron reduction where both nitrogen atoms of the monoanionic and are η^2-coordinated to the samarium atom at the centre (similar to **D** in **Fig 3.1**). However, adding an excess of the reducing agent [Cp*$_2$Sm(THF)$_2$] to the first reaction or alternatively doing the same reaction in a 2:1 stoichiometric ratio (Cp*$_2$Sm(THF)$_2$:azobenzene) in toluene proceeds through a different pathway to afford complex **B** (in **Fig 3.3**) in blue solution. Unlike the first reaction, azobenzene underwent a two-electron reduction in this case where each nitrogen forms Sm-N single bond to the samarium atom, forming an unusual η^1,η^1-$Ph_2N_2^{2-}$ complex. Here the coordinating pattern is different (**A** in **Fig 3.1**) from complex **A**, demonstrating that stoichiometry could also be a factor in determining the binding modes. Finally, the addition of THF to **B** caused a colour change to orange forming a trivalent dinuclear complex of samarium with two bridged azobenzene moieties (complex **C** in **Fig 3.3**). This is due to the non-redox ligand redistribution of **B** in THF, in which the coordinating ability of the solvent effected the formation of a third structure. Here again, the coordination mode changed (similar to **D** in **Fig 3.1**) where it showed that a single *trans*-azobenzene ligand is capable of coordinating with two samarium atoms. Overall, this study using a single divalent reagent exhibited the ability of azobenzene to undergo one- and two-electron reductions and their capability to coordinate metal atoms through various binding modes.

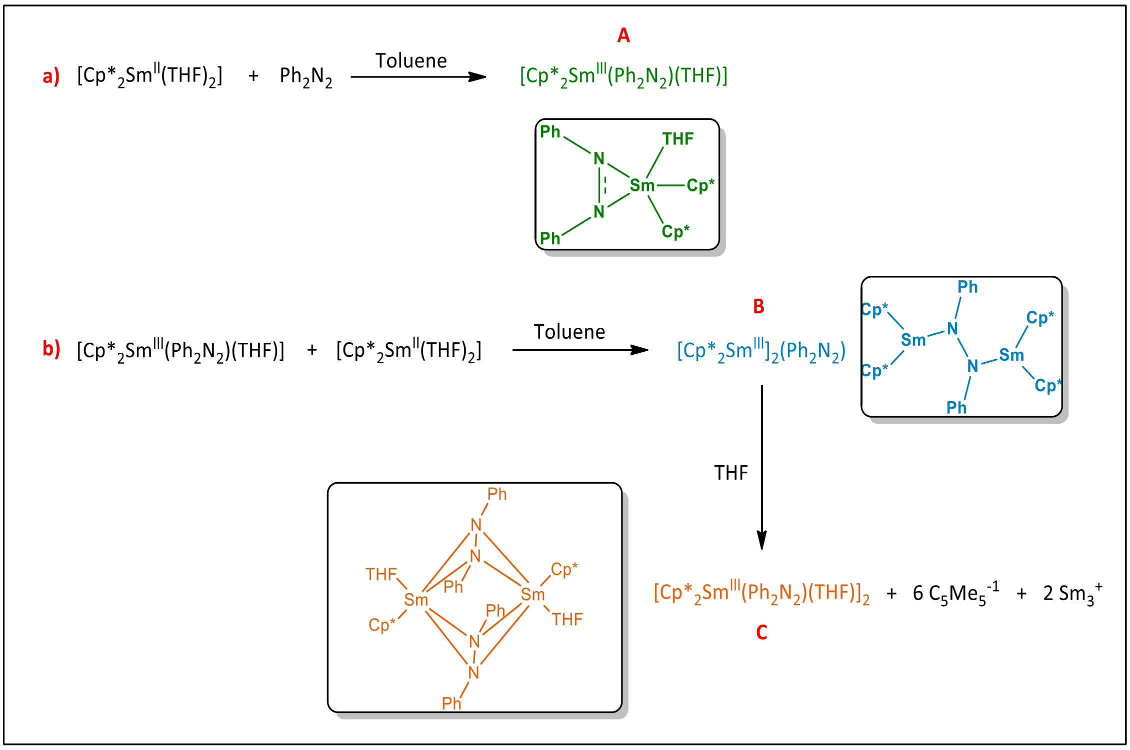

Fig 3.3. The reaction of azobenzene with $[Cp^*_2Sm(THF)_2]$ in both 1:1 (a) and 2:1 (b) stoichiometric ratio and structures of obtained products.[26]

Evans *et al* also investigated the reaction of $[Cp_2Yb(THF)]$ with azobenzene with a focus on obtaining additional details and looking for possibilities of similar chemistry in related compounds.[26] Since the samarium complex $[Cp_2Sm(THF)]_n$ was insoluble in THF and toluene,[35] its ytterbium analogue was the viable option for the studies. The reaction carried out in a 1:1 stoichiometric ratio provided an immediate colour change to green in both THF and toluene. The products they obtained were $[Cp_3Yb(THF)]$ and $[Cp(THF)Yb]_2[N_2Ph_2]_2$, and they deduced that reaction chemistry is comparable to that of the samarium-azobenzene system as shown in their proposed mechanism (**Scheme 3.1**). The structure of $[Cp(THF)Yb]_2[N_2Ph_2]_2$ is identical to complex **C** in **Fig 3.3**, where we can see two trivalent ytterbium ions bridged by two $Ph_2N_2^{2-}$ species.

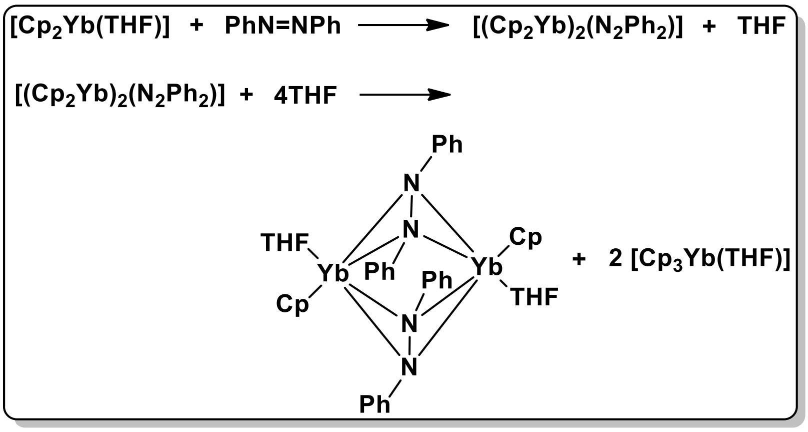

Scheme 3.1. Proposed mechanism of the reaction of [$Cp_2Yb(THF)$] with azobenzene (where Cp = C_5H_5).[26]

1*H*-1,2,3-benzotriazole (BtzH) is another ligand containing an NN linkage which could be useful in this reductive trapping application. Heterocycles containing a 1,2,3-triazole molecular skeleton have enormous applications in pharmaceutical, agrochemical and industrial fields.[36] However, compared to azobenzene, benzotriazole is new to this sort of chemistry. Even organolanthanoid complexes containing benzotriazole or benzotriazolates are very limited. Coordination polymers of rare earth benzotriazolates containing divalent and mixed valent lanthanoid metals have been reported in which BtzH is used for the stabilization of the complexes.[37, 38] Other applications include the synthesis of homoleptic rare earth 3D-benozotriazolate frameworks (MOFs),[39] high-temperature oxidations of lanthanoid metals with amines using triazolates[40] and in organometallic dysprosium single-molecular magnets (SMMs).[41, 42]

3.1.2 *Formation of organosamarium diarylpnictide complexes through reduction by divalent lanthanoid precursors*

Aryl-substituted group 15 ligands other than azobenzene have also proved to be successful in single electron transfer reactions even though comparatively few complexes were reported so far. Ligands of Ph_2EEPh_2 (E = P, As, Sb & Bi) type were reacted with low valent Ln^{2+} species resulting in coordination, E-E bond cleavage or E-C bond cleavage. E-E cleavage is the most common reaction albeit heavier pnictogens undergo E-C cleavage due to weaker bonds. In 1996, Evans *et al* reported a series of reactions where tetraphenyl diphosphide and its other pnictogen analogues were treated with both solvated and unsolvated [SmCp*$_2$] complexes (**Scheme 3.2**).[43] Both Ph_2PPPh_2 and $Ph_2AsAsPh_2$ underwent E-E cleavage leading to the trapping of diphenyl P/As species upon reaction with [SmCp*$_2$] (Eqn 1 in **Scheme 3.2**). Similar reactivity is also exhibited with solvated samarocene [SmCp*$_2$(THF)$_2$] (Eqn 2 in **Scheme 3.2**), which eventually led to nucleophilic ring opening of THF forming a butoxide component when the reaction is carried out in THF in place of toluene (Eqn 3 in **Scheme 3.2**). The formation of a dinuclear mixed-valent complex also occurred when [SmCp*$_2$] was reacted with P_2Ph_4 in a 4:1 stoichiometric ratio (Eqn 4 in **Scheme 3.2**). In addition, heavier pnictogen compounds ($Ph_2SbSbPh_2$ and $Ph_2BiBiPh_2$) were subjected to additional E-C cleavage resulting in trivalent samarium complexes where the phenyl group was trapped (Eqn 5 & 6 in **Scheme 3.2**). Recently, the reaction of another bulky Sm(II) complex [SmCp''$_2$] (Cp'' = $C_5H_3{}^tBu_2$) with tetraphenyl diphosphide was also reported which resulted in three different products (Eqn **7** in **Scheme 3.2**).[44]

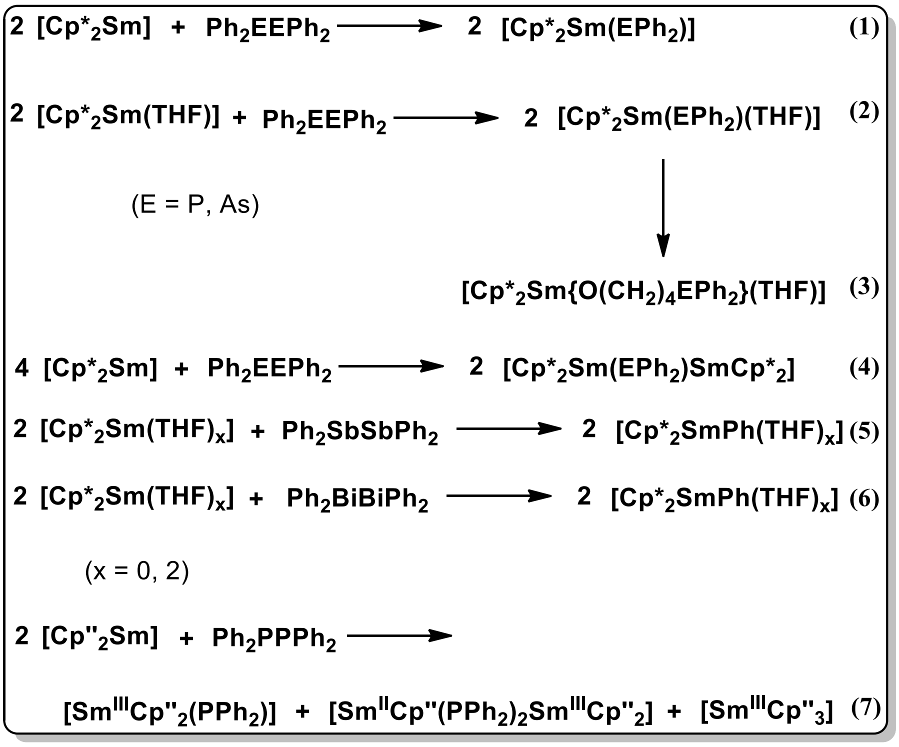

Scheme 3.2. The reaction of tetraphenyl diphosphide and its other pnictogen analogues with divalent samarium complexes.[43, 44]

3.2 Research Plan

The reactivity shown by azobenzene towards different types of divalent lanthanoid complexes is very promising. It is reasonable to assume that $[Sm(DippForm)_2(THF)_2]$ can reduce *trans*-azobenzene to its both monoanionic and dianionic forms due to the large reduction potential of divalent samarium. Its ytterbium counterpart $[Yb(DippForm)_2(THF)_2]$ can also be an interesting candidate in this anionic reductive trapping reaction even though it is not as powerful a reducing agent as samarium. Other ligands with NN linkage to be examined are 1*H*-1,2,3-benzotriazole and 4,4'-azopyridine, which are rarely used in this area and have the potential to undergo the anticipated reductive trapping chemistry. Among ligands with other dipnictide linkages, tetraphenyl diphosphide is the best choice to start with as it has already shown reacting with Sm(II) complexes in surprising ways. Its arsenic analogue As_2Ph_4 could also be useful in this application.

3.3 Results and Discussion

3.3.1 *Synthesis and characterization*

3.3.1.1 *The reaction of [Sm(DippForm)$_2$(THF)$_2$] with azobenzene in a 1:1 stoichiometric ratio*

The reaction was carried out in THF owing to the high solubility of reagents [Sm(DippForm)$_2$(THF)$_2$] and *trans*-azobenzene in this solvent. They were dissolved in THF separately and both solutions were mixed using a cannula immediately giving a dark blue solution. The solution was stirred for 24 hours and yellow/colourless crystals of **[(DippForm)$_2$Sm^{III}(Ph$_2$N$_2$)(THF)]·3THF (1)** were obtained from toluene or THF by storing the concentrated solution at -18°C for several weeks. Alternatively, DME was the better choice for more rapid crystallization since crystals of complex **1** formed within 3 days at -18°C. The reaction scheme and product structure are given below **(Scheme 3.1)**. The formation of the same product was identified when the reaction was performed in toluene in place of THF. Complex **1** is highly air and moisture sensitive, and minor exposure results in a colour change from dark blue to orange due to decomposition.

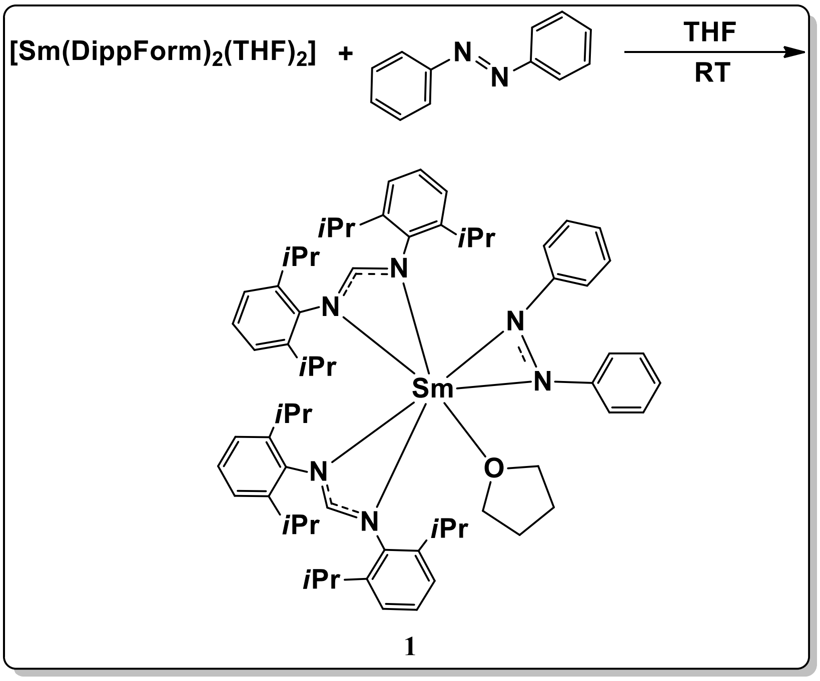

Scheme 3.3. The reaction of [Sm(DippForm)$_2$(THF)$_2$] with azobenzene in a 1:1 stoichiometric ratio.

Complex **1** was characterized by ^{1}H NMR, ^{13}C NMR, IR, and elemental analysis. Even though the broadening of signals due to paramagnetic effects of trivalent samarium can be seen, the data is interpretable and is consistent with the obtained X-ray crystal structure (see **Fig 3.4**). The NC*H*N (DippForm) proton appears as a singlet at δ = 10.51 ppm with an integration value of 2, while proton signals observed at δ = 8.03 ppm are accounted for unreacted *trans*-azobenzene. Coordinated THF resonances with less intensity can be located at δ = 1.37 ppm and δ = 3.39 ppm, where the latter signal is broadened a little. A broad signal at δ = 2.66 ppm is attributed to C*H* protons of the isopropyl group (DippForm). ^{1}H NMR data was obtained using the crystals formed in toluene (toluene signals can be seen at δ = 2.11 ppm (CH_3) and aromatic region) while complex **1** crystals obtained from DME were used for ^{13}C NMR analysis (see **Fig 3.5**), where DME substituted the coordinated THF molecules. It is evident from the two additional DME signals at δ = 72.26 ppm ($\boldsymbol{C}H_2$) and δ = 58.74 ppm ($\boldsymbol{C}H_3$) in ^{13}C NMR spectrum. The DippForm backbone N*C*HN resonance was not observed in the spectrum. ^{13}C NMR and IR spectra are also matching with the obtained crystal structure along with the elemental analysis result. In the IR spectrum, several intense bands around 700 – 1700 cm^{-1} can be seen which are typical for anionic formamidinate ligands. A strong absorption at 1667 cm^{-1} is attributed to delocalized NCN stretching mode.

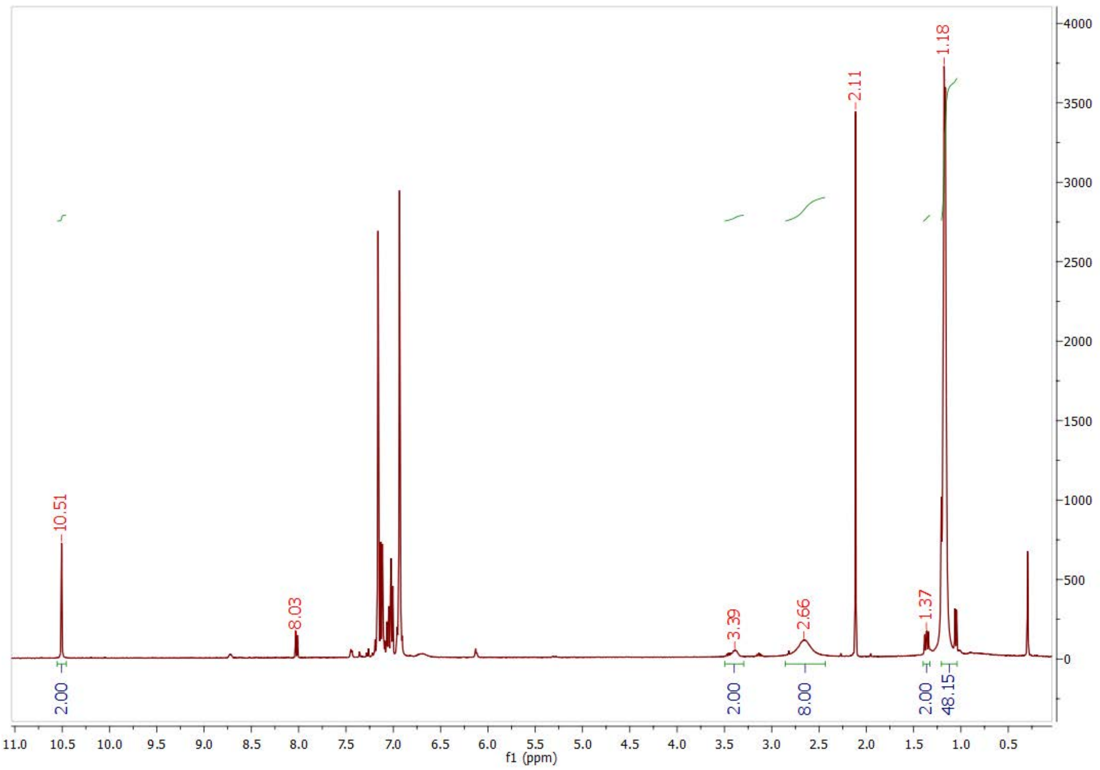

Fig 3.4 ^{1}H NMR spectrum of [(DippForm)$_2$Sm^{III}(Ph$_2$N$_2$)(THF)]·3THF (**1**)

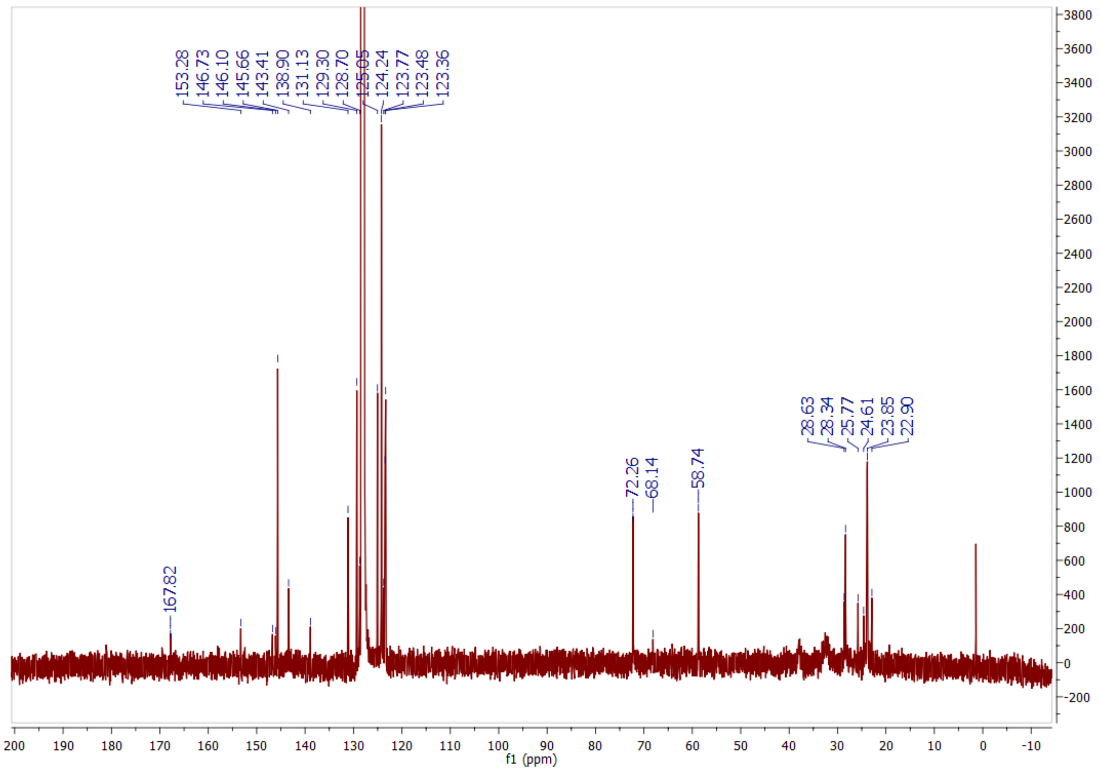

Fig 3.5 ^{13}C NMR spectrum of [(DippForm)$_2$Sm^{III}(Ph$_2$N$_2$)(THF)]·3THF (**1**)

3.3.1.2 The reaction of [Sm(DippForm)$_2$(THF)$_2$] with azobenzene in a 2:1 stoichiometric ratio

The reaction of [Sm(DippForm)$_2$(THF)$_2$] and *trans*-azobenzene in a 2:1 stoichiometric ratio was also carried out under similar reaction conditions to that for the 1:1 stoichiometry (above). THF is the most suitable solvent even though the reaction could also be performed in toluene. After mixing both reagents, the solution immediately changed to a dark blue colour. The colour then gradually changed to yellowish green after stirring for two days, and eventually became an orange/yellow solution after a week. Yellow crystals of **[(DippForm)Sm^{III}(Ph$_2$N$_2$)(THF)]$_2$·2THF (2)** and [Sm(DippForm)$_3$] (**Scheme 3.4**) can be obtained from THF or toluene by keeping the concentrated solution at -18°C for several weeks. Using DME instead of THF/toluene for crystallization could be a viable alternative which can form complex **2** crystals within 3-4 days at -18°C, where coordinated THF will be replaced by DME. Crystallization of [Sm(DippForm)$_3$] along with complex **2** is a barrier in obtaining pure crystals of the product which makes its purification and characterization difficult. Adding a minimal amount of hexane to the solid product (after removal of the THF/toluene) is an effective method to separate product **2** from [Sm(DippForm)$_3$] to a certain extent since the latter has low solubility in hexane. This gave a green solution of compound **2** with a lot of yellow solid material. Even though there was a solubility difference of compound **2** and [Sm(DippForm)$_3$] in hexane, complete separation still was not able to be achieved.

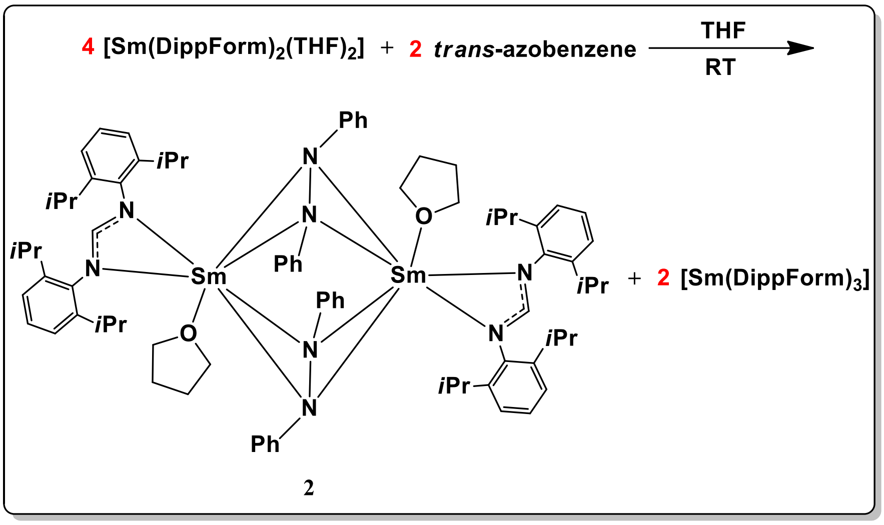

Scheme 3.4. The reaction of [Sm(DippForm)$_2$(THF)$_2$] with azobenzene in a 2:1 stoichiometric ratio.

3.3.1.3 The reaction of [Yb(DippForm)$_2$(THF)$_2$] with azobenzene

The reaction using the ytterbium analogue of [Sm(DippForm)$_2$(THF)$_2$] was also performed in a similar way to the 1:1 stoichiometric ratio used in the formation of compound **1**. Both reagents were dissolved in THF individually before mixing using a cannula transfer. The red/brown solution gradually changed to dark green after stirring for 3 days. Keeping the concentrated solution at -18°C for several weeks afforded small yellow blocks of **[(DippForm)Yb^{III}(Ph$_2$N$_2$)(THF)]$_2$(OH)$_2$·2THF (3)** along with a few DippFormH crystals. Further attempts to synthesize the desired complex without hydroxide as a ligand were unsuccessful even after repeated attempts to dry solvents and to modify the solvent conditions. The scheme of the reaction and structure of complex **3** is shown below (**Scheme 3.5**).

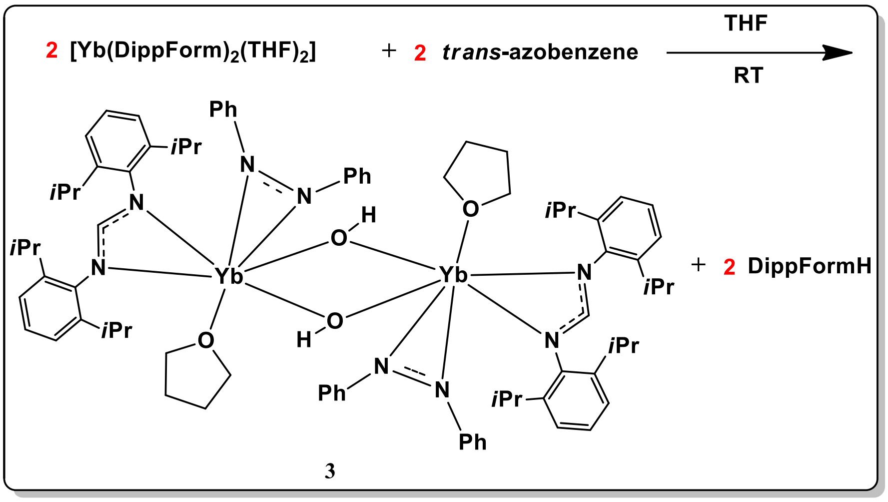

3

Scheme 3.5. The reaction of [Yb(DippForm)$_2$(THF)$_2$] with azobenzene in a 2:1 stoichiometric ratio.

3.3.1.4 The reaction of [Sm(DippForm)$_2$(THF)$_2$] with 1H-1,2,3-benzotriazole

The reaction was performed using an equimolar mixture of [Sm(DippForm)$_2$(THF)$_2$] and 1*H*-1,2,3-benzotriazole in THF. The colour of the solution changed from dark green to yellowish green after stirring for three days. Formation of off-white crystals of **[Sm^{III}(DippForm)$_2$(Btz)(THF)]·THF (4)** were isolated after keeping the concentrated solution at 4°C overnight. The reaction scheme is given below (**Scheme 3.6**). The formation of hydrogen gas as a by-product was confirmed by an NMR scale reaction of the same reagents in d_8-THF, which is shown in **Fig. 3.6.** A small resonance peak at δ = 4.72 ppm was detected which is attributable to H_2.[45, 46]

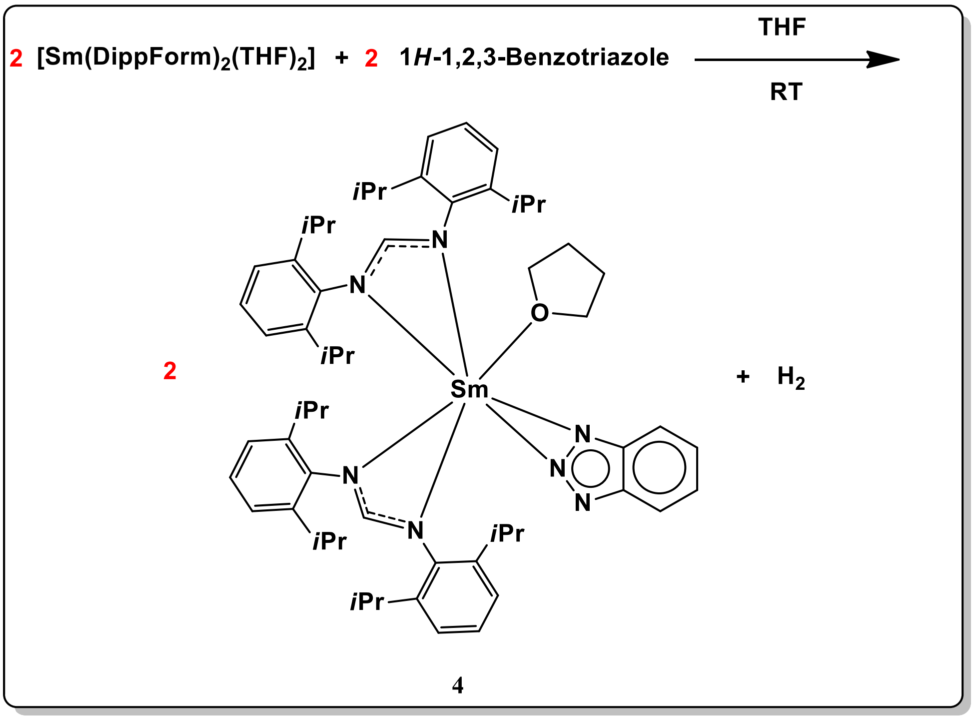

Scheme 3.6. The reaction of $Sm(DippForm)_2(THF)_2$ with 1*H*-1,2,3-benzotriazole.

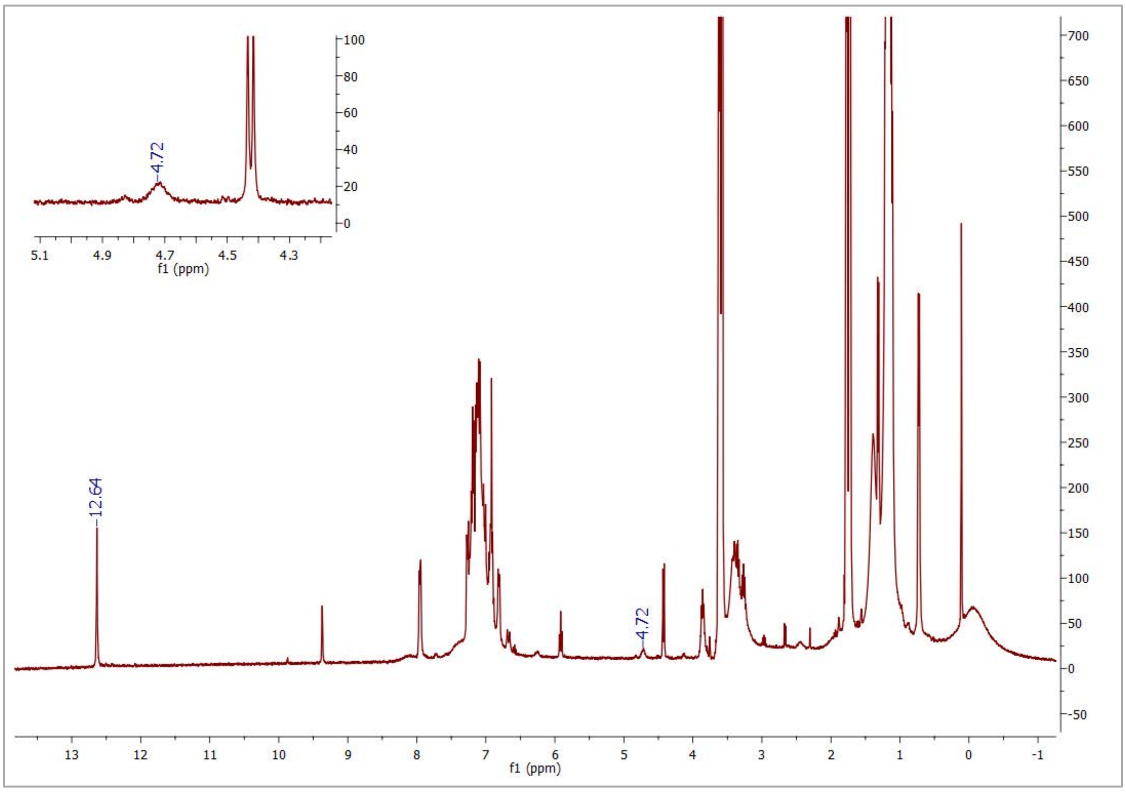

Fig 3.6. The ^{1}H NMR spectrum of NMR scale reaction of $Sm(DippForm)_2(THF)_2$ with 1H-1,2,3-benzotriazole.

^{1}H NMR signals of the isopropyl groups of the DippForm ligands are broadened due to the paramagnetic nature of the metal centre (Sm^{3+}) causing overlapping of the signals, particularly in the upfield region of the spectrum. This makes satisfactory integration and assignment of some peaks difficult. However, a strong downfield shift of the DippForm backbone NC*H*N was easily identifiable, which is detected as a singlet at δ= 12.85 ppm (**Fig 3.7**). Proton signals of some unreacted ligand (1*H*-1,2,3-benzotriazole) can be observed as a multiplet δ= 6.66 ppm. The ^{13}C NMR spectrum is shown in **Fig 3.8** where the resonance at δ = 192.29 ppm is assigned to the N*C*HN formamidinate backbone carbon atom. Moreover, satisfactory IR and elemental analysis were also obtained for complex **4**. The carbon content measured by elemental analysis is slightly lower than the expected value in the microanalysis, which is not uncommon for lanthanoid complexes owing to ease of metal carbide formation during combustion.[47, 48]

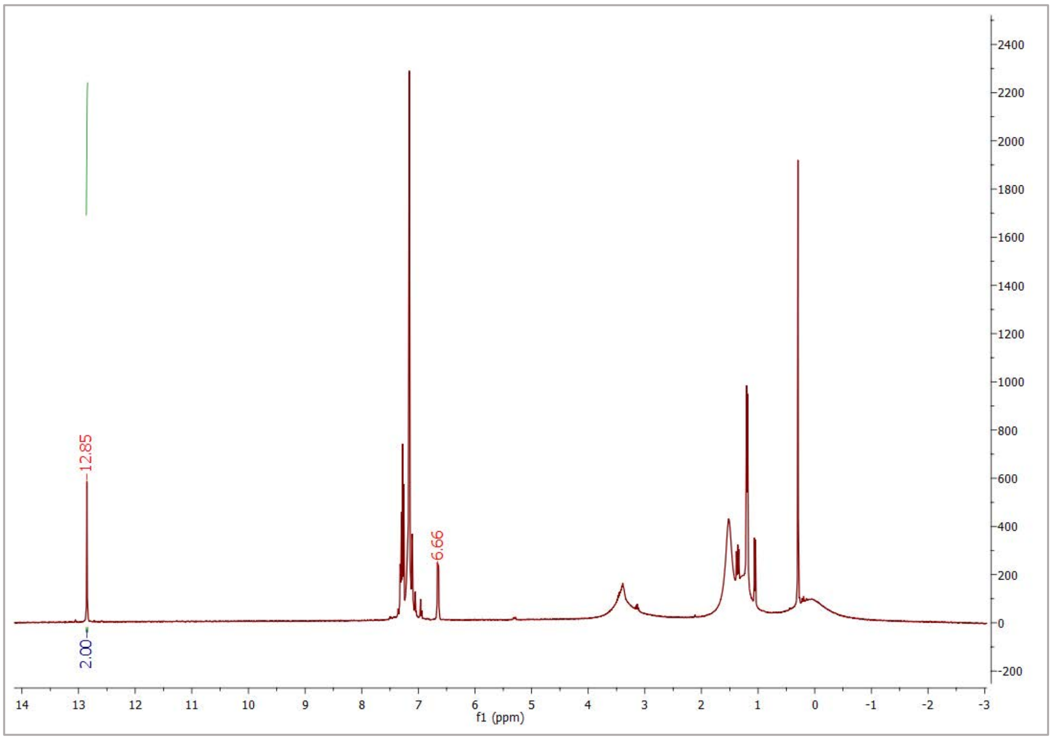

Fig 3.7 ^{1}H NMR spectrum of $[Sm^{III}(DippForm)_2(Btz)(THF)]\cdot THF$ (**4**)

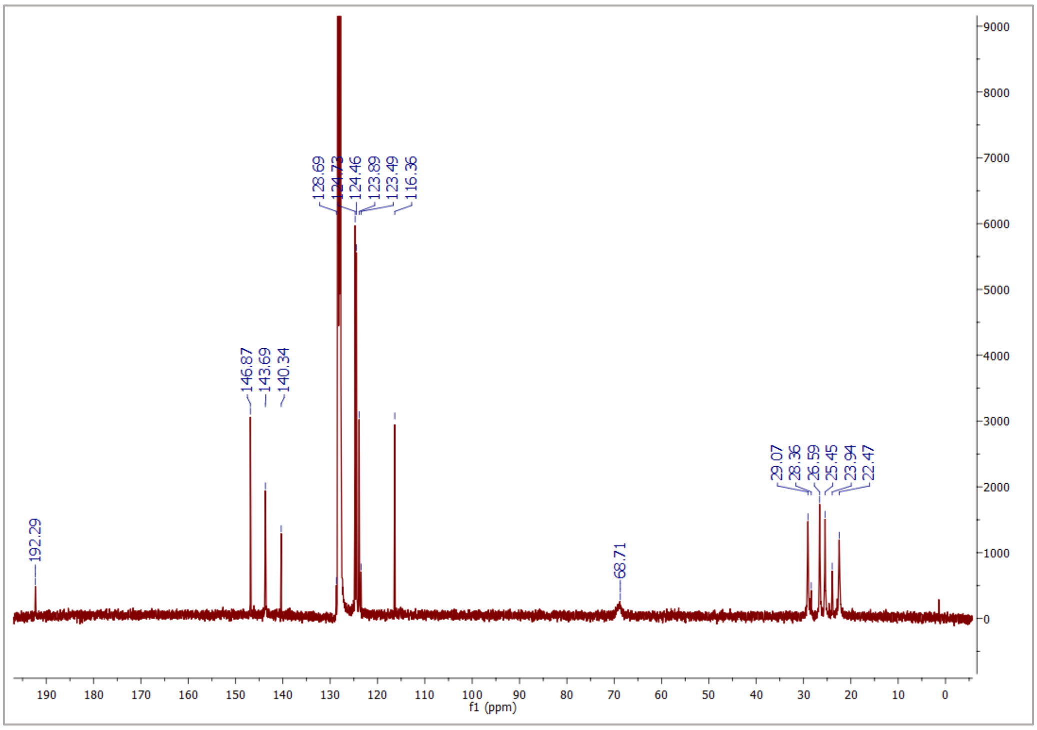

Fig 3.8 ^{13}C NMR spectrum of [Sm^{III}(DippForm)$_2$(Btz)(THF)]·THF (**4**)

3.3.1.5 The reaction of [Sm(DippForm)$_2$(THF)$_2$] with P_2Ph_4

[Sm(DippForm)$_2$(THF)$_2$] was treated with tetraphenyldiphosphine in a 2:1 stoichiometric ratio using the non-coordinating solvent toluene. Toluene was added to the Schlenk charged with both reagents and heated at 100°C for 3 days along with stirring. The colour of the solution changed from dark green to dark yellow during this period and the reaction was monitored using ^{31}P NMR spectroscopy. **Figure 3.9** shows the ^{31}P NMR spectrum of the reaction mixture where two distinct peaks were observed. The first resonance at δ = -14.94 ppm accounts for the unreacted starting material Ph_2P-PPh_2, while the doublet at δ = -40.31 and -41.63 ppm (coupling constant $J_{P\text{-}H}$ = 213.8 Hz) is attributable to diphenylphosphine (Ph_2PH) (the spectrum was not proton decoupled). The intensity of the P_2Ph_4 signal remains unchanged even after allowing the reaction to continue for a few more days, indicating that the reaction is complete. After filtration, the toluene was removed under vacuum and the residue was washed with hexane in order to remove remaining starting material (P_2Ph_4), which resulted in isolation of a yellow solid. The addition of toluene and concentration of the solution led to the formation of [Sm(DippForm)$_3$] crystals at room temperature. The hexane solution was concentrated and stored at 4°C overnight, which resulted in the formation of numerous yellow crystals of **[(Sm^{III}(DippForm)$_2$(μ-DippForm)(PPh$_2$)O] (5)**. The ^{1}H NMR spectrum of the solid isolated from hexane also shows the presence of [Sm(DippForm)$_3$], making the characterization of complex **5** difficult. Even though the reaction was performed in a 2:1 ratio, the product has a stoichiometric ratio of DippForm to PPh$_2^-$ of 3:1. The reaction scheme and product structure are given below (**Scheme 3.7**).

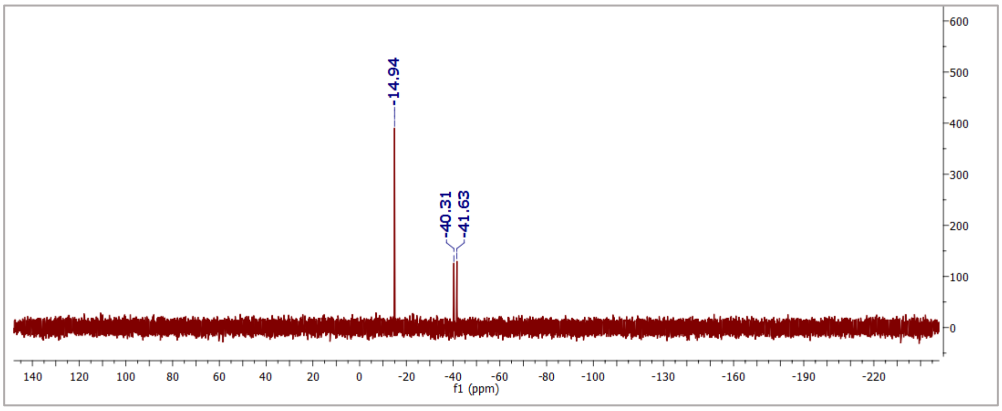

Fig 3.9 ^{31}P NMR spectrum of the reaction mixture of [Sm(DippForm)$_2$(THF)$_2$] and P$_2$Ph$_4$.

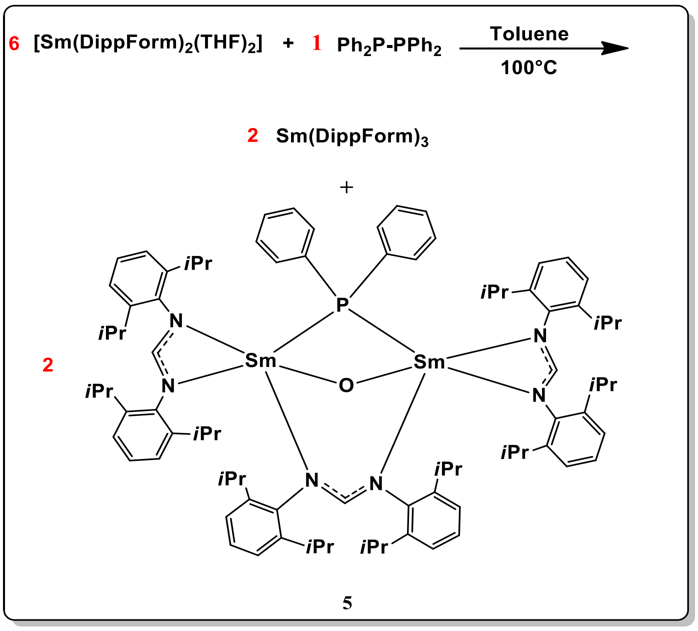

Scheme 3.7. The reaction of [Sm(DippForm)$_2$(THF)$_2$] with P$_2$Ph$_4$. The origin of oxygen in complex **5** is derived from THF (see discussion below).

3.3.2 X-ray Crystal Structures

*3.3.2.1 [(DippForm)$_2$Sm^{III}(Ph$_2$N$_2$)(THF)]·3THF **1***

Complex **1** crystallizes in the monoclinic space group *P*2$_1$/*n* with three lattice THF molecules in the asymmetric unit and there is a disorder in one of the lattice THF molecules. Two DippForm ligands bind in κ^1: κ^1 fashion to the samarium atom, along with one coordinating THF molecule. The N_2Ph_2 moiety is η^2-bonded to the samarium centre through the NN vector where coplanarity and *trans* orientation of the phenyl rings no longer exist. The *cis*-azobenzene moiety has a dihedral angle of 71.2^o (C_{Ph}-NN-C_{Ph}) which is in line with the values of the analogous complex [(C_5Me_5)$_2$Sm(N_2Ph_2)(THF)] (63.1^o and 70.8^o for two crystallographically independent molecules)[26] although some structural features are slightly different from other monomeric azobenzene samarium complexes. The Sm-N$_{azobenzene}$ bond lengths show two distinct values, 2.267(2) Å and 2.586(2) Å. The first value is close to the typical Sm^{3+}-NR_2 σ bond length (2.284 Å)[49] while the latter falls in the range of conventional $R_3N{:}\rightarrow Sm^{3+}$ donor bond length (2.53-2.77 Å),[50] suggesting that the N_2Ph_2 ligand is involved in one single bond and one donor bond to the samarium atom. The N-N bond length in trapped azobenzene ligand is 1.438(3) Å which is significantly longer relative to the NN double bond length in free azobenzene (1.25 Å) and slightly shorter with respect to the typical N-N single bond length (1.45 Å).[51] The substantial elongation in the N-N bond implies the reduction of the ligand which points towards the presence of the metal in the trivalent state. The average N-C(Ph) bond distance between nitrogen and carbon atoms of *cis*-oriented C_6H_5 rings in azobenzene is 1.412 Å, which is marginally shorter compared with 1.433 Å of free *trans*-azobenzene. All these structural dimensions indicate the presence of significant electron delocalization in the azobenzene ligand. Moreover, the Sm-N$_{DippForm}$ bond lengths are shorter [between 2.267(2) Å & 2.586(4) Å] compared with the divalent starting material [Sm(DippForm)$_2$(THF)$_2$] [2.529(4) Å & 2.617(4) Å] and the same trend can be observed in the case of Sm-O(THF) bond length [2.4973(16) Å compared to 2.56(3) Å and 2.599(3) Å of starting material].[52] This suggests a trivalent oxidation state for the samarium atom which is attributed to the high Lewis acidity of the Sm^{3+} and smaller ionic radius compared with Sm^{2+}.[53]

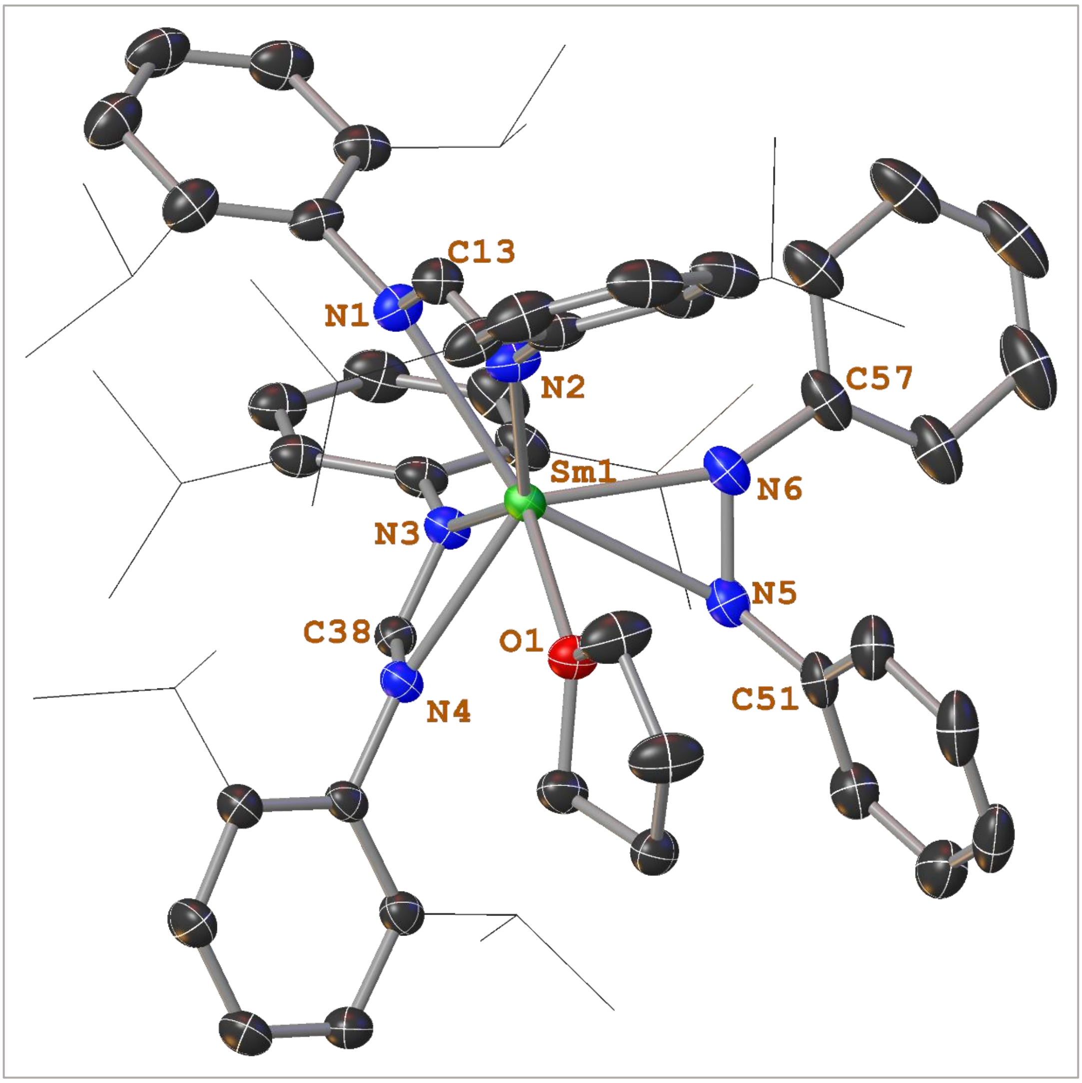

Fig. 3.10 ORTEP diagram of complex **1** in which relevant atoms are labelled. Thermal ellipsoids are drawn at a 50% probability level. Isopropyl groups of DippForm are shown as lines and hydrogen atoms along with three lattice THF molecules are omitted for clarity. Selected bond angles (°) and lengths (Å): Sm1-O1 2.4973(16), Sm1-N6 2.267(2), Sm1-N5 2.586(2), Sm1-N1 2.479(2), Sm1-N2 2.503(2), Sm1-N3 2.5301(19), Sm1-N4 2.4754(19), N5-N6 1.438(3), N5-C51 1.427(3), N6-C57 1.397(3), N1-C13 1.323(3), N2-C13 1.323(3), N3-C38 1.320(3), N4-C38 1.323(3), N6-Sm1-N5 33.66(7), N5-N6-Sm1 85.41(12), C57-N6-Sm1 154.42(19), C57-N6-N5 116. 2(2), N6-N5-Sm1 60.93(11), C51-N5-Sm1 130.67(15), C51-N5-N6 118.47(19), N3-C38-N4 120.2(2), N2-C13-N1 118.8(2).

3.3.2.2 [(DippForm)Sm^{III}(Ph_2N_2)(THF)]$_2$·2THF 2

The X-ray crystal structure of complex **2** was solved and refined in the triclinic space group *P*-1 with two lattice THF molecules in the asymmetric unit. One DippForm ligand is $\kappa^1 : \kappa^1$ coordinated to each samarium atom whereas two azobenzene units act as a bridge between two samarium ions by using two η^2:η^2 binding modes (Similar to **figure 3.1c**), along with one coordinating THF molecule on each metal. Here again, a considerable difference is evident regarding the shape of coordinated N_2Ph_2 moieties compared to the free azobenzene. The phenyl rings in the bridged azobenzene molecules are oriented in a *trans* fashion having a dihedral angle of 81.1°, which is comparable to that of analogous complex $[(C_5Me_5)(THF)Sm]_2[\mu\text{-}\eta^2\text{:}\eta^2\text{-}N_2Ph_2]_2$ (76°).[26] The N-N bond length in bridged azobenzene ligand is 1.456(3) Å which is clearly elongated compared to the typical NN double bond in free azobenzene (1.25 Å) and similar to the normal N-N single bond length (1.45 Å), indicating the formation of an sp^3-sp^3 NN single bond.[51] The Sm-$N_{azobenzene}$ bond lengths on each metal atom are 2.2815(19) Å (Sm1-N3), 2.3256(19) Å (Sm-N4*), 2.6165(19) Å (Sm-N4) and 2.600(2) Å (Sm-N3*) displaying two distinct ranges of bond length values. Here again, the first two values are close to the typical Sm-N sigma bond length (2.284 Å)[49] while the latter two fall in the range of conventional Sm-N donor bond length (2.41-2.65 Å).[54] This indicates that each samarium atom is forming two different types of bonds to each bridged N_2Ph_2 unit: one single bond and another donor bond. In the same way, one azobenzene ligand creates two different bonds to each samarium atom in addition to N-C(Ph) bonds. These structural features imply the existence of two completely reduced $N_2Ph_2^{2-}$ moieties which are complexed by two trivalent samarium ions. All these bond parameters discussed above along with a few significant bond angles are comparable to that of $[(C_5Me_5)(THF)Sm]_2[\mu\text{-}\eta^2\text{:}\eta^2\text{-}N_2Ph_2]_2$ including the Sm-Sm* distance. Like $[(C_5Me_5)(THF)Sm]_2[\mu\text{-}\eta^2\text{:}\eta^2\text{-}N_2Ph_2]_2$, here also two samarium ions exist relatively closely, being 3.519 Å apart [3.491(2) Å for Cp* analogue].[26] The trivalent state of the samarium ions can also be confirmed by comparing the Sm-$N_{DippForm}$ and Sm-O(THF) bond lengths of divalent starting material [Sm(DippForm)$_2$(THF)$_2$]. The Sm-$N_{DippForm}$ bond lengths are slightly shorter [2.482(2) Å & 2.531(4) Å] compared with the divalent starting material [Sm(DippForm)$_2$(THF)$_2$] [2.529(4) Å & 2.617(4)] reflecting the smaller size of Sm^{III} compared with Sm^{II}.[53] Likewise, a similar result can also be noticed in the case of Sm-O(THF) bond length, which is 2.4759(17) Å compared to 2.56(3) Å and 2.599(3) Å of the starting material.[52]

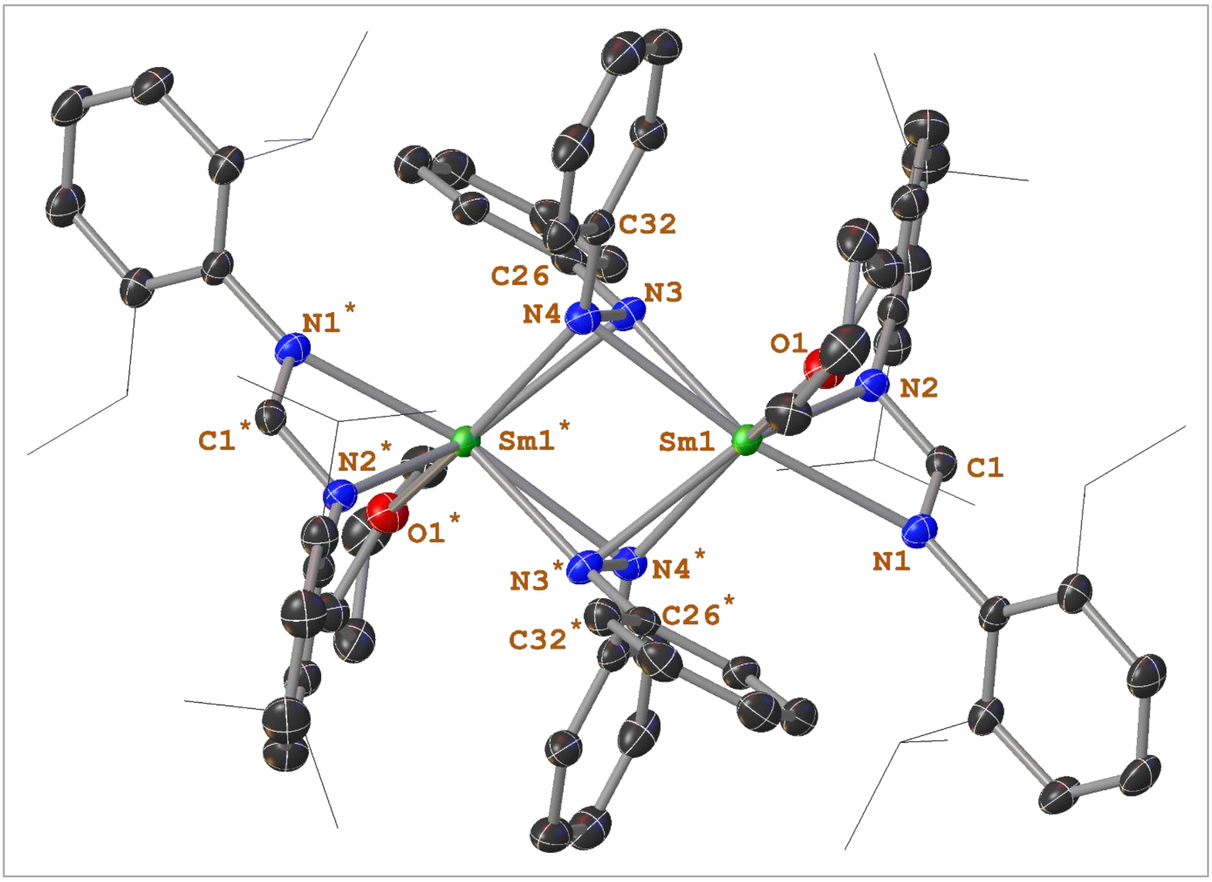

Fig. 3.11 ORTEP diagram of complex **2** in which relevant atoms are labelled. Thermal ellipsoids are drawn at a 50% probability level. Isopropyl groups of DippForm are shown as lines and hydrogen atoms along with two lattice THF molecules are omitted for clarity. Selected bond angles (°) and lengths (Å): Sm1-N3 2.2815(19), Sm1-N3* 2.600(2), Sm1-N4 2.6165(19), Sm1-N4* 2.3256(19), Sm1-N1 2.500(2), Sm1-O1 2.4759(17), Sm1-N2 2.482(2), N2-C1 1.329(3), N2-C2 1.427(3), N1-C1 1.316(3), N1-C14 1.430(3), N3-N4 1.456(3), N3-C26 1.390(3), N4-C32 1.397(3), N3-Sm1-N4 33.70(6), N4*-Sm1-N3* 33.79(6), N4-N3-Sm1* 62.70(10), N4-N3-Sm1 85.87(11), N3-N4-Sm1* 83.51(11), N3-N4-Sm1 60.43(10), C26-N3-N4 118.03(18), C32-N4-N3 116.94(19), N3-Sm1-N3* 87.97(7), N4*-Sm1-N4 89.37(6), Sm1-N3-Sm1* 92.03(7), Sm1*-N4-Sm1 90.63(6), C26-N3-Sm1* 89.97(13), C26-N3-Sm1 153.69(16), C32-N4-Sm1* 148.71(15), C32-N4-Sm1 119.66(14), N1-C1-N2 118.4(2).

3.3.2.3 [(DippForm)Yb^{III}(Ph$_2$N$_2$)(THF)]$_2$(OH)$_2$·2THF ***3***

Complex **3** crystallizes in the triclinic space group *P*-1 in which the unit cell contains two crystallographically independent molecules (**3a** & **3b**) along with two lattice THF molecules in the asymmetric unit. There is disorder in one of the lattice THF molecules. As observed in the previous structure, one DippForm ligand binds in κ^1: κ^1 fashion to each ytterbium atom, along with one coordinating THF molecule. Two ytterbium centres are bridged by two hydroxyl groups forming a Yb(μ-OH)$_2$Yb molecular cage. The average Yb-O$_{OH}$ bond length is 2.217 Å, which is in the range expected for that of similar trivalent ytterbium complexes [Yb(Oar^R)$_2$OH(THF)$_2$] (R = H, ^{t}Bu)[55] and [Yb(*o*-TolForm)$_2$(μ-OH)(THF)]$_2$ [56]. The same trend is also visible in the case of Yb-O$_{OH}$-Yb bond angle which is 111.5(3)° (Yb1-O1-Yb1^1) and 111.4(3)° (Yb2-O6-Yb2^2) for complex **3**. Similar to complex **1**, the N$_2$Ph$_2$ moiety is η^2-bonded to the ytterbium centre through the dinitrogen backbone where coplanarity and phenyl rings are in *cis* orientation. This is evident from the dihedral angle (C$_{Ph}$-NN-C$_{Ph}$) values 71.9^0 and 72.0^0. As shown by samarium complexes, the Yb-N$_{azobenzene}$ bond lengths also have two distinct values 2.210(7) Å [2.228(8) Å for **3b**] and 2.575(7) Å [2.514 Å(8) for **3b**]. The shorter bonds are accounted for the Yb-NR$_2$ single bond while the longer ones fall in the range of typical R$_3$N:→Yb donor bond lengths, which are comparable to previously reported ytterbium complexes.[26, 34] The N-N bond length in η^2-bonded azobenzene ligand is different in both crystallographically independent molecules [1.433(9) Å in **3a** and 1.393(10) Å in **3b**]. Both are obviously longer compared to the NN double bond length in free azobenzene (1.25 Å) and shorter with respect to the typical N-N single bond length (1.45 Å). The N-C(Ph) bond distances between nitrogen and carbon atoms of *cis*-oriented C$_6$H$_5$ rings in azobenzene are 1.381(11) Å [1.394(12) Å for **3b**] and 1.433(11) Å [1.442(12) Å for **3b**], where one bond is elongated than the other one. This indicates significant electron delocalization in trapped azobenzene moieties is clearly visible from all these structural features which point towards the trivalent state of ytterbium metal in the complex. This is also perceptible by comparing complex **3** bond parameters with the divalent starting material. The Yb-N$_{DippForm}$ bond lengths are lower [between 2.384(6) Å & 2.409(7) Å] compared with the divalent starting reagent [Yb(DippForm)$_2$(THF)$_2$] [2.462(2) Å & 2.496(4) Å] and the same trend can be observed in the case of Yb-O(THF) bond length [2.299 Å (2.318 Å in **3b**) compared to 2.461(2) Å and 2.420 (4) Å of starting material].[57]

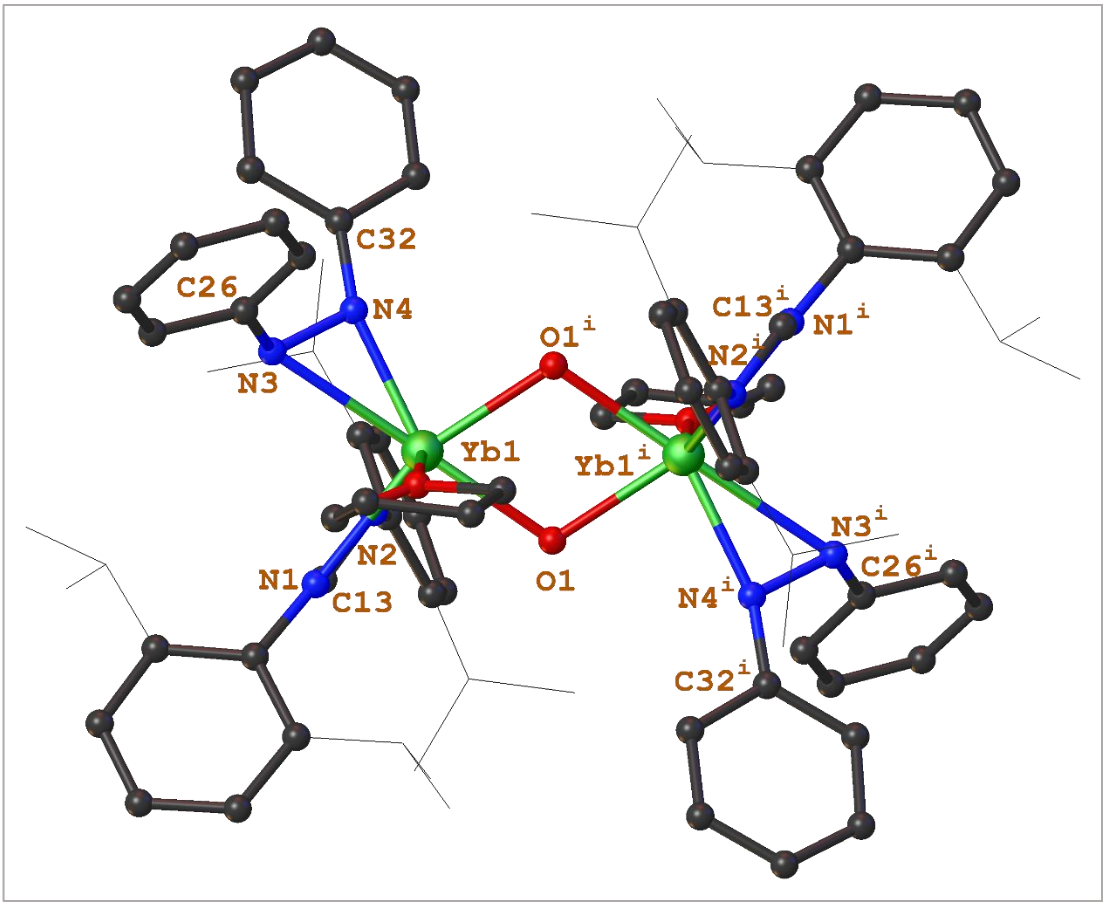

Fig. 3.12 ORTEP diagram of complex **3** in which relevant atoms are labelled. Thermal ellipsoids are drawn at a 50% probability level. Figure showing only one of the two crystallographically independent molecules present in the unit cell (**3a**). Isopropyl groups of DippForm are shown as lines and hydrogen atoms along with two lattice THF molecules are omitted for clarity. Selected bond angles and lengths are listed in the table below (**Table 3.1**) for both molecules.

Table 3.1: Selected bond angles (°) and lengths (Å) for two crystallographically independent molecules of complex **3**.

	3a	3b
Yb-O_{OH}	Yb1-O1 2.221(6) Yb1-O1^1 2.225(6)	Yb2-O6 2.199(6) Yb2-O6^1 2.224(6)
Yb-O_{OH}-Yb	Yb1-O1-Yb1^1 111.5(3)	Yb2-O6-Yb2^2 111.4(3)
O_{OH}-Yb- O_{OH}	O1-Yb1-O1^1 68.5(3)	O6-Yb2-O6^2 68.6(3)
Yb-$N_{azobenzene}$	Yb1-N4 2.210(7) Yb1-N3 2.575(7)	Yb2-N7 2.228(8) Yb2-N8 2.514(8)
N-N	N3-N4 1.433(9)	N7-N8 1.393(10)
$C_{(Ph)}$-$N_{azobenzene}$	N4-C32 1.381(11) N3-C26 1.433(11)	N7-C84 1.394(12) N8-C78 1.442(12)
Yb-$N_{DippForm}$	Yb1-N2 2.384(6) Yb1-N1 2.409(7)	Yb2-N6 2.407(7) Yb2-N5 2.385(7)
Yb-$O_{(THF)}$	Yb1-O2 2.299(5)	Yb2-O7 2.318(5)

3.3.2.4 [Sm^{III}(DippForm)$_2$(Btz)(THF)]·THF **4**

Complex **3** crystallizes in the monoclinic space group $P2_1/n$ with one lattice THF molecule in the asymmetric unit. The samarium atom is ligated by two DippForm moieties in a κ^1: κ^1 fashion along with one coordinating THF molecule. The benzotriazolate moiety is η^2-bonded to the samarium centre through two nitrogen atoms. The Sm-N$_{Btz}$ bond lengths are 2.422(3) Å (Sm-N1) and 2.460(3) Å (Sm-N2) which are similar and longer than the typical Sm-N sigma bond length (2.284 Å)[49] but falls in the range of conventional Sm-N donor bond length (2.41-2.65 Å)[54]. The two N-N bond lengths are approximately equal, which are 1.342(4) Å for N1-N2 and 1.322(5) Å for N2-N3. These values are intermediate between the usually observed values for NN double bond in free azobenzene (1.25 Å) and definitely shorter than the normal N-N single bond length (1.45 Å).[51] 1.354(4) Å (N1-C1) and 1.363(4) Å (N3-C6) are the N$_{Btz}$-C$_{Btz}$ bond lengths for trapped benzotriazolate. Delocalization of π electrons of NN double bond owing to the deprotonation is clear from these structural features. In addition, these N-N and N-C bond distances are comparable to the previously reported bond length ranges of rare earth benzotriazolates.[38-40] Similar to two previous structures (**1** & **2**), the Sm-N$_{DippForm}$ bond lengths are shorter [2.423(3) Å & 2.471(3) Å] compared to the 2.529(4) Å & 2.617(4) Å of divalent starting material [Sm(DippForm)$_2$(THF)$_2$] and the same trend can be observed in the case of Sm-O(THF) bond length [2.4973(16) Å compared to 2.56(3) Å and 2.599(3) Å of starting material].[52] Again, this suggests that samarium ion is in the trivalent oxidation state due to high Lewis acidity of the Sm^{3+} and smaller ionic radius compared with Sm^{2+}.[53]

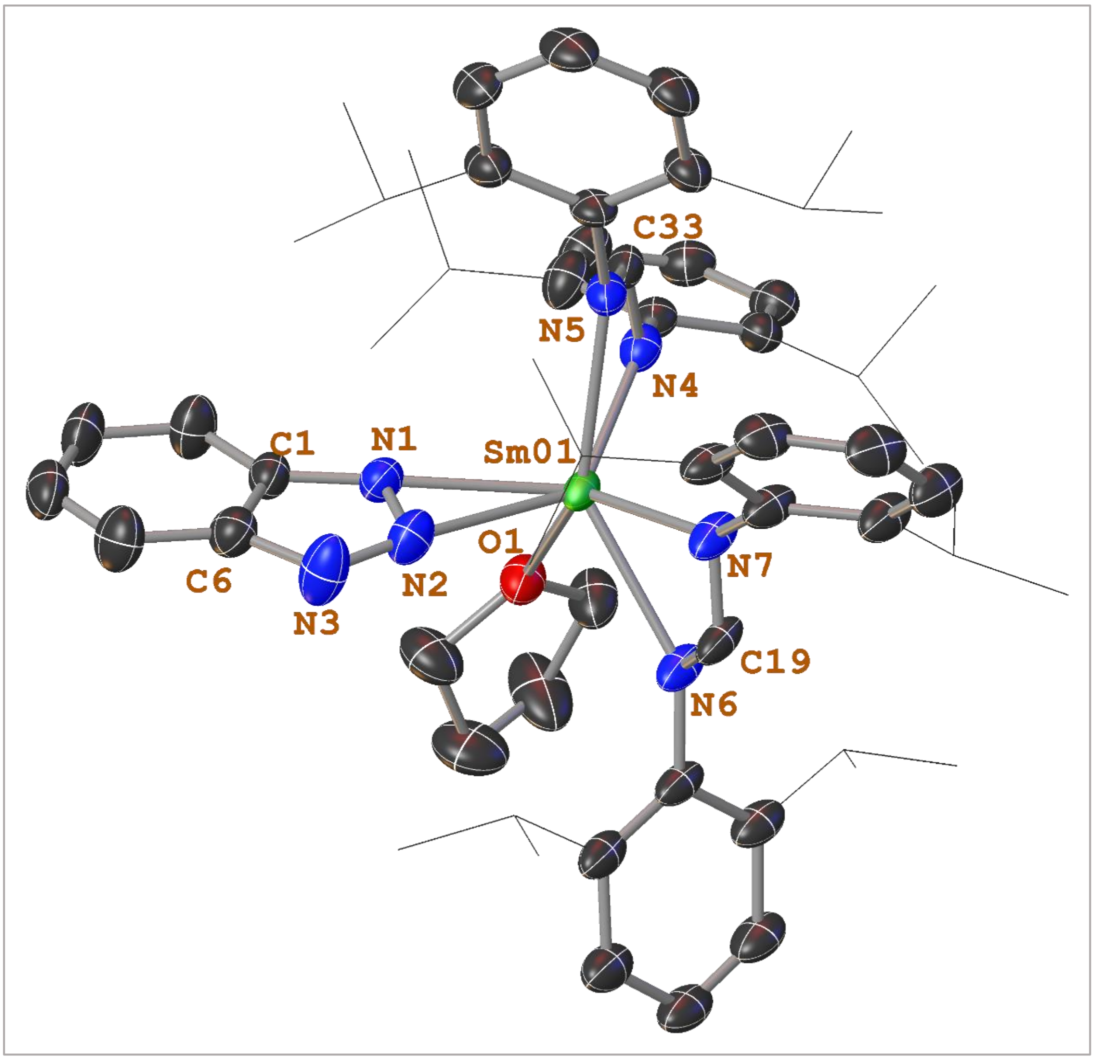

Fig. 3.13 ORTEP diagram of complex **4** in which relevant atoms are labelled. Thermal ellipsoids are drawn at a 50% probability level. Isopropyl groups of DippForm are shown as lines and hydrogen atoms along with one lattice THF molecule are omitted for clarity. Selected bond angles (°) and lengths (Å): Sm01-N1 2.422(3), Sm01-N2 2.460(3), N1-N2 1.342(4), N1-C1 1.354(4), N2-N3 1.322(5), N3-C6 1.363(4), Sm01-O1 2.452(2), Sm01-N4 2.423(3), Sm01-N5 2.471(3), Sm01-N7 2.440(3), Sm01-N6 2.457(3), N1-Sm01-N2 31.90(10), N2-N1- Sm01 75.59(19), C1-N1- Sm01 176.8(2), N1-N2- Sm01 72.51(19), N3-N2- Sm01 174.6(3), N2-N1-C1 106.6(3), N3-C6-C1 107.9(3), N3-N2-N1 112.5(3), N2-N3-C6 106.1(3), N4-Sm01-N5 55.46(9), N7-Sm01-N6 55.34(9), N5-C33-N4 118.4(3), N7-C19-N6 118.4(3).

3.3.2.5 [(Sm^{III}(DippForm)$_2$(DippForm)(PPh$_2$)O] **5**

The X-ray crystal structure of complex **5** was solved and refined in the triclinic space group *P*-1 and the structure has some disorder in the phosphorus atom and isopropyl phenyl group of one of the DippForm ligands. Two samarium metal centres are bridged by three different ligand species. One of them was μ-oxo linkage with Sm-O bond lengths 2.068(3) Å and 2.066(2) Å, which are comparable to that of other structurally verified oxo-bridged trivalent samarium complexes such as [(Cp*$_2$Sm)μ-O]^{58} and [Sm[N(SiMe$_3$)$_2$]$_2$(thf)]$_2$(μ^2-O)^{28}. However, the Sm1-O-Sm2 bond is a little bent [120.73(11)°] while it is linear in the case of the above-mentioned complexes. This also suggests the relative proximity of two samarium ions similar to complex **2**, with a distance of 3.593 Å. Two samarium ions are also connected by a diphenylphosphide ligand, where phosphorus shows some disorder and the existence of two parts (P1 and P1A) can be seen. Sm-P distance of one part is comparable to previously reported complex [Sm^{II}Cp''(PPh$_2$)$_2$Sm^{III}Cp''$_2$] (Cp'' = C$_5$H$_3$^{t}Bu$_2$)^{44} - 2.986(6) Å and 2.960(9) Å. On the other hand, the other Sm-P bond distances are comparatively longer, being 3.324(17) Å and 3.12(3) Å. Similarly, the Sm-P-Sm bond angle is also different for each phosphorus atom part, which is 74.39(15)° (Sm2-P1-Sm1) and 67.7(4)° (Sm2-P1A-Sm1). Two DippForm ligands bind in κ^1: κ^1 fashion to the samarium atom while a third DippForm moiety is bridged between two samarium centres. The Sm-N$_{\mathrm{DippForm}}$ bond lengths for all three DippForm ligands look similar, where they all fall between 2.439(3) Å and 2.493(3) Å. These are well shorter compared to that divalent starting material [Sm(DippForm)$_2$(THF)$_2$] [2.529(4) Å & 2.617(4) Å] implying trivalent state of samarium ions in complex **5**.^{52} In addition, the N-C-N bond angle in the bridged DippForm species is more obtuse [125.6(3)°] than that of terminal DippForm ligands [119.4(3)° & 120(3)°].

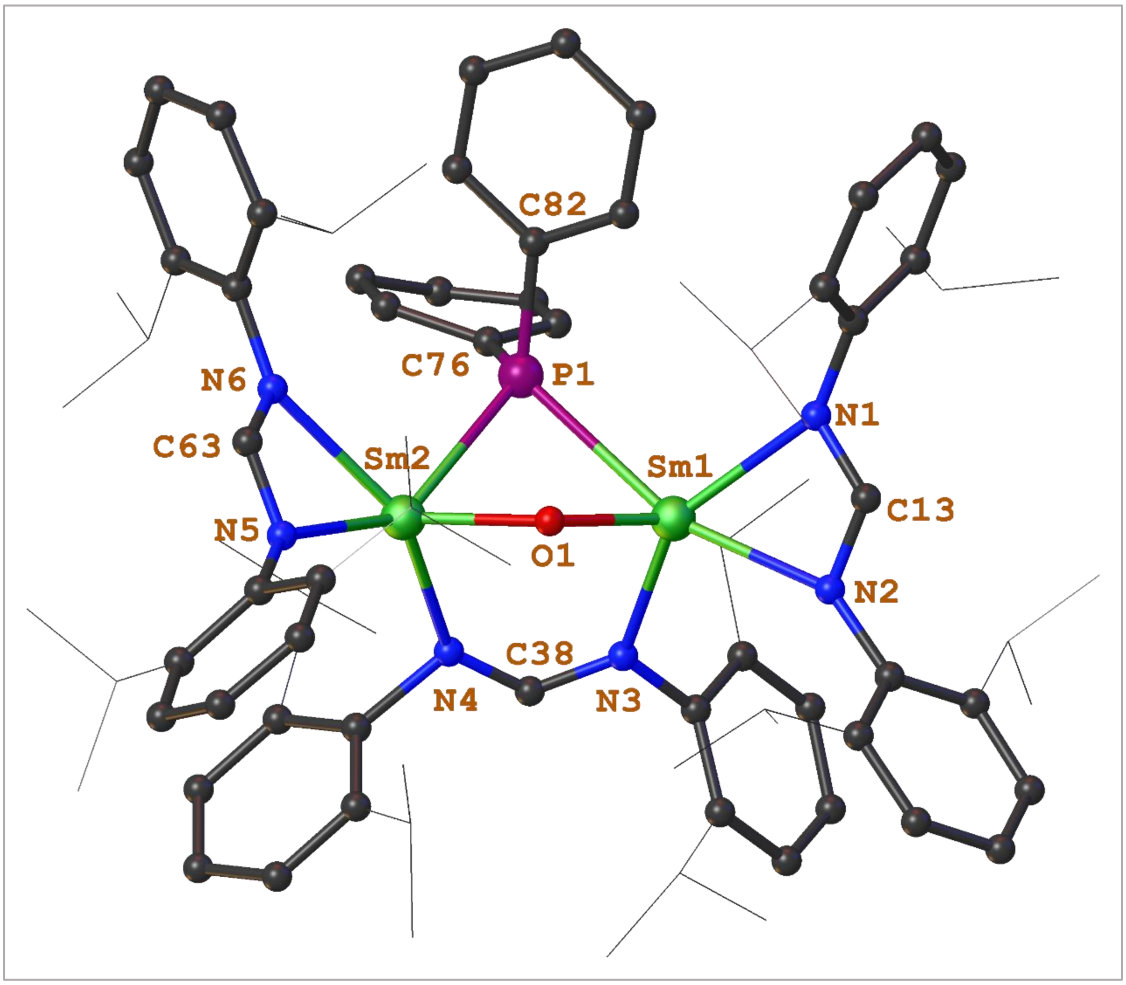

Fig. 3.14 ORTEP diagram of complex **5** in which relevant atoms are labelled. Thermal ellipsoids are drawn at a 50% probability level. Only one part of the disordered atoms is shown here. Isopropyl groups of DippForm are presented as lines and hydrogen atoms are omitted for clarity. Selected bond angles (°) and lengths (Å): Sm1-P1 2.986(6), Sm1-P1A 3.324(17), Sm2-P1 2.960(9), Sm2-P1A 3.12(3), Sm1-O1 2.068(3), Sm2-O1 2.066(2), Sm1-N1 2.470(3), Sm1-N2 2.446(3), Sm1-N3 2.454(3), Sm1-N4 2.439(3), Sm1-N5 2.446(3), Sm1-N6 2.493(3), P1-C82 1.884(9), P1-C76 1.861(9), P1A-C82 1.67(3), P1A-C76 1.70(3), N1-C13 1.322(4), N2-C13 1.327(4), N3-C38 1.316(5), N4-C38 1.319(5), N5-C63 1.322(4), N6-C63 1.323(5), Sm1-O1-Sm2 120.73(11), Sm2-P1-Sm1 74.39(15), Sm2-P1A-Sm1 67.7(4), C76-P1-C82 97.3(4), N3-C38-N4 125.6(3), N1-C13-N2 120.0(3), N5-C63-N6 119.4(3), C13-N1-Sm1 91.53(19), C13-N2-Sm1 92.5 (2), C38-N3-Sm1 123.7(2), C38-N4-Sm2 140.2(3), C63-N5-Sm2 93.2(2), C63-N6-Sm2 91.0(2).

3.3.3 Discussion

3.3.3.1 Reaction of [Sm(DippForm)$_2$(THF)$_2$] with trans-azobenzene

The capability of *trans*-azobenzene to undergo two one-electron reductions is already discussed in the introduction part of this chapter. Consequently, the high reactivity of *trans*-azobenzene towards the divalent samarium complex [Sm(DippForm)$_2$(THF)$_2$] was strongly anticipated. The initial reaction in a stoichiometric ratio of 1:1 in solvent THF immediately resulted in a colour change of the reaction mixture to dark blue. The obtained product, complex **1**, turned out to be analogous to the trivalent samarium pentamethylcyclopentadienyl complex [Cp*$_2$Sm(N$_2$Ph$_2$)(THF)] reported by Evans *et al* 34 years ago (Complex **A** in **Scheme 3.8a**).[26] Use of THF instead of toluene as solvent was the only difference in the reaction conditions between both reactions. We preferred THF for most of the reactions involving [Sm(DippForm)$_2$(THF)$_2$] due to the appropriate solubility of reagents. Parallel reactivity between [SmCp*$_2$] and [Sm(DippForm)$_2$(THF)$_2$] demonstrated in chapter 2 motivated us to look for other similar products [Cp*$_2$Sm]$_2$(N$_2$Ph$_2$) and [Cp*$_2$(THF)Sm]$_2$[N$_2$Ph$_2$]$_2$ (Complexes **B** & **C** in **Scheme 3.8**) in the same reaction chemistry. Repeating the first reaction in a different stoichiometric ratio (2:1) in the same solvent witnessed the reaction getting carried out in a different direction in terms of both colour and resulting products. The initial dark blue colour of the solution slowly changed to greenish yellow after stirring for one week. Crystals obtained from the solution were of complex **2** [which is analogous to Evans' product **C**] and the homoleptic trivalent complex [Sm(DippForm)$_3$]. The search for the DippForm analogue of the remaining complex [Cp*$_2$Sm]$_2$(N$_2$Ph$_2$) was in vain even after changing the solvent to toluene. Repetition of the reaction in toluene in both stoichiometric ratios resulted in the formation of the same products (complexes **1** & **2**) as those obtained in THF. Since the products are similar, it can be inferred that the reaction pathway in both cases might be identical.

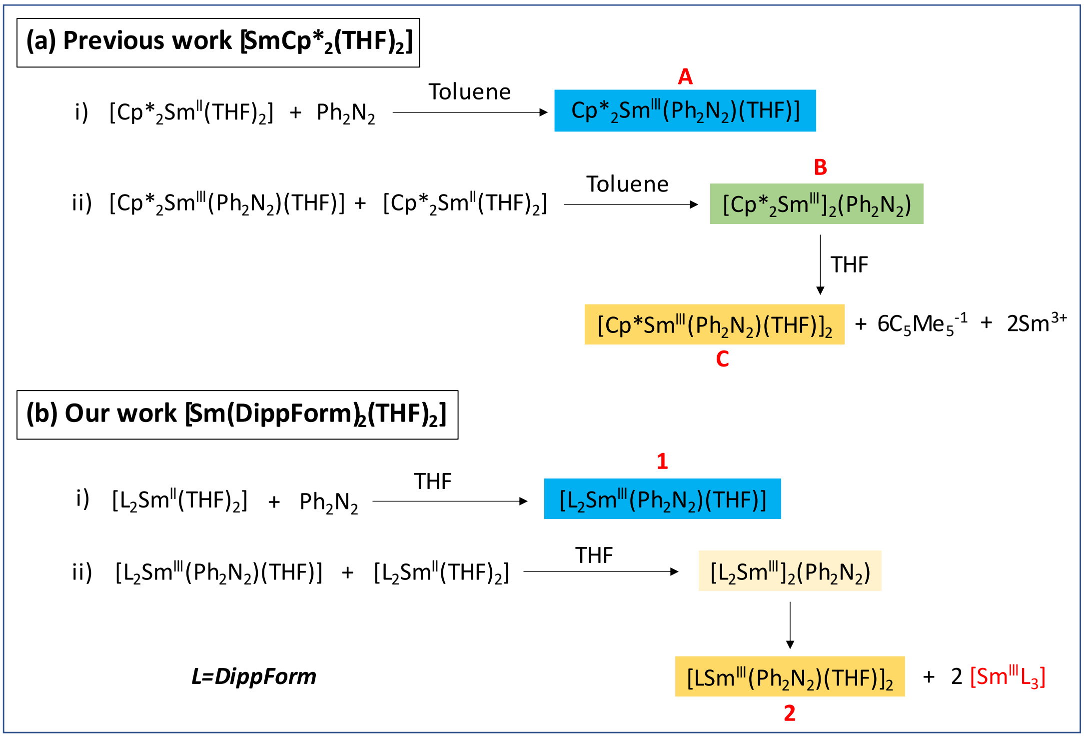

Scheme 3.8. (a) The reaction of *trans*-azobenzene with [SmCp*$_2$] *(Previous work)*. (b) The reaction of *trans*-azobenzene with [Sm(DippForm)$_2$(THF)$_2$] (*Our work*). Colours of the complexes are matched with the shading used in the Scheme.[26]

The correlation of reaction products with previously reported complexes helped in unravelling the complex reaction chemistry in this case. Initially, when the reaction was carried out in a 1:1 stoichiometric ratio, the solution immediately changed to dark blue. Even though the blue colour is considered a characteristic property of divalent samarium complexes in normal cases,[59] structural features of complex **1** point towards the presence of a trivalent samarium centre. The N_2Ph_2 species is η^2-bonded to the samarium centre through each nitrogen atom where azobenzene undergoes one-electron reduction. Therefore, the colour might be due to the presence of monoanionic azobenzene moiety in complex **1**. Previously, a dark blue colour was observed for $N_2Ph_2^-$ containing Ln(III) complexes such as [Tm(dtp)$_2$(N_2Ph_2)], [Sm(dtp)$_2$(N_2Ph_2)] and [Sm(dsp)$_2$(N_2Ph_2)] (dsp = $PC_4Me_2(SiMe_3)_2$, dtp = $PC_4Me_2{}^tBu_2$).[60] Since the reaction proceeds quickly and azobenzene can undergo two-electron reduction, chances for further reduction can be prevented by the addition of excess azobenzene.

Addition of 1 mole of *trans*-azobenzene per 2 moles of [Sm(DippForm)$_2$(THF)$_2$] also results in the initial dark blue colouration of the reaction mixture. This suggests that here the reaction proceeds via the initial formation of complex **1** and the same reaction can be performed alternatively through the addition of [Sm(DippForm)$_2$(THF)$_2$] to complex **1**. The excess samarium reducing agent, therefore, reacts with complex **1**, which is also evident from the reaction mechanism of [SmCp*$_2$(THF)$_2$] reactivity towards azobenzene.[26] This might be facilitating another one-electron reduction of the $Ph_2N_2^{1-}$ unit and leading to the formation of a particular Sm^{3+} intermediate [Sm(DippForm)$_2$]$_2$(Ph$_2$N$_2$) (a DippForm analogue of complex **B** in **Scheme 3.1**). This intermediate complex containing dianionic azobenzene species is not regarded as being favoured thermodynamically and while it was observed in the case of complex **B**, mild conditions such as adding THF triggered the formation of complex **C** through ligand redistribution.[26] Likewise, non-redox ligand redistribution of [Sm(DippForm)$_2$]$_2$(Ph$_2$N$_2$) in the presence of THF might have resulted in the formation of a yellow solution containing reduced azo-bridged bilanthanoid complex **2** and another already reported trivalent samarium complex [Sm(DippForm)$_3$].[61] In complex **2**, two samarium ions are connected by two azobenzene bridge units where each using two $\eta^2:\eta^2$ binding modes. Bond parameters and other structural features of complex **2** imply that both samarium ions are in a trivalent state while each azobenzene unit has undergone two-electron reduction. The presence of two types of Sm-N$_{\text{azobenzene}}$ bonds refers to the formation of single bonds and donor bonds. Hence, in addition to single bonds between each $Ph_2N_2^{2-}$ moiety and samarium atoms, a lone pair on each nitrogen atom also creates two extra donor bonds to samarium metals. The yellow colour of the solution predominantly comes from the characteristics of the trivalent samarium ion.

Attempts to isolate the intermediate (the DippForm analogue of compound **B** in **Scheme 3.8**) by repeating the reaction in toluene were unsuccessful. Less stability and the presence of coordinated THF in the divalent starting material could have facilitated the final non-redox ligand redistribution. The reaction proceeds in a similar way in both THF and toluene. Even though synthesis of bulky [Sm(DippForm)$_3$] was not expected, the formation of an analogous complex [SmCp*$_3$] can be elucidated from the reaction mechanism of [SmCp*$_2$(THF)$_2$] (**scheme 3.1a**). At that time, it was predicted that high steric crowding would deter the formation of [SmCp*$_3$]. However, three years later, the first tris(pentamethylcyclopentadienyl) samarium complex was synthesized upon reaction with COT, as mentioned in Chapter 2.[62]

3.3.3.2 Reaction of [Yb(DippForm)$_2$(THF)$_2$] with trans-azobenzene

Azobenzene is very reactive and it is well-known to oxidize even the less powerful divalent ytterbium (compared to samarium), which is mentioned in detail in the introduction. So, the reaction of [Yb(DippForm)$_2$(THF)$_2$] with *trans*-azobenzene was expected and the initial colour change of the reaction mixture to dark green was an indication of that result. Like samarium, there is a possibility for [Yb(DippForm)$_2$(THF)$_2$] to show a parallel reaction compared to the Cp analogue [YbCp$_2$(THF)$_2$] (where Cp = C_5H_5) as shown in **Scheme 3.9**, which ultimately results in the formation of [Cp$_3$Yb(THF)] and [Cp(THF)Yb]$_2$[N$_2$Ph$_2$]$_2$. However, the obtained crystals of complex **3** after several attempts were not the expected product. The μ-bridged hydroxyl groups indicate the partial hydrolysis of ytterbium complex, plausibly due to traces of adventitious water. This is not surprising since the ingress of water was possible after keeping the solution over a prolonged period while attempting to get crystals. This decomposition surely highlights the highly reactive nature of these types of compounds. Similar types of incidents and complexes have already been reported previously.[28, 58] A retrospective approach might help to understand the sort of chemistry occurring in this reaction. Complex **3** might be formed due to hydrolysis of another intermediate product [Yb(DippForm)$_2$(THF)(N$_2$Ph$_2$)], which is analogous to complex **1** (**Scheme 3.9**). A variety of methods such as changing solvents and crystallization techniques were employed to isolate [Yb(DippForm)$_2$(THF)(N$_2$Ph$_2$)], but it has remained elusive.

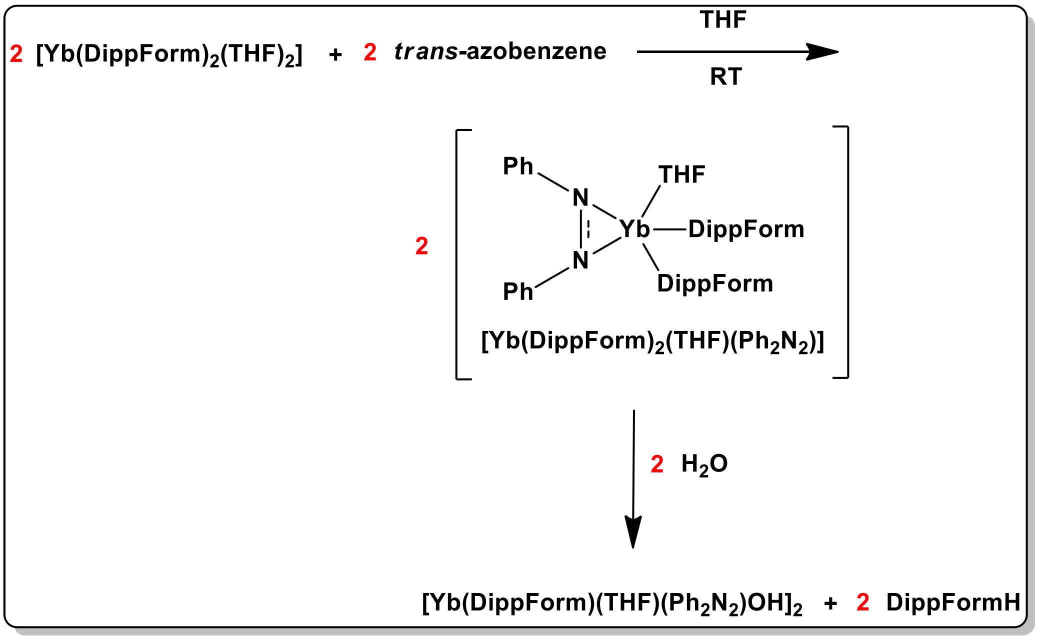

Scheme 3.9. A proposed reaction mechanism of the reaction of [Yb(DippForm)₂(THF)₂] with *trans*-azobenzene.

3.3.3.3 The reaction of [Sm(DippForm)₂(THF)₂] with 1H-1,2,3-benzotriazole

The organolanthanoid chemistry with 1*H*-1,2,3-benzotriazole was not as straightforward as the *trans*-azobenzene reaction. The latter was a proven oxidant while 1*H*-1,2,3-benzotriazole's complexation with rare earth metals is much more limited in number. Even though, 1*H*-1,2,3-benzotriazole possesses N=N linkages, the reaction with [Sm(DippForm)₂(THF)₂] could be rather complex. Compared to *trans*-azobenzene, the most important feature is the presence of an acidic proton near the NN bond. Therefore, the formation of a 1,2,3-benzotriazolate anion (Btz$^-$) was expected through deprotonation.

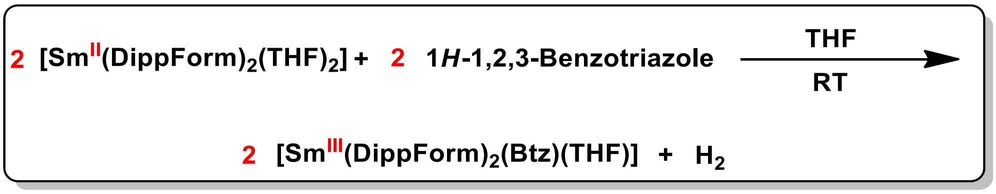

Scheme 3.10. A proposed reaction mechanism of the reaction of [Sm(DippForm)₂(THF)₂] with 1*H*-1,2,3-benzotriazole.

The colour change from dark green to yellowish green was the first indication that the reaction had occurred. A possible reaction scheme is given above where synthesis of complex **4** is accompanied by the release of the H_2. The formation of H_2 was confirmed by carrying out the reaction on an NMR scale using *d*-THF as solvent. In addition, the H atom is missing in the crystal structure of **4** and the delocalization of π electrons around NNN bonds in trapped benzotriazole ligand is evident from structural features (especially the N-N bond lengths). So, the divalent samarium complex $[Sm(DippForm)_2(THF)_2]$ traps 1,2,3-benzotriazolate anion (Btz^-) through single electron transfer resulting in the formation of trivalent samarium complex **4**, where H_2 is eliminated during the process. To the best of our knowledge, the complexation of 1,2,3-benzotriazolate with trivalent samarium is not reported to date.

3.3.3.4 *The reaction of $[Sm(DippForm)_2(THF)_2]$ with P_2Ph_4*

The primary target compound of the reaction was the DippForm analogue of $[Cp^*_2Sm(PPh_2)]$[43] with diphenylphosphine being the solely expected by-product. That was the reason for carrying out the reaction in a 2:1 stoichiometric ratio. In order to circumvent any reactions where ring-opening of THF occurs, toluene was chosen as the solvent of choice. Initially, stirring wasn't enough for the reaction to proceed as it didn't display any colour change and only signals of starting material were detected by ^{31}P NMR of the reaction mixture. After heating at 100°C, the reaction began to change colour to dark yellow and a resonance corresponding to the formation of diphenylphosphine (PPh_2H) began to emerge in the ^{31}P NMR spectrum. The reaction was monitored by ^{31}P NMR daily and an unchanging spectrum was obtained after three days, indicating reaction completion. Instead of our desired outcome, we obtained three different products, which were complex **5**, $[Sm(DippForm)_3]$ and PPh_2H. This suggests the reaction proceeded in a 6:1 stoichiometric ratio and this is also evident from the presence of a lot of starting material P_2Ph_4 in the ^{31}P NMR of the reaction mixture.

When we look into the products, we have one unexpected μ-oxo component in complex **5** and similar complexes have been reported before.[63-65] The possible oxygen source in this reaction environment is the THF ligand coordinated to starting material

[Sm(DippForm)$_2$(THF)$_2$]. While the source of oxygen in the complex could be from adventitious moisture, we have previously observed THF molecules interacting (due to ring opening) with reaction pathways leading to the formation of unanticipated products in chapter 1, the introduction part of this chapter and a few previously reported findings.[43, 44, 66] Hence, a possible reaction mechanism is shown in **Scheme 3.11**. Upon reacting with P_2Ph_4, the formation of a dinuclear Sm(II) intermediate [Sm(DippForm)]$_2$(DippForm)(PPh$_2$) might have occurred in addition to the trivalent samarium complex [Sm(DippForm)$_3$]. The slow and irreversible two electron attack of this intermediate on THF might trigger the formation of complex **5**. A similar reaction has been reported previously by Guan *et al*, where they obtained a dinuclear trivalent oxo derivative of a (calix-tetrapyrrole)Sm(II) complex upon reaction with THF.[66] The formation of diphenylphosphine can be ascribed to radical cleavage of unreacted P_2Ph_4 caused by the remaining THF fragments. Presumably the H$^\bullet$ is obtained from the solvent.

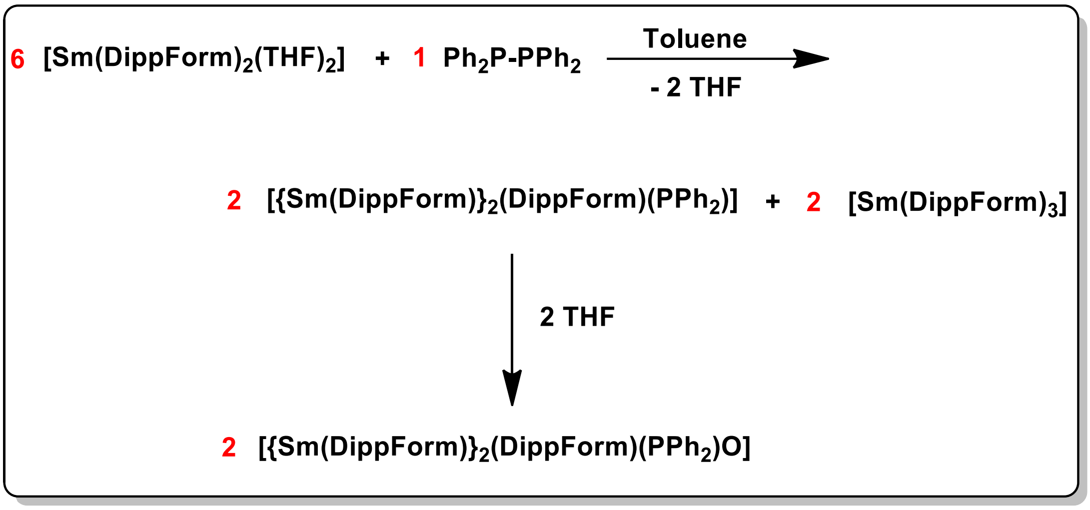

Scheme 3.11. A proposed reaction mechanism of the reaction of [Sm(DippForm)$_2$(THF)$_2$] with P_2Ph_4.

Removal of THF from the starting material might be the better approach to overcome the oxide formation in this reaction. The only way to do it is to sublime the starting material, which is out of the scope of this project at this point.

3.4 Conclusions & Future Outlook

The reactivity shown by [Sm(DippForm)$_2$(THF)$_2$] and ytterbium analogue towards substrates containing dipnictide linkages are very promising and the chapter is concluded by opening up new vistas for future exploration. Reaction with *trans*-azobenzene underlines the fact that [Sm(DippForm)$_2$(THF)$_2$] is demonstrating parallel reactivity with renowned divalent complex [SmCp*$_2$(THF)$_2$]. The use of [Sm(DippForm)$_2$(THF)$_2$] as a reducing agent proved to be effective in synthesizing DippForm analogues of trivalent samarium complexes formed by the reaction of [SmCp*$_2$(THF)$_2$] with Ph_2N_2, where azobenzene has undergone both one and two electron reduction. Less powerful [Yb(DippForm)$_2$(THF)$_2$] also reacts with *trans*-azobenzene (obvious colour changes were observed) but needs more effort to crystallize and isolate the 'yet to be achieved' trivalent ytterbium complex, in which the azobenzene moiety is reductively trapped. The reaction of [Sm(DippForm)$_2$(THF)$_2$] to accomplish benzotriazolate entrapment was amazing and it points towards the requirement of more utilization of 1*H*-1,2,3-benzotriazole in divalent lanthanoid reduction chemistry. Treatment of 1*H*-1,2,3-benzotriazole with divalent ytterbium complexes [Yb(DippForm)$_2$(THF)$_2$] and [Yb(XylForm)$_2$(THF)$_2$] appears to work as both form purple precipitates immediately. The low solubility of the products obtained prevented advancements. Another reagent with NN linkage to investigate is 4,4'-azopyridine, which also provided an immediate colour change upon reaction. But obtaining characterizable crystals of the product remain beyond reach and so the results of this chemistry were not included in this thesis.

Results obtained by treatment of [Sm(DippForm)$_2$(THF)$_2$] with P_2Ph_4 only provide a head start in reductive trapping of substrates containing dipnictogen bonds other than azo linkages. This reaction might need a different approach to prevent unnecessary deviation in the reaction pathway and to achieve the desired outcome. The utility of tetraphenyl diarsenide and its other pnictogen analogues in this particular project is yet to be analyzed. Altogether, a wide range of synthesis and reactivity can be produced.

3.5 Experimental

3.5.1 General Considerations

The lanthanoid compounds described here are highly air and moisture sensitive and were prepared and handled with vacuum-nitrogen line techniques and in a dry box in an atmosphere of purified nitrogen. [Sm(DippForm)$_2$(THF)$_2$],[52] [Yb(DippForm)$_2$(THF)$_2$][57] and P_2Ph_4[67] were prepared by the literature method. Lanthanoid metals were from Santoku/Molycorp/Eutectix. Large chunks were filed in the drybox before use. Solvents (thf, DME, C_6D_6, toluene and hexane) were pre-dried by distillation over sodium or sodium benzophenone ketyl before being stored under an atmosphere of nitrogen. *Trans*-azobenzene and 1*H*-1,2,3-benzotriazole were purchased from Sigma Aldrich and dried under vacuum prior to use. IR spectra were recorded as Nujol mulls between NaCl plates using an Agilent Technologies Cary 630 FTIR instrument within the range 4000–700 cm^{-1}. ^{1}H NMR, ^{13}C NMR and ^{31}P CPD NMR spectra were recorded with a Bruker 400MHz instrument. Chemical shifts were referenced to the residual ^{1}H resonances of the deuterated solvents (^{1}H). Microanalyses were determined by the Chemical Analysis Facility, Macquarie University, and all the samples were sealed in tubes under nitrogen. Melting points were determined in sealed glass capillaries under nitrogen and are uncalibrated. Crystals were immersed in viscous hydrocarbon oil and were measured on a Rigaku SynergyS diffractometer or the MX1 beamline at the Australian Synchrotron.

3.5.2 General Procedure

For N_2Ph_2 reactions, the reagents placed in a Schlenk flask and individually dissolved in solvent (THF/toluene) first and then mixed using a cannula under a nitrogen atmosphere. For other reactions, the solvent was added to a Schlenk charged with reagents.

3.5.3 [(DippForm)$_2$Sm^{III}(Ph$_2$N$_2$)(THF)] 1

Two separate solutions of [Sm(DippForm)$_2$(THF)$_2$] (0.2 mmol) and N_2Ph_2 (0.2 mmol) in 5mL THF were mixed and stirred for 24 hours giving a dark blue solution. Adding N_2Ph_2 in excess is advantageous. Added DME and concentrated in vacuo before storing the solution at -18°C for 3 days to afford yellow/colourless crystals. (0.573g, 42.5%), (Found: C, 69.88; H, 8.39; N, 7.64; $C_{78}H_{112}N_6O_4Sm$ (1348.08) requires C, 69.49; H, 8.37; N, 6.23 %). IR (Nujol): 1667s, 1587w, 1521m, 1334m,1295m, 1260m, 1235w, 1189w, 1098w, 1014w, 934w, 799m, 766w, 755m, 722w, 690w cm $^{-1}$. ^{1}H NMR (C_6D_6, 300 MHz): 10.51 (s, 2H, NC***H***N), 7.2 - 6.9 (m, 22H, aromatic Hs), 3.39 (4H, THF: 2,5-C$\boldsymbol{H}_2$), 2.66 (m,8H, Dipp-C***H***), 2.11 (s, 3H, Toluene-C$\boldsymbol{H}_3$) 1.37 (4H, THF: 3,4-C$\boldsymbol{H}_2$), 1.18 (m, 48H, Dipp-C$\boldsymbol{H}_3$). ^{13}C NMR (75.5 MHz, C_6D_6, 296K): 22.90 (Dipp-***C***H$_3$), 23.85 (Dipp-***C***H$_3$), 24.61 (Dipp-***C***H$_3$), 25.77 (THF: 3,4-***C***H$_2$), 28.34 (Dipp-***C***H), 28.63 (Dipp-***C***H), 58.74 (DME: ***C***H$_3$), 68.14 (THF: 2,5-***C***H$_2$), 72.26 (DME: ***C***H$_2$), 123.36, 123.48, 123.77, 125.05, 128.70, 129.30, 131.13, 138.90, 143.41, 145.66, 146.10, 146.73, 153.28, 167.82 (aromatic C resonances – not assigned).

3.5.4 [(DippForm)Sm^{III}(Ph$_2$N$_2$)(THF)]$_2$ 2

Two separate solutions solution of [Sm(DippForm)$_2$(THF)$_2$] (0.2 mmol) and N_2Ph_2 (0.1 mmol) in 5mL THF were mixed and stirred for one week, causing a colour change to yellow/orange from dark blue. Added DME and concentrated in vacuo before storing the solution at -18°C for 3-4 days to obtain yellow crystals.

3.5.5 [(DippForm)Yb^{III}(Ph$_2$N$_2$)(THF)]$_2$(OH)$_2$·2THF 3

Two separate solutions of [Yb(DippForm)$_2$(THF)$_2$] (0.2 mmol) and N_2Ph_2 (mmol) in 5mL THF were mixed and stirred for 3 days, resulting in a colour change of the solution from red/brown to dark green. Concentrated the solution in vacuo and left the solution undisturbed at -18°C for a few weeks resulting in the formation of small yellow crystals.

3.5.6 [Sm^{III}(DippForm)$_2$(Btz)(THF)] 4

10mL of THF was added to a Schlenk charged with [Sm(DippForm)$_2$(THF)$_2$] (0.2 mmol) and 1*H*-1,2,3-benzotriazole (0.2mmol) and stirred for three days causing a colour change from dark green to yellowish green. The solution was concentrated in vacuo and stored at 4°C overnight to afford off-white crystals. (0.605g, 53.1%), (Found: C, 63.65; H, 8.121; N, 8.97; $C_{64}H_{90}N_7O_2Sm$ (1139.77) requires C, 67.44; H, 7.96; N, 8.60 %). IR (Nujol): 3061m, 1666m, 1593m, 1522s, 1361m, 1318s, 1278s, 1233s, 1190s, 1138w, 1107m, 1070s, 1044m, 1021m, 972w, 942m, 911m, 867m, 802m, 776m, 758m, 748s, 629m cm $^{-1}$. ^{1}H NMR (C_6D_6, 300 MHz): 12.85 (s, 2H, NC***H***N), 7.4 - 6.9 (m, 16H, aromatic Hs). ^{13}C NMR (75.5 MHz, C_6D_6, 296K): 22.47 (Dipp-***C***H$_3$), 23.94 (Dipp-***C***H$_3$), 25.45 (Dipp-***C***H$_3$), 26.59 (THF: 3,4-***C***H$_2$), 28.36 (Dipp-***C***H), 29.07 (Dipp-***C***H), 68.71 (THF: 2,5-***C***H$_2$), 116.36, 123.49, 123.89, 124.46, 124.73, 128.69, 140.34, 143.69, 146.87 (aromatic **C** resonances – not assigned), 192.29 (Dipp-N***C***HN).

3.5.7 [Sm^{III}(DippForm)]$_2$(DippForm)(PPh$_2$)O 5

10mL of toluene was added to a Schlenk charged with [Sm(DippForm)$_2$(THF)$_2$] (0.3 mmol) and P_2Ph_4 (0.05mmol), and heated at 100°C for 3 days along with stirring giving a dark yellow solution. Filtered and dried the solution to obtain yellow/green solid. Added hexane and filtered again. Concentrating the hexane solution in vacuo and storing it at 4°C overnight resulted in the formation of yellow crystals.

3.6 X-ray crystal data

Single crystals coated with viscous hydrocarbon oil were mounted on glass fibres or loops. Complex **1, 2, 3** and **5** were measured at the Australian Synchrotron on the MX1 macromolecular beamlines, data integration was completed using Blue-ice[68] and XDS[69] software programs. Complexes **4** was measured on a Rigaku SynergyS diffractometer. The SynergyS operated using microsource Cu-Kα radiation (λ = 1.54184 Å) at 123 K. Data processing was conducted using CrysAlisPro.55 software suite.[70] Structural solutions were obtained by either direct methods[71] or charge flipping[70] methods and refined using full-matrix least-squares methods against F^2 using SHELX2015,[72] in conjunction with Olex2[70] graphical user interface. All hydrogen atoms were placed in calculated positions using the riding model. Crystal data and refinement details are given in **Table 3.1**. Data was collected by my colleague Dr. Zhifang Guo and she solved and refined the X-ray structures of **3** and **5**. Crystal structures of other complexes were solved and refined by me.

Table 3.1 Crystal data and structure refinement for lanthanoid complexes **1-3**

	1	**2**	**3**
Formula	$C_{78}H_{112}N_6O_4Sm$	$C_{98}H_{138}N_8O_6Sm_2$	$C_{90}H_{124}N_8O_6Yb_2$
M_r	1348.08	1824.86	1758.03
Crystal System	Monoclinic	Triclinic	Triclinic
Space group	$P2_1/n$	P-1	P-1
a (Å)	13.930(3)	12.87040(10)	14.750(3)
b (Å)	25.320(5)	13.01920(10)	16.270(3)
c (Å)	20.770(4)	14.91580(10)	20.580(4)
α (°)	90	106.0950(10)	101.96(3)
β (°)	103.32(3)	106.1290(10)	94.29(3)
γ (°)	90	91.8730(10)	91.23(3)
V (Å^3)	7129(3)	2290.49(3)	4814.6(18)
Z	4	1	2
ρ_{calc}, g cm^{-3}	1.256	1.323	1.213
μ, mm^{-1}	0.876	9.959	1.980

N_τ	117941	46899	81560
N (R_{int})	12938 (0.0481)	9553 (0.0419)	16594 (0.0444)
$R_1(I > 2\sigma(I))$	0.0335	0.0273	0.0693
wR_2 (all data)	0.0910	0.0700	0.2222
GOF	1.063	1.088	1.071

Table 3.2 Crystal data and structural refinement for lanthanoid complexes **4** & **5.**

	4	**5**
Formula	$C_{64}H_{90}N_7O_2Sm$	$C_{87}H_{115}N_6OPSm_2$
M_r	1139.77	1592.51
Crystal System	Monoclinic	Triclinic
Space group	$P2_1/n$	P-1
a (Å)	15.3800(2)	12.650(3)
b (Å)	16.5828(2)	13.240(3)
c (Å)	25.1684(3)	26.730(5)
α (°)	90	90.65(3)
β (°)	95.5170(10)	98.37(3)
γ (°)	90	115.67(3)
V (Å^3)	6389.30(14)	3978.0(17)
Z	4	2
ρ_{calc}, g cm^{-3}	1.185	1.330
μ, mm^{-1}	7.239	1.530
N_τ	67249	68051
N (R_{int})	13245 (0.0496)	13846 (0.0267)
$R_1(I > 2\sigma(I))$	0.0447	0.0364
wR_2 (all data)	0.1285	0.0979
GOF	1.048	1.031

3.7 References

1. F. T. Edelmann, *Coord. Chem. Rev.*, 2016, **306**, 346-419.
2. D. A. Atwood, *The rare earth elements : fundamentals and applications*, John Wiley & Sons, Inc., Chichester, West Sussex, United Kingdom ; Hoboken, 2012.
3. T. Pugh, A. Kerridge and R. A. Layfield, *Angew. Chem. Int. Ed.*, 2015, **54**, 4255-4258.
4. T. Li, S. Kaercher and P. W. Roesky, *Chem. Soc. Rev.*, 2014, **43**, 42-57.
5. W. J. Evans, T. A. Ulibarri and J. W. Ziller, *J. Am. Chem. Soc.*, 1988, **110**, 6877-6879.
6. W. J. Evans, G. Kociok-Koehn, V. S. Leong and J. W. Ziller, *Inorg. Chem.*, 1992, **31**, 3592-3600.
7. W. J. Evans and D. K. Drummond, *J. Am. Chem. Soc.*, 1989, **111**, 3329-3335.
8. W. J. Evans, L. A. Hughes, D. K. Drummond, H. Zhang and J. L. Atwood, *J. Am. Chem. Soc.*, 1986, **108**, 1722-1723.
9. W. J. Evans, J. W. Grate, L. A. Hughes, H. Zhang and J. L. Atwood, *J. Am. Chem. Soc.*, 1985, **107**, 3728-3730.
10. W. J. Evans and D. K. Drummond, *J. Am. Chem. Soc.*, 1988, **110**, 2772-2774.
11. W. J. Evans and D. K. Drummond, *J. Am. Chem. Soc.*, 1986, **108**, 7440-7441.
12. N. Arleth, S. Bestgen, M. T. Gamer and P. W. Roesky, *J. Am. Chem. Soc.*, 2014, **136**, 14023-14026.
13. C. Schoo, S. Bestgen, R. Köppe, S. N. Konchenko and P. W. Roesky, *Chem. Commun.*, 2018, **54**, 4770-4773.
14. N. Arleth, M. T. Gamer, R. Köppe, N. A. Pushkarevsky, S. N. Konchenko, M. Fleischmann, M. Bodensteiner, M. Scheer and P. W. Roesky, *Chem. Sci.*, 2015, **6**, 7179-7184.
15. C. Schoo, S. Bestgen, A. Egeberg, J. Seibert, S. N. Konchenko, C. Feldmann and P. W. Roesky, *Angew. Chem. Int. Ed.*, 2019, **58**, 4386-4389.
16. S. N. Konchenko, N. A. Pushkarevsky, M. T. Gamer, R. Koppe, H. Schnöckel and P. W. Roesky, *J. Am. Chem. Soc.*, 2009, **131**, 5740–5741.
17. C. Schoo, S. Bestgen, M. Schmidt, S. N. Konchenko, M. Scheer and P. W. Roesky, *Chem. Commun.*, 2016, **52**, 13217-13220.

18. T. Li, N. Arleth, M. T. Gamer, R. Köppe, T. Augenstein, F. Dielmann, M. Scheer, S. N. Konchenko and P. W. Roesky, *Inorg. Chem.*, 2013, **52**, 14231-14236.
19. S. Patai, *The chemistry of the hydrazo, azo, and azoxy groups*, John Wiley, London ; New York, 1975.
20. C.-L. Pan, W. Chen and J. Song, *Organometallics*, 2011, **30**, 2252-2260.
21. F. Nief, B. T. de Borms, L. Ricard and D. Carmichael, *Eur. J. Inorg. Chem.*, 2005, **2005**, 637-643.
22. M. A. Katkova, G. K. Fukin, A. A. Fagin and M. N. Bochkarev, *J. Organomet. Chem.*, 2003, **682**, 218-223.
23. Z. Hou, T.-a. Koizumi, M. Nishiura and Y. Wakatsuki, *Organometallics*, 2001, **20**, 3323-3328.
24. W. J. Evans, D. S. Lee, J. W. Ziller and N. Kaltsoyannis, *J. Am. Chem. Soc.*, 2006, **128**, 14176-14184.
25. W. J. Evans, R. A. Keyer and J. W. Ziller, *Organometallics*, 1993, **12**, 2618-2633.
26. W. J. Evans, D. K. Drummond, L. R. Chamberlain, R. J. Doedens, S. G. Bott, H. Zhang and J. L. Atwood, *J. Am. Chem. Soc.*, 1988, **110**, 4983-4994.
27. W. J. Evans, T. M. Champagne and J. W. Ziller, *Organometallics*, 2007, **26**, 1204-1211.
28. E. D. Brady, D. L. Clark, D. W. Keogh, B. L. Scott and J. G. Watkin, *J. Am. Chem. Soc.*, 2002, **124**, 7007-7015.
29. J. Andrez, J. Pécaut, P.-A. Bayle and M. Mazzanti, *Angew. Chem. Int. Ed.*, 2014, **53**, 10448-10452.
30. M. Nishiura, Z. Hou and Y. Wakatsuki, *Organometallics*, 2004, **23**, 1359-1368.
31. J. Takats, X. W. Zhang, V. W. Day and T. A. Eberspacher, *Organometallics*, 1993, **12**, 4286-4288.
32. W. J. Evans, *Coord. Chem. Rev.*, 2000, **206–207**, 263–283.
33. C. A. P. Goodwin, N. F. Chilton, G. F. Vettese, E. Moreno Pineda, I. F. Crowe, J. W. Ziller, R. E. P. Winpenny, W. J. Evans and D. P. Mills, *Inorg. Chem.*, 2016, **55**, 10057-10067.
34. A. R. Willauer, A. M. Dabrowska, R. Scopelliti and M. Mazzanti, *Chem. Commun.*, 2020, **56**, 8936-8939.
35. G. W. Watt and E. W. Gillow, *J. Am. Chem. Soc.*, 1969, **91**, 775-776.

36. A. R. Katritzky, C. W. Rees and E. F. V. Scriven, *Comprehensive heterocyclic chemistry II : a review of the literature 1982-1995 : the structure, reactions, synthesis, and uses of heterocyclic compounds*, Pergamon, Oxford ; New York, 1st edn., 1996.
37. J.-C. Rybak and K. Müller-Buschbaum, *Z. Anorg. Allg. Chem.*, 2010, **636**, 126-131.
38. K. Müller-Buschbaum and Y. Mokaddem, *Z. Anorg. Allg. Chem.*, 2007, **633**, 521-523.
39. K. Müller-Buschbaum and Y. Mokaddem, *Z. Anorg. Allg. Chem.*, 2008, **634**, 2360-2366.
40. K. Müller-Buschbaum and Y. Mokaddem, *Eur. J. Inorg. Chem.*, 2006, **2006**, 2000-2010.
41. Y.-S. Meng, Y.-S. Qiao, M.-W. Yang, J. Xiong, T. Liu, Y.-Q. Zhang, S.-D. Jiang, B.-W. Wang and S. Gao, *Inorg. Chem. Front.*, 2020, **7**, 447-454.
42. R. A. Layfield, J. J. W. McDouall, S. A. Sulway, F. Tuna, D. Collison and R. E. P. Winpenny, *Chem. Eur. J.*, 2010, **16**, 4442-4446.
43. W. J. Evans, J. T. Leman, J. W. Ziller and S. I. Khan, *Inorg. Chem.*, 1996, **35**, 4283-4291.
44. N. A. Pushkarevsky, I. Y. Ilyin, P. A. Petrov, D. G. Samsonenko, M. R. Ryzhikov, P. W. Roesky and S. N. Konchenko, *Organometallics*, 2017, **36**, 1287-1295.
45. S. Hamidi, G. B. Deacon, P. C. Junk and P. Neumann, *Dalton Trans.*, 2012, **41**, 3541-3552.
46. G. R. Fulmer, A. J. Miller, N. H. Sherden, H. E. Gottlieb, A. Nudelman, B. M. Stoltz, J. E. Bercaw and K. I. Goldberg, *Organometallics*, 2010, **29**, 2176-2179.
47. M. Salehisaki, N. E. Rad, G. B. Deacon, J. Wang, Z. Guo and P. C. Junk, *Inorg. Chim. Acta.*, 2022, **539**, 120997.
48. R. F. Culmo and C. Shelton, *Shelton, CT*, 2013.
49. H.-X. Li, Q.-F. Xu, J.-X. Chen, M.-L. Cheng, Y. Zhang, W.-H. Zhang, J.-P. Lang and Q. Shen, *J. Organomet. Chem.*, 2004, **689**, 3438-3448.
50. W. J. Evans, T. P. Hanusa, J. H. Meadows, W. E. Hunter and J. L. Atwood, *Organometallics*, 1987, **6**, 295-301.
51. C. Brown, *Acta Crystallogr.*, 1966, **21**, 146-152.

52. M. L. Cole and P. C. Junk, *Chem. Commun.*, 2005, 2695-2697.
53. R. D. Shannon, *Acta Crystallogr. Sect. A.*, 1976, **32**, 751-767.
54. F. Yuan, Q. Shena and J. Sun, *Polyhedron*, 1998, **17**, 2009-2012.
55. G. B. Deacon, G. Meyer, D. Stellfeldt, G. Zelesny, B. W. Skelton and A. H. White, *Z. Anorg. Allg. Chem.*, 2001, **627**, 1652-1658.
56. M. L. Cole, G. B. Deacon, C. M. Forsyth, P. C. Junk, K. Konstas and J. Wang, *Chem. Eur. J.*, 2007, **13**, 8092-8110.
57. M. L. Cole, G. B. Deacon, C. M. Forsyth, P. C. Junk, K. Konstas, J. Wang, H. Bittig and D. Werner, *Chem. Eur. J.*, 2013, **19**, 1410-1420.
58. W. J. Evans, J. W. Grate, I. Bloom, W. E. Hunter and J. L. Atwood, *J. Am. Chem. Soc.*, 1985, **107**, 405-409.
59. W. J. Evans, *Polyhedron*, 1987, **6**, 803-835.
60. D. Turcitu, F. Nief and L. Ricard, *Chem. Eur. J.*, 2003, **9**, 4916-4923.
61. M. L. Cole, G. B. Deacon, C. M. Forsyth, P. C. Junk, D. P. Ceron and J. Wang, *Dalton Trans.*, 2010, **39**, 6732-6738.
62. W. J. Evans, S. L. Gonzales and J. W. Ziller, *J. Am. Chem. Soc.*, 1991, **113**, 7423-7424.
63. W. J. Evans, B. L. Davis, G. W. Nyce, J. M. Perotti and J. W. Ziller, *J. Organomet. Chem.*, 2003, **677**, 89-95.
64. W. J. Evans and S. L. Gonzales, *J. Organomet. Chem.*, 1994, **480**, 41-44.
65. W. J. Evans, E. Montalvo, S. E. Foster, K. A. Harada and J. W. Ziller, *Organometallics*, 2007, **26**, 2904-2910.
66. J. Guan, T. Dubé, S. Gambarotta and G. P. Yap, *Organometallics*, 2000, **19**, 4820-4827.
67. W. Kuchen and H. Buchwald, *Chem. Ber.*, 1958, **91**, 2871-2877.
68. T. M. McPhillips, S. E. McPhillips, H. J. Chiu, A. E. Cohen, A. M. Deacon, P. J. Ellis, E. Garman, A. Gonzalez, N. K. Sauter, R. P. Phizackerley, S. M. Soltis and P. Kuhn, *J. Synchrotron Radiat.*, 2002, **9**, 401-406.
69. W. Kabsch, *J. Appl. Crystallogr.*, 1993, **26**, 795-800.
70. O. V. Dolomanov, L. J. Bourhis, R. J. Gildea, J. A. K. Howard and H. Puschmann, *J. Appl. Crystallogr.*, 2009, **42**, 339-341.
71. G. M. Sheldrick, *Acta Crystallogr. A.*, 2008, **64**, 112-122.

72. G. M. Sheldrick, *Acta Crystallogr. C.*, 2015, **71**, 3-8.

Chapter 4

Reactivity of [Ln(DippForm)$_2$(THF)$_2$] (Ln = Sm, Yb) towards unsaturated small organic molecules

4.1 Introduction

The interesting factor in studying the reactivities of divalent organolanthanoid complexes is their uncertainty and often uniqueness in the reaction outcome. This is mainly due to their high reactivity and often the lack of selectivity is due to this reactivity. Optimising the selectivity is the impetus for many studies. The results obtained in the previous two chapters were very exciting and those signify the importance of carrying out studies on the reactivity of these divalent organolanthanoid complexes towards other unsaturated chemical bonds. Since Ln(II) complexes hardly follow a set of rules compared to d-block metals, their reaction in the vicinity of multiple bonded substrates can be unpredictable. One early example which underlines this statement is illustrated in **Scheme 4.1**, where reductive homologation of CO using [SmCp*$_2$(THF)$_2$], results in the formation of a tetranuclear Sm(III) complex with two ketenecarboxylate units as a skeleton.[1] The [SmCp*$_2$(THF)$_2$] has triggered the reduction of six CO ligands by four electrons and a complete cleavage of a CO unit is obvious here since an oxygen-free C=C-C linkage is observed. This distinctiveness of lanthanoid complexes from others is evident in this reaction because even more soluble, strongly reducing, and low valent transition metal complexes usually form carbonyl complexes upon reaction with CO.[2]

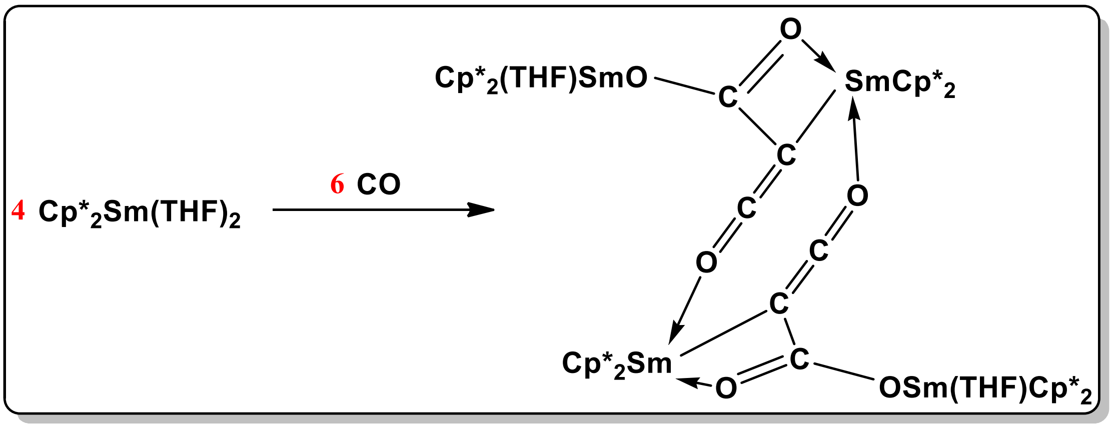

Scheme 4.1. Reductive homologation of CO using [SmCp*$_2$(THF)$_2$] results in the formation of [Cp*$_4$Sm$_2$(O$_2$CCCO)(THF)]$_2$.[1]

Similarly, a couple of recent examples are depicted in **Scheme 4.2**, in which [Ln(DippForm)$_2$(THF)$_2$] (where Ln = Sm and Yb) were treated with C=O (benzophenone) and C=S (carbon disulfide) multiple bonds. The Sm complex shows the trapping of a rare dianionic bridging ligand thioformyl carbonotrithioate ((SCSCS$_2$)$^{2-}$) by [Sm(DippForm)$_2$(THF)$_2$] when treated with CS$_2$.[3] Usually, a C-C coupling is expected on these occasions, instead, a C-S bond formation induced by the amidinatolanthanoid species is observed. The second example exhibits the formation of a highly unusual complex [Ln(DippForm)$_2$]$_2$(THF)[OC(Ph)=(C$_6$H$_5$)C(Ph)$_2$O], when [Sm(DippForm)$_2$(THF)$_2$] and its Yb analogue is treated with benzophenone.[3] The observation of a trapped bridging anion involved a rare C-C coupling, which was not between two carbonyl carbons of two benzophenone ligands (similar to pinacolate complexes). Rather, the carbon at the *para* position of one of the phenyl groups formed a bond with other carbonyl carbon. In addition, the reaction of Ln(II) complexes towards nitro groups are also well studied using [Sm[N(SiMe$_3$)$_2$]$_2$], where aryl nitro compounds (ArNO$_2$) were reduced to corresponding arylamines (ArNH$_2$), which proceed *via* O abstraction and later resulted in the isolation of unusual intermediates.[4]

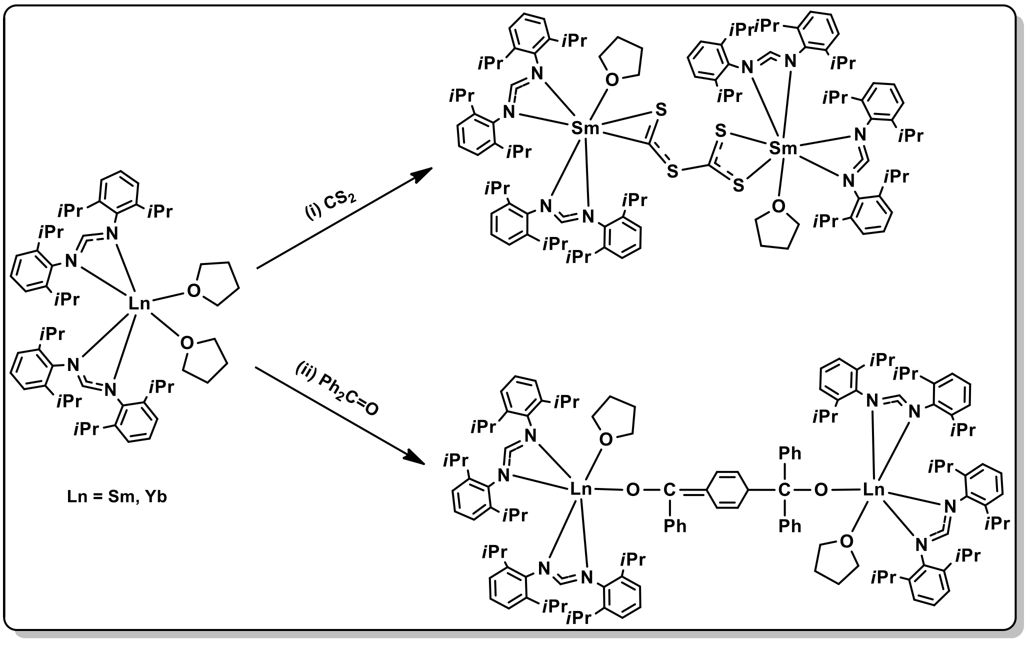

Scheme 4.2. [Ln(DippForm)$_2$(THF)$_2$] was treated with (i) carbon disulfide (Ln = Sm) and (ii) benzophenone (Ln = Sm, Yb).[3]

4.1.1 Entrapment of ketyl radical ligands using divalent organolanthanoid complexes.

The reduction and formation of pinacolate complexes via C-C coupling often resulted when a C=O bond in an organic molecule was targeted by divalent lanthanoid complexes.[5] We have already seen this type of reaction in **Scheme 4.2 (ii)** and a similar transformation was successfully achieved previously using $[Yb(NCS)_2(THF)_2]$ upon reaction with benzophenone.[6] The reaction pathway for these reductions involves the development of ketyl intermediates, where 'ketyl' denotes a radical anion which consists of a $^{\cdot}C\text{-}O^{-}$ unit, which usually forms as a product of one-electron reduction of a ketone. Metal ketyl complexes have a few important applications in organic chemistry, which include organic synthesis promoted by transient samarium ketyls in the SmI_2/ketone system[7-11] together with a universal role in the drying of organic solvents. Since they are highly reactive and only transient existence is observed,[9, 12-14] their isolation is extremely difficult. Besides, they might undergo radical C-C coupling as shown previously. However, careful selection of co-ligand (normally those capable of steric saturation)[15, 16] and solvents[17, 18] would help to prevent decomposition and stabilization of metal ketyls can be achieved.[5, 18, 19] The single-electron reduction of 9-fluorenone facilitated by $[Sm^{II}(OAr)_2(THF)_3]$ resulted in the formation of first crystallographically characterized metal ketyl complex $[Sm^{III}(OAr)(THF)_2(fn^{\cdot}\text{-}O)]$, where $fn^{\cdot}\text{-}O^{-}$ = 9-fluorenone ketyl and OAr = $2,6\text{-}tBu_2\text{-}4\text{-}MeC_6H_2O$.[20] But, the dissolution of the same complex in Et_2O causes radical C-C coupling which results in pinacolate-type complexes (see **Scheme 4.3**).[20]

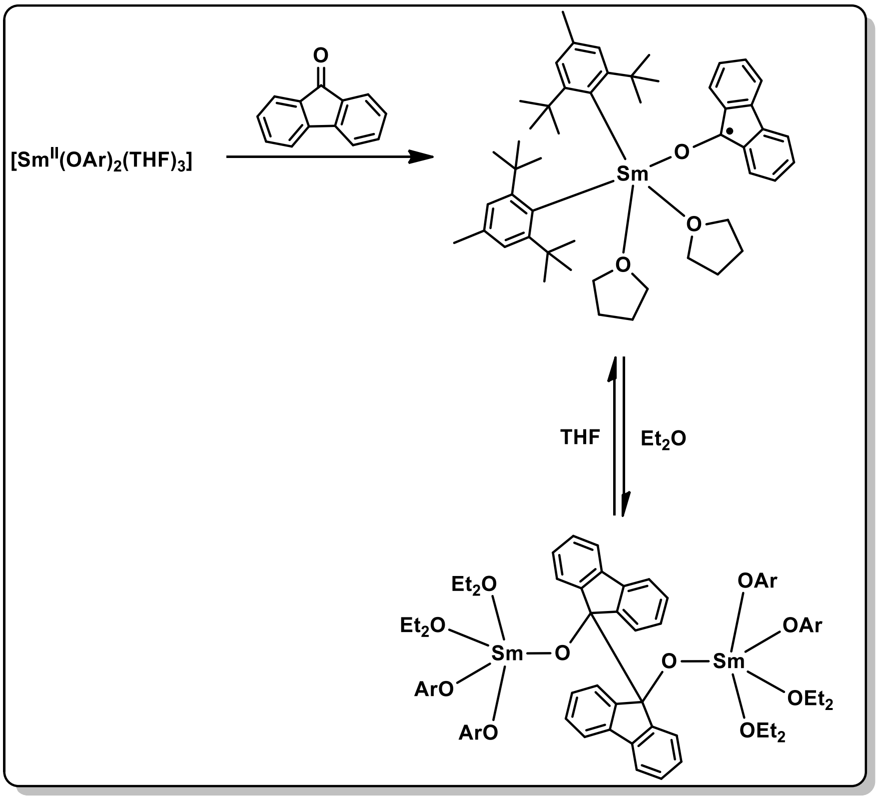

Scheme 4.3. The reduction of 9-fluorenone by [Sm^{II}(OAr)$_2$(THF)$_3$] and dissolution of metal ketyl complex [Sm^{III}(OAr)(THF)$_2$(fn$^{\cdot}$-*O*)] in Et$_2$O.[20]

Studies were continued and synthesis of several crystallographically characterizable metal ketyl (fn$^{\cdot}$-*O* or bp$^{\cdot}$-*O* from benzophenone) complexes were reported utilizing different metals[19, 21-26] and co-ligand groups.[18-20, 26-28] Amidinate and formamidinate based ligands were limited among them and recently utilization of [Ln(DippForm)$_2$(THF)$_2$] (Ln = Sm, Yb) were unsuccessful since reaction with benzophenone resulted in unusual C-C coupling as shown in **Scheme 4.2** above. Further studies using more rigid or bulkier ketones (than benzophenone) paved the way for trapping a range ketyl radical ligands using [Yb(DippForm)$_2$(THF)$_2$]. **Figure 4.1** shows the ytterbium ketyl radical complexes synthesized by [Yb(DippForm)$_2$(THF)$_2$] through reduction of various ketones such as 9-fluorenone, 9,10-phenanthrenequinone (phen), 3,5-di-tert-butyl-1,2-benzoquinone (tbbq), 2,3,4,5-tetraphenylcyclopentadienone and 1,2-acenaphthenequinone(acen).[29]

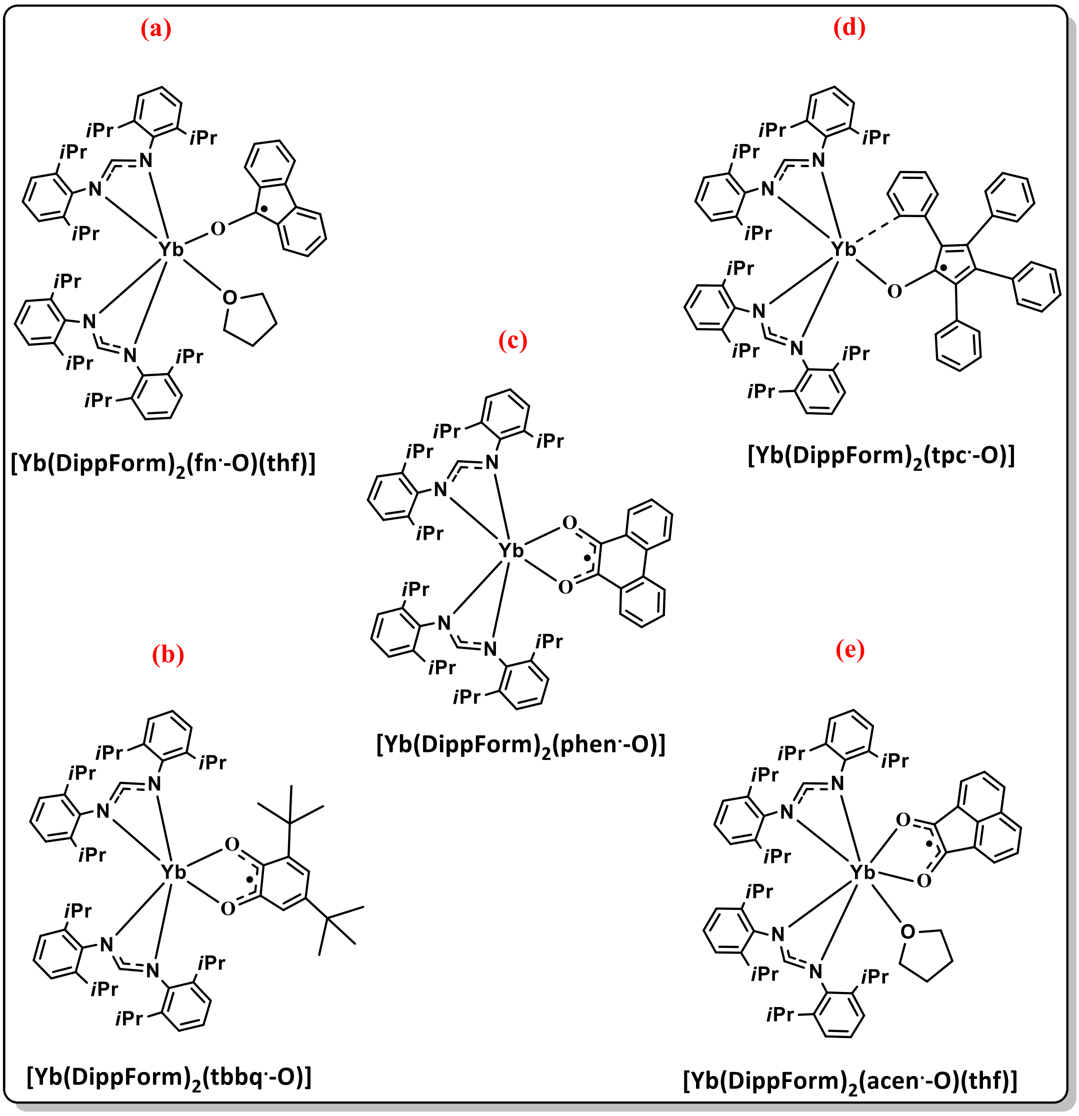

Fig 4.1. [Yb(DippForm)$_2$(THF)$_2$] has been used for trapping ketyl radical complexes (a) [Yb(DippForm)$_2$(fn$^{\cdot}$-O)(thf) from 9-fluorenone; (b) [Yb(DippForm)$_2$(tbbq$^{\cdot}$-O_2)] from 3,5-di-tert-butyl-1,2-benzoquinone (tbbq); (c) [Yb(DippForm)$_2$(phen$^{\cdot}$-O_2)] from 9,10-phenanthrenequinone (phen); (d) [Yb(DippForm)$_2$(tpc$^{\cdot}$-O)] from 2,3,4,5-tetraphenylcyclopentadienone; (e) [Yb(DippForm)$_2$(acen$^{\cdot}$-O_2)(thf)] from 1,2-acenaphthenequinone(acen).[29]

4.1.2 Reaction with substrates containing C=N

Lanthanoid metal-based reactivity studies have been carried out for many substrates containing C=N bonds and a few important ones among them are imines, carbodiimides, isothiocyanates, isocyanates and nitriles.[30-41] Carbodiimides can be termed as one of the most studied among them of their reactivity towards divalent organolanthanoid complexes. Reduction reactions using carbodiimides are highly influenced by the size of the substrate and ligation of Sm(II), which results in the formation of unusual reaction products, as seen in **Scheme 4.4**. Initially, the formation of an oxalamidinate ($(CyN)_2CC(NCy)_2$) was observed through C-C coupling when N,N'-dicyclohexylcarbodiimide (Cy-N=C=N-Cy) was treated with the samarium (II) bis(trimethylsilyl)amide complex **[Scheme 4.4. a(i)]**.[32] The C-C coupling occurred in this case between central diimide carbon atoms of Cy-N=C=N-Cy fragments, whereas coupling of two methine carbon atoms was seen when the cyclohexyl groups on the carbodiimide were replaced by diisopropylphenyl groups, and resulted in the formation of a dinuclear diformamidinate complex when treated with the same Sm(II) complex **[Scheme 4.4. a(ii)]**.[32] However, the reaction proceeded in a different way when a divalent samarium complex ligated by two DippForm ligands was employed and resulted in the formation of two mononuclear complexes instead of C-C coupling **[Scheme 4.4. (b)]**.[31] In the case of imines, reactions involving divalent organosamarium complexes $[SmCp^*_2(THF)_2]$, $[Sm[N(SiMe_3)_2]_2(THF)_3]$, and $[Sm(OAr)_2(THF)_3]$ (where Ar = $C_6H_2{}^tBu_2$-2,6-Me-4) were treated with *N*-phenyl benzophenone imine, *N*-phenyl fluorenone imine and benzophenone imines, which resulted in the synthesis of various trivalent samarium η^1-amine/η^1-ketimido and η^2-ketimine complexes (**Figure 4.2**).[42]

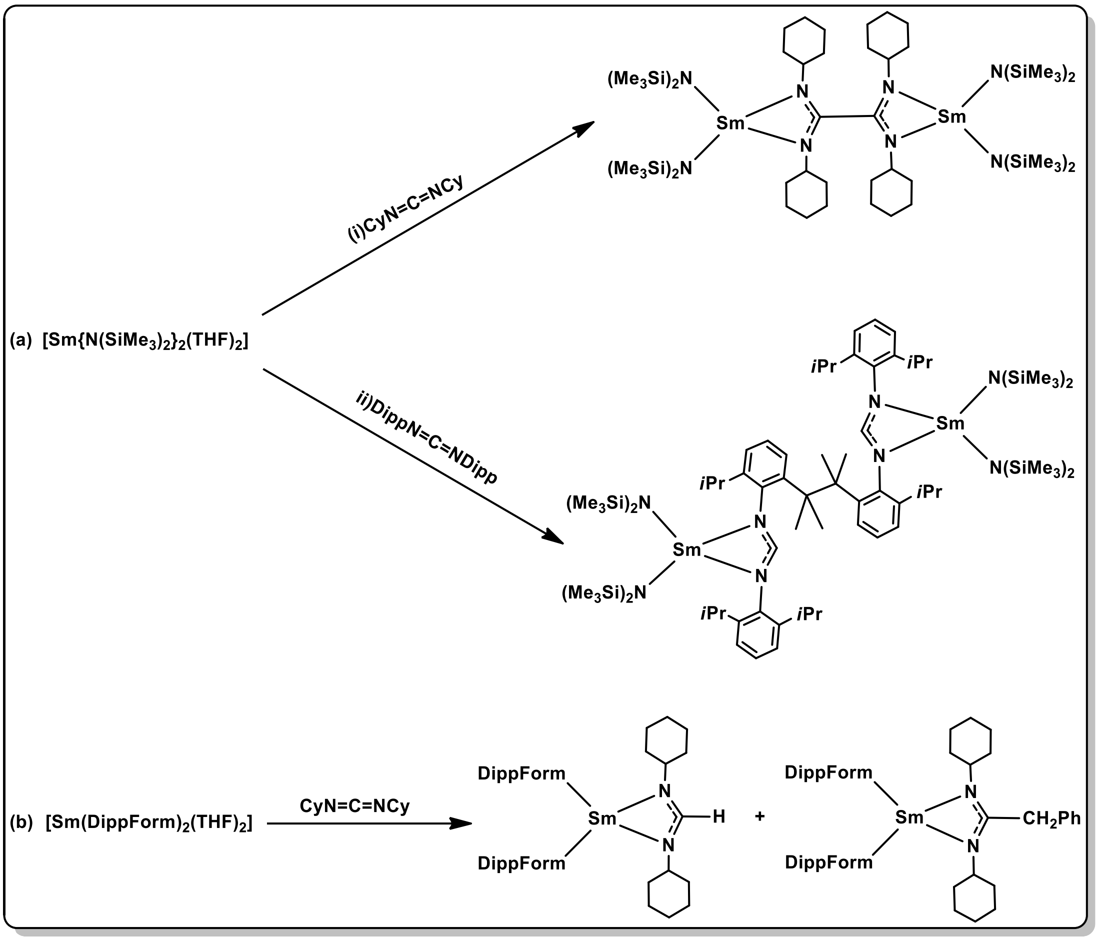

Scheme 4.4. The reaction of [SmL$_2$(THF)$_2$] towards RN=C=NR, where [a(i)] L = N(SiMe$_3$)$_2$, R = Cy; [a(ii)] L = N(SiMe$_3$)$_2$, R = Dipp; [b] L = DippForm, R = Cy.[31,32]

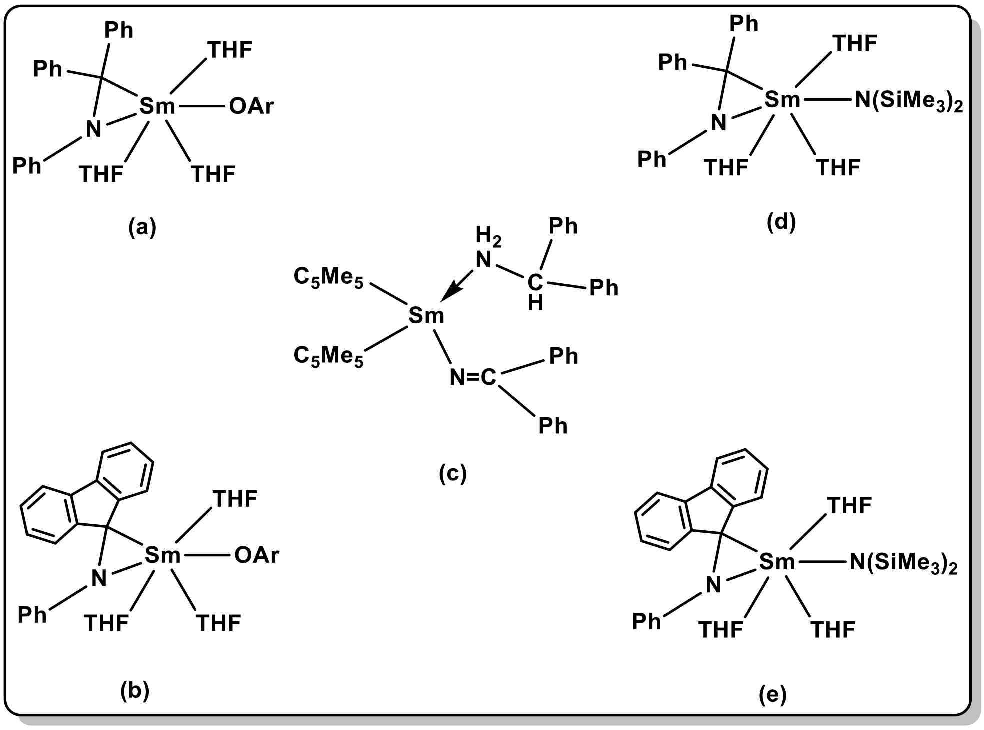

Fig 4.2. Structurally characterizable Sm(III) complexes formed by reaction of **(a)** [Sm(OAr)$_2$(THF)$_3$] (Ar = C$_6$H$_2$^{t}Bu$_2$-2,6-Me-4) with *N*-phenyl benzophenone imine **(b)** [Sm(OAr)$_2$(THF)$_3$] (Ar = C$_6$H$_2$^{t}Bu$_2$-2,6-Me-4) with *N*-phenyl fluorenone imine **(c)** [SmCp*$_2$(THF)$_2$] with benzophenone imine **(d)** [Sm[N(SiMe$_3$)$_2$]$_2$(THF)$_3$] with *N*-phenyl benzophenone imine **(e)** [Sm[N(SiMe$_3$)$_2$]$_2$(THF)$_3$] with *N*-phenyl fluorenone imine.[42]

The reaction of divalent organolanthanoid complexes towards isocyanates and isothiocyanates has been much less studied and notable reductive trapping products have not been obtained so far. In organolanthanoid chemistry, substrates containing NCX (X = S, O) moieties are mainly used for insertion-type reactions towards trivalent rare-earth complexes[43-45] and cyclotrimerization of PhNCX (X = S, O) ligands occurred in some cases.[43] Nitriles and isonitriles are very useful reagents in organic and organometallic chemistry,[35, 37] but their interactions with organolanthanoid complexes are reported only a few.[30, 33, 40] Reactivity of nitriles and isonitriles towards Sm(II) SET reagents normally results in their reduction and formation of trivalent samarium cyanides, which proceed via C-N or C-C bond cleavage and form various samarium-containing complexes along with some organic products.[46, 47] The reaction of dimetallated N,N'-dimethyl substituted porphyrinogen Sm(II) complex

$[(Me_2N_4)Sm(THF)_2]$ with the nitrile ^tBuCN is a very good example, which leads to the formation of a trimeric Sm(III) cyanide (μ-CN^-) complex and reductive entrapment of ^tBu moiety by forming Sm(III)-iminoacyl $(^tBuC{=}N{-}^tBu)^-$ complex (**Scheme 4.5**).[48]

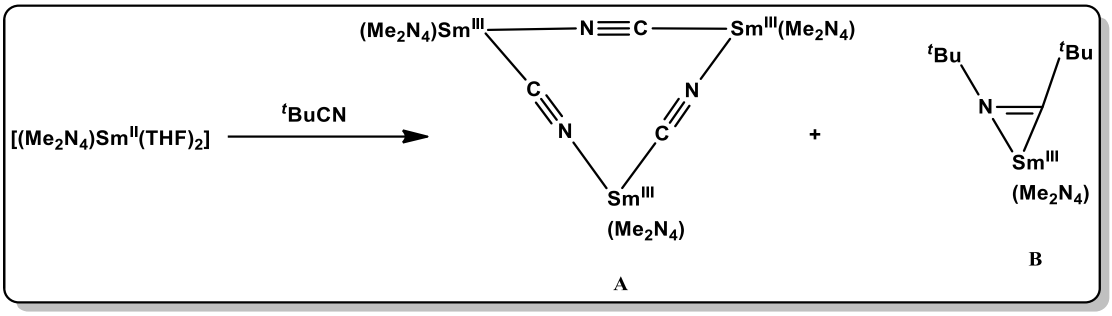

Scheme 4.5. The reaction of $[(Me_2N_4)Sm(THF)_2]$ with ^tBuCN giving trimeric Sm(III) cyanide (μ-CN^-) complex (A) and Sm(III)-iminoacyl $(^tBuC{=}N{-}^tBu)^-$ complex (B).[48]

Sm(II) mediated catalytic cyclotrimerization of arylnitriles has been reported previously, where Sm(II) complexes alone (SmI_2, $[Sm(CH_3C_5H_4)_2]$, $[Sm(Ar'O)_2]$ Ar' = 2,6-di-^{t}Bu-4-methylphenyl) or combined with n-hexylamine proved to be highly efficient (**Scheme 4.6**).[49] Divalent samarium complexes were successfully employed in the cyclotrimerization of benzonitrile, *p*-chlorophenylnitrile and 2-pyridylnitrile, which results in the formation of triphenyl-s-triazine, tri-*p*-chlorophenyl-s-triazine and tri-2-pyridyl-s-triazine respectively. This could be one reason for their low utility in reductive trapping applications using divalent organolanthanoid complexes.

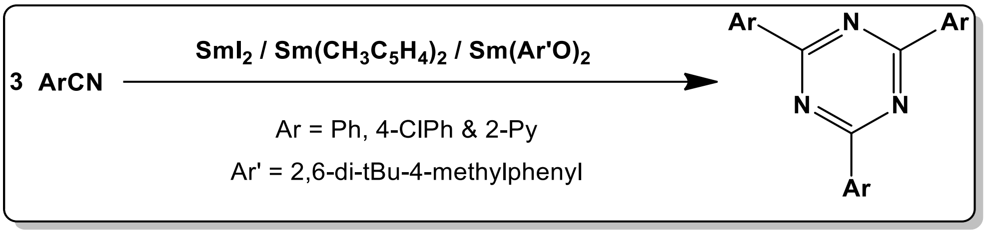

Scheme 4.6. Sm(II) mediated catalytic cyclotrimerization of arylnitriles.[49]

4.2 Research Plan

The reaction of divalent organolanthanoid complexes towards each type of unsaturated small organic molecule is distinct. Substrates containing dissimilar types of bonds will give different outcomes, which mainly depend on ligand nature and steric saturation around the central lanthanoid ion. The formation of rare-earth ketyl complexes when [Yb(DippForm)$_2$(THF)$_2$] was treated with 1,2-diketones were interesting, but their reaction outcome with samarium analogue [Sm(DippForm)$_2$(THF)$_2$] was different. Selection of the appropriate di-ketone will be the key here as stabilization of metal ketyls has very high requirements. Benzil will be a good choice in this case because of its slightly larger size than benzophenone and flexibility compared to other rigid diketones.

Isocyanates and isothiocyanates are less-studied organic substrates in the application of reduction chemistry using organolanthanoids. The reaction of phenyl isocyanates (PhNCO) and phenyl isothiocyanates (PhNCS) towards [Sm(DippForm)$_2$(THF)$_2$] and [Yb(DippForm)$_2$(THF)$_2$] will be interesting. Since steric saturation is one of the key factors in organolanthanoid chemistry, naphthyl isothiocyanate ($C_{10}H_8$-NCS) also can be an attractive reagent in this application. The use of various nitriles such as benzonitrile, *o*-tolunitrile etc. can also be included as part of the research plan, even though the chance for catalytic cyclotrimerization of these arylnitriles are very high. Large bulky amidinate ligand systems of [Sm(DippForm)$_2$(THF)$_2$] and [Yb(DippForm)$_2$(THF)$_2$] complexes might react in a contrasting way compared to previous divalent lanthanoid compounds.

4.3 Results and Discussion

4.3.1 *Synthesis and characterization*

4.3.1.1 The reaction of [Sm(DippForm)$_2$(THF)$_2$] with benzil

The reaction was performed using an equimolar mixture of [Sm(DippForm)$_2$(THF)$_2$] and benzil in THF. An immediate colour change from dark green to maroon was observed soon after stirring the reaction mixture. The solution was stirred overnight and dark red crystals of **[(DippForm)$_2$Sm^{III}(bnzl$^{\cdot}$-O)(THF)]·PhMe (1)** were obtained after storing the concentrated solution in toluene at -18°C for several weeks. Alternatively, DME was the better choice for more rapid crystallization since crystals of complex **1** formed within 3 days at -18°C, where it could possibly replace the coordinating THF. The reaction scheme and product structure are given below **(Scheme 4.7)**. The formation of the same product was identified when the reaction was performed in toluene in place of THF. Slight exposure to the air of complex **1** results in an immediate decomposition as the complex is highly air and moisture sensitive.

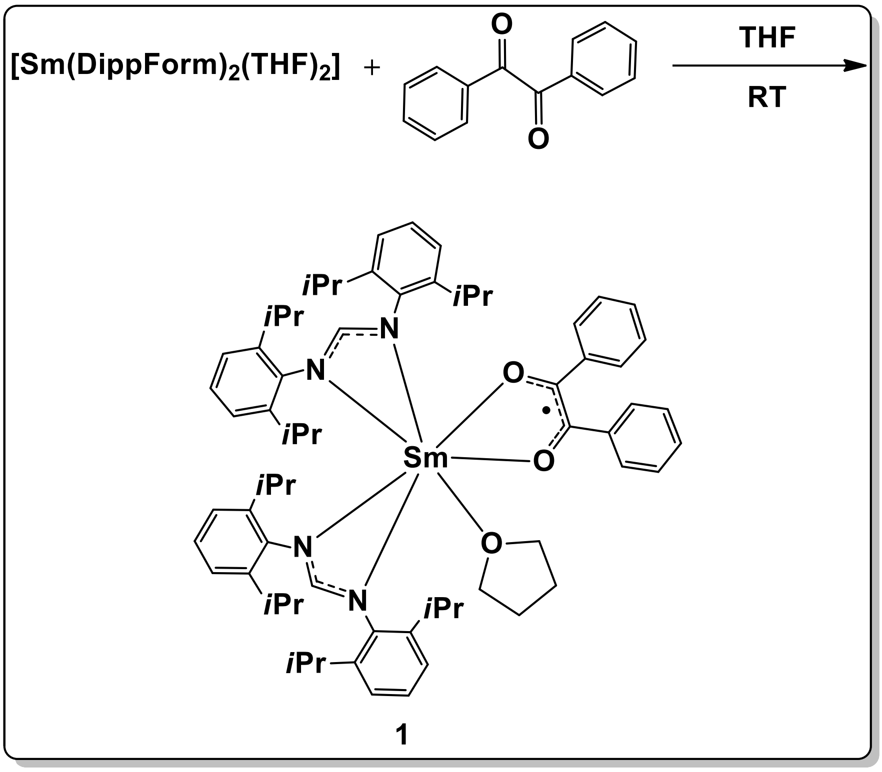

Scheme 4.7. The reaction of [Sm(DippForm)$_2$(THF)$_2$] with benzil yielding complex **1**.

Complex **1** was characterized by ^{1}H NMR, ^{13}C NMR, IR, and elemental analysis. The ^{1}H NMR spectrum (see **Fig. 4.3**) was rather complex even though it was interpretable to a certain extent. This was expected because of the combined effect of the paramagnetic samarium centre and the presence of ketyl radical species. A huge shift can be seen in the case of DippForm backbone (NC*H*N) protons, which appear as a singlet at δ = 42.08 ppm. A similar shift can be seen in a previously reported related complex [Yb(DippForm)$_2$(phen$^{\cdot}$-O_2)] from the reaction of [Yb(DippForm)$_2$(THF)$_2$] with 9,10-phenanthrenequinone (phen).[29] In this case the resonance appeared at δ = 41.88 ppm (very close to the present value), even though the resonances were not assigned due to the broadness of resonances at other regions of the spectrum due to the paramagnetic nature of Yb(III). The isopropyl C-*H* resonances appear as a septet at δ = 3.44 ppm. The CH_3 protons of the isopropyl group showed signals at three different shifts, as two separate groups for each DippForm ligand. The first two splitting at δ = 1.06 & 1.17 ppm in a 3:1 ratio with a total integration value of 24 is quite common in usual samarium complexes with DippForm ligands owing to the existence of one isopropyl group directed towards the paramagnetic samarium centre. See earlier chapters 2 and 3 in this work. The resonance at δ = 1.86 ppm is attributed to the CH_3 protons of isopropyl groups of the second DippForm moiety. The presence of the protons of THF and DME are also clearly visible in the spectrum. We can see the occupancy of two additional resonances at δ = 11.39 & 1.36 ppm, which were unable to be assigned. A satisfactory ^{13}C NMR spectrum was also obtained (**Fig. 4.4**) where we can see an unexpected shift in the resonance of one of the Dipp-*C*H carbons, which appears at δ = 37.08 ppm. In addition, the product is also confirmed by IR spectroscopy and elemental analysis.

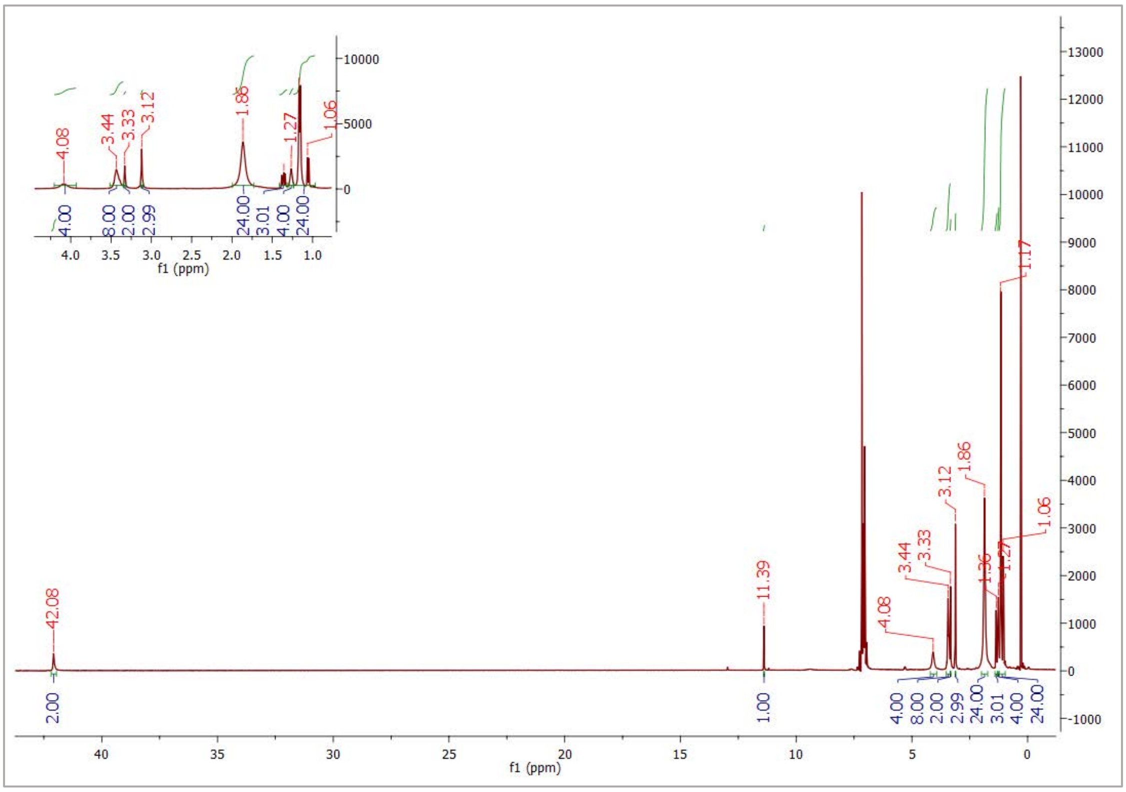

Fig 4.3 ^{1}H NMR spectrum of [(DippForm)$_2$Sm^{III}(bnzl$^{\cdot}$-O)(THF)]·PhMe (**1**)

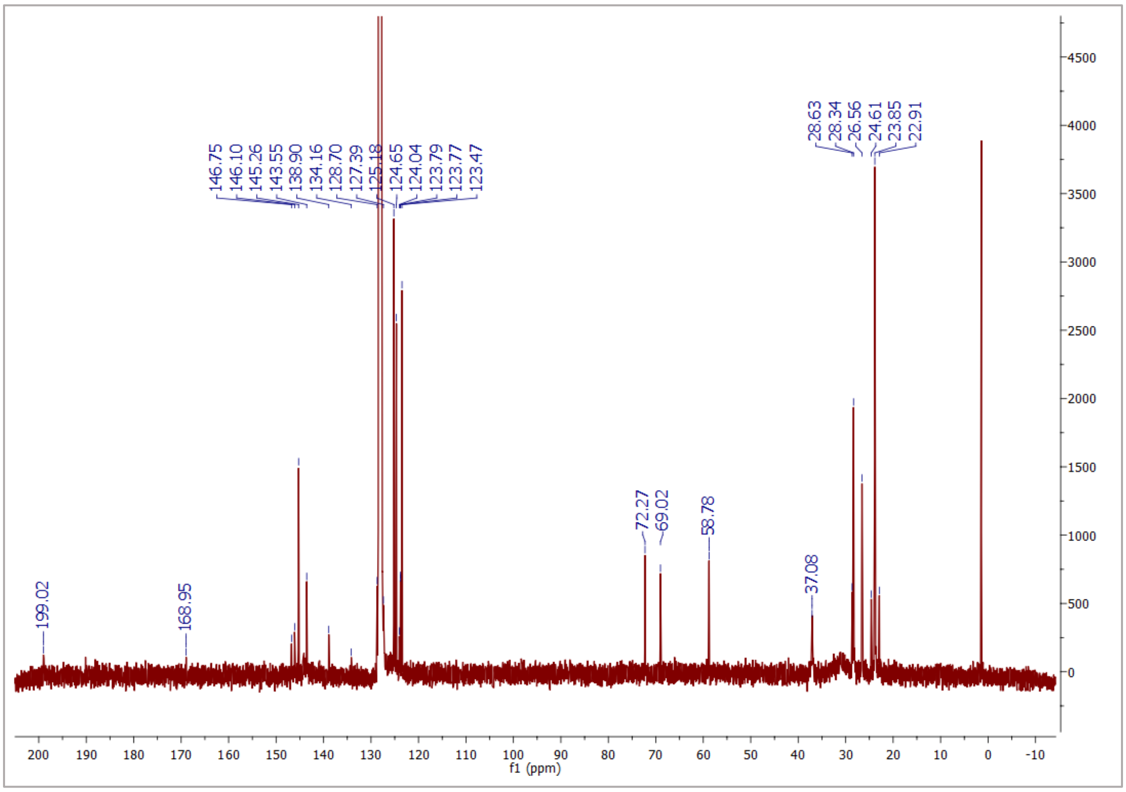

Fig 4.4 ^{13}C NMR spectrum of [(DippForm)$_2$Sm^{III}(bnzl$^{\cdot}$-O)(THF)]·PhMe (**1**)

4.3.1.2 The reaction of [Sm(DippForm)$_2$(THF)$_2$] with naphthyl isothiocyanate

The reaction was carried out in THF owing to the high solubility of reagents in this solvent. [Sm(DippForm)$_2$(THF)$_2$] was treated with naphthyl isothiocyanate in a 1:1 stoichiometric ratio. The colour of the solution changed to orange-red immediately and it persisted even after stirring for 2 days. Yellow crystals of **[Sm^{III}(DippForm)$_2$(Nap-NCHS)(THF)]·THF (2)** were obtained after keeping the concentrated solution at -18°C for two weeks thereafter. The reaction scheme and product structure are given below **(Scheme 4.8)**.

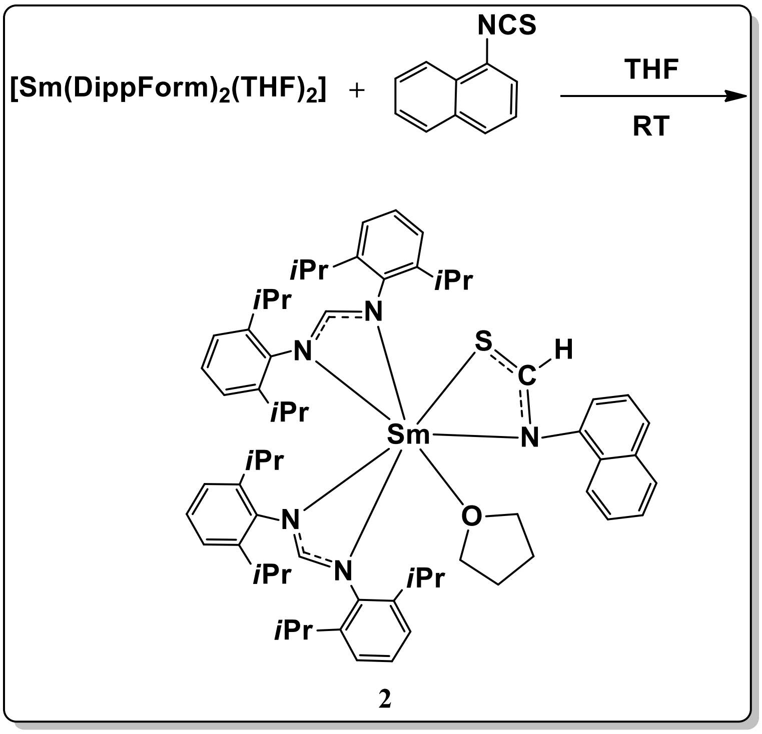

2

Scheme 4.8. The reaction of [Sm(DippForm)$_2$(THF)$_2$] with naphthyl isothiocyanate gives complex **2.**

Complex **2** was characterized by ^{1}H NMR, ^{13}C NMR, and IR spectroscopy. Signals in the ^{1}H NMR spectrum of complex **2** are broadened due to the paramagnetic nature of the metal centre (Sm^{3+}) making assignment and integration difficult, particularly in the upfield region of the spectrum. However, a strong downfield shift of the DippForm backbone NC*H*N was easily identifiable, which is detected as a singlet at δ= 11.45 ppm with an integration value of 2 (**Fig 4.5**). In addition, solvent signals also can be detected for DME. The resonance of the NC*H*S proton of trapped naphthyl isothiocyanate fragment could be in the aromatic region (δ = 6.9 – 7.4 ppm). The ^{13}C NMR spectrum is shown in **Fig 4.6** and a satisfactory IR spectrum was also obtained.

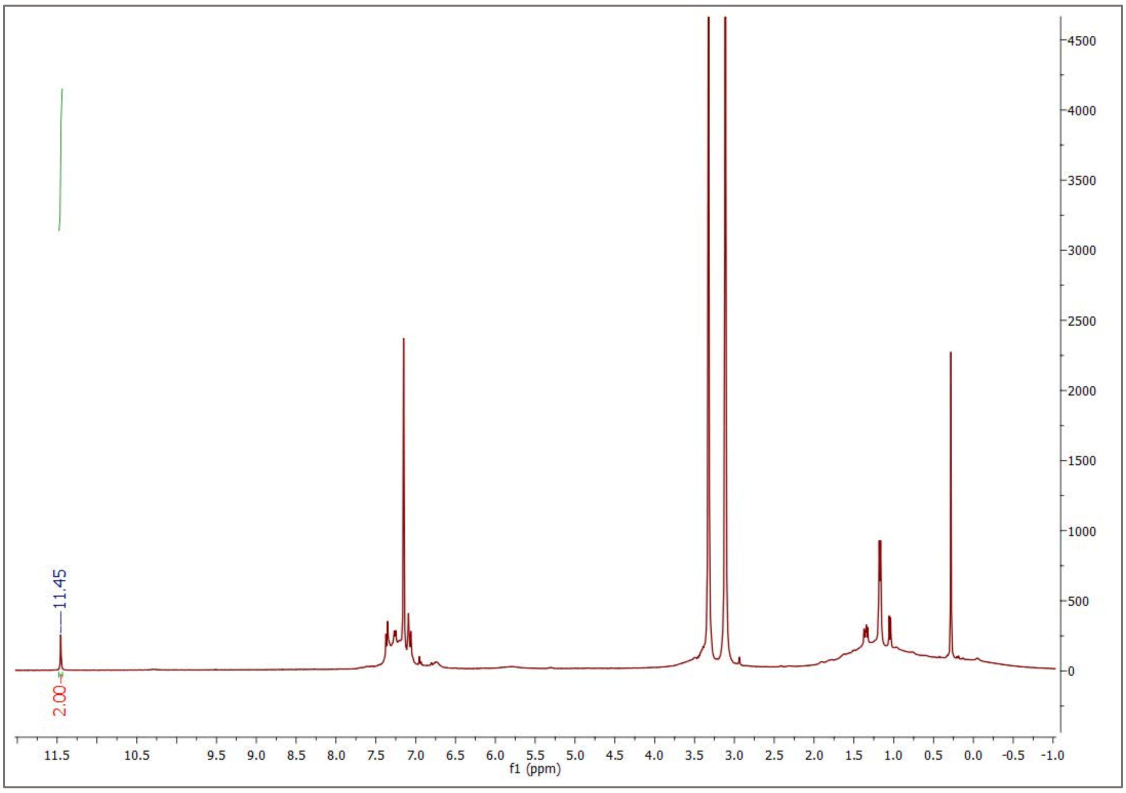

Fig 4.5 ^{1}H NMR spectrum of [Sm^{III}(DippForm)$_2$(Nap-NCHS)(THF)]·THF (**2**)

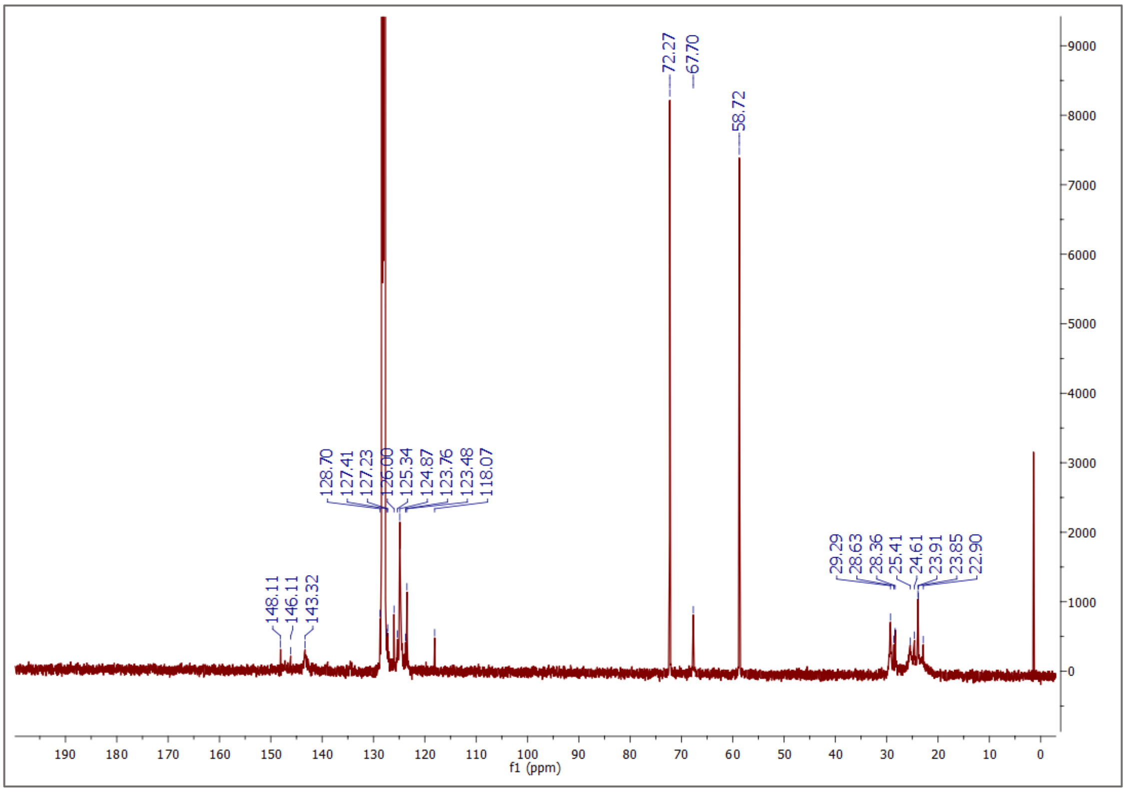

Fig 4.6 ^{13}C NMR spectrum of [Sm^{III}(DippForm)$_2$(Nap-NCHS)(THF)]·THF (**2**)

4.3.1.3 The reaction of [Sm(DippForm)$_2$(THF)$_2$] with phenyl isothiocyanate

The reaction was performed using an equimolar mixture of [Sm(DippForm)$_2$(THF)$_2$] and phenylisothiocyanate in THF. Phenylisothiocyanate was added dropwise to [Sm(DippForm)$_2$(THF)$_2$] solution in THF and the colour immediately changed from dark green to red-brown. After stirring overnight, the solution was concentrated and stored at 4°C for one week to afford rectangular prism-type crystals of ***N,N'*-diphenyl-*N*-(phenylcarbamothioyl)formimidamide (3)**. Crystals of another trivalent samarium complex [Sm(DippForm)$_3$] were also obtained by the fractional crystallization of the remaining solution. The reaction scheme and structures of products are given below **(Scheme 4.9).** Organic product **3** can be isolated by treating it with water and organic solvent, separating the organic layer, and crystallizing it in the open air in THF or toluene.

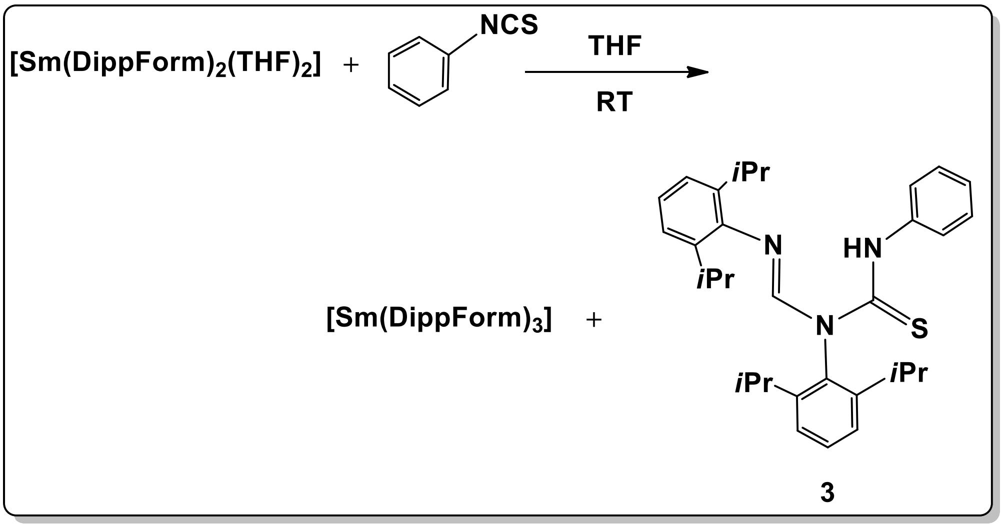

3

Scheme 4.9. The reaction of [Sm(DippForm)$_2$(THF)$_2$] with phenyl isothiocyanate yielding compound **3** and [Sm(DippForm)$_3$]**.**

Satisfactory ^{1}H NMR and ^{13}C NMR spectra were obtained for compound **3** (**Fig. 4.7 & 4.8**). The Dipp-NC*H*N proton appears as a small singlet at δ = 7.36 ppm while aromatic hydrogen resonances are observed at δ = 7.11, 6.70 and 6.59 for *meta*, *ortho* and *para* aromatic hydrogens respectively. The multiplet at δ = 1.36 ppm is attributed to Dipp-C*H* protons, while usual 3:1 splitting can be observed for CH_3 protons of isopropyl groups which shows resonances at δ = 1.19 & 1.05 ppm. The resonance for the backbone N*C*HN carbon is observed at δ = 139.30 ppm in the ^{13}C NMR spectrum. In addition, a suitable IR spectrum was also obtained for compound **3**.

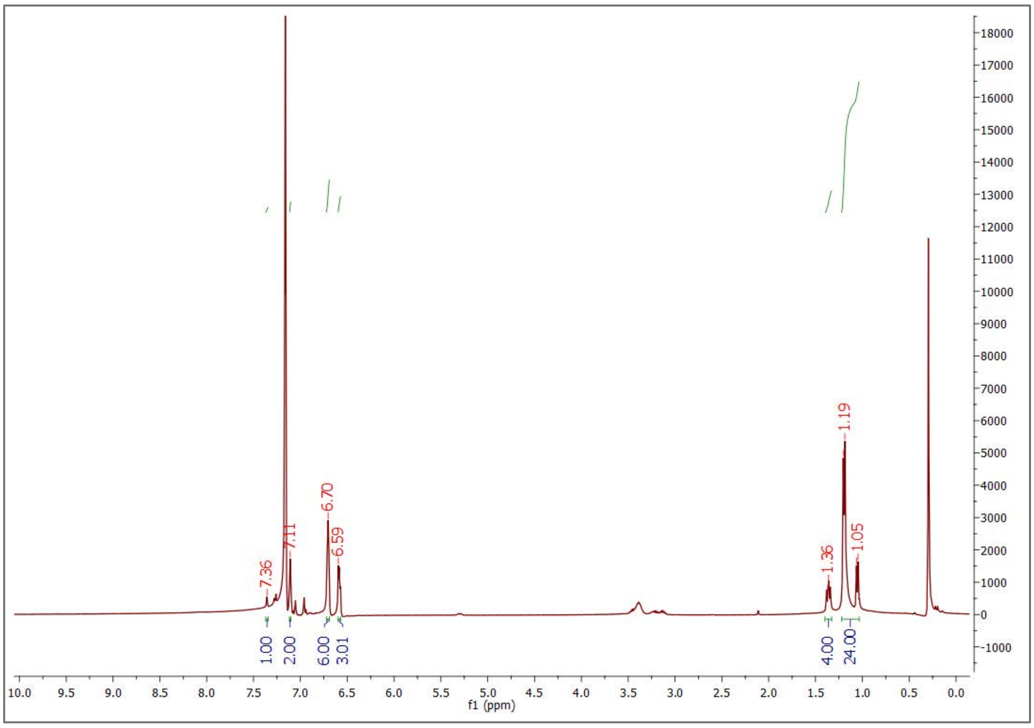

Fig 4.7 ^{1}H NMR spectrum of *N,N'*-diphenyl-*N*-(phenylcarbamothioyl)formimidamide (**3**).

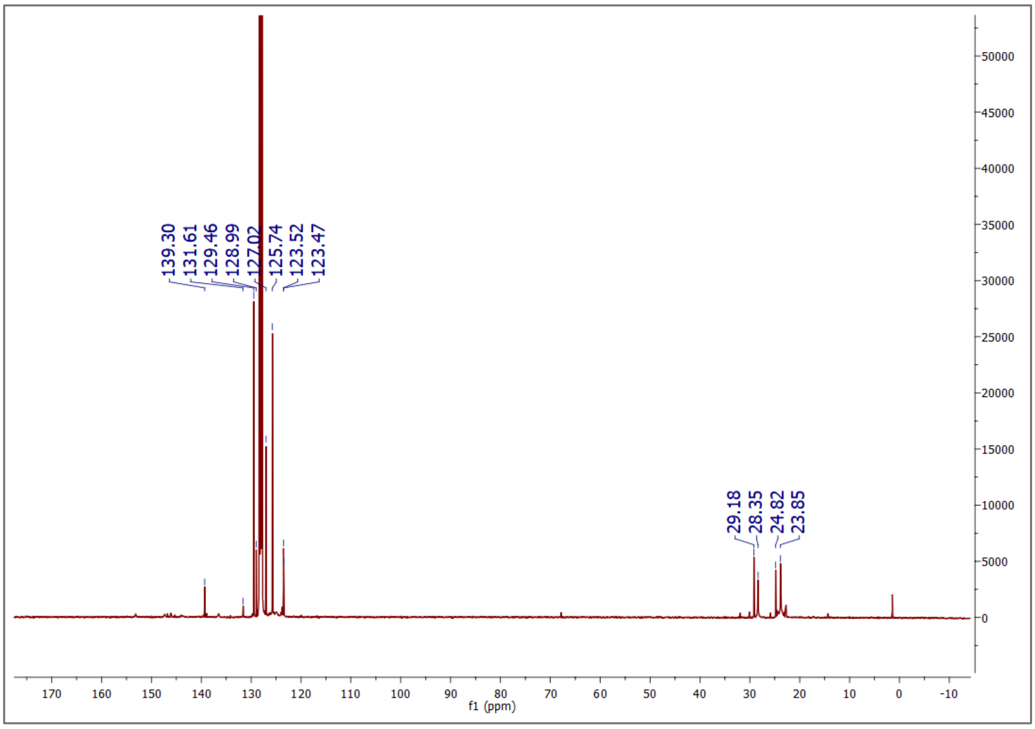

Fig 4.8 ^{13}C NMR spectrum of *N,N'*-diphenyl-*N*-(phenylcarbamothioyl)formimidamide (**3**).

4.3.1.4 The reaction of [Sm(DippForm)$_2$(THF)$_2$] with phenyl isocyanate

Sm(DippForm)$_2$(THF)$_2$ was treated with phenyl isocyanate in a 1:1 stoichiometric ratio, using THF as solvent. Dropwise addition of phenyl isocyanate triggered a colour change from dark green to a pale yellowish green immediately and the reaction was allowed to stir overnight. Colourless crystals of ***N,N′*-diphenyl-*N*-(phenylcarbamoyl) formimidamide (4)** were obtained after keeping the concentrated solution at 4°C for 24 hours. Fractional crystallization of the remaining solution resulted in the formation of yellow crystals of [Sm(DippForm)$_3$]. Here again, organic product **4** can be separated from the samarium complex by water and solvent treatment in the open air. Crystals of phenyl isothiocyanate trimer (1,3,5-triphenyl-1,3,5-triazinane-2,4,6-trione) were also isolated occasionally after the water treatment (see **Fig. 4.9**) (see discussion below). The reaction scheme and structures of products are given below **(Scheme 4.10).**

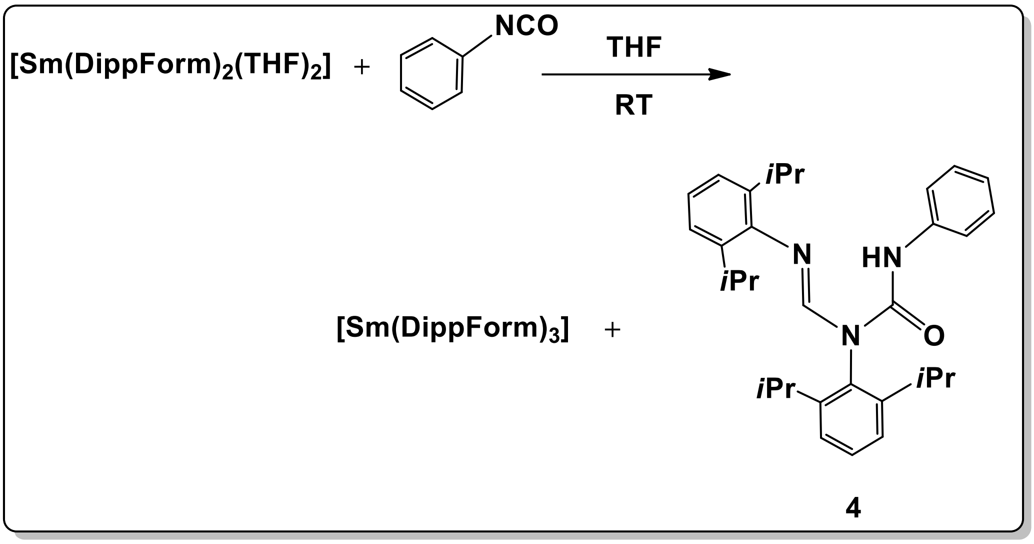

Scheme 4.10. The reaction of [Sm(DippForm)$_2$(THF)$_2$] with phenyl isocyanate gives compound **4** and [Sm(DippForm)$_3$].

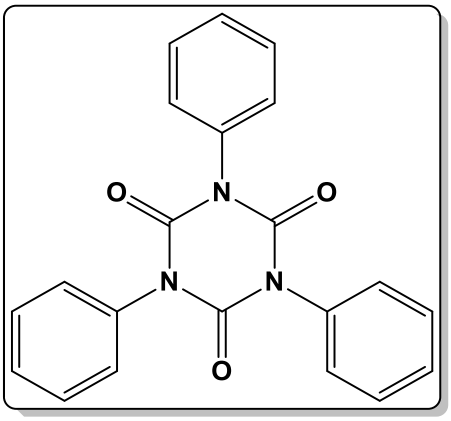

Fig. 4.9 Structure of 1,3,5-triphenyl-1,3,5-triazinane-2,4,6-trione.

Compound **4** was characterized by ^{1}H NMR, ^{13}C NMR, and IR spectroscopies. **Fig 4.10** shows the ^{1}H NMR spectrum where the broad singlet at δ = 7.78 ppm is attributed to the DippForm backbone proton (NC*H*N). The aromatic hydrogen resonances are located close to the C_6D_6 solvent signal, except for one triplet at δ = 6.87 ppm, which represents the *para*-hydrogen atom in the phenyl ring of phenyl isocyanate component. The spectrum also shows residual solvent peaks for THF at δ = 3.62 & 1.46 ppm. Dipp-C*H* protons appear as a multiplet at δ = 3.27 ppm, which is shifted to the downfield region compared to complex **3**. Regarding Dipp- CH_3 protons, we can see a third resonance at δ = 1.29 ppm in addition to usual splitting at δ = 1.23 & 1.20 ppm. The ^{13}C NMR spectrum (**Fig. 4.11**) also shows the presence of a minute amount of residual solvent THF, which appears at δ = 68.07 & 26.07 ppm, and the resonance for the backbone N*C*HN carbon is observed at δ = 120.14 ppm. Moreover, a satisfactory IR spectrum was also obtained for compound **4**.

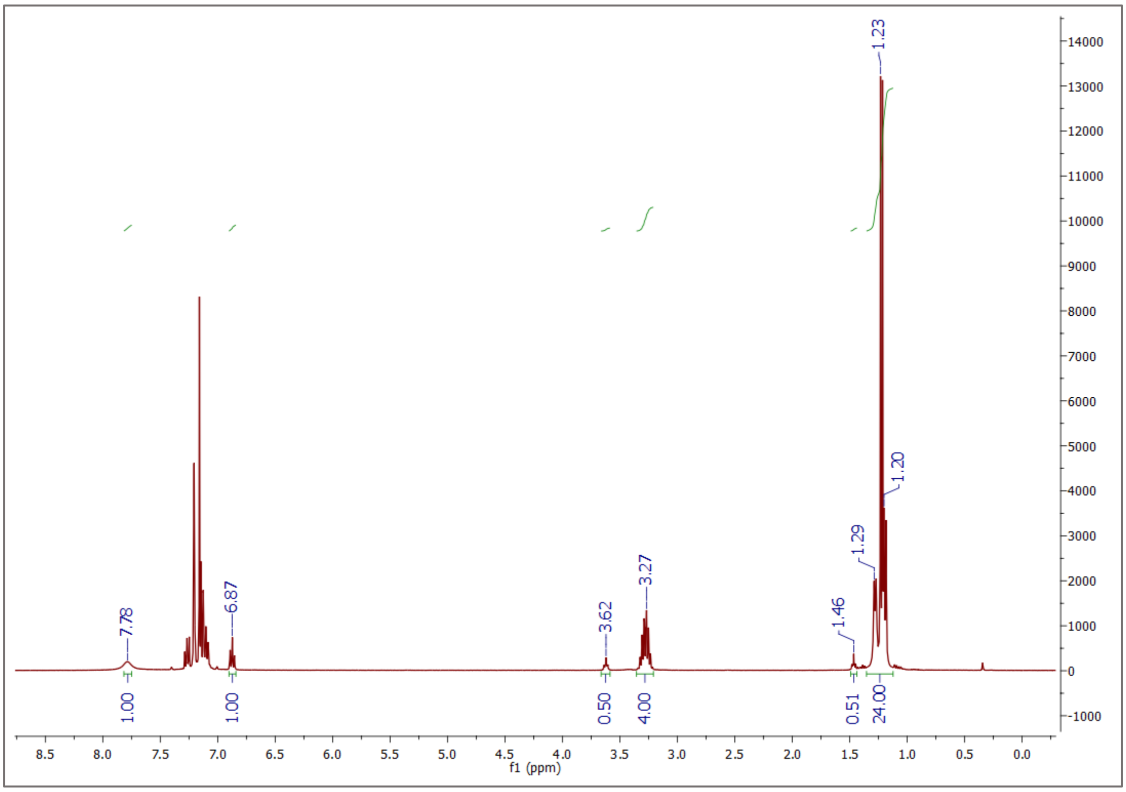

Fig 4.10 ^{1}H NMR spectrum of *N,N′*-diphenyl-*N*-(phenylcarbamoyl)formimidamide (**4**).

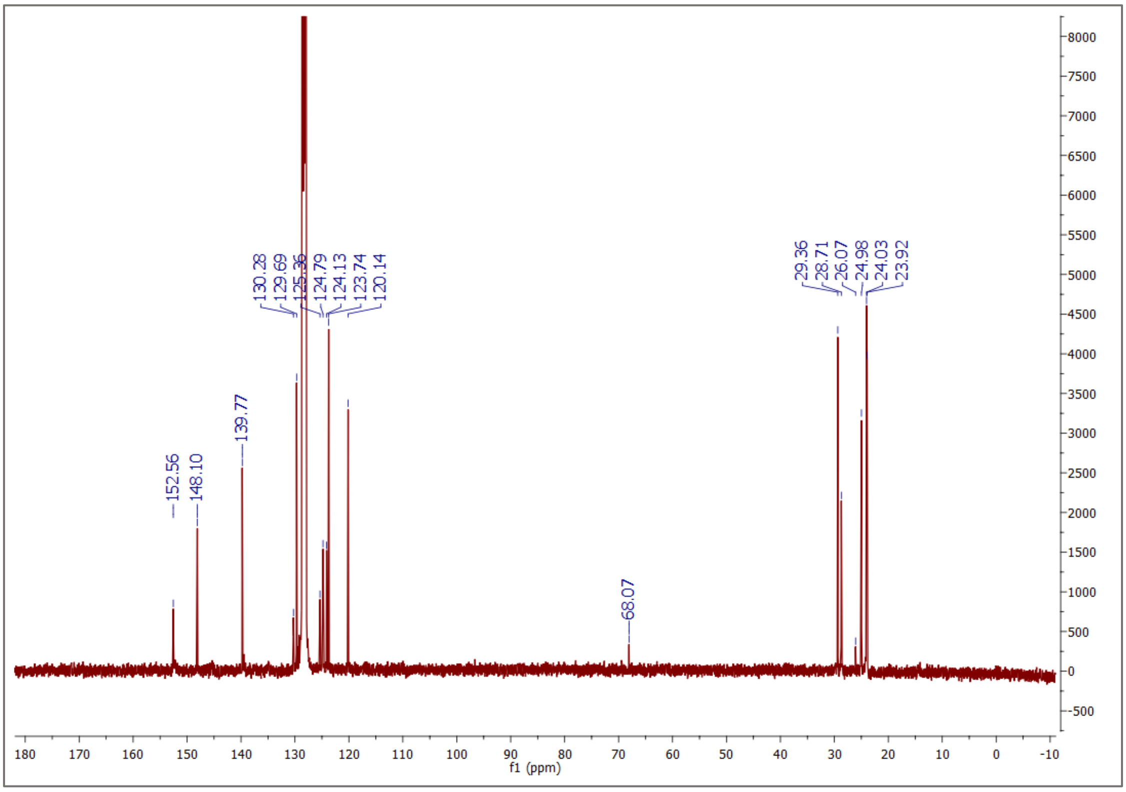

Fig 4.11 ^{13}C NMR spectrum of *N,N′*-diphenyl-*N*-(phenylcarbamoyl)formimidamide (**4**).

4.3.1.5 The reaction of [Sm(DippForm)$_2$(THF)$_2$] with benzonitrile

[Sm(DippForm)$_2$(THF)$_2$] was treated with benzonitrile in a 1:1 stoichiometric ratio using the non-coordinating solvent toluene. The solution immediately turned dark red and stirred overnight. Yellow crystals of [Sm(DippForm)$_3$] were formed after leaving the concentrated solution at 4°C for a few days. The formation of triphenyl-s-triazine in the reaction mixture was identified. The reaction scheme is given below (**Scheme 4.11**).

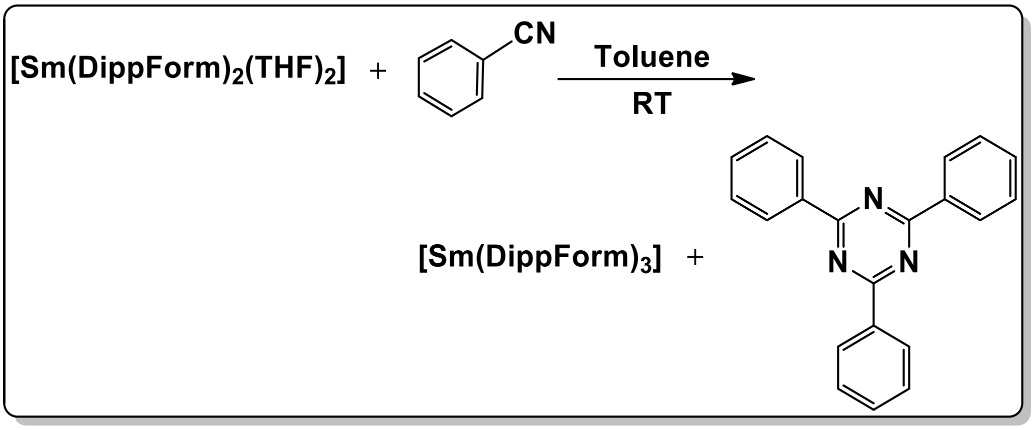

Scheme 4.11. The reaction of [Sm(DippForm)$_2$(THF)$_2$] with benzonitrile gives [Sm(DippForm)$_3$].

4.3.1.6 The reaction of [Sm(DippForm)$_2$(THF)$_2$] with o-tolunitrile

The reaction of [Sm(DippForm)$_2$(THF)$_2$] with *o*-tolunitrile was similar to the reaction discussed above. Dropwise addition of *o*-tolunitrile to a solution of [Sm(DippForm)$_2$(THF)$_2$] in toluene resulted in an immediate colour change to dark red and the reaction was allowed to stir overnight. The formation of colourless and yellow crystals was observed after keeping the concentrated solution at 4°C for several days. The yellow crystals were identified as the trivalent organolanthanoid complex [Sm(DippForm)$_3$], but the crystal quality of colourless crystals was not good enough to obtain adequate crystal data. Attempts to obtain diffractable crystals were in vain. The reaction scheme is given below (**Scheme 4.12**).

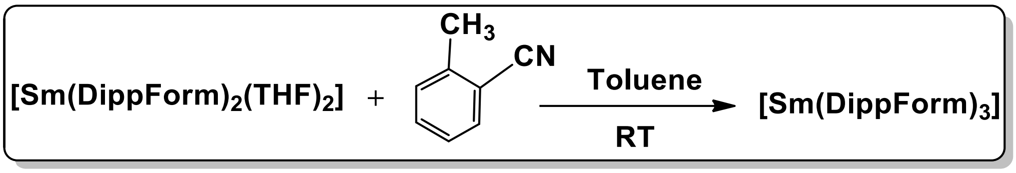

Scheme 4.12. The reaction of [Sm(DippForm)$_2$(THF)$_2$] with *o*-tolunitrile gives [Sm(DippForm)$_3$].

4.3.2 X-ray Crystal Structures

4.3.2.1 [(DippForm)$_2$Sm^{III}(bnzl$^\cdot$-O)(THF)]·PhMe ***1***

Complex **1** crystallizes as maroon plates with the X-ray crystal structure modelled in the triclinic space group *P*-1. Two terminal κ(*N,N′*)-DippForm ligands are coordinated to the samarium metal along with one coordinating THF molecule. The Sm-O$_{\mathrm{bnzl}}$ bond length is 2.3850(16) Å for Sm1-O1 and 2.3313(14) Å for Sm1-O2, suggesting the existence of an asymmetrically chelating bnzl$^\cdot$-*O$_2$* ketyl. Similar asymmetric coordination is observed in one previously reported ytterbium ketyl radical [Yb(DippForm)$_2$(acen$^\cdot$-*O$_2$*)(thf)], synthesized by reduction of another 1,2-diketone 1,2-acenaphthenequinone(acen) using [Yb(DippForm)$_2$(THF)$_2$].[29] The Yb-O bond lengths for [Yb(DippForm)$_2$(acen$^\cdot$-*O$_2$*)(thf)] are 2.266(2) Å and 2.354(2) Å, and the difference is attributed to the close proximity of O1 to the coordinated THF (O1···O3: 2.874 Å), which induce an electrostatic and steric repulsion between O1 and O3. As a result, the Sm1-O2 bond is shorter because of the preference of the radical/anion for less crowded O2 (O2···O3: 4.022 Å). On the other hand, symmetrical chelation of a ketyl ligand is observed in the case of a similar Yb(III) complex [Yb(DippForm)$_2$(phen$^\cdot$-*O$_2$*)] (Yb-O1/O2 bond distances are 2.234(2) and 2.229(2) Å), where THF is absent in the coordination sphere.[29] The C-O bond lengths of the trapped benzil ligand (O1-C51: 1.281(2) Å & O2-C58: 1.284(2) Å) are slightly longer and the C-C bond length (C51-C58: 1.446(2) Å) is slightly shorter compared to the neutral benzil molecule (1.211 Å for C=O & 1.522 Å for C-C), which implies the resonance stabilization of free-electron and anionic charge across the OCCO unit. Charge/radical distribution in the vicinity of ketyl ligand chelation to the metal center and the effect of coordinated thf of ketyl ligand is shown in **Scheme 4.13**.

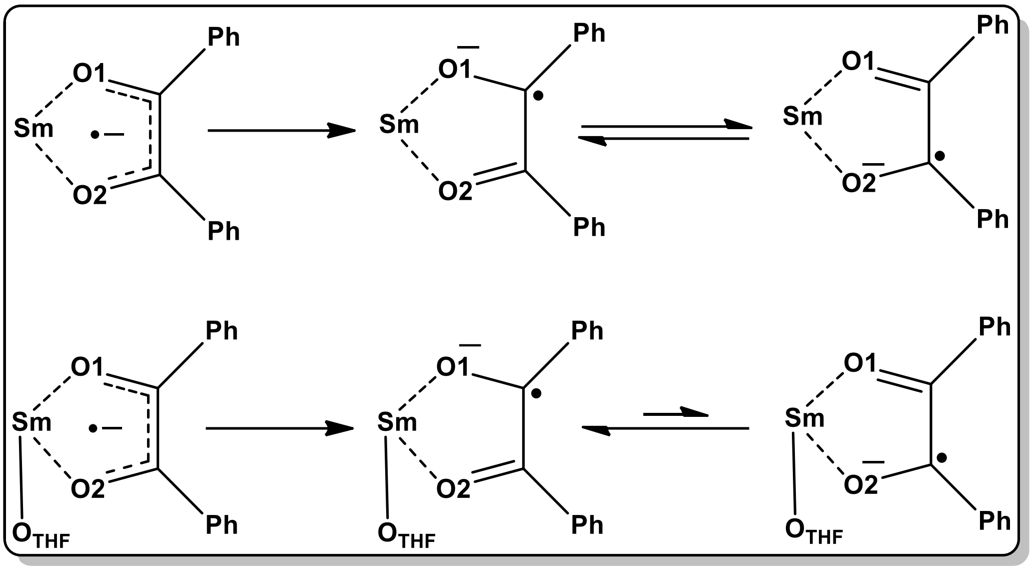

Scheme 4.13. Charge/radical distribution in complex **1** with (bottom) and without (top) the effect of coordinated in THF.

In addition, the Sm-N$_{\mathrm{DippForm}}$ bond lengths are shorter [between 2.4427(15) Å and 2.4990(15) Å] compared with the divalent starting material [Sm(DippForm)$_2$(THF)$_2$] [2.529(4) Å & 2.617(4) Å] and the same trend can be observed in the case of Sm-O(THF) bond length [2.4929(15) Å compared to 2.56(3) Å and 2.599(3) Å of starting material].[50] This suggests a trivalent oxidation state for the samarium atom which is attributed to the high Lewis acidity of the Sm^{3+} and smaller ionic radius compared with Sm^{2+}.[51]

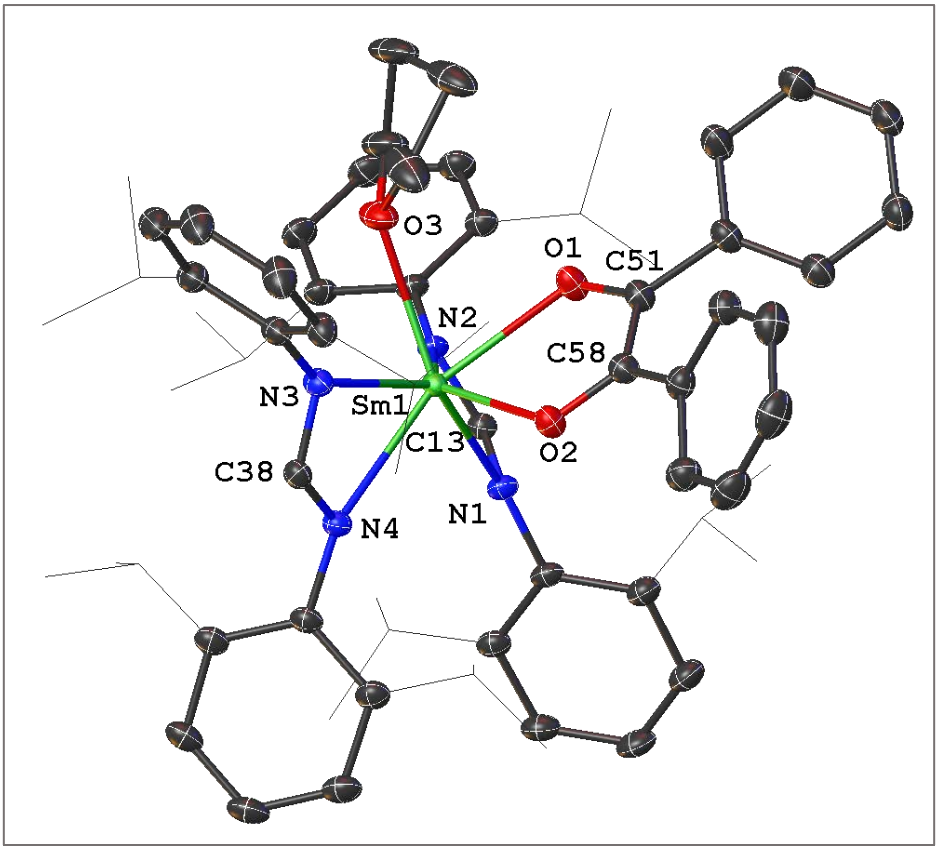

Fig. 4.12 ORTEP diagram of complex **1** in which relevant atoms are labelled. Thermal ellipsoids are drawn at a 50% probability level. Two β-carbon atoms in the coordinated THF ligand are disordered and only one part is shown here. Isopropyl groups of DippForm are shown as lines and hydrogen atoms along with one lattice toluene molecule are omitted for clarity. Selected bond angles (°) and lengths (Å): Sm1-O1 2.3850(16), Sm1-O2 2.3313(14), O1-C51 1.281(2), O2-C58 1.284(2), C51-C58 1.446(2), Sm1-N1 2.4427(15), Sm1-N2 2.4718(15), Sm1-N3 2.4955(16), Sm1-N4 2.4990(15), Sm1-O3 2.4929(15), N2-C13 1.325(2), N1-C13 1.323(2), N3-C38 1.325(2), N4-C38 1.322(2), O2-Sm1-O1 66.20(5), C58-O2-Sm1 121.29(11), C51-O1-Sm1 119.59(11), O2-C58-C51 115.94(15), O1-C51-C52 118.28(15), O2-C58-C59 117.87(15), O1-C51-C58 116.18(15), N1-Sm1-N2 55.55(5), N3-Sm1-N4 54.41(5), N1-C13-N2 119.72(14), N4-C38-N3 119.21(15).

4.3.2.2 [(DippForm)$_2$Sm^{III}(Nap-NCS)(THF)] 2

The X-ray crystal structure of complex **2** was solved and refined in the monoclinic space group *P*2$_1$/*n* without any lattice solvent molecules in the asymmetric unit. Two DippForm ligands are $\kappa^1 : \kappa^1$ coordinated to the samarium metal along with one coordinating THF molecule. The naphthyl isothiocyanate moiety is ligated to samarium through nitrogen and sulfur. The Sm-S1 and Sm-N5 bond distance values are 2.8094(12) Å & 2.549(3) Å respectively, which are in line with previously reported Sm-N$_{\text{isothiocyanate}}$ and Sm-S$_{\text{isothiocyanate}}$ bond distances.[52, 53] The C-S and C-N bond lengths of the isothiocyanate unit are 1.637(3) Å (for S1-C51) and 1.314(5) Å (for N5-C51) respectively, which are clearly shorter compared to single-bond distances of C-S (1.81 Å) and C-N (1.51 Å),[54, 55] and higher than the values of corresponding double-bond distances of C=S (1.56 Å) and C=N (1.15 Å).[56] This indicates the substantial electronic delocalization over the NCS unit. The N-C-S bond angle value is 124.5(3)° and the Sm1-N5-C51-S1 unit is substantially planar within experimental error.

Moreover, the trivalent state of the samarium ions can also be confirmed by comparing the Sm-N$_{\text{DippForm}}$ and Sm-O(THF) bond lengths of divalent starting material Sm(DippForm)$_2$(THF)$_2$.[51] The Sm-N$_{\text{DippForm}}$ bond lengths are slightly shorter [2.430(3) Å & 2.533(3) Å] compared with the divalent starting material Sm(DippForm)$_2$(THF)$_2$ [2.529(4) Å & 2.617(4)] reflecting the smaller size of Sm^{III} compared with Sm^{II}. Likewise, a similar observation can also be made in the case of Sm-O(THF) bond length, which is 2.440(2) Å compared to 2.56(3) Å and 2.599(3) Å of the starting material. [50]

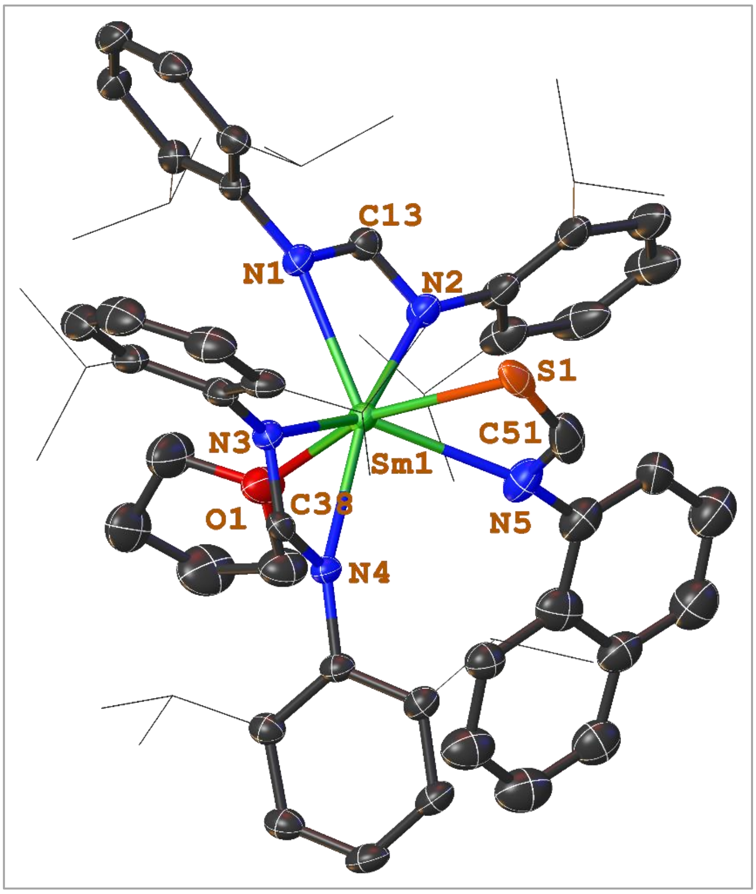

Fig. 4.13 ORTEP diagram of complex **2** in which relevant atoms are labelled. Thermal ellipsoids are drawn at a 50% probability level. One carbon atom in the coordinated THF ligand is disordered and only one part is shown here. Isopropyl groups of DippForm are shown as lines and hydrogen atoms are omitted for clarity. Selected bond angles (°) and lengths (Å): Sm1-S1 2.8094(12), Sm1-O1 2.440(2), Sm1-N5 2.549(3), S1-C51 1.637(3), N5-C51 1.314(5), Sm1-N1 2.514(3), Sm1-N2 2.457(3), Sm1-N3 2.430(3), Sm1-N4 2.533(3), N2-C13 1.319(4), N1-C13 1.322(4), N3-C38 1.337(4), N4-C38 1.313(4), N5-Sm1-S1 58.20(8), C51-S1-Sm1 80.19(14), C51-N5-Sm1 96.7(2), N5-C51-S1 124.5(3), N2-Sm1-N1 54.64(9), N3-Sm1-N4 55.03(8), N2-C13-N1 119.5(3), N3-C38-N4 119.9(3).

4.3.2.3 [PhNCS-DippForm]·THF ***3***

Complex **3** crystallizes in the triclinic space group *P*-1 with one lattice THF molecule in the asymmetric unit and there is a disorder in the oxygen atom of the lattice THF molecule. N1-C7 and C7-S1 bond lengths are 1.3406(18) Å & 1.6653(14) Å respectively, which are corresponding to single bond and double bond values of C-N and C-S. The new bond between N2 and C7 is clearly a single bond as the bond length value of 1.4092(18) Å is in the range of a normal C-N single bond. The DippForm backbone N2-C20-N3 is not delocalized anymore. This is evident from their bond lengths, where we can see an N2-C20 single bond [1.3920(17) Å] and a C20-N3 double bond [1.2781(18) Å].

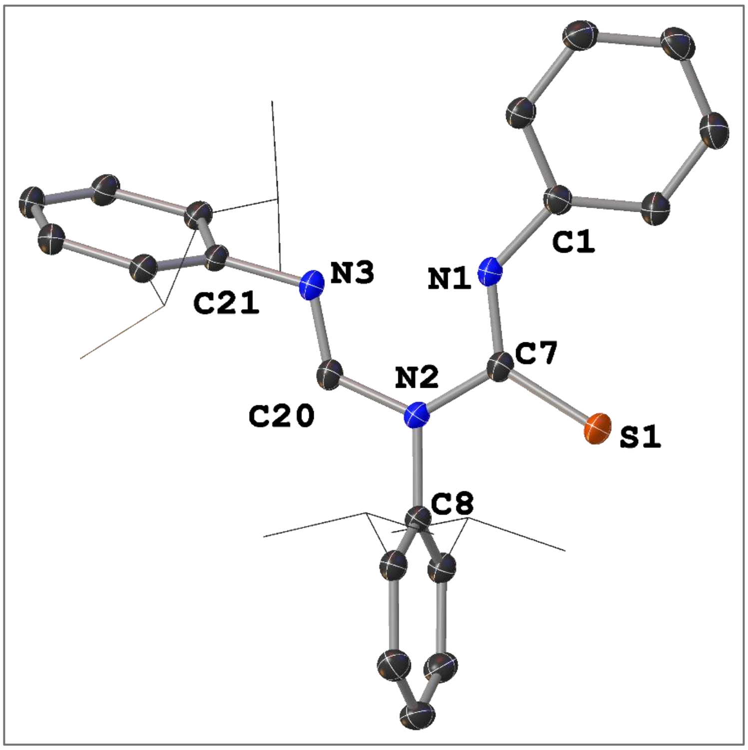

Fig. 4.14 ORTEP diagram of compound **3** in which relevant atoms are labelled. Thermal ellipsoids are drawn at a 50% probability level. Isopropyl groups of DippForm are shown as lines and hydrogen atoms along with one lattice THF molecule are omitted for clarity. Selected bond angles (°) and lengths (Å): S1-C7 1.6653(14), N2-C8 1.4578(17), N2-C20 1.3920(17), N2-C7 1.4092(18), N3-C21 1.4361(17), N3-C20 1.2781(18), N1-C1 1.4166(19), N1-C7 1.3406(18), C20-N2-C8 114.82(11), C20-N2-C7

126.92(12), C7-N2-C8 118.13(11), C20-N3-C21 116.52(12), C7-N1-C1 130.14(12), N3-C20-N2 124.88(13), N2-C7-S1 119.53(10), N1-C7-S1 126.71(11), N1-C7-N2 113.76(12).

4.3.2.4 [PhNCO-DippForm] ***4***

Complex **4** crystallizes in the monoclinic space group *C*2/*c* without any lattice solvent molecule in the asymmetric unit. The bond length value of 1.4214(16) Å between N2 and C7 implies the formation of a new single bond. The N1-C7 and C7-O1 bond lengths are 1.3614(16) Å and 1.2168(15) respectively, suggesting a single bond between N1 & C7 and a double bond between C7 & O1. The electronic delocalization in the NCN moiety of the DippForm is absent. This is evident from the single bond length value of N2-C8 [1.3797(16) Å] and the double bond value of N3-C8 [1.2803(16) Å].

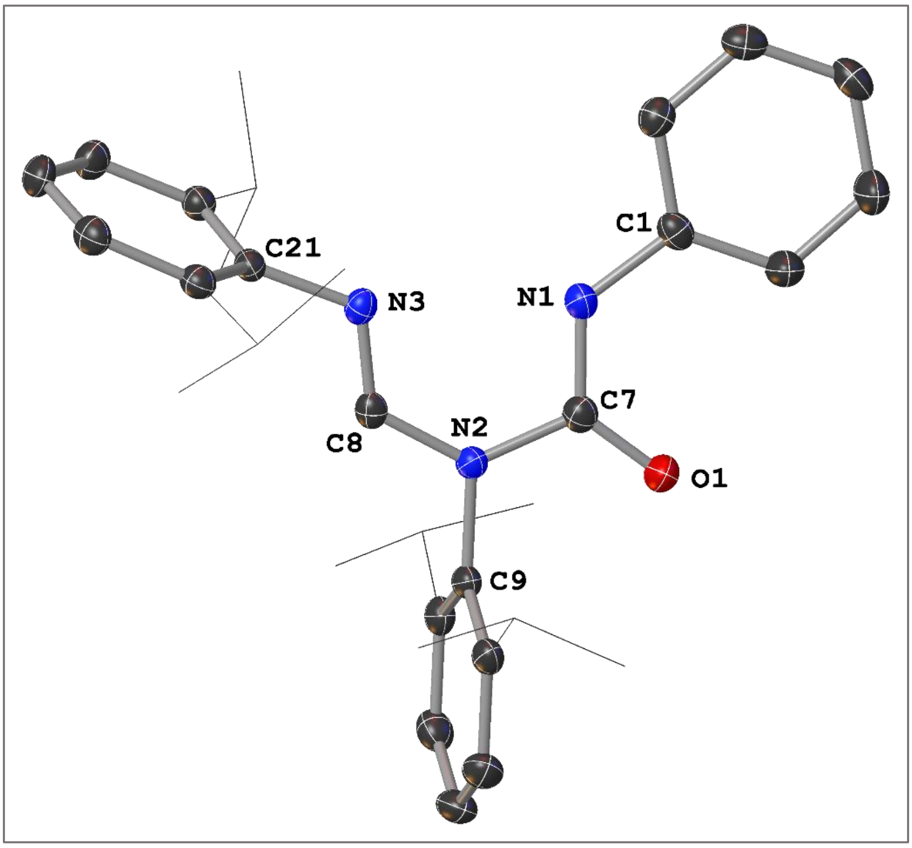

Fig. 4.15 ORTEP diagram of compound **4** in which relevant atoms are labelled. Thermal ellipsoids are drawn at a 50% probability level. Isopropyl groups of DippForm are shown as lines and hydrogen atoms are omitted for clarity. Selected bond angles (°) and lengths (Å): O1-C7 1.2168(15), N2-C8 1.3797(16), N2-C9 1.4542(15), N2-C7

1.4214(16), N3-C8 1.2803(16), N3-C21 1.4331(15), N1-C1 1.4106(16), N1-C7 1.3614(16), C8-N2-C9 116.35(10), C8-N2-C7 127.50(10), C7-N2-C9 116.15(9), C8-N3-C21 117.39(10), C7-N1-C1 126.59(11), N3-C8-N2 124.58(11), N1-C7-N2 114.37(10), O1-C7-N2 119.33(11), O1-C7-N1 126.30(12).

4.3.3 Discussion

4.3.3.1 Reaction of [Sm(DippForm)$_2$(THF)$_2$] with benzil

The formation of rare-earth ketyl complexes when [Yb(DippForm)$_2$(THF)$_2$] was treated with 1,2-diketones 3,5-di-tert-butyl-1,2-benzoquinone (tbbq), 9,10-phenanthrenequinone (phen) and 1,2-acenaphthenequinone(acen) were interesting and questions regarding the capability of the samarium analogue [Sm(DippForm)$_2$(THF)$_2$] arose.[29] As mentioned before, stabilization of metal ketyls has high requirements, in which the participating co-ligand and solvents will play a great role to avoid decomposition. In addition, the choice of diketone is also important as it should be able to provide steric saturation. Otherwise, it may form the pinacolate-type complexes, as we have seen in the case of [Sm(DippForm)$_2$(THF)$_2$] and benzophenone.[3] The selection of benzil as a di-ketone oxidant emerged as a result of a search for a di-ketone which is slightly larger than benzophenone and not as rigid as 9,10-phenanthrenequinone (phen) or 1,2-acenaphthenequinone(acen).

The reactivity of benzil with [Sm(DippForm)$_2$(THF)$_2$] was highly anticipated and the immediate colour change to maroon was the first indication, which could be the formation of a pinacolate-type complex or the desired metal ketyl radical complex. The reaction was very straightforward, and it resulted in the formation of complex **1**, which is a samarium amidinate ketyl complex. The bond parameters of the coordinated OCCO moiety confirmed the existence of a ketyl radical and the trivalent state of samarium was also validated by analysing the relevant bond lengths. Complex **1** showed exceptional stability in non-coordinating solvents (C_6D_6, PhMe), which is not common for rare-earth ketyl complexes.

4.3.3.2 The reaction of [Sm(DippForm)$_2$(THF)$_2$] with naphthyl isothiocyanate

Initially, naphthyl isothiocyanate was not a favourite candidate in reductive trapping using divalent organolanthanoids because of a couple of reasons. The reaction of isothiocyanates towards Ln(II) complexes is very limited and the chances of the bulkiness of naphthyl moiety hampering the reactivity was another reason. However, an immediate colour change to orange-red when the solvent was added to reagents signified that a reaction occurred.

Coordination of the samarium centre to both N and S atoms of naphthyl isocyanate and their bond parameters indicate sufficient delocalization in the NCS unit. The formation of complex **2** might be proceeding *via* organometallic radical intermediate evolution and subsequent hydrogen abstraction from the solvent. The reduction of naphthyl isothiocyanate by the [Sm(DippForm)$_2$(THF)$_2$] resulting from the transfer of a single electron to the N=C=S fragment, generates a radical intermediate as shown in **Scheme 4.14**, which later forms into complex **2** by abstracting a hydrogen atom from the solvent THF. Similar reactions mediated by radical mechanism and H atom abstractions from solvent have been previously reported.[18, 42, 57, 58]

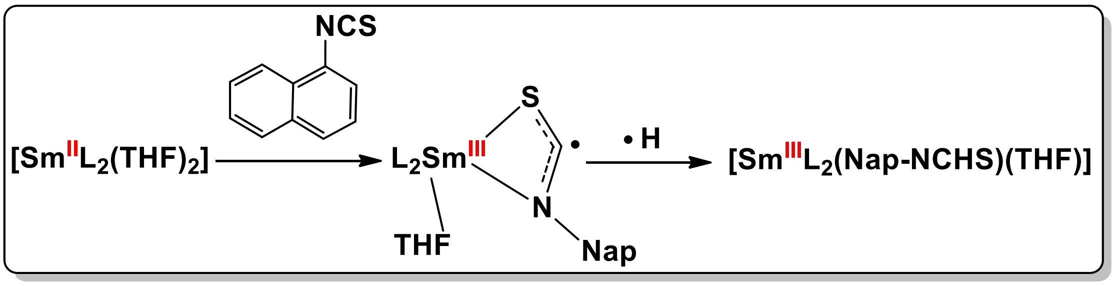

Scheme 4.14. A proposed reaction mechanism of the reaction of [Sm(DippForm)$_2$(THF)$_2$] with naphthyl isothiocyanate.

4.3.3.3 The reaction of [Sm(DippForm)$_2$(THF)$_2$] with phenyl isocyanate and phenyl isothiocyanate

Phenyl isocyanate (PhNCO) and phenyl isothiocyanate (PhNCS) are similar unsaturated organic substrates and a related reactivity was predicted for them. Their reaction with divalent organolanthanoid complex [Sm(DippForm)$_2$(THF)$_2$] was also similar, where both show immediate colour change and ultimately produce analogous compounds. Each reaction resulted in the synthesis of a new organic product and previously reported bulky homoleptic [Sm(DippForm)$_3$]. The formation of [Sm(DippForm)$_3$] suggests single electron transfer and possible reduction chemistry. However, elucidating the complete reaction mechanism is difficult here because of the mismatch in the reaction stoichiometry and the identified products. The presence of one more samarium-containing component was expected, but it remained elusive even after changing the reaction conditions and crystallization techniques. The possible formation of **A** is shown in **Scheme 4.15**, where the ideal stoichiometric ratio and expected products are illustrated. The unknown product (complex **A** in **Scheme 4.15**) could be a binucleated samarium complex bridged by two PhNCX (X = O, S) moieties.

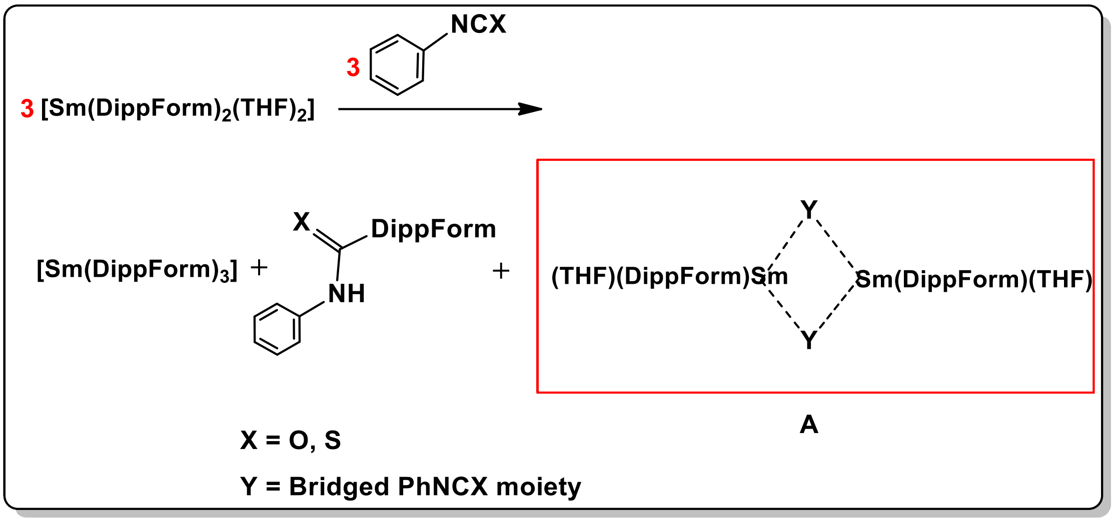

Scheme 4.15. The reaction of [Sm(DippForm)$_2$(THF)$_2$] with phenyl isothiocyanate (X = S) and phenyl isocyanate (X = O). Complex **A** is the expected binuclear samarium product, along with [Sm(DippForm)$_3$] and organic compound.

The two reactions were repeated several times in various stoichiometric ratios and the results did not provide much explanation. In the case of PhNCO reaction, the formation of 1,3,5-triphenyl-1,3,5-triazinane-2,4,6-trione was identified once, which might be resulted from cyclotrimerization of phenyl isocyanate by [Sm(DippForm)$_2$(THF)$_2$] acting as catalyst (see **Scheme 4.16**). Catalytic cyclotrimerization of C=N containing substrates by Sm(II) are reported before and also mentioned in the introduction part of this chapter.[49]

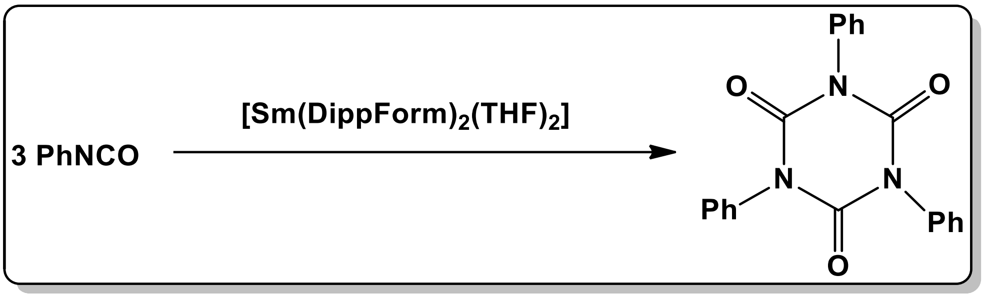

Scheme 4.16. The formation of 1,3,5-triphenyl-1,3,5-triazinane-2,4,6-trione by catalytic cyclotrimerization of phenyl isocyanate using [Sm(DippForm)$_2$(THF)$_2$].

4.3.3.4 The reaction of [Sm(DippForm)$_2$(THF)$_2$] with benzonitrile and o-tolunitrile

The reaction of nitriles (benzonitrile and *o*-tolunitrile) towards the divalent samarium complex [Sm(DippForm)$_2$(THF)$_2$] were identical. The colour change of the reaction mixture and the obtained product are similar in both cases. Formation [Sm(DippForm)$_3$] confirms the redox mechanism in the reaction chemistry. However, unravelling the chemistry is very difficult here without the isolation of other products. Multiple attempts were made in search of the remaining products, but no promising results were obtained even after changing reaction conditions. The presence of triphenyl-s-triazine in benzonitrile reaction could be an after effect of catalytic cyclotrimerization by divalent samarium starting material (**Scheme 4.17**), like previously reported examples.[49]

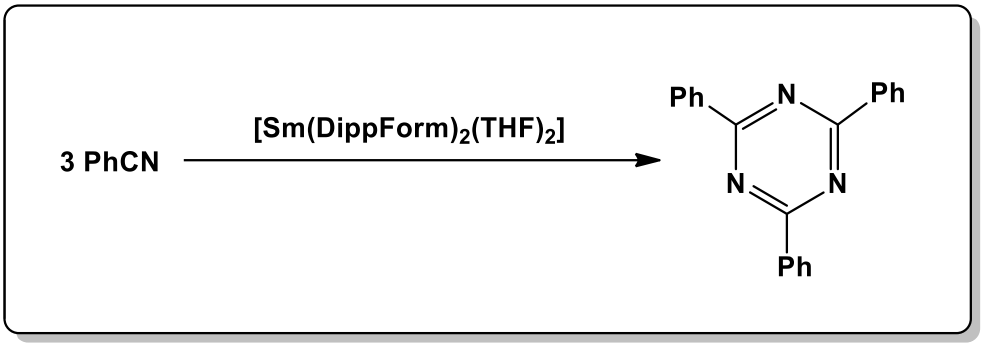

Scheme 4.17. The formation of triphenyl-s-triazine by catalytic cyclotrimerization of benzonitrile using [Sm(DippForm)$_2$(THF)$_2$].

4.4 Related chemistry - Interaction with methyl benzoate

4.4.1 The reaction of [Sm(DippForm)$_2$(THF)$_2$] with methyl benzoate

Methyl benzoate was added to the solution of [Sm(DippForm)$_2$(THF)$_2$] in THF dropwise. The reagents were added in a 1:1 stoichiometric ratio and the colour gradually began to change from dark green to yellowish green without stirring or heating. The colour of the solution eventually changed to orange completely within a time span of three hours. Keeping the concentrated solution at 4°C for a few weeks afforded yellow crystals of **[Sm$_4$(benzoate)$_4$(DippForm)$_2$(THF)$_2$(O-CH$_3$)$_4$(O)$_2$]** (**5**) and colourless crystals of DippFormH. The X-ray crystal structure of complex **5** is shown in **Fig. 4.16**.

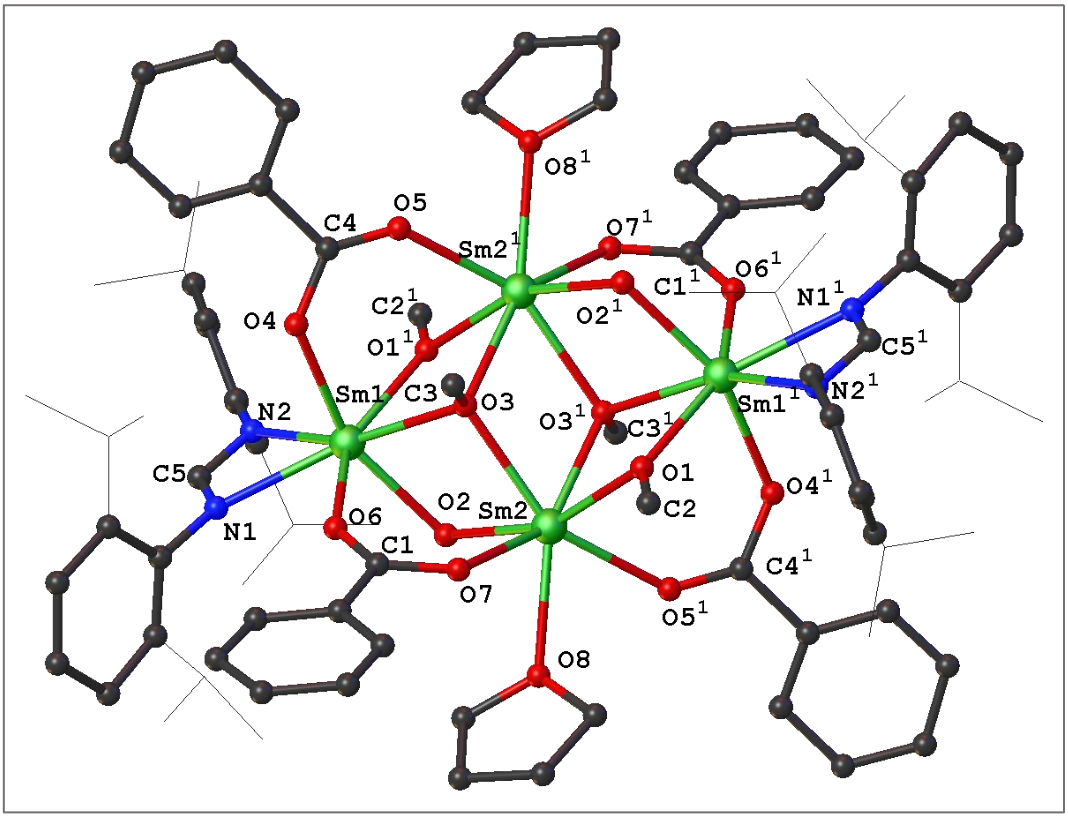

Fig 4.16. ORTEP diagram of complex **5** in which relevant atoms are labelled. Isopropyl groups of DippForm are shown as lines and hydrogen atoms are omitted for clarity.

The crystals obtained from this reaction were very poor and diffracted weakly. The X-ray crystal data obtained was only able to provide unambiguous connectivity as to the structure of this compound. Each samarium is in a trivalent state and dissociation of methyl benzoate into benzoate and methoxy groups can be seen. The complex is tetranuclear with four benzoate moieties and methoxy groups act as a bridge between two samarium centres. Furthermore, two methoxy groups connecting three samarium ions each also can be observed, along with two oxygen atoms acting as a bridge between two samarium atoms. Efforts to make quality crystals of complex **5** were futile. However, the obtained crystal structure hints toward the possibility of a successful reaction of [Sm(DippForm)$_2$(THF)$_2$] with methyl benzoate. More details regarding reactivity and related products can only be elucidated after collecting more adequate data.

4.4.2 The reaction of [Yb(DippForm)$_2$(THF)$_2$] with methyl benzoate

The reaction was performed using an equimolar mixture of [Yb(DippForm)$_2$(THF)$_2$] and methyl benzoate in THF. The reaction mixture was left undisturbed for one week and the colour of the solution was red. Very small colourless crystals of **[Yb$_2$(DippForm)$_2$(O-CH$_3$)$_4$(THF)$_2$]** (**6**) were obtained after keeping the concentrated solution at 4°C for a few weeks. The X-ray crystal structure of complex **6** is shown in **Fig. 4.17**. The quality of crystals was very poor and they were not diffracting enough to provide acceptable x-ray crystal data. Obtained data can only be used to confirm the explicit connectivity as to the structure of this compound.

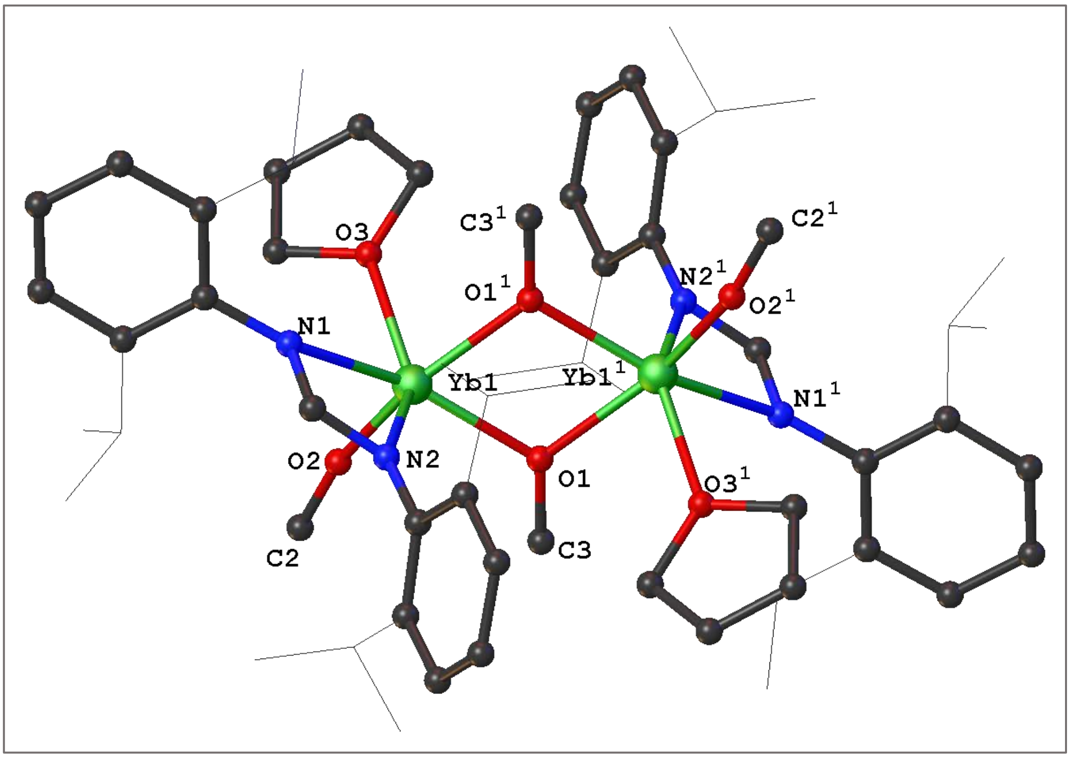

Fig 4.17. ORTEP diagram of complex **6** in which relevant atoms are labelled. Thermal ellipsoids are drawn at a 50% probability level. Isopropyl groups of DippForm are shown as lines and hydrogen atoms are omitted for clarity.

The reaction of [Yb(DippForm)$_2$(THF)$_2$] with methyl benzoate was confirmed as the methoxy group dissociated from the methyl benzoate ligand and can be observed in the obtained crystal structure. This also suggests the likelihood of the presence of more additional products in the reaction mixture. Two methoxy units act as bridging between two ytterbium centres while the remaining two terminal methoxy groups coordinated to each ytterbium ion. The possibility of ytterbium being in a trivalent state can also be inferred from the crystal structure. Nonetheless, more comments on these reactions cannot be made without additional data.

4.5 Conclusions & Future Outlook

The results of the reaction of [Sm(DippForm)$_2$(THF)$_2$] and its ytterbium analogue [Yb(DippForm)$_2$(THF)$_2$] with different types of unsaturated small organic molecules highlighted the fact that divalent organolanthanoid complexes are powerful reagents and always produce unusual and unexpected outcomes. Interaction of [Sm(DippForm)$_2$(THF)$_2$] with benzil resulted in a rare samarium amidinate ketyl complex, which shows exceptional stability in non-coordinating solvents benzene-d$_6$ and toluene. Moreover, the reaction of benzil with [Yb(DippForm)$_2$(THF)$_2$] and [Yb(XylForm)$_2$(THF)$_2$] also showed similar colour change, suggesting that reaction is working but failed to obtain crystals.

The reaction of isocyanate and isothiocyanates were promising, pointing toward their successful application in reductive trapping. The result with naphthyl isothiocyanate is highly remarkable, where it forms a trivalent samarium complex in which both nitrogen and sulfur coordinate to the samarium centre. The reaction proceeds through a radical intermediate mechanism, which resulted in a significant H-abstraction from the solvent. However, the reaction of phenyl isocyanates and phenyl isothiocyanates is incomplete, where a putative third samarium complex has yet to be identified.

The reaction with C≡N-containing substrates (nitriles and cyanides) is an area which needs to be studied extensively. Benzonitrile and o-tolunitrile reactions succeeded in synthesizing [Sm(DippForm)$_3$], which confirms the redox chemistry but missing other crucial products, which remained elusive even after multiple attempts. In addition, a colour change can be seen in the reaction of [Sm(DippForm)$_2$(THF)$_2$] with other nitriles such as 1,2-dicyanobenzene (dark blue), 9-anthracenecarbonitrile (dark red), benzyl cyanide (orange) and 1,4-dicyanobenzene (dark purple). These results indicate the need for a further thorough investigation as this field holds a bright future for reductive trapping.

The use of methyl benzoate in reductive trapping using [Ln(DippForm)$_2$(THF)$_2$] will provide new insight into the feasibility of more unsaturated substrates in this application. Cleaved methyl benzoate moieties can be seen in both crystal structures, suggesting more efforts on these particular reactions will provide amazing results. Using a related organic substrate methyl *p*-anisate also can be a useful reagent, which demonstrated a colour change to red upon reaction with [Sm(DippForm)$_2$(THF)$_2$].

Overall, the use of small unsaturated organic molecules in this particular application is still in its infancy. [Sm(DippForm)$_2$(THF)$_2$] (and its ytterbium analogue to a certain extent) could become one of the phenomenal complexes in organolanthanoid chemistry if more ligands are employed and novel crystallization techniques are applied.

4.6 Experimental

4.6.1 General Considerations

The lanthanoid compounds described here are highly air and moisture sensitive and were prepared and handled with vacuum-nitrogen line techniques and in a dry box in an atmosphere of purified nitrogen. [Sm(DippForm)$_2$(THF)$_2$],[50] and [Yb(DippForm)$_2$(THF)$_2$][59] were prepared by the literature method. Lanthanoid metals were from Santoku/Molycorp/Eutectix. Large chunks were filed in the drybox before use. Solvents (THF, DME, C_6D_6, toluene and hexane) were pre-dried by distillation over sodium or sodium benzophenone ketyl before being stored under an atmosphere of nitrogen. Benzil was purchased from Alfa Aesar and all other reagents were purchased from Sigma Aldrich, and dried under vacuum prior to use. IR spectra were recorded as Nujol mulls between NaCl plates using an Agilent Technologies Cary 630 FTIR instrument within the range 4000–700 cm^{-1}. ^{1}H NMR and ^{13}C NMR spectra were recorded with a Bruker 400MHz instrument. Chemical shifts were referenced to the residual ^{1}H resonances of the deuterated solvents (^{1}H). Microanalyses were determined by the Chemical Analysis Facility, Macquarie University, and all the samples were sealed in tubes under nitrogen. Melting points were determined in sealed glass capillaries under nitrogen and are uncalibrated. Crystals were immersed in viscous hydrocarbon oil and were measured on a Rigaku SynergyS diffractometer or the MX1 beamline at the Australian Synchrotron.

4.6.2 [(DippForm)$_2$Sm^{III}(bnzl$^{\cdot}$-O)(THF)]·PhMe 1

5mL of THF was added to a Schlenk charged with [Sm(DippForm)$_2$(THF)$_2$] (0.1 mmol) and benzil (0.1mmol) and stirred overnight causing a colour change from dark green to maroon. Added DME and concentrated in vacuo before storing the solution at -18°C for 3 days to afford maroon crystals. (0.58g, 46%), (Found: C, 71.73; H, 7.63; N, 4.65; $C_{78}H_{112}N_6O_4Sm$ (1348.08) requires C, 71.95; H, 7.73; N, 4.48 %) IR (Nujol): 3056m, 1667s, 1593m, 1525s, 1361s, 1319s, 1282s, 1232s, 1189w, 1158m, 1098s, 1055s, 1023s, 931m, 865w, 822m, 801s, 783w, 766m, 757s, 723w, 694m, 695m, 674w, 661w, 607w cm $^{-1}$. ^{1}H NMR (C_6D_6, 300 MHz): 42.08 (s, 2H, NC***H***N), 11.39 (s, 1H, not assigned), 7.4 - 6.9 (m, 22H, aromatic Hs), 4.08 (4H, THF: 2,5-C***H***$_2$), 3.44 (m,8H, Dipp-C***H***), 3.33

(DME-C***H***$_3$), 3.12 (DME-C***H***$_3$), 1.86 (24H, Dipp-C***H***$_3$), 1.36 (3H, not assigned), (1.27 (4H, THF: 3,4-C***H***$_2$), 1.17 & 1.06 (24H, Dipp-C***H***$_3$). ^{13}C NMR (75.5 MHz, C_6D_6, 296K): 22.91 (Dipp-***C***H$_3$), 23.85 (Dipp-***C***H$_3$), 24.61 (Dipp-***C***H$_3$), 26.56 (THF: 3,4-***C***H$_2$), 28.34 (Dipp-***C***H), 28.63 (Dipp-***C***H), 37.08 (Dipp-***C***H), 58.78 (DME: ***C***H$_3$), 69.02 (THF: 2,5-***C***H$_2$), 72.27 (DME: ***C***H$_2$), 123.47, 123.77, 123.79, 124.04, 124.65, 125.18, 127.39, 128.70, 134.16, 138.90, 143.55, 145.26, 146.10, 146.75, 168.95 (aromatic C resonances – not assigned), 199.02 (Dipp-N***C***HN).

4.6.3 [(DippForm)$_2$Sm^{III}(Nap-NCHS)(THF)] 2

10mL of THF was added to a Schlenk charged with [Sm(DippForm)$_2$(THF)$_2$] (0.2 mmol) and Naphthyl isothiocyanate (0.2mmol) and stirred for two days causing a colour change from dark green to orange red. Concentrated in vacuo before storing the solution at -18°C for 3 days to obtain small yellow crystals. (0.31g, 27%). IR (Nujol): 1663s, 1587m, 1528s, 1379s, 1319m, 1286s, 1260m, 1233m, 1180m, 1098m, 1057m, 1043m, 1017m, 925w, 890w, 863w, 799s, 770m, 753m, 722w, 669w, 648w cm $^{-1}$. ^{1}H NMR (C_6D_6, 300 MHz): 11.45 (s, 2H, NC***H***N), 7.4 - 6.9 (m, 20H, aromatic Hs). ^{13}C NMR (75.5 MHz, C_6D_6, 296K): 22.90 (Dipp-***C***H$_3$), 23.85 (Dipp-***C***H$_3$), 23.91 (Dipp-***C***H$_3$) 24.61 (Dipp-***C***H$_3$), 25.41 (THF: 3,4-***C***H$_2$), 28.36 (Dipp-***C***H), 28.63 (Dipp-***C***H) 29.29 (Dipp-***C***H), 58.72 (DME: ***C***H$_3$), 67.70 (THF: 2,5-***C***H$_2$), 72.27 (DME: ***C***H$_2$), 118.07, 123.48, 123.76, 124.87, 125.34, 126.00, 127.23, 127.41, 128.70, 143.32, 146.11, 148.11 (aromatic **C** resonances – not assigned).

4.6.4 N,N'-diphenyl-N-(phenylcarbamothioyl)formimidamide 3

8mL of THF was added to a Schlenk charged with [Sm(DippForm)$_2$(THF)$_2$] (0.2 mmol) and phenylisothiocyanate (0.2mmol) was added dropwise and stirred overnight causing a colour change from dark green to red-brown. The solution was concentrated in vacuo before storing the solution at 4°C for one week to obtain colourless rectangular prisms. IR (Nujol): 3334w, 3061w, 2961m, 2926m, 2866m, 2070m, 1633m, 1589m, 1531m, 1490s, 1466m, 1445m, 1380m, 1361m, 1322m, 1277m, 1223s, 1154s, 1096m, 1057m, 1025m, 956m, 933m, 903w, 871w, 846m, 799m, 750s, 686s, 604w, 553m, 520m, 491m cm $^{-1}$. ^{1}H NMR (C_6D_6, 300 MHz): 7.36 (s, 1H, NC***H***N), 7.11 (m, 2H, *o*-

Ph-H), 6.70 (m, 6H, *m*-Ph) 6.59 (m, 3H, *p*-Ph), 1.36 (m,4H, Dipp-C***H***), 1.19 & 1.05 (24H, Dipp-C$\boldsymbol{H}_3$). ^{13}C NMR (75.5 MHz, C_6D_6, 296K): 23.85 (Dipp-***C***H_3), 24.82 (Dipp-***C***H_3), 28.35 (Dipp-***C***H), 29.18 (Dipp-***C***H), 123.47, 123.52, 125.74, 127.02, 128.99, 129.46, 131.61, (aromatic C resonances – not assigned), 139.30 (Dipp-N***C***HN).

4.6.5 N,N'-diphenyl-N-(phenylcarbamoyl) formimidamide 4

8mL of THF was added to a Schlenk charged with [Sm(DippForm)$_2$(THF)$_2$] (0.2 mmol) and phenylisocyanate (0.2mmol) was added dropwise and stirred overnight causing a colour change from dark green to pale yellowish green. The solution was concentrated in vacuo before storing the solution at 4°C for 24 hours to obtain colourless crystals. IR (Nujol): 3277w, 3026w, 2961m, 2869w, 1703m, 1638s, 1594s, 1557s, 1498m, 1447s, 1438s, 1383m, 1362w, 1311m, 1290m, 1223s, 1183m, 1155m, 1096m, 1079m, 1057m, 1026m, 986w, 963w, 935w, 914w, 894m, 811m, 798m, 776w, 752s, 727m, 690s, 641m, 612m, 578m, 557m, 523m, 509m, 452w cm $^{-1}$. ^{1}H NMR (C_6D_6, 300 MHz): 7.78 (s, 1H, NC***H***N),7.3 – 7.05 (m, 10H, aromatic Hs), 6.87 (m, 1H, *p*-Ph-H), 3.62 (4H, THF: 2,5-C$\boldsymbol{H}_2$), 3.27 (m,4H, Dipp-C***H***), 1.46 (4H, THF: 3,4-C$\boldsymbol{H}_2$), 1.29, 1.23 & 1.20 (24H, Dipp-C$\boldsymbol{H}_3$). ^{13}C NMR (75.5 MHz, C_6D_6, 296K): 23.92 (Dipp-***C***H_3), 24.03 (Dipp-***C***H_3), 24.98 (Dipp-***C***H_3), 26.07 (THF: 3,4-***C***H_2), 28.71 (Dipp-***C***H), 29.38 (Dipp-***C***H), 68.07 (THF: 2,5-***C***H_2), 120.14 (Dipp-N***C***HN), 123.74, 124.13, 124.79, 125.36, 129.69, 130.28, 139.77, 148.10, 152.56 (aromatic C resonances – not assigned.

4.6.6 The reaction of [Sm(DippForm)$_2$(THF)$_2$] with benzonitrile & o-tolunitrile

Benzonitrile (0.2mmol) / *o*-tolunitrile (0.2mmol) was added dropwise to a Schlenk flask charged with [Sm(DippForm)$_2$(thf)$_2$] (0.2mmol) in 10mL of toluene under a nitrogen atmosphere. Both solutions turned dark red immediately and the reaction was allowed to stir overnight. Yellow crystals of [Sm(DippForm)$_3$] were formed in both cases after leaving the concentrated solution at 4°C for a few days.

4.7 X-ray crystal data

Single crystals coated with viscous hydrocarbon oil were mounted on glass fibres or loops. All four complexes were measured at the Australian Synchrotron on the MX1 macromolecular beamlines, data integration was completed using Blue-ice[60] and XDS[61] software programs. Structural solutions were obtained by either direct methods[62] or charge flipping[63] methods and refined using full-matrix least-squares methods against F^2 using SHELX2015,[64] in conjunction with Olex2[63] graphical user interface. All hydrogen atoms were placed in calculated positions using the riding model. Crystal data and refinement details are given in **Table 3.1**. Data was collected by my colleague Dr. Zhifang Guo and she solved and refined the X-ray structures of **1** and **2**. Crystal structures of other complexes were solved and refined by me.

Table 3.1 Crystal data and structural refinement for lanthanoid complexes **1** & **2.**

	1	**2**
Formula	$C_{75}H_{96}N_4O_3Sm$	$C_{65}H_{86}N_5OSSm$
M_r	1251.90	1135.79
Crystal System	Triclinic	Monoclinic
Space group	P-1	$P2_1/n$
a (Å)	12.325(3)	15.060(3)
b (Å)	13.336(3)	22.200(4)
c (Å)	22.609(5)	17.850(4)
α (°)	101.40(3)	90
β (°)	91.66(3)	97.42(3)
γ (°)	112.08(3)	90
V (Å^3)	3353.8(14)	5918(2)
Z	2	4
ρ_{calc}, g cm^{-3}	1.240	1.275
μ, mm^{-1}	0.924	1.072
N_τ	137644	106289
N (R_{int})	15917 (0.0339)	11214 (0.0523)
$R_1(I > 2\sigma(I))$	0.0254	0.0386

wR_2 (all data)	0.0610	0.0932
GOF	1.092	1.047

Table 3.1 Crystal data and structural refinement for lanthanoid complexes **3** & **4.**

	3	**4**
Formula	$C_{36}H_{49}N_3OS$	$C_{32}H_{41}N_3O$
M_r	571.84	483.68
Crystal System	Triclinic	Monoclinic
Space group	*P*-1	*C*2/*c*
a (Å)	8.9800(18)	40.992(8)
b (Å)	11.170(2)	9.1240(18)
c (Å)	17.650(4)	16.470(3)
α (°)	104.38(3)	90
β (°)	94.89(3)	112.94(3)
γ (°)	104.47(3)	90
V (Å^3)	1640.0(6)	5673(2)
Z	2	8
ρ_{calc}, g cm^{-3}	1.158	1.133
μ, mm^{-1}	0.130	0.068
N_τ	51987	31828
N (R_{int})	6593 (0.0278)	4764 (0.0155)
$R_1(I > 2\sigma(I))$	0.0472	0.0441
wR_2 (all data)	0.1209	0.1093
GOF	1.065	1.072

4.8 References

1. W. J. Evans, J. W. Grate, L. A. Hughes, H. Zhang and J. L. Atwood, *J. Am. Chem. Soc.*, 1985, **107**, 3728-3730.
2. J. E. Bercaw, R. H. Marvich, L. G. Bell and H. H. Brintzinger, *J. Am. Chem. Soc.*, 1972, **94**, 1219-1238.
3. G. B. Deacon, P. C. Junk, J. Wang and D. Werner, *Inorg. Chem.*, 2014, **53**, 12553-12563.
4. E. D. Brady, D. L. Clark, D. W. Keogh, B. L. Scott and J. G. Watkin, *J. Am. Chem. Soc.*, 2002, **124**, 7007-7015.
5. Z. Hou, A. Fujita, H. Yamazaki and Y. Wakatsuki, *J. Am. Chem. Soc.*, 1996, **118**, 7843-7844.
6. G. B. Deacon, C. M. Forsyth and D. L. Wilkinson, *Chem. Eur. J.*, 2001, **7**, 1784-1795.
7. M. Szostak, N. J. Fazakerley, D. Parmar and D. J. Procter, *Chem. Rev.*, 2014, **114**, 5959-6039.
8. G. A. Molander and C. R. Harris, *Chem. Rev.*, 1996, **96**, 307-338.
9. G. A. Molander, *Acc. Chem. Res.*, 1998, **31**, 603-609.
10. G. A. Molander, *Chem. Rev.*, 1992, **92**, 29-68.
11. K. Gopalaiah and H. B. Kagan, *Chem. Rec.*, 2013, **13**, 187-208.
12. T. Skrydstrup, *Angew. Chem.*, 1997, **109**, 355-358.
13. T. Skrydstrup, *Angew. Chem. Int. Ed. Engl.*, 1997, **36**, 345-347.
14. N. G. Connelly and W. E. Geiger, *Chem. Rev.*, 1996, **96**, 877-910.
15. I. L. Fedushkin, A. A. Skatova, V. K. Cherkasov, V. A. Chudakova, S. Dechert, M. Hummert and H. Schumann, *Chem. Eur. J.*, 2003, **9**, 5778-5783.
16. C. Cui, S. Köpke, R. Herbst-Irmer, H. W. Roesky, M. Noltemeyer, H.-G. Schmidt and B. Wrackmeyer, *J. Am. Chem. Soc.*, 2001, **123**, 9091-9098.
17. O. P. Lam, C. Anthon, F. W. Heinemann, J. M. O’Connor and K. Meyer, *J. Am. Chem. Soc.*, 2008, **130**, 6567-6576.
18. Z. Hou, A. Fujita, Y. Zhang, T. Miyano, H. Yamazaki and Y. Wakatsuki, *J. Am. Chem. Soc.*, 1998, **120**, 754-766.

19. W. Clegg, K. Izod, P. O'Shaughnessy, C. Eaborn and J. D. Smith, *Angew. Chem. Int. Ed. Engl.*, 1997, **36**, 2815-2817.
20. Z. Hou, T. Miyano, H. Yamazaki and Y. Wakatsuki, *J. Am. Chem. Soc.*, 1995, **117**, 4421-4422.
21. T. A. Scott, B. A. Ooro, D. J. Collins, M. Shatruk, A. Yakovenko, K. R. Dunbar and H.-C. Zhou, *Chem. Commun.*, 2009, 65-67.
22. Z. Hou, X. Jia, M. Hoshino and Y. Wakatsuki, *Angew. Chem.*, 1997, **109**, 1348-1350.
23. Z. Hou, X. Jia, M. Hoshino and Y. Wakatsuki, *Angew. Chem. Int. Ed. Engl.*, 1997, **36**, 1292-1294.
24. Z. Hou, X. Jia, A. Fujita, H. Tezuka, H. Yamazaki and Y. Wakatsuki, *Chem. Eur. J.*, 2000, **6**, 2994-3005.
25. Z. Hou, A. Fujita, T.-a. Koizumi, H. Yamazaki and Y. Wakatsuki, *Organometallics*, 1999, **18**, 1979-1985.
26. W. Clegg, K. Izod, P. O'Shaughnessy, C. Eaborn and J. D. Smith, *Angew. Chem.*, 1997, **109**, 2925-2926.
27. F. Jaroschik, F. Nief and X.-F. Le Goff, *Polyhedron*, 2009, **28**, 2744-2748.
28. Â. Domingos, I. Lopes, J. C. Waerenborgh, N. Marques, G. Lin, X. Zhang, J. Takats, R. McDonald, A. C. Hillier and A. Sella, *Inorg. Chem.*, 2007, **46**, 9415-9424.
29. D. Werner, X. Zhao, S. P. Best, L. Maron, P. C. Junk and G. B. Deacon, *Chem. Eur. J.*, 2017, **23**, 2084-2102.
30. J. E. Bercaw, D. L. Davies and P. T. Wolczanski, *Organometallics*, 1986, **5**, 443-450.
31. M. L. Cole, G. B. Deacon, C. M. Forsyth, P. C. Junk, D. Polo-Cerón and J. Wang, *Dalton Trans.*, 2010, **39**, 6732-6738.
32. G. B. Deacon, C. M. Forsyth, P. C. Junk and J. Wang, *Inorg. Chem.*, 2007, **46**, 10022-10030.
33. R. Duchateau, T. Tuinstra, E. A. Brussee, A. Meetsma, P. T. van Duijnen and J. H. Teuben, *Organometallics*, 1997, **16**, 3511-3522.
34. E. J. Enholm, D. C. Forbes and D. P. Holub, *Synth. Commun.*, 1990, **20**, 981-987.
35. V. Y. Kukushkin and A. J. Pombeiro, *Chem. Rev.*, 2002, **102**, 1771-1802.

36. Y. Makioka, Y. Taniguchi, Y. Fujiwara, K. Takaki, Z. Hou and Y. Wakatsuki, *Organometallics*, 1996, **15**, 5476-5478.
37. R. A. Michelin, M. Mozzon and R. Bertani, *Coord. Chem. Rev.*, 1996, **147**, 299-338.
38. Y. Tanaka, N. Taniguchi and M. Uemura, *Org. Lett.*, 2002, **4**, 835-838.
39. N. Taniguchi and M. Uemura, *J. Am. Chem. Soc.*, 2000, **122**, 8301-8302.
40. J. Wang, F. Xu, T. Cai and Q. Shen, *Org. Lett.*, 2008, **10**, 445-448.
41. W. Yi, J. Zhang, F. Zhang, Y. Zhang, Z. Chen and X. Zhou, *Chem. Eur. J.*, 2013, **19**, 11975-11983.
42. Z. Hou, C. Yoda, T.-a. Koizumi, M. Nishiura, Y. Wakatsuki, S.-i. Fukuzawa and J. Takats, *Organometallics*, 2003, **22**, 3586-3592.
43. W. Yi, J. Zhang, L. Hong, Z. Chen and X. Zhou, *Organometallics*, 2011, **30**, 5809-5814.
44. F. A. Watt, N. Dickmann, R. Schoch and S. Hohloch, *Inorg. Chem.*, 2020, **59**, 13621-13631.
45. Y. Han, J. Zhang, F. Han, Z. Zhang, L. Weng and X. Zhou, *Organometallics*, 2009, **28**, 3916-3921.
46. W. J. Evans and D. K. Drummond, *Organometallics*, 1988, **7**, 797-802.
47. W. J. Evans, E. Montalvo, S. E. Foster, K. A. Harada and J. W. Ziller, *Organometallics*, 2007, **26**, 2904-2910.
48. M. G. Gardiner, A. N. James, C. Jones and C. Schulten, *Dalton Trans.*, 2010, **39**, 6864-6870.
49. F. Xu, X. H. Zhu, Q. Shen, J. Lu and J. Q. Li, *Chin. J. Chem.*, 2002, **20**, 1334-1339.
50. M. L. Cole and P. C. Junk, *Chem. Commun.*, 2005, 2695-2697.
51. R. D. Shannon, *Acta Crystallogr. Sect. A.*, 1976, **32**, 751-767.
52. A. A. Maleev, A. P. Pushkarev, V. A. Ilichev, M. A. Lopatin, M. A. Samsonov, G. K. Fukin, G. L. Pakhomov, V. V. Travkin, I. D. Grishin and M. N. Bochkarev, *J. Rare Earths.*, 2014, **32**, 1101-1108.
53. K. Mashima, T. Shibahara, Y. Nakayama and A. Nakamura, *J. Organomet. Chem.*, 1998, **559**, 197-201.
54. G. Häfelinger, *Chem. Ber.*, 1970, **103**, 2902-2921.

55. L. Pauling, *The nature of the chemical bond and the structure of molecules and crystals : an introduction to modern structural chemistry*, Third edition. edn.
56. H.-P. Deng and M. Shi, *Eur. J. Org. Chem.*, 2012, **2012**, 183-187.
57. M. L. Cole, G. B. Deacon, C. M. Forsyth, P. C. Junk, D. P. Ceron and J. Wang, *Dalton Trans.*, 2010, **39**, 6732-6738.
58. G. B. Deacon, C. M. Forsyth, P. C. Junk and J. Wang, *Inorg. Chem.*, 2007, **46**, 10022−10030.
59. M. L. Cole, G. B. Deacon, C. M. Forsyth, P. C. Junk, K. Konstas, J. Wang, H. Bittig and D. Werner, *Chem. Eur. J.*, 2013, **19**, 1410-1420.
60. T. M. McPhillips, S. E. McPhillips, H. J. Chiu, A. E. Cohen, A. M. Deacon, P. J. Ellis, E. Garman, A. Gonzalez, N. K. Sauter, R. P. Phizackerley, S. M. Soltis and P. Kuhn, *J. Synchrotron Radiat.*, 2002, **9**, 401-406.
61. W. Kabsch, *J. Appl. Crystallogr.*, 1993, **26**, 795-800.
62. G. M. Sheldrick, *Acta Crystallogr. A.*, 2008, **64**, 112-122.
63. O. V. Dolomanov, L. J. Bourhis, R. J. Gildea, J. A. K. Howard and H. Puschmann, *J. Appl. Crystallogr.*, 2009, **42**, 339-341.
64. G. M. Sheldrick, *Acta Crystallogr. C.*, 2015, **71**, 3-8.

Chapter 5

Reactivity of transition metal carbonyls towards the divalent organolanthanoid complexes

5.1 Introduction

Heterometallic complexes comprised of lanthanoids and transition metals (TM) (mainly, 4d-4f and 3d-4f) have received a lot of interest because of their potential applications in catalysis,[1, 2] magnetism,[3-5] and their photophysical characteristics.[6, 7] The vast majority of these properties primarily arise from their possession of different affinities for N and O donor ligands by lanthanoids and transition metal ions, which is mainly based on the hard-soft acid/base categorization.[8] Ln-TM carbonyl complexes are one of the significant classes of compounds among them, as they provide diverse reactive aspects from both fundamental and application perspectives.[9-11] Single-molecule magnetic behaviour exhibited by Dy-TM carbonyl complexes is an effective illustration of that.[12, 13] Highly reactive divalent organolanthanoid complexes have been used in synthesizing novel Ln-TM carbonyl complexes. Reduction of $[Cp^*Fe(CO)_2]_2$ using solvated decamethyl samarocene $[SmCp^*_2(THF)_2]$ resulted in the formation of a Sm^{III}-Fe^0 heterometallic complex,[14] while trapping of a $[W_2(CO)_{10}]^{2-}$ anion in a mixed-valent samarium complex has been achieved using divalent samarium *meso*-octaethylcalyx[4]pyrrolide complex $[Sm_2(N_4Et_8)(thf)_4]$ upon treating with tungsten hexacarbonyl.[15] Among Yb(II) complexes, $[Cp^*_2Yb(OEt_2)]$ has been applied for the synthesis of various Yb^{III}-TM isocarbonyl complexes [Yb^{III}-OC-TM] through the reduction of carbonyl complexes of d-block metals.[16-19]

Ln-TM carbonyl complexes can be classified into different types based on the bonding between lanthanoids and transition metals, which includes solvent-separated ion pairs[20, 21] and Ln-TM bonded compounds.[9, 10, 12, 22-24] Ln-TM heterometallic complexes with isocarbonyl linkages[11, 17, 25] represents a large fraction among them as they exploit the oxophilic nature of lanthanoid cations. In addition, π back-bonding between TM(d_π) and C-O(π^*) provides enhanced stability to the negative charge on the transition metal.[26] Application of divalent organolanthanoid complexes as single-electron transfer (SET) reagents has been utilized in making or breaking TM-TM bonds through the transfer of electrons to TM carbonyl moiety, which leads to the formation of isocarbonyl-bridged Ln-TM systems. $[SmCp^*_2(THF)_2]$ and its DippForm analogue $[Sm(DippForm)_2(THF)_2]$ are the two Sm(II) complexes of interest, which were recently employed in the reduction of [$Re_2(CO)_{10}$].[27] Reaction with [$SmCp^*_2(THF)_2$] resulted in the isolation of a Fischer-type rhenacycle (**A** in **Scheme 5.1**) while treatment with [$Sm(DippForm)_2(THF)_2$] leads to trapping of a novel dianionic ligand [$Re_2(CO)_8$]$^{2-}$ (**B** in **Scheme 5.1**).

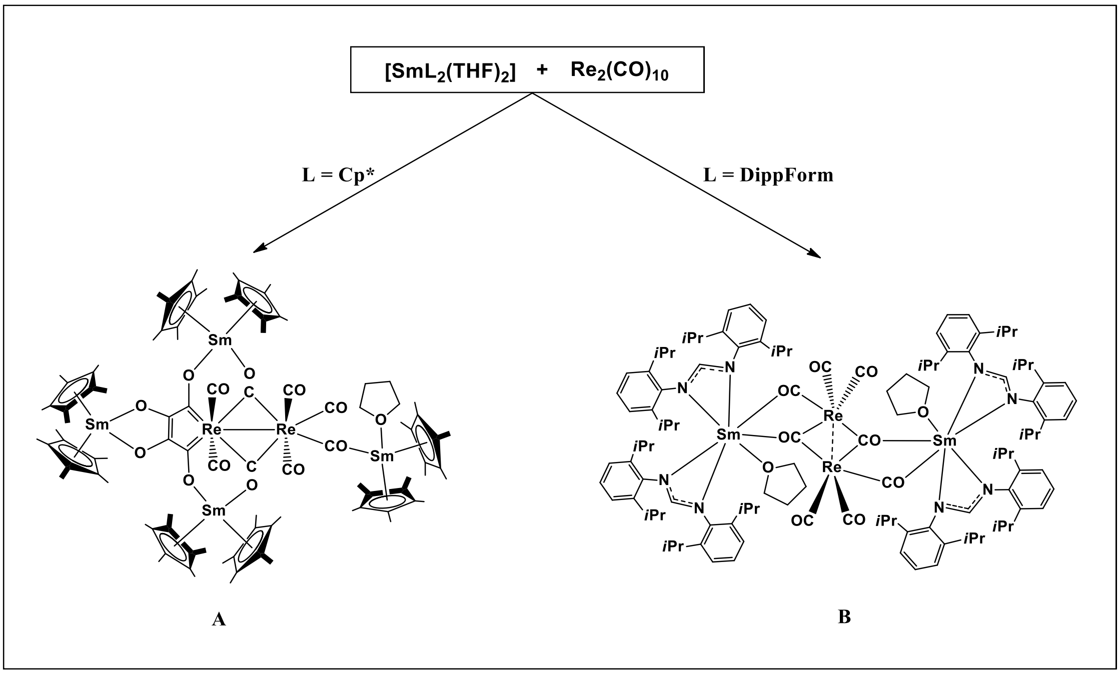

Scheme 5.1. The reaction of [$SmL_2(THF)_2$] (L = Cp* or DippForm) with $Re_2(CO)_{10}$. [27]

5.2 Results & Discussion

Reactivity of transition metal carbonyls (especially groups 8 and 9) towards the divalent organolanthanoid complexes is of great interest, particularly using highly powerful reductant Sm(II) and Yb(II) complexes ligated by bulky amidinate DippForm moieties. As a part of an expanding investigation on group 8 and 9 metal carbonyls, our lab treated $Co_2(CO)_8$ with $[Yb(DippForm)_2(THF)_2]$ in different solvents and obtained crystal structures of two separate products in toluene and THF (**Scheme 5.2**). This project involved resynthesizing product **B** (in **Scheme 5.2**) and its characterization which aided in the completion of this aspect of the project.

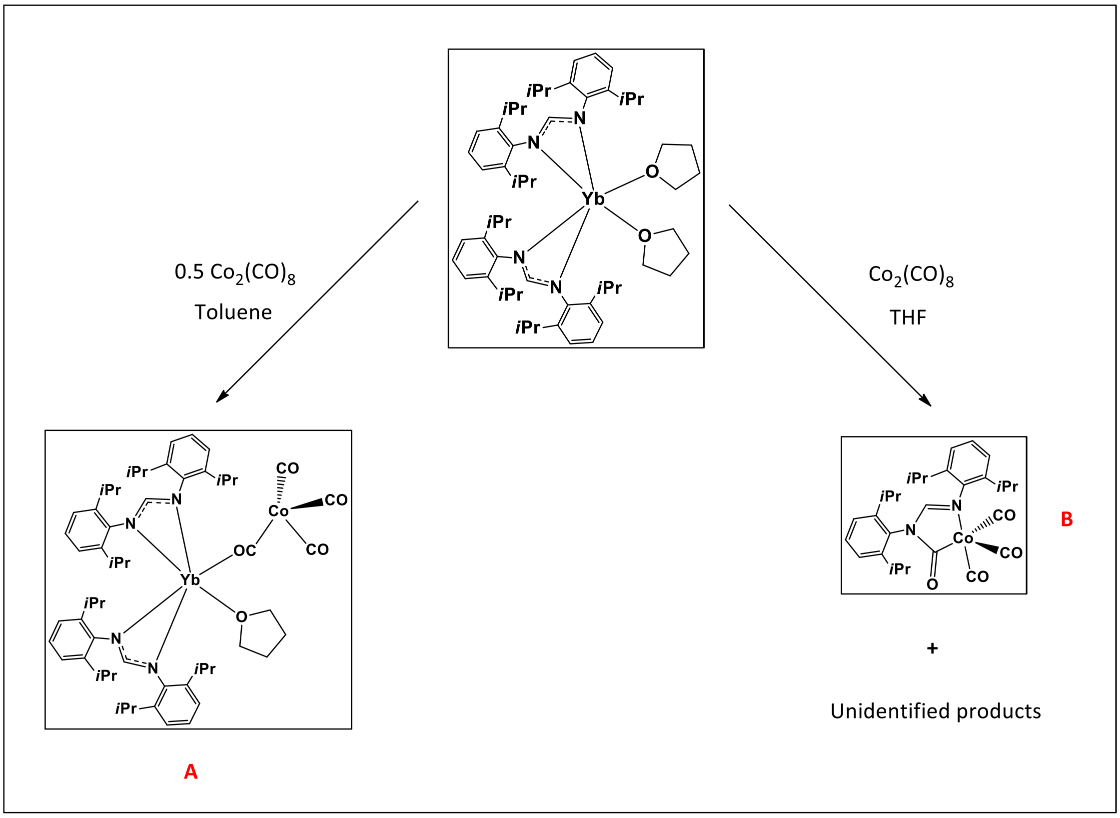

Scheme 5.2. The reaction of $Co_2(CO)_8$ towards $[Yb(DippForm)_2(THF)_2]$ giving two separate products **A** (in toluene) and **B** (in THF).

5.3 Synthesis and characterization

[Yb(DippForm)$_2$(THF)$_2$] and Co$_2$(CO)$_8$ were stirred for 12h under nitrogen in THF at room temperature, resulting in a colour change from orange to dark brown. Solid materials were removed from the solution through filtration and concentrated under vacuum, giving colourless needle-type crystals of **[Co(DippFormCO)(CO)$_3$]·THF**. The compound was successfully characterized using ^{1}H NMR and IR spectroscopy.

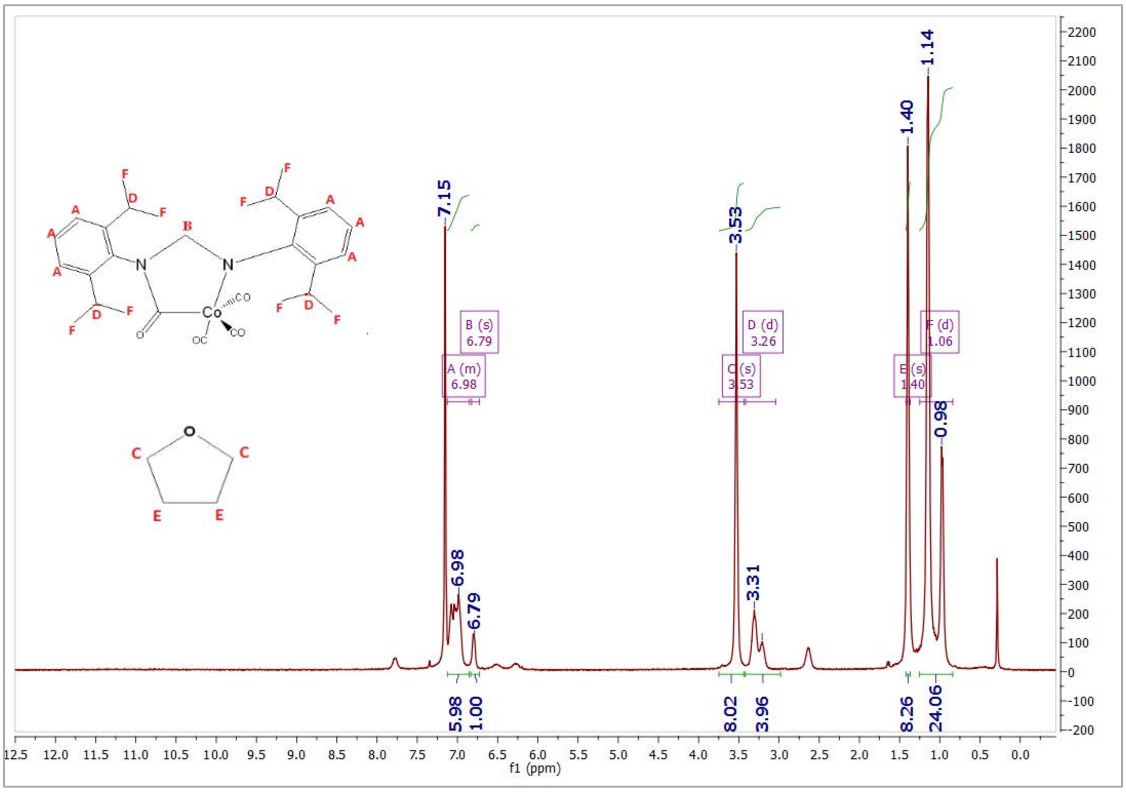

Fig. 5.1. ^{1}H NMR spectrum of **[Co(DippFormCO)(CO)$_3$]·THF**.

The ^{1}H NMR spectrum indicates the formation of the proposed compound although there areminor impurities. The spectrum shows an agreement with the ^{1}H NMR spectrum of an analogous compound Co(CO)$_3$[C(=O)N(Ar)C(tBu)N(Ar)] reported by the Jones group.[28] The splitting in the chemical shift of isopropyl protons can also be seen here at 1.06 ppm (for CH(C***H***$_3$)$_2$) and 3.26 ppm (for C***H***(CH$_3$)$_2$). The DippForm backbone proton (NC*H*N) resonance is identified as a singlet at δ = 6.79 ppm with an integration value of one while the peaks at δ = 1.40 and 3.31 ppm can be attributed to α- and β-hydrogens of solvent THF respectively. A satisfactory IR spectrum of **[Co(DippFormCO)(CO)$_3$]·THF** was also obtained where the absorptions at 2066s, 2009s and 1983m can be ascribed to C-O stretching frequencies of carbonyl groups. These values are very similar to the IR spectrum of the previously mentioned analogous compound, Co(CO)$_3$[C(=O)N(Ar)C(tBu)N(Ar)], where they identified 2064s, 2004s and 1970br as CO stretching frequencies.[28]

The crystal structure of **[Co(DippFormCO)(CO)$_3$]·THF** is given in **Fig. 5.2**. The complex crystallizes in the monoclinic space group $P2_1/n$ with one lattice THF molecule in the asymmetric unit. The cobalt centre in the complex is connected to three carbonyl groups (CO), one C(=O)N unit and to one of the two nitrogen atoms in N-C-N backbone of DippForm. The bond lengths and bond angles of this complex are similar to that of analogous compound Co(CO)$_3$[C(=O)N(Ar)C(tBu)N(Ar)].[28] The crystal structure matches with spectroscopy data (NMR and IR) described above.

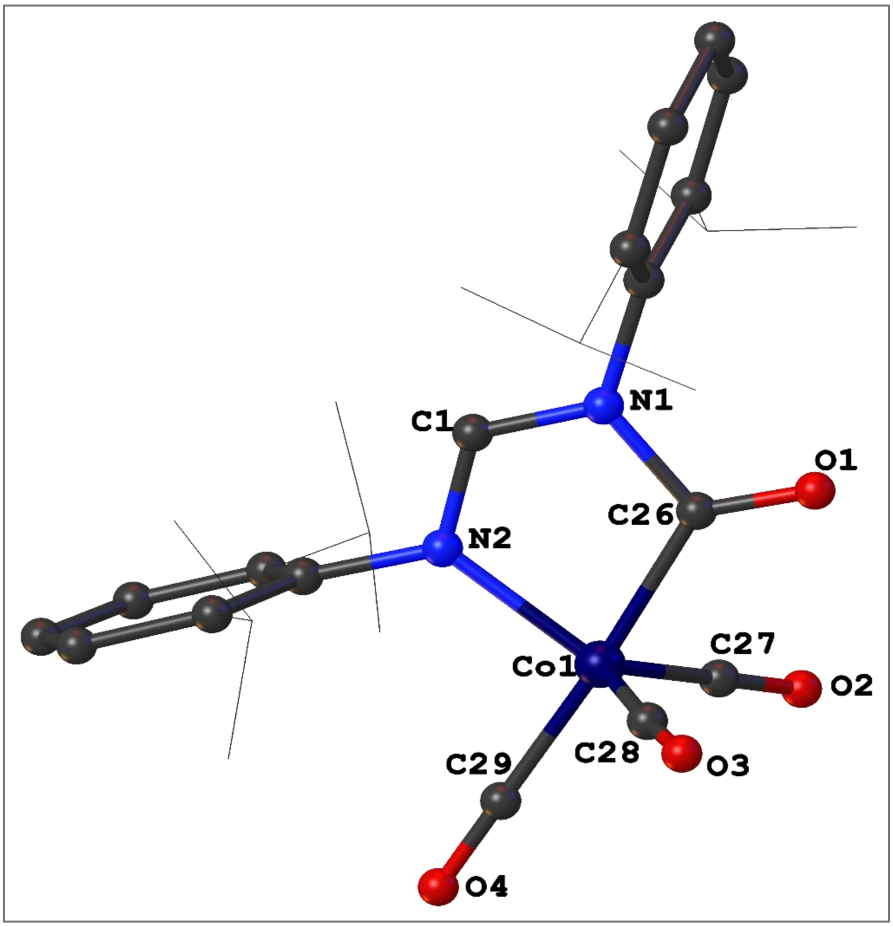

Fig. 5.2 ORTEP diagram of complex **[Co(DippFormCO)(CO)$_3$]·THF** in which relevant atoms are labelled. Thermal ellipsoids are drawn at a 50% probability level. Isopropyl groups of DippForm are shown as lines and hydrogen atoms along with one lattice THF molecule are omitted for clarity. Selected bond angles (°) and lengths (Å): Co1-N2 1.968(3), Co1-C29 1.799(5), Co1-C28 1.755(6), Co1-C27 1.755(6), Co1-C26 1.930(4), C29–O4 1.138(6), C28–O3 1.134(7), C27–O2 1.135(6), C26–O1 1.201(5), N1–C26 1.430(5), C1–N2 1.285(3), C1–N1 1.346(5), C29–Co1–N2 93.6(2), C28–Co1–N2 117.7(2), C27–Co1–N2 121.6(2), C26–Co1–N2 82.7(2), C28–Co1–C29 96.7(2), C27–Co1–C28 118.5(3), C26–Co1–C29 176.1(2), C26–Co1–C28 86.0(2), C26–Co1–C27 86.2(2), N1-C1-N2 118.3(4).

5.4 Conclusions & Future Outlook

The compound **[Co(DippFormCO)(CO)$_3$]·THF** was successfully resynthesized and characterized using ^{1}H NMR and IR spectra. The X-ray crystal structure details are also described here. This part of the project resulted in a publication in the journal *Dalton Transactions* (see reprint in appendix 1). Divalent organolanthanoid complexes [Sm(DippForm)$_2$(THF)$_2$] and it's ytterbium analogue [Yb(DippForm)$_2$(THF)$_2$] have been used in the formation of various 3d-4f heterometallic complexes upon reaction with carbonyl complexes of 3d transition metals cobalt and iron. These studies opened up the wide possibilities of synthesis of diverse 3d-4f heterometallic complexes by utilizing the high reduction potential of divalent lanthanoid complexes samarium and ytterbium coordinated by the DippForm ligand.

5.5 Experimental

5.5.1 General Considerations

The lanthanoid compounds described here are highly air and moisture sensitive and were prepared and handled with vacuum-nitrogen line techniques and in a dry box in an atmosphere of purified nitrogen. [Yb(DippForm)$_2$(THF)$_2$] was prepared by the literature method.[29] Lanthanoid metals were from Santoku/Molycorp/Eutectix. Large chunks were filed in the drybox before use. Solvents (THF and C_6D_6) were pre-dried by distillation over sodium or sodium benzophenone ketyl before being stored under an atmosphere of nitrogen. $Co_2(CO)_8$ was purchased from Sigma Aldrich and dried under a vacuum prior to use. IR spectra were recorded as Nujol mulls between NaCl plates using an Agilent Technologies Cary 630 FTIR instrument within the range 4000–700 cm^{-1}. ^{1}H NMR spectrum was recorded with a Bruker 400MHz instrument. Chemical shifts were referenced to the residual ^{1}H resonances of the deuterated solvents (^{1}H).

5.5.2 Synthesis of [Co(DippFormCO)(CO)$_3$]

30mL of THF was added to a Schlenk flask charged with [Yb(DippForm)$_2$(THF)$_2$] (0.4 mmol) and $Co_2(CO)_8$ (0.47mmol) and stirred for 12 hours at room temperature causing a colour change from orange to dark brown. The solution was concentrated *in vacuo* and stored at 3°C for three days to afford colourless needle-like crystals. IR *v*/cm^{-1} (Nujol): 2066(s), 2009(s), 1983(m), 1897(w), 1666(s), 1587(m), 1287(m), 1234(w), 1180(m), 1098(w), 1058(w), 1000(w), 935(w), 821(w), 799(m), 753(w), 767(m), 722(m). ^{1}H NMR (C_6D_6, 300 MHz) δ 7.13 – 6.85 (m, 6H, Ar-*H*), 6.79 (s, 1H, NC*H*N), 3.53 (s, 8H, OC*H*$_2$(thf)), 3.31 (sept, 3H, *J* 868, C*H*(CH$_3$)$_2$), 3.21 (sept, 1H, *J* 892, C*H*(CH$_3$)$_2$), 1.40 (s, 8H, C*H*$_2$(thf)), 1.14 (d, 18H, *J* 868, CH(C*H*$_3$)$_2$), 0.98 (d, 6H, *J* 892, CH(C*H*$_3$)$_2$).

5.6 References

1. A. Bhunia, M. A. Gotthardt, M. Yadav, M. T. Gamer, A. Eichhöfer, W. Kleist and P. W. Roesky, *Chem. Eur. J.*, 2013, **19**, 1986-1995.
2. M. Yadav, A. Bhunia, S. K. Jana and P. W. Roesky, *Inorg. Chem.*, 2016, **55**, 2701-2708.
3. A. Bhunia, M. T. Gamer, L. Ungur, L. F. Chibotaru, A. K. Powell, Y. Lan, P. W. Roesky, F. Menges, C. Riehn and G. Niedner-Schatteburg, *Inorg. Chem.*, 2012, **51**, 9589-9597.
4. J. L. Liu, J. Y. Wu, Y. C. Chen, V. Mereacre, A. K. Powell, L. Ungur, L. F. Chibotaru, X. M. Chen and M. L. Tong, *Angew. Chem. Int. Ed.*, 2014, **53**, 12966-12970.
5. J. Wu, L. Zhao, L. Zhang, X. L. Li, M. Guo, A. K. Powell and J. Tang, *Angew. Chem.*, 2016, **128**, 15803-15807.
6. S. V. Eliseeva and J.-C. G. Bünzli, *Chem. Soc. Rev.*, 2010, **39**, 189-227.
7. T. D. Pasatoiu, C. Tiseanu, A. M. Madalan, B. Jurca, C. Duhayon, J. P. Sutter and M. Andruh, *Inorg. Chem.*, 2011, **50**, 5879-5889.
8. R. G. Pearson, *J. Am. Chem. Soc.*, 1963, **85**, 3533-3539.
9. P. L. Arnold, J. McMaster and S. T. Liddle, *Chem. Commun.*, 2009, 818-820.
10. C. P. Burns, X. Yang, S. Sung, J. D. Wofford, N. S. Bhuvanesh, M. B. Hall and M. Nippe, *Chem. Commun.*, 2018, **54**, 10893-10896.
11. C. E. Plecnik, S. Liu and S. G. Shore, *Acc. Chem. Res.*, 2003, **36**, 499-508.
12. C. P. Burns, X. Yang, J. D. Wofford, N. S. Bhuvanesh, M. B. Hall and M. Nippe, *Angew. Chem.*, 2018, **130**, 8276-8280.
13. T. Pugh, N. F. Chilton and R. A. Layfield, *Angew. Chem. Int. Ed.*, 2016, **55**, 11082-11085.
14. A. Recknagel, A. Steiner, S. Brooker, D. Stalke and F. T. Edelmann, *Chem. Ber.*, 1991, **124**, 1373-1375.
15. G. B. Deacon, Z. Guo, P. C. Junk and J. Wang, *Angew. Chem. Int. Ed.*, 2017, **56**, 8486-8489.
16. T. D. Tilley and R. A. Andersen, *J. Chem. Soc., Chem. Commun.*, 1981, 985-986.
17. T. D. Tilley and R. Andersen, *J. Am. Chem. Soc.*, 1982, **104**, 1772-1774.
18. J. M. Boncella and R. A. Andersen, *Inorg. Chem.*, 1984, **23**, 432-437.

19. J. M. Boncella and R. A. Andersen, *J. Chem. Soc., Chem. Commun.*, 1984, 809-810.
20. P. V. Poplaukhin, X. Chen, E. A. Meyers and S. G. Shore, *Inorg. Chem.*, 2006, **45**, 10115-10125.
21. W. J. Evans, I. Bloom, J. W. Grate, L. A. Hughes, W. E. Hunter and J. L. Atwood, *Inorg. Chem.*, 1985, **24**, 4620-4623.
22. I. Beletskaya, A. Voskoboynikov, E. Chuklanova, N. Kirillova, A. Shestakova, I. Parshina, A. Gusev and G. Magomedov, *J. Am. Chem. Soc.*, 1993, **115**, 3156-3166.
23. M. P. Blake, N. Kaltsoyannis and P. Mountford, *J. Am. Chem. Soc.*, 2011, **133**, 15358-15361.
24. C. Döring, A. M. Dietel, M. V. Butovskii, V. Bezugly, F. R. Wagner and R. Kempe, *Chem. Eur. J.*, 2010, **16**, 10679-10683.
25. B. Oelkers, M. V. Butovskii and R. Kempe, *Chem. Eur. J.*, 2012, **18**, 13566-13579.
26. R. Green, A. C. Walker, M. P. Blake and P. Mountford, *Polyhedron*, 2016, **116**, 64-75.
27. R. Yadav, T. Simler, M. T. Gamer, R. Köppe and P. W. Roesky, *Chem. Commun.*, 2019, **55**, 5765-5768.
28. C. Jones, C. Schulten, R. P. Rose, A. Stasch, S. Aldridge, W. D. Woodul, K. S. Murray, B. Moubaraki, M. Brynda and G. La Macchia, *Angew. Chem. Int. Ed.*, 2009, **48**, 7406-7410.
29. M. L. Cole, G. B. Deacon, C. M. Forsyth, P. C. Junk, K. Konstas, J. Wang, H. Bittig and D. Werner, *Chem. Eur. J.*, 2013, **19**, 1410-1420.

Appendix 1

Publication

Volume 49
Number 23
21 June 2020
Pages 7631-7994

Dalton Transactions

An international journal of inorganic chemistry

rsc.li/dalton

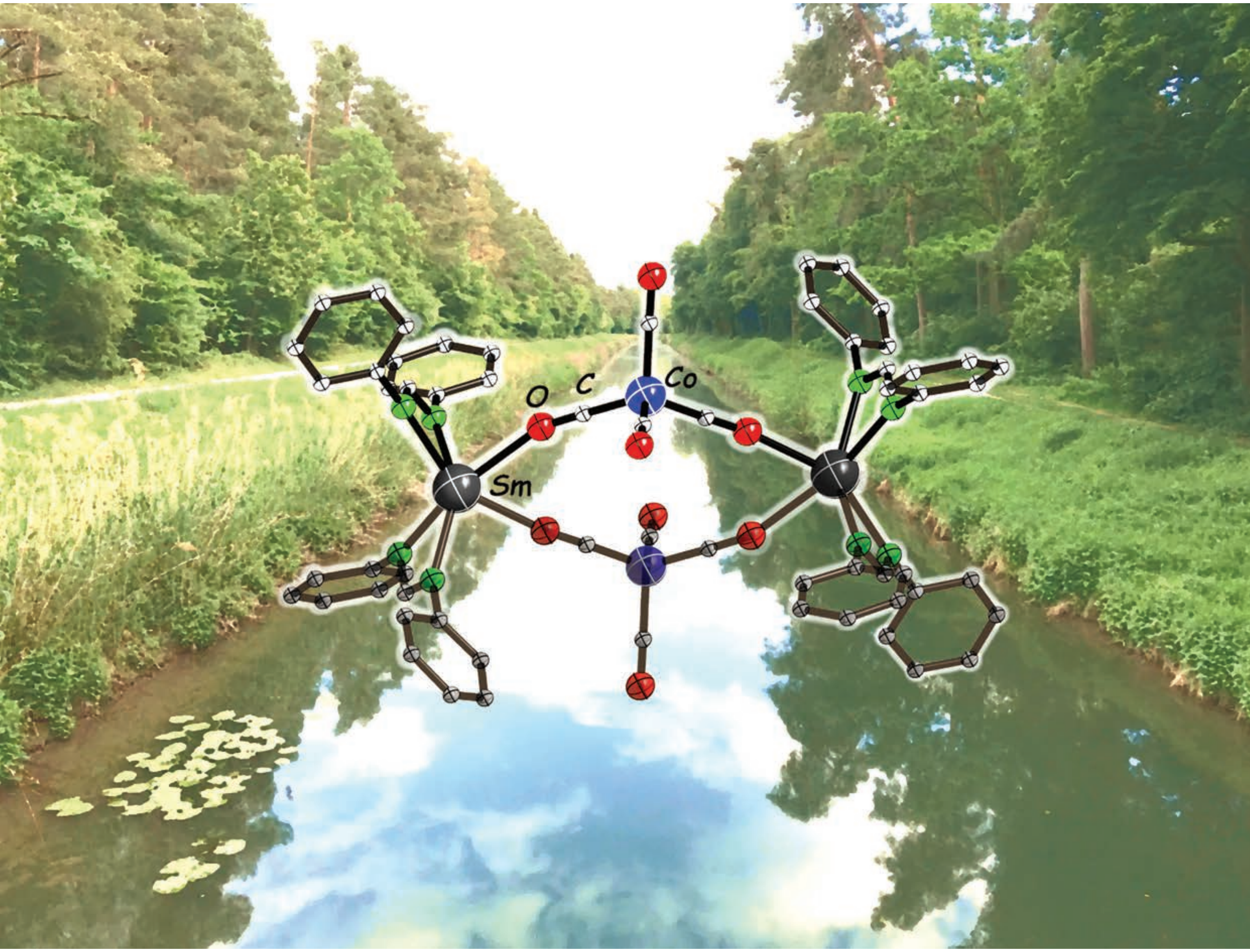

ISSN 1477-9226

ROYAL SOCIETY OF **CHEMISTRY**

PAPER
Peter W. Roesky *et al.*
3d–4f heterometallic complexes by the reduction of transition metal carbonyls with bulky Ln^{II} amidinates

Dalton Transactions

ROYAL SOCIETY OF CHEMISTRY

PAPER

View Article Online
View Journal | View Issue

Cite this: *Dalton Trans.*, 2020, **49**, 7701

3d–4f heterometallic complexes by the reduction of transition metal carbonyls with bulky Ln^{II} amidinates†

Ravi Yadav, [a] Md Elius Hossain, [b] Ramees Peedika Paramban, [b] Thomas Simler, [a] Christoph Schoo, [a] Jun Wang,[b] Glen B. Deacon, [c] Peter C. Junk [b] and Peter W. Roesky *[a]

Received 6th April 2020,
Accepted 1st May 2020

DOI: 10.1039/d0dt01271h

rsc.li/dalton

The redox chemistry between divalent lanthanide complexes bearing bulky amidinate ligands has been studied with 3d transition metal carbonyl complexes (iron and cobalt). The reaction of $[(\text{DippForm})_2\text{Sm}^{II}(\text{thf})_2]$ (DippForm = *N*,*N*′-bis(2,6-diisopropylphenyl)formamidinate) with $[\text{Co}_2(\text{CO})_8]$ resulted in the formation of a tetranuclear Sm–Co complex, $[\{(\text{DippForm})_2\text{Sm}^{III}(\text{thf})\}_2\{(\mu\text{-CO})_2\text{Co}(\text{CO})_2\}_2]$. The product of the reaction of $[(\text{DippForm})_2\text{Yb}^{II}(\text{thf})_2]$ and $[\text{Co}_2(\text{CO})_8]$ gives the dinuclear Yb–Co complex $[\{(\text{DippForm})_2\text{Yb}^{III}(\text{thf})\}\{(\mu\text{-CO})\text{Co}(\text{CO})_3\}]$ in toluene. The reaction of $[(\text{DippForm})_2\text{Sm}^{II}(\text{thf})_2]$ was also carried with the neighbouring group 8 carbonyl complexes $[\text{Fe}_2(\text{CO})_9]$ and $[\text{Fe}_3(\text{CO})_{12}]$, resulting in a pentanuclear Sm^{III}–Fe complex, $[\{(\text{DippForm})_2\text{Sm}^{III}\}_2\{(\mu_3\text{-CO})_2\text{Fe}_3(\text{CO})_9\}]$, featuring a triangular iron carbonyl cluster core.

Introduction

Heterometallic complexes have gained widespread attention due to the viable synergistic effect that may result from a judicious choice of metal centres.[1,2] Ln–TM (TM = transition metal) heterometallic complexes have especially attracted interest due to their magnetic,[3–5] and photophysical properties,[6,7] as well as their catalytic activity.[8,9] Among them, Ln–TM carbonyl complexes are a major class of compounds from both fundamental and application points of view.[10–12] For example, Dy–TM carbonyl complexes have demonstrated single-molecule magnetic behaviour.[13,14] Andersen and co-workers have synthesized several Yb^{III}–TM isocarbonyl complexes, [Yb^{III}-OC-TM], by reduction of TM carbonyl complexes with $[\text{Cp}^*{}_2\text{Yb}^{II}(\text{OEt}_2)]$.[15–18] Edelmann and co-workers have isolated the formally Sm^{III}–Fe^0 complex $[\text{Cp}^*{}_2\text{Sm}(\mu\text{-OC})_2\text{FeCp}^*]_2$ by reducing $[\text{Cp}^*\text{Fe}(\text{CO})_2]_2$ with $[\text{Cp}^*{}_2\text{Sm}(\text{thf})_2]$.[19] Some of us isolated the elusive $[\text{W}_2(\text{CO})_{10}]^{2-}$ anion in a mixed-valent Sm$^{II/III}$ calix[4]pyrrolide sandwich by the reduction of $[\text{W}(\text{CO})_6]$ with a divalent samarium *meso*-octaethylcalix[4]pyrrolide.[20] Also, Ln^{II}–TM carbonyl complexes have been accessed either by redox-transmetallation between Hg salts of TM carbonyl complexes and elemental Ln^0 or by reduction of TM carbonyl complexes with Ln/Hg amalgam.[10,21–26] Depending on the bonding situation between the two metal centres, Ln–TM carbonyl complexes can be divided into three major categories: (i) solvent-separated ion pairs,[22,27] (ii) Ln–TM bonded compounds,[11,12,14,23,28,29] and (iii) compounds with isocarbonyl-linkages[10,16,30] between both metals. Isocarbonyl bridged Ln–TM complexes are the major representatives, which can be explained by the oxophilic nature of lanthanide cations and the additional stabilisation of the negative charge on the TM centre through π back-donation from TM(d$_\pi$) to C–O(π*).[26] Usually, the reaction of divalent lanthanide complexes with TM-carbonyls leads to isocarbonyl-bridged systems, resulting from a single-electron transfer (SET) to the TM carbonyl moiety and leading to either cleavage or formation of TM–TM bonds.

The chemistry of divalent lanthanide complexes is dominated by the use of cyclopentadienyl-based ligands.[31–33] Investigating the effects of the nature of the supporting ligands, we have examined the reactivity of the divalent lanthanide complexes $[(\text{DippForm})_2\text{Ln}^{II}(\text{thf})_2]$ (Ln = Sm,[35] Yb[36]) in the reduction of main group elements and compounds. By using different electronic and steric environments around divalent lanthanide elements, a different reactivity can be

---

[a] *Institute of Inorganic Chemistry, Karlsruhe Institute of Technology, Engesserstr. 15, 76131 Karlsruhe, Germany. E-mail: roesky@kit.edu*
[b] *College of Science and Engineering, James Cook University, Townsville, QLD, 4811, Australia*
[c] *School of Chemistry, Monash University, Clayton, Vic, 3800, Australia*

† Electronic supplementary information (ESI) available: IR spectra and X-ray crystallographic details of complexes **1–4**, 1994647 (**1**), 1994648 (**2**), 1952438 (**3**), and 1994649 (**4**). For ESI and crystallographic data in CIF or other electronic format see DOI: 10.1039/d0dt01271h

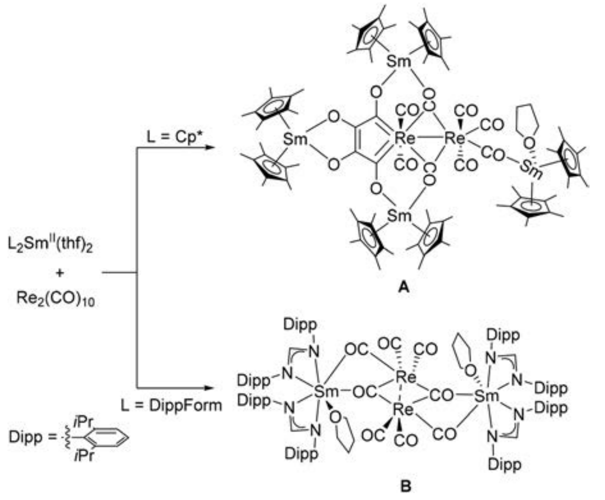

Scheme 1 Reactivity of $[Re_2(CO)_{10}]$ towards Sm(II) complexes bearing different ligands.[34]

achieved with a same substrate.[37–45] For example, Evans and co-workers have reported the formation of $[\{Cp^{*}{}_2Sm^{III}\}_2(S_3)]$ by reaction of $[Cp^{*}{}_2Sm^{II}(thf)_2]$ with elemental sulfur,[46] whereas some of us have isolated lanthanide polysulfide coordination clusters, $[(DippForm)_3Ln_3^{III}S_{12}]$ (Ln = Sm and Yb), by using $[(DippForm)_2Ln^{II}(thf)_2]$ (Ln = Sm, Yb) as divalent lanthanide reagents.[42] In addition, activation of white phosphorous and yellow arsenic by $[(DippForm)_2Sm^{II}(thf)_2]$ led to the formation of $[\{(DippForm)_2Sm^{III}\}_2(\mu\text{-}\eta^4\text{-}Pn_4)]$ (Pn = P, As).[43] These products contrast with the cage-type molecules $[\{Cp^{*}{}_2Sm^{III}\}_4(Pn)_8]$ (Pn = P,[37] As,[44] and Sb[47]) that were obtained by reaction of $[Cp^{*}{}_2Sm^{II}]$ with white phosphorous, nanoscale arsenic, and nanoscale antimony, respectively. We were then interested to extend the study of the influence of the ligands on the reductive behaviour of divalent lanthanide complexes from main group compounds to transition metal complexes. Very recently, some of us have reported the reduction of $[Re_2(CO)_{10}]$ with $[L_2Sm^{II}(thf)_2]$ (L = Cp* or DippForm) and, depending on the nature of the ligands around samarium, were able to isolate either a Fischer-type rhenacycle (**A**) or a novel $[Re_2(CO)_8]^{2-}$ dianion (**B**) in the coordination sphere of $[L_2Sm^{III}]^+$ moieties (Scheme 1).[34] Inspired by the above results, we further explored the reactivity of group 8 and 9 metal carbonyls towards divalent lanthanide complexes supported by the bulky amidinate DippForm ligand and report herein the synthesis and characterisation of the resulting 3d–4f metal complexes obtained.

Results and discussion

Ln–Co carbonyl complexes

The reaction of $[(DippForm)_2Sm^{II}(thf)_2]$ with half an equivalent of $[Co_2(CO)_8]$ in toluene at room temperature resulted in the formation of the heterometallic complex $[\{(DippForm)_2Sm^{III}(thf)\}_2\{(\mu\text{-}CO)_2Co(CO)_2\}_2]$ (**1**) (Scheme 2).

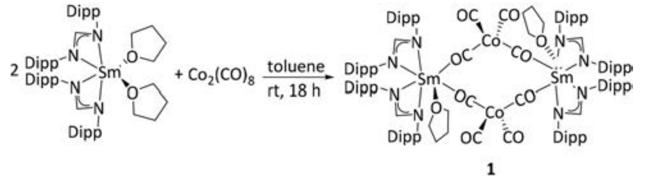

Scheme 2 Synthesis of complex **1**.

After a short work-up, analytically pure yellow-coloured crystals of complex **1** were grown in a 56% yield by slow evaporation of toluene. The solid-state IR spectrum of complex **1** showed characteristic $\tilde{\nu}_{CO}$ bands at 2020 (m), 1951 (br), 1935 (br), 1922 (br), 1904 (br), 1842 (s), 1819 (s) and 1782 (s) cm^{-1}. The low-frequency stretch at 1782 (s) cm^{-1} suggests the presence of bridging isocarbonyls between the Sm and Co atoms. The terminal CO stretches from 2020 to 1819 cm^{-1} and the low-frequency isocarbonyl stretch at 1782 cm^{-1} are apparent for complex **1**. Similar low-frequency stretches at 1798 (m) and 1761 (s) cm^{-1} were observed for $[\{(Cp^{*})_2Yb^{III}(thf)\}\{(\mu\text{-}CO)Co(CO)_3\}]$.[15] Furthermore, the molecular structure of complex **1** was determined by single crystal X-ray crystallography. Complex **1** crystallizes in the monoclinic space group $P2_1/n$ with half a molecule in the asymmetric unit. The solid-state structure showed that two $[(DippForm)_2Sm^{III}(thf)]^+$ moieties are bridged by two $[(\mu\text{-}CO)_2Co(CO)_2]^-$ units (Fig. 1). The formation of complex **1** can be rationalized by single-electron transfer steps from two $[(DippForm)_2Sm^{II}(thf)_2]$ molecules to one molecule of $[Co_2(CO)_8]$, resulting in the homolytic cleavage of the Co–Co bond and the formation of two $[Co(CO)_4]^-$ anions along with two $[(DippForm)_2Sm^{III}(thf)]^+$ cations.

Each samarium atom is heptacoordinated, surrounded by two bidentate amidinate ligands, two bridging isocarbonyls,

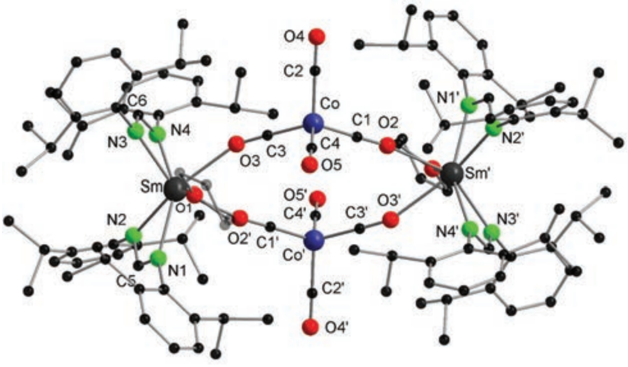

Fig. 1 Molecular structure of **1**. Hydrogen atoms are omitted for clarity. Selected bond distances (Å) and angles [°]: Sm–O1 2.422(2), Sm′–O2 2.488(3), Sm–O3 2.552(3), Sm–N1 2.431(3), Sm–N2 2.449(3), Sm–N3 2.409(3), Sm–N4 2.449(3), Co–C1 1.733(4), Co–C2 1.787(4), Co–C3 1.747(4), Co–C4 1.782(4), O2–C1 1.175(4), O3–C3 1.170(4), O4–C2 1.138(5), O5–C4 1.145(5), N1–C5 1.322(4), N2–C5 1.318(4), N3–C6 1.330(5), N4–C6 1.326(5); O2′–Sm–O3 67.27(8), N1–Sm–N2 55.35(9), N1–Sm–N4 143.10(10), C1–Co–C2 108.8(2), C1–Co–C3 116.1(2), C1–Co–C4 110.1(2), C3–Co–C2 109.7(2), C3–Co–C4 105.8(2), C4–Co–C2 105.8(2), N2–C5–N1 118.4(3), N4–C6–N3 120.3(3).

and one coordinating thf. The average Sm–N bond length (2.434(3) Å) in complex **1** is significantly shorter than that in $[(\text{DippForm})_2\text{Sm}^{\text{II}}(\text{thf})_2]$ (Sm–N(average) 2.573(3) Å). This shortening is consistent with a decrease in the ionic radius of the metal cation upon oxidation of Sm^{II} to Sm^{III}.[48] Besides, the shortening of the Sm–O1(thf) bond length, from 2.560(3) Å in $[(\text{DippForm})_2\text{Sm}^{\text{II}}(\text{thf})_2]$ to 2.422(2) Å in **1**, further supports the oxidation of the Sm centre to the +3 oxidation state. The cobalt centre in the bridging tetracarbonylcobaltate anion has a distorted tetrahedral coordination geometry with C–Co–C angles ranging from 105.8(2)° to 116.1(2)°. Owing to the coordination to the $[(\text{DippForm})_2\text{Sm}^{\text{III}}(\text{thf})]^+$ moiety, the O2–C1 (1.175(4) Å) and O3–C3 (1.170(4) Å) bond distances are longer than the O4–C2 (1.138(5) Å) and O5–C4 (1.145(5) Å) analogues involving terminal CO ligands. A further effect of the formation of bridging isocarbonyls can be seen by analysis of the Co–C bond lengths: the Co–C(bridging) bonds are shortened and strengthened as compared to the Co–C(terminal) bonds (Co–C1 (1.733 (4) Å) and Co–C3 (1.747(4) Å) *vs.* Co–C4 (1.782(4) Å) and Co–C2 (1.787(4) Å), respectively).[15] To the best of our knowledge, complex **1** is a rare example of a Sm^{III}–Co carbonyl complex featuring bridging isocarbonyls between the two metal centres. Mountford and co-workers have reported the Sm^{III}–Co carbonyl complex $[\text{Sm}^{\text{III}}\{(\mu\text{-CO})\text{Co(CO)}_2(\text{PCy}_3)\}\{\text{Co(CO)}_3(\text{PCy}_3)\}(\text{thf})_3]$ (Cy = cyclohexyl) by a reaction between SmI_2 with $\text{K}[\text{Co(CO)}_3(\text{PCy}_3)(\text{thf}_2)]$.[25] Although the reduction of $[\text{Co}_2(\text{CO})_8]$ by $[\text{Cp*}_2\text{Sm}^{\text{II}}(\text{thf})_2]$ has been studied by Evans *et al.*, no solid-state structure of the product has been reported.[27] Besides, the reaction between $[\text{Sm}^{\text{II}}\text{I}_2(\text{thf})_2]$ and $[\text{Co}_2(\text{CO})_8]$ in thf led to the solvent-separated ion pair, $[\text{Sm}^{\text{III}}\text{I}_2(\text{thf})_4][\text{Co(CO)}_4]$, which was structurally characterized.[27]

The ytterbium analogue of complex **1** was synthesized following a similar procedure (Scheme 3) and orange-coloured crystals were isolated in 63% yield. The IR spectrum of complex **2**, $[\{(\text{DippForm})_2\text{Yb}^{\text{III}}(\text{thf})\}\{(\mu\text{-CO})\text{Co(CO)}_3\}]$, shows $\tilde{\nu}_{\text{CO}}$ stretches in the carbonyl region from 2031 to 1748 cm^{-1}, in a similar range to those of $[\{\text{Cp*}_2\text{Yb}^{\text{III}}\}(\text{thf})(\mu\text{-CO})\text{Co(CO)}_3]$ (2023 to 1761 cm^{-1}).[15] The lowest stretch at 1748 cm^{-1} indicates bridging isocarbonyls between the tetracarbonylcobaltate anion and the $[(\text{DippForm})_2\text{Yb}^{\text{III}}(\text{thf})]^+$ moiety. Similar $\tilde{\nu}_{\text{CO}}$ stretches (2017 to 1780 cm^{-1}) have been observed in the related complex $[\text{Cp}_2\text{Lu(thf)}\{\text{Co(CO)}_4\}]$.[49] The solid-state structure was established by single-crystal X-ray crystallography (Fig. 2). Complex **2** crystallizes in the triclinic space group $P\bar{1}$ with one molecule in the asymmetric unit cell. In contrast to the dimeric form of complex **1**, the solid-state structure of complex **2** reveals a monomeric arrangement. A possible reason for this difference could be a combined effect of the smaller ionic radius of Yb^{3+} as compared to Sm^{3+} and the sterically demanding nature of the DippForm ligands.[48] The ytterbium centre is in a distorted octahedral environment, coordinated by two chelating amidinate ligands, one isocarbonyl O donor, and one thf ligand. In complex **2**, the shortening of the Yb–N bond distances involving the amidinate ligands (2.315(2) Å, average) and of Yb–O5 (2.304(2) Å), in comparison to the corresponding separations in $[(\text{DippForm})_2\text{Yb}^{\text{II}}(\text{thf})_2]$ (Yb–N (2.447 Å) and Yb–O (2.461 Å), average),[36] is consistent with the oxidation of the Yb metal centre from the +2 to the +3 oxidation state.[48] As observed in **1**, the cobalt centre in the tetracarbonylcobaltate anion of **2** has a distorted tetrahedral coordination environment with C–Co–C angles varying from 104.6(2)° to 115.8(2)°. The Co–C1 bond length (1.705(3) Å) in **2** is almost the same as the Co–C(bridged) (1.699(3) Å) bond distance in $[\{\text{Cp*}_2\text{Yb}^{\text{III}}\}(\text{thf})(\mu\text{-CO})(\text{Co(CO)}_3]$.[15] The average Co–C (terminal) bond lengths in **2** and $[\{\text{Cp*}_2\text{Yb}^{\text{III}}\}(\text{thf})(\mu\text{-CO})\text{Co(CO)}_3]$ are also similar (*ca.* 1.77 Å in both cases).

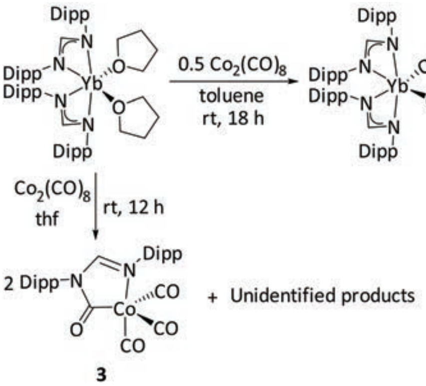

Scheme 3 Synthesis of complex **2** and **3** (**3** is not fully characterized).

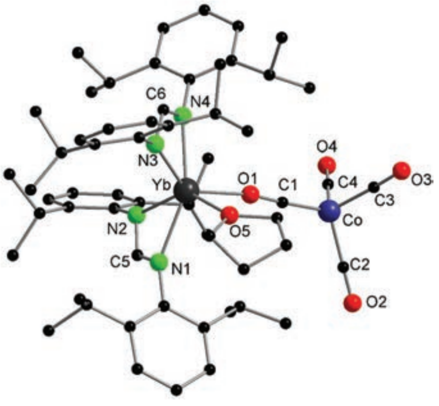

Fig. 2 Molecular structure of **2**. Hydrogen atoms are omitted for clarity. Selected bond distances (Å) and angles [°]: Yb–O1 2.248(2), Yb–O5 2.304(2), Yb–N1 2.307(2), Yb–N2 2.337(2), Yb–N3 2.292(2), Yb–N4 2.324(2), Yb–C5 2.697(3), Yb–C6 2.686(3), Co–C1 1.705(3), Co–C2 1.783(5), Co–C3 1.787(4), Co–C4 1.763(3), O1–C1 1.200(3), O2–C2 1.143(5), O3–C3 1.152(5), O4–C4 1.140(4), N1–C5 1.317(3), N2–C5 1.315(3), N3–C6 1.319(3), N4–C6 1.315(3); O1–Yb–O5 81.70(8), N1–Yb–N2 58.23(7), N1–Yb N4 99.80(8), N3–Yb–N1 112.08(8), N3–Yb–N2 114.88(8), C1–Co–C2 111.8(2), C1–Co–C3 115.8(2), C1–Co–C4 109.6(2), C2–Co–C3 107.5(2), C4–Co–C2 104.6(2), C4–Co–C3 106.8(2).

In a different approach to synthesize complex **2**, $[(\text{DippForm})_2\text{Yb}(\text{thf})_2]$ was treated with cobalt carbonyl at room temperature in thf for 12 hours. In this case, we did not obtain the bimetallic species **2**. Instead, crystals of the metallacyclic cobalt(I) complex $[(\text{DippFormCO})(\text{CO})_3\text{Co}]$ (**3**) were isolated (Scheme 3). Despite our attempts, complex **3** could not

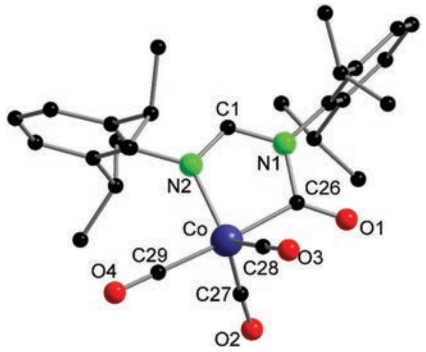

Fig. 3 Molecular structure of **3**. Hydrogen atoms and solvent of crystallisation have been omitted for clarity. Selected bond lengths (Å) and angles [°]: Co1–N2 1.968(3), Co1–C26 1.930(4), Co1–C27 1.755(6), Co1–C28 1.755(6), Co1–C29 1.799(5), C1–N1 1.346(5), C1–N2 1.285(3), N1–C26 1.430(5), C26–O1 1.201(5), C27–O2 1.135(6), C28–O3 1.134(7), C29–O4 1.138(6); C26–Co1–N2 82.7(2), C27–Co1–N2 121.6(2), C28–Co1–N2 117.7(2), C29–Co1–N2 93.6(2), C26–Co1–C27 86.2(2), C26–Co1–C28 86.0(2), C26–Co1–C29 176.1(2), C27–Co1–C28 118.5(3), C28–Co1–C29 96.7(2), N1–C1–N2 118.3(4).

be obtained in analytically pure form. However, the isolation of **3** gave some insight into occurring side reactions. Complex **3** was unambiguously identified by single crystal X-ray diffraction studies. Complex **3** crystallizes in the monoclinic space group $P2_1/n$, with one molecule in the asymmetric unit (Fig. 3). This complex consists of a five-coordinate cobalt centre, connected to three carbonyl groups ($C{\equiv}O$), one $-C({=}O)N$ donor and a nitrogen atom from the N–C–N backbone of the methanide ligand. Previously, Jones and coworkers have reported a very similar complex, $[Co\{C({=}O)N(Dipp)C(tBu)N(Dipp\}(CO)_3]$, by reacting CO gas with an amidinate stabilized cobalt(I) complex.[50] In the IR spectrum of complex **3** taken from the reaction mixture bands at 2066 (s), 2009 (s), and 1983 (m) cm^{-1} can be attributed to C–O stretching frequencies of carbonyl groups. These values have close resemblance to the IR spectrum reported by Jones' group, where they identified 2064 (s), 2004 (s), and 1970 (br) cm^{-1} as C–O stretching frequencies. The bond lengths and angles of complex **3** and $[Co\{C({=}O)N(Dipp)C(tBu)N(Dipp\}(CO)_3]$ are very similar.[50] The ligand in complex **3** showed a band at 1666 (s) cm^{-1} corresponding to the ketonic carbonyl $-C({=}O)N$ stretching. Complex **3** presumably arises from $[(DippForm)Yb^{III}(\mu\text{-}DippForm)(\mu\text{-}OC)Co(CO)_3]$, the latter formed by partial transmetallation from the bimetallic complex **2**. The bridging DippForm is bound to the cobalt(I) centre through the imine N atom, providing an 18 electron Co species which undergoes CO insertion into the Co–N bond resulting in complex **3**, where the new *N,N′*-(Dipp)formimidamidomethanide ($C({=}O)N(Dipp)C(H)N(Dipp)$ now C,N′-chelates the cobalt.

Sm–Fe carbonyl complex

Further reactivity studies of $[(DippForm)_2Sm^{II}(thf)_2]$ were carried out with iron-carbonyl complexes. The reaction between $[(DippForm)_2Sm^{II}(thf)_2]$ and half an equivalent of $[Fe_3(CO)_{12}]$ or one equivalent of $[Fe_2(CO)_9]$ in thf at

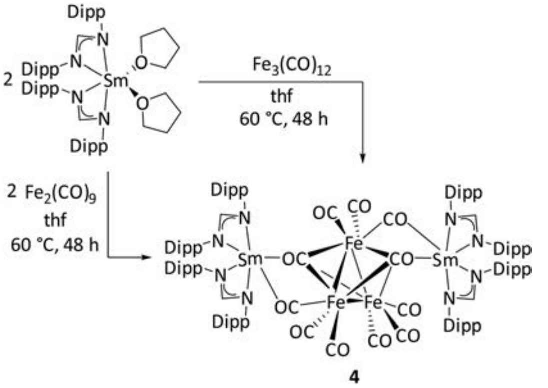

Scheme 4 Synthesis of complex **4** *via* two routes.

60 °C resulted in the formation of $[\{(DippForm)_2Sm^{III}\}_2\{(\mu_3\text{-}CO)_2Fe_3(CO)_9\}]$ (**4**) (Scheme 4). Red-coloured crystals were isolated in 33% yield after a short work-up. The solid-state IR spectrum showed characteristic $\tilde{\nu}_{CO}$ absorption bands at 2011(vs), 1979 (vs), 1967 (s), 1878 (m), 1830 (w), and 1696 (w) cm^{-1}. Similar $\tilde{\nu}_{CO}$ absorption bands were observed for $[(NEt_4)_2][Fe_3(CO)_{11}]$ at 1938, 1910, 1890, and 1670 cm^{-1}.[51] The low-frequency band at 1696 cm^{-1} is characteristic of the occurrence of bridging isocarbonyls. The solid-state structure of complex **4** was unambiguously determined by single crystal X-ray diffraction studies, revealing two $[(DippForm)_2Sm^{III}]^+$ moieties associated together by a $[(\mu_3\text{-}CO)_2Fe_3(CO)_9]^{2-}$ fragment *via* bridging isocarbonyls (Fig. 4). In complex **4**, each Sm atom is hexacoordinated, surrounded by two bidentate amidinate ligands and two bridging isocarbonyls. Notably, the $[(DippForm)_2Sm^{III}]^+$ moiety is free of coordinating thf molecules, which may result from the crystallisation of the complex from hot toluene and also the steric crowding around

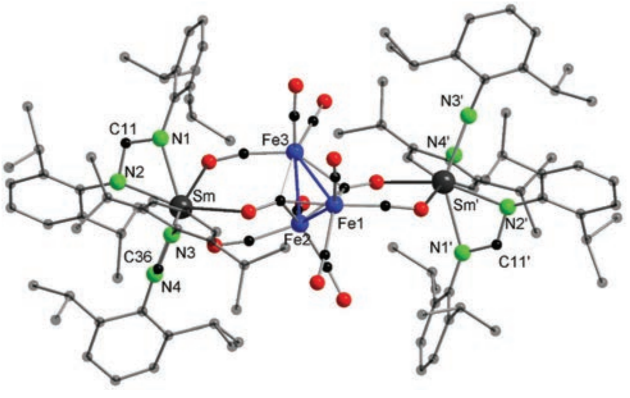

Fig. 4 Simplified view of the molecular structure of **4** in the solid state. H atoms are omitted for clarity. Selected bond distances (Å) and angles [°]: N1–Sm 2.409(2), N2–Sm 2.426(2), N3–Sm 2.381(2), N4–Sm 2.418(2), N1–C11 1.329(3), N2–C11 1.329(3), N3–C36 1.336(3), N4–C36 1.323(3); N1–C11–N2 117.87(2), N4–C36–N3 117.9(2), N1–Sm–N2 56.20(6), N1–Sm–N4 142.11(6), N3–Sm–N1 108.16(6), N3–Sm–N2 109.53(6), N3–Sm–N4 56.65(6). Discussion of the bond lengths and angles for the $[Fe_3(CO)_{11}]^{2-}$ moiety is precluded due to the disorder.

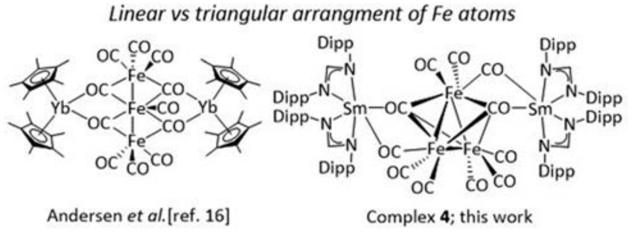

Scheme 5 Different conformations of the $[Fe_3(CO)_{11}]^{2-}$ anion.

the Sm metal centre. The average Sm–N bond length (2.408(2) Å) in complex **4** is significantly shorter than in $[(DippForm)_2Sm^{II}(thf)_2]$ (Sm–N(average) 2.573(3) Å).[35] The $[(\mu_3\text{-}CO)_2Fe_3(CO)_9]^{2-}$ moiety is formed by a two-electron reduction of $[Fe_3(CO)_{12}]$ or $[Fe_2(CO)_9]$ by two $[(DippForm)_2Sm^{II}(thf)_2]$ molecules through SET steps. The $[(\mu_3\text{-}CO)_2Fe_3(CO)_9]^{2-}$ moiety features three Fe atoms arranged in a triangular shape. Upon reaction, formally one CO group in $[Fe_3(CO)_{12}]$ is replaced by a di-negative charge leading to the $[(\mu_3\text{-}CO)_2Fe_3(CO)_9]^{2-}$ anion. In contrast, the related Yb^{III} complex $[(Cp^*{}_2Yb^{III})_2((\mu_2\text{-}CO)_4Fe_3(CO)_7)]$ isolated by Andersen and co-workers exhibits a linear arrangement for the three Fe atoms (Scheme 5).[16] The possible reason for this different arrangement in the solid state may be the sterically demanding nature of the DippForm ligands. Due to disorder of the $[(\mu_3\text{-}CO)_2Fe_3(CO)_9]^{2-}$ moiety the bond lengths and angles cannot be precisely discussed (Fig. S8, ESI†). Despite several attempts, the product formed upon the reaction between $[Fe_3(CO)_{12}]$ and $[(DippForm)_2Yb^{II}(thf)_2]$ could not be crystallized and its true identification remains unknown. The structural motive of $[(\mu_3\text{-}CO)_2Fe_3(CO)_9]^{2-}$ observed in complex **4** is very rare as compared to the $[(\mu\text{-}CO)(\mu_3\text{-}CO)Fe_3(CO)_9]^{2-}$ unit observed in $[(NEt_4)_2][Fe_3(CO)_{11}]$.[51] Previously, the $[(\mu_3\text{-}CO)_2Fe_3(CO)_9]^{2-}$ moiety has been observed in coordination with main group elements such as Li,[52] Ca,[25] C,[53] and B.[54] For example, the Ca complex $[Ca\{(\mu_3\text{-}CO)_2Fe_3(CO)_9\}(MeCN)_4]_n$, was obtained by reduction of $[Fe_3(CO)_{12}]$ with Ca amalgam in liquid ammonia.[25] In contrast, the reactions of $[Fe_3(CO)_{12}]$ with Yb metal, resulted in $[\{(MeCN)_3YbFe(CO)_4\}_2{\cdot}MeCN]_n$ featuring a Yb–Fe bond,[55] and that of $[Fe_3(CO)_{12}]$ with $[(Cp^*{}_2Yb(OEt_2)]$, gave $[(Cp^*{}_2Yb^{III})_2((\mu_2\text{-}CO)_4Fe_3(CO)_7)]$ (Scheme 5).[16]

Conclusions

In conclusion, we have studied the reactivity of two divalent lanthanide (Sm and Yb) complexes coordinated by bulky amidinate ligands towards 3d transition metal carbonyl complexes of groups 8 and 9. The reaction of $[(DippForm)_2Sm^{II}(thf)_2]$ with $[Co_2(CO)_{10}]$ resulted in a tetranuclear Sm^{III}–Co heterometallic complex (**1**) representing a rare example of a Sm^{III}–Co carbonyl complex featuring a bridging isocarbonyl. An analogous reactivity was also observed when $[(DippForm)_2Yb^{II}(thf)_2]$ was reacted with $[Co_2(CO)_{10}]$ in toluene resulting in a dinuclear Yb^{III}–Co heterometallic complex (**2**). Interestingly, the reaction between $[(DippForm)_2Yb^{II}(thf)_2]$ and $[Co_2(CO)_{10}]$ in thf resulted in a mononuclear cobalt(I) complex (**3**). The possible reason for the formation of complex **3** when using thf as solvent may be due to solvent induced displacement of DippForm from the Yb centre. The reaction of $[(DippForm)_2Sm^{II}(thf)_2]$ was also carried out with two iron carbonyl complexes, $[Fe_2(CO)_9]$ and $[Fe_3(CO)_{12}]$. In both cases, a pentanuclear Sm^{III}–Fe heterometallic complex (**4**) was isolated. Complex **4** exhibits a $[(\mu_3\text{-}CO)_2Fe_3(CO)_9]^{2-}$ anion with a triangular Fe core. The $[(\mu_3\text{-}CO)_2Fe_3(CO)_9]^{2-}$ anion is sandwiched between two $[(DippForm)_2Sm^{III}]^+$ moieties. Interestingly, the $[(\mu_3\text{-}CO)_2Fe_3(CO)_9]^{2-}$ anion in complex **4** is in a triangular arrangement which is in sharp contrast to the linear arrangement observed in $[(Cp^*{}_2Yb^{III})_2((\mu_2\text{-}CO)_4Fe_3(CO)_7)]$.[16]

Experimental

General procedures

All the manipulations of air- and water-sensitive reactions were performed with rigorous exclusion of oxygen and moisture in flame-dried Schlenk-type glassware either on a dual manifold Schlenk line, interfaced to a high vacuum (10^{-3} Torr) line or in an argon-filled MBraun glove box. Tetrahydrofuran was distilled under nitrogen from potassium benzophenoneketyl before storage *in vacuo* over $LiAlH_4$. Hydrocarbon solvents were dried by using an MBraun solvent purification system (SPS 800) and degassed and stored *in vacuo* over $LiAlH_4$. Elemental analyses were carried out with an Elementar vario Micro cube. IR spectra were obtained on a Bruker Tensor 37 spectrometer equipped with a room temperature DLaTGS detector and a diamond ATR (attenuated total reflection) unit. $[(DippForm)_2Sm^{II}(thf)_2]$[35,41] and $[(DippForm)_2Yb^{II}(thf)_2]$[36] were prepared according to literature procedure. $[Fe_3(CO)_{12}]$, $[Fe_2(CO)_9]$, and $[Co_2(CO_8)]$ were purchased from commercial suppliers and used as received. No reasonable NMR could be obtained due to low solubility and paramagnetic character.

Synthesis of $[\{(DippForm)_2Sm^{III}(thf)\}_2\{(\mu\text{-}CO)_2Co(CO)_2\}_2]$ (1)[56]

To a mixture of $[(DippForm)_2Sm^{II}(thf)_2]$ (205 mg, 0.20 mmol) and $[Co_2(CO)_8]$ (34 mg, 0.10 mmol) was condensed toluene (15 mL) at −78 °C and then the reaction mixture was stirred for 18 hours at room temperature. The reaction mixture was filtered through P4 frit in a double ampule and flame sealed. Yellow-coloured crystals were grown by slow evaporation of toluene. Crystals were washed carefully with cold toluene and dried under vacuum. **Yield**: 127 mg, (based on crystals), 0.056 mmol, 56%. **Anal. calcd** for $C_{116}H_{156}N_8O_{10}Co_2Sm_2$ (2241.16): C, 62.17; H, 7.02; N, 5.00. **Found**: C, 62.34; H, 6.84; N, 4.81. **IR (ATR)** $\tilde{\nu}$ (cm^{-1}): 2959 (s), 2927 (m), 2866 (m), 2020 (m), 1951 (br), 1935 (br), 1922 (br), 1904 (br), 1842 (s), 1819 (s), 1782 (s), 1665 (vs), 1636 (m), 1587 (m), 1527 (m), 1518 (m), 1464 (s), 1457 (s), 1439 (s), 1383 (s), 1361 (m), 1332 (m), 1314 (m), 1289 (m), 1272 (m), 1255 (m), 1236 (s), 1185 (m), 1107 (m), 1098 (m), 1057 (m), 1043 (m), 1016 (m), 934 (m), 912 (m), 865 (br), 800 (s), 753 (vs), 673 (s), 565 (w), 553 (s), 550 (s), 531 (s) 522 (s), 506 (s) 435 (w).

Synthesis of [{(DippForm)$_2$Yb^{III}(thf)}{(μ-CO)Co(CO)$_3$}] (2)[56]

Following the procedure described above for **1**, the reaction of [(DippForm)$_2$Yb^{II}(thf)$_2$] (209 mg, 0.20 mmol) and [Co$_2$(CO)$_8$] (34 mg, 0.10 mmol) afforded orange-coloured crystals of **2**. **Yield**: 146 mg, (based on crystals), 0.127 mmol, 63%. **Anal. calcd** for $C_{58}H_{78}N_4O_5CoYb$ (1143.27): C, 60.93; H, 6.88; N, 4.90. **Found**: C, 61.30; H, 6.89; N, 4.90. **IR (ATR)** $\tilde{\nu}$ (cm^{-1}): 2960 (s), 2927 (m), 2869 (m), 2031 (m), 2016 (m), 1915 (br), 1792 (m), 1748 (w), 1665 (vs), 1636 (m), 1587 (s), 1521 (m), 1465 (m), 1458 (m), 1439 (s), 1383 (s), 1361 (m), 1331 (m), 1331 (m), 1319 (m), 1290 (m), 1268 (m), 1255 (w), 1236 (m), 1186 (m), 1107 (m), 1107 (w), 1097 (w), 1058 (w), 1043 (w), 1025 (w), 1007 (w), 934 (w), 883 (w), 871 (w), 822 (w), 799 (s), 767 (w), 753 (w), 712 (w), 673 (w), 564 (w), 551 (vs), 510 (m), 434 (m), 418 (m).

Synthesis of [Co(DippFormCO)(CO)$_3$] (3)

THF (30 mL) was added to a Schlenk flask charged with [Yb(DippForm)$_2$(thf)$_2$] (418 mg, 0.40 mmol) under purified nitrogen Co$_2$(CO)$_8$ (160 mg, 0.47 mmol) was added to the orange solution with stirring and the mixture was stirred for 12 hours at ambient temperature. The colour of the solution turned from orange to dark brown. The solution was filtered to remove any solid materials and the volume reduced under vacuum. The solution was then stored at 3 °C for 3 days during which time needle like crystals formed. IR (Nujol) $\tilde{\nu}$ (cm^{-1}): 2066 (s), 2009 (s), 1983 (m), 1897 (w), 1666 (s), 1587 (m), 1287 (m), 1234 (w), 1180 (m), 1098 (w), 1058 (w), 1000 (w), 935 (w), 821 (w), 799 (m), 753 (w), 767 (m), 722 (m). Complex **3** could not be obtained as analytically pure material.

Synthesis of [{(DippForm)$_2$Sm^{III}}$_2${(μ$_3$-CO)$_2$Fe$_3$(CO)$_9$}] (4)[56]

To a mixture of [(DippForm)$_2$Sm^{II}(thf)$_2$] (205 mg, 0.20 mmol) and [Fe$_3$(CO)$_{12}$] (51 mg, 0.10 mmol) or [Fe$_2$(CO)$_9$] (72 mg, 0.20 mmol) was condensed thf (15 mL) at −78 °C and the reaction mixture was stirred for 48 hours at 60 °C. All the volatiles were removed *in vacuo*. Toluene (15 mL) was added to the residue and refluxed for five minutes and the hot reaction mixture was filtered. Dark red-coloured crystals were obtained upon slowly cooling the filtrate to room temperature. The mother liquor was decanted off and the product was dried under vacuum. **Yield**: 74 mg (based on crystals), 0.033 mmol, 33% (average). **Anal. calcd** for $C_{111}H_{140}N_8O_{11}Fe_3Sm_2$ (2230.64): C, 59.77; H, 6.33; N, 5.02. **Found**: C, 59.77; H, 6.20; N, 4.81. **IR (ATR)** $\tilde{\nu}$ (cm^{-1}): 2962 (vs), 2926 (m), 2869 (m), 2011 (vs), 1979 (vs), 1967 (s), 1878 (m), 1830 (w), 1696 (w), 1667 (s), 1640 (s), 1636 (m), 1586 (s), 1512 (s), 1464 (s) 1457 (m), 1437 (m), 1384 (s), 1362 (m), 1346 (m), 1332 (m), 1314 (s), 1278 (s), 1368 (m), 1254 (s), 1236 (m), 1186 (m), 1112 (w), 1098 (m), 1054 (m), 1042 (m), 1023 (w), 1004 (w), 947 (w), 935 (m), 823 (s), 800 (s) 768 (m), 753 (s), 681 (s), 645 (m), 612 (s), 585 (s), 508 (w), 474 (w), 458 (w), 444 (w), 438 (w), 433 (w), 420 (w).

Conflicts of interest

There are no conflicts to declare.

Acknowledgements

RY and PWR acknowledge funding for the current project from the SFB 1176 funded by the German Research Council (DFG). TS thanks the Alexander von Humboldt Foundation for a post-doctoral fellowship. PCJ and GBD thank the Australian research Council for grant DP190100798.

Notes and references

1 J. A. Mata, F. E. Hahn and E. Peris, *Chem. Sci.*, 2014, **5**, 1723–1732.

2 P. Buchwalter, J. Rosé and P. Braunstein, *Chem. Rev.*, 2015, **115**, 28–126.

3 A. Bhunia, M. T. Gamer, L. Ungur, L. F. Chibotaru, A. K. Powell, Y. Lan, P. W. Roesky, F. Menges, C. Riehn and G. Niedner-Schatteburg, *Inorg. Chem.*, 2012, **51**, 9589–9597.

4 J.-L. Liu, J.-Y. Wu, Y.-C. Chen, V. Mereacre, A. K. Powell, L. Ungur, L. F. Chibotaru, X.-M. Chen and M.-L. Tong, *Angew. Chem., Int. Ed.*, 2014, **53**, 12966–12970.

5 J. Wu, L. Zhao, L. Zhang, X.-L. Li, M. Guo, A. K. Powell and J. Tang, *Angew. Chem., Int. Ed.*, 2016, **55**, 15574–15578.

6 S. V. Eliseeva and J.-C. G. Bünzli, *Chem. Soc. Rev.*, 2010, **39**, 189–227.

7 T. D. Pasatoiu, C. Tiseanu, A. M. Madalan, B. Jurca, C. Duhayon, J. P. Sutter and M. Andruh, *Inorg. Chem.*, 2011, **50**, 5879–5889.

8 A. Bhunia, M. A. Gotthardt, M. Yadav, M. T. Gamer, A. Eichhöfer, W. Kleist and P. W. Roesky, *Chem. – Eur. J.*, 2013, **19**, 1986–1995.

9 M. Yadav, A. Bhunia, S. K. Jana and P. W. Roesky, *Inorg. Chem.*, 2016, **55**, 2701–2708.

10 C. E. Plečnik, S. Liu and S. G. Shore, *Acc. Chem. Res.*, 2003, **36**, 499–508.

11 P. L. Arnold, J. McMaster and S. T. Liddle, *Chem. Commun.*, 2009, 818–820.

12 C. P. Burns, X. Yang, S. Sung, J. D. Wofford, N. S. Bhuvanesh, M. B. Hall and M. Nippe, *Chem. Commun.*, 2018, **54**, 10893–10896.

13 T. Pugh, N. F. Chilton and R. A. Layfield, *Angew. Chem., Int. Ed.*, 2016, **55**, 11082–11085.

14 C. P. Burns, X. Yang, J. D. Wofford, N. S. Bhuvanesh, M. B. Hall and M. Nippe, *Angew. Chem., Int. Ed.*, 2018, **57**, 8144–8148.

15 T. D. Tilley and R. A. Andersen, *J. Chem. Soc., Chem. Commun.*, 1981, 985–986.

16 T. D. Tilley and R. Andersen, *J. Am. Chem. Soc.*, 1982, **104**, 1772–1774.

17 J. M. Boncella and R. A. Andersen, *J. Chem. Soc., Chem. Commun.*, 1984, 809–810.

18 J. M. Boncella and R. A. Andersen, *Inorg. Chem.*, 1984, **23**, 432–437.

19 A. Recknagel, A. Steiner, S. Brooker, D. Stalke and F. T. Edelmann, *Chem. Ber.*, 1991, **124**, 1373–1375.

20 G. B. Deacon, Z. Guo, P. C. Junk and J. Wang, *Angew. Chem., Int. Ed.*, 2017, **56**, 8486–8489.

21 C. E. Plečnik, S. Liu, X. Chen, E. A. Meyers and S. G. Shore, *J. Am. Chem. Soc.*, 2004, **126**, 204–213.

22 P. V. Poplaukhin, X. Chen, E. A. Meyers and S. G. Shore, *Inorg. Chem.*, 2006, **45**, 10115–10125.

23 M. P. Blake, N. Kaltsoyannis and P. Mountford, *J. Am. Chem. Soc.*, 2011, **133**, 15358–15361.

24 M. P. Blake, N. Kaltsoyannis and P. Mountford, *Chem. Commun.*, 2013, **49**, 3315–3317.

25 M. P. Blake, N. Kaltsoyannis and P. Mountford, *J. Am. Chem. Soc.*, 2015, **137**, 12352–12368.

26 R. Green, A. C. Walker, M. P. Blake and P. Mountford, *Polyhedron*, 2016, **116**, 64–75.

27 W. J. Evans, I. Bloom, J. W. Grate, L. A. Hughes, W. E. Hunter and J. L. Atwood, *Inorg. Chem.*, 1985, **24**, 4620–4623.

28 I. P. Beletskaya, A. Z. Voskoboynikov, E. B. Chuklanova, N. I. Kirillova, A. K. Shestakova, I. N. Parshina, A. I. Gusev and G. K. I. Magomedov, *J. Am. Chem. Soc.*, 1993, **115**, 3156–3166.

29 C. Döring, A.-M. Dietel, M. V. Butovskii, V. Bezugly, F. R. Wagner and R. Kempe, *Chem. – Eur. J.*, 2010, **16**, 10679–10683.

30 B. Oelkers, M. V. Butovskii and R. Kempe, *Chem. – Eur. J.*, 2012, **18**, 13566–13579.

31 W. J. Evans and B. L. Davis, *Chem. Rev.*, 2002, **102**, 2119–2136.

32 W. J. Evans, *Organometallics*, 2016, **35**, 3088–3100.

33 H. M. Nicholas and D. P. Mills, Lanthanides: Divalent Organometallic Chemistry, in *Encyclopedia of Inorganic and Bioinorganic Chemistry*, ed. R. A. Scott, John Wiley & Sons, 2017.

34 R. Yadav, T. Simler, M. T. Gamer, R. Köppe and P. W. Roesky, *Chem. Commun.*, 2019, **55**, 5765–5768.

35 M. L. Cole and P. C. Junk, *Chem. Commun.*, 2005, 2695–2697.

36 M. L. Cole, G. B. Deacon, C. M. Forsyth, P. C. Junk, K. Konstas, J. Wang, H. Bittig and D. Werner, *Chem. – Eur. J.*, 2013, **19**, 1410–1420.

37 S. N. Konchenko, N. A. Pushkarevsky, M. T. Gamer, R. Köppe, H. Schnöckel and P. W. Roesky, *J. Am. Chem. Soc.*, 2009, **131**, 5740–5741.

38 T. Li, J. Wiecko, N. A. Pushkarevsky, M. T. Gamer, R. Köppe, S. N. Konchenko, M. Scheer and P. W. Roesky, *Angew. Chem., Int. Ed.*, 2011, **50**, 9491–9495.

39 T. Li, M. T. Gamer, M. Scheer, S. N. Konchenko and P. W. Roesky, *Chem. Commun.*, 2013, **49**, 2183–2185.

40 M. Kühling, R. McDonald, P. Liebing, L. Hilfert, M. J. Ferguson, J. Takats and F. T. Edelmann, *Dalton Trans.*, 2016, **45**, 10118–10121.

41 C. Schoo, S. Bestgen, M. Schmidt, S. N. Konchenko, M. Scheer and P. W. Roesky, *Chem. Commun.*, 2016, **52**, 13217–13220.

42 Y.-Z. Ma, S. Bestgen, M. T. Gamer, S. N. Konchenko and P. W. Roesky, *Angew. Chem., Int. Ed.*, 2017, **56**, 13249–13252.

43 C. Schoo, S. Bestgen, R. Köppe, S. N. Konchenko and P. W. Roesky, *Chem. Commun.*, 2018, **54**, 4770–4773.

44 C. Schoo, S. Bestgen, A. Egeberg, J. Seibert, S. N. Konchenko, C. Feldmann and P. W. Roesky, *Angew. Chem., Int. Ed.*, 2019, **58**, 4386–4389.

45 D. Werner, G. B. Deacon and P. C. Junk, *Inorg. Chem.*, 2019, **58**, 1912–1918.

46 W. J. Evans, G. W. Rabe, J. W. Ziller and R. J. Doedens, *Inorg. Chem.*, 1994, **33**, 2719–2726.

47 C. Schoo, S. Bestgen, A. Egeberg, S. Klementyeva, C. Feldmann, S. N. Konchenko and P. W. Roesky, *Angew. Chem., Int. Ed.*, 2018, **57**, 5912–5916.

48 R. Shannon, *Acta Crystallogr., Sect. A: Cryst. Phys., Diffr., Theor. Gen. Crystallogr.*, 1976, **32**, 751–767.

49 I. P. Beletskaya, A. Z. Voskoboynikov, E. B. Chuklanova, A. I. Gusev and G. K. Magomedov, *Metalloorg. Khim.*, 1988, **1**, 1383–1390.

50 C. Jones, C. Schulten, R. P. Rose, A. Stasch, S. Aldridge, W. D. Woodul, K. S. Murray, B. Moubaraki, M. Brynda, G. La Macchia and L. Gagliardi, *Angew. Chem., Int. Ed.*, 2009, **48**, 7406–7410.

51 F. Y.-K. Lo, G. Longoni, P. Chini, L. D. Lower and L. F. Dahl, *J. Am. Chem. Soc.*, 1980, **102**, 7691–7701.

52 W. Petz and B. Neumüller, *Z. Anorg. Allg. Chem.*, 2010, **636**, 551–556.

53 A. A. Aradi, F. W. Grevels, C. Krueger and E. Raabe, *Organometallics*, 1988, **7**, 812–818.

54 T. V. Laine, M. Klinga and M. Leskelä, *Eur. J. Inorg. Chem.*, 1999, **1999**, 959–964.

55 H. Deng and S. G. Shore, *J. Am. Chem. Soc.*, 1991, **113**, 8538–8540.

56 R. Yadav, *Synthesis of Heterometallic Zinc-Gold and Lanthanide-Transition Metal carbonyl complexes and Reactivity Study of Pentaphosphaferrocene Towards Low-Valent Main Group Species*, PhD Thesis, Karlsruhe Institute of Technology (KIT), Kalrsruhe, Germany, 2019.

Appendix 2

This manuscript has now been accepted by Dalton Transactions on 5th January 2023.

(Dalton Transactions, 2023, DOI: 10.1039/D2DT04164B)

View Article Online
View Journal

Dalton Transactions

An international journal of inorganic chemistry

Accepted Manuscript

This article can be cited before page numbers have been issued, to do this please use: R. Peedika Paramban, Z. Guo, G. B. Deacon and P. C. Junk, *Dalton Trans.*, 2023, DOI: 10.1039/D2DT04164B.

Volume 46
Number 10
14 March 2017
Pages 3073-3412

Dalton Transactions

An international journal of inorganic chemistry

rsc.li/dalton

ISSN 0306-0012

COMMUNICATION
Douglas W. Stephen *et al.*
N-Heterocyclic carbene stabilized parent sulfenyl, selenenyl, and tellurenyl cations (XH^+, X = S, Se, Te)

rsc.li/dalton

COMMUNICATION

Formation of a cyclooctatetraenylsamarium(III) inverse sandwich that ring-opens tetrahydrofuran

R. Peedika Paramban,[a] Zhifang Guo,[a] Glen B. Deacon,[b] and Peter C. Junk.[a]*

Received 00th January 20xx,
Accepted 00th January 20xx

DOI: 10.1039/x0xx00000x

Reductive trapping of the cyclooctatetraenyl dianion (COT^{2-}) by treatment of [Sm(DippForm)$_2$(thf)$_2$] (DippFormH = N,N′-bis(2,6-diisopropylphenyl)formamidine; thf = tetrahydrofuran) with 1,3,5,7-cyclooctatetraene (C_8H_8) in toluene yields an inverse sandwich dinuclear complex [Sm$_2$(DippForm)$_4$(COT)] (1), but [Sm(DippForm)(COT)(thf)$_2$] (2) and [Sm(DippForm)$_2$(O-C_4H_8-DippForm)(thf)] (3) in thf, and 1 yields 2 and 3 on treatment with thf.

---

[a] *College of Science & Engineering, James Cook University, Townsville, QLD, 4811, Australia.*
[b] *School of Chemistry, Monash University, Clayton, VIC, 3800, Australia.*
[c] ** Corresponding Author: Email: peter.junk@jcu.edu.au*

Electronic Supplementary Information (ESI) available: Synthetic details, spectra, and crystallographic information. For ESI and crystallographic data in CIF or other electronic format see DOI:10.1039/x0xx00000x